

**EFFECTS OF ORGANOPHOSPHATE ESTERS ON
THE ADRENAL GLAND**

By

Zixuan Li

Department of Pharmacology and Therapeutics

Faculty of Medicine and Health Sciences

McGill University, Montréal

December 2024

A Thesis Submitted to McGill University in Partial Fulfillment of the Requirements of the
Degree of Doctor of Philosophy

© Zixuan Li, 2024

ABSTRACT

Organophosphate esters (OPEs) have become increasingly prevalent following the phase-out of polybrominated diphenyl ethers (PBDEs). Their widespread presence in both the environment and human matrices has raised concerns about their potential as endocrine disrupting chemicals. However, the effects of OPEs on one of the most critical endocrine glands, the adrenal glands, have received relatively little attention. In this thesis, I aim to elucidate the *in vitro* and *in vivo* effects of exposure to commonly used OPEs on the adrenal glands. First, I evaluated the impact of six OPEs on the phenotypes and functions of H295R cells. Through benchmark modeling and Toxicological Prioritization Index (ToxPi) analyses, I identified OPEs that are more potent than legacy PBDEs, as well as OPEs that could serve as potential replacement chemicals. Functional assays revealed that OPEs exerted contrasting effects on the ability of cells to produce cortisol and aldosterone by targeting key transcripts involved in cholesterol and steroid biosynthesis pathways. Next, I investigated the effects of an environmentally relevant mixture of OPEs designed to replicate the profile of OPEs found in Canadian house dust on the phenotype, function, and lipidome of H295R cells. Exposure to this mixture resulted in alterations in the quantity and composition of lipid droplets, suggesting that lipid disruption could serve as a sensitive biomarker of OPE exposure. In line with the effects of individual OPEs, the mixture also impacted levels of cortisol and aldosterone produced by the cells. Notably, the mixture induced significant effects at concentrations where individual OPEs showed little or no activity, indicating that studies focused on single compounds may underestimate the risks associated with OPE exposure. Lastly, I assessed the effects of the environmentally relevant mixture of OPEs on the adrenal glands of Sprague Dawley rats. OPE exposure led to sex-specific alterations in the weight, function, and serum lipid profiles of adrenal glands. Transcriptomic analysis of whole adrenal glands revealed that, in females, the

cholesterol biosynthesis pathway was targeted, while in males, potassium channel activity was affected. Together, these findings provide the first direct comparison of the effects of OPEs with those of legacy compounds and offer new insights into the real-life exposure risks of mixture of OPEs on the adrenal gland. Exposure to OPEs may impair steroidogenesis in the adrenal glands through sex-specific mechanisms, with lipid and cholesterol homeostasis identified as particularly sensitive targets. The integration of *in vitro* and *in vivo* assessments, high-content screening, and omics analyses offers powerful tools for identifying endocrine disrupting chemicals that require regulation, as well as safer alternatives for future use.

RÉSUMÉ

Les esters organophosphorés (EOP) sont devenus de plus en plus répandus à la suite de l'élimination progressive des polybromodiphényléthers (PBDE). Leur omniprésence dans l'environnement et dans les matrices biologiques humaines a suscité des inquiétudes quant à leur potentiel rôle comme perturbateurs endocriniens. Cependant, les effets des EOP sur la glande surrénale, une des glandes les plus essentielles, ont suscité relativement peu d'intérêt. Dans cette thèse, je cherche à élucider les effets *in vitro* et *in vivo* des EOP les plus couramment utilisés sur les glandes surrénales. Tout d'abord, j'ai évalué l'effet de six EOP sur les phénotypes et les fonctions des cellules H295R. À l'aide de la modélisation de référence et des analyses de l'indice de priorisation toxicologique (ToxPi), j'ai identifié parmi les EOP certains qui sont plus puissants que les anciens PBDE, ainsi que d'autres qui pourraient potentiellement les remplacer. Des essais fonctionnels ont révélé que les EOP avaient des effets négatifs sur la capacité des cellules à produire du cortisol et de l'aldostérone en ciblant l'expression de transcrits essentiels à la biosynthèse du cholestérol et à la stéroïdogénèse. Ensuite, j'ai étudié les effets d'un mélange d'EOP pouvant se trouver dans l'environnement, conçu pour reproduire le profil des EOP trouvés dans la poussière domestique au Canada, sur le phénotype, la fonction et le lipidome des cellules H295R. L'exposition à ce mélange a modifié la quantité et la composition des gouttelettes lipidiques, suggérant qu'un changement dans les lipides pourrait constituer un biomarqueur sensible de l'exposition aux EOP. En accord avec les effets des EOP individuels, le mélange a également affecté les niveaux de cortisol et d'aldostérone produits par les cellules. Notamment, le mélange a induit des effets importants à des concentrations où les EOP individuels n'ont montré que peu ou pas d'activité. Ceci indique que les études portant sur des substances chimiques individuelles pourraient sous-estimer les risques associés à l'exposition aux EOP. Dans la dernière expérimentale section de ma thèse, j'ai évalué les effets du mélange

d'EOP pouvant se trouver dans l'environnement sur les glandes surrénales de rats Sprague-Dawley. L'exposition aux EOP a mené à des changements spécifiques en fonction du sexe dans les glandes surrénales, à savoir le poids, la fonction et le profil des lipides sériques. L'analyse transcriptomique des glandes surrénales entières a révélé que chez les femelles, la voie de biosynthèse du cholestérol était ciblée, tandis que chez les mâles, l'activité des canaux potassiques était affectée. Ensemble, ces résultats constituent la première comparaison directe entre les effets des EOP et ceux des composés anciens. Ces résultats nous donnent également de nouvelles perspectives sur les risques d'exposition réelle aux mélanges d'EOP sur les glandes surrénales. L'exposition aux EOP pourrait altérer la stéroïdogénèse dans les glandes surrénales par des mécanismes spécifiques selon le sexe, avec l'homéostasie des lipides et du cholestérol étant identifiée comme une cible particulièrement sensible. Les évaluations *in vitro* et *in vivo*, l'imagerie cellulaire à haut débit et les analyses en «-omiques» sont des outils puissants pour identifier les perturbateurs endocriniens qui nécessitent d'être régulés, ainsi que trouver des alternatives plus sûres pour une utilisation future.

TABLE OF CONTENTS

ABSTRACT.....	II
RÉSUMÉ	IV
TABLE OF CONTENTS.....	VI
LIST OF TABLES AND FIGURES	X
LIST OF ABBREVIATIONS.....	XIII
ACKNOWLEDGEMENTS	XVI
FORMAT OF THE THESIS.....	XVIII
CONTRIBUTION OF AUTHORS.....	XIX
SOURCES OF FUNDING.....	XXI
CHAPTER 1 INTRODUCTION.....	1
1.1 The adrenal glands	1
1.1.1 Origin and development of the adrenal gland	1
1.1.2 The morphology of the adrenal gland.....	4
1.1.3 Adrenal steroidogenesis.....	5
1.1.3.1 Cholesterol pathway	6
1.1.3.1.1 Source of cholesterol.....	6
1.1.3.1.2 Regulation of cholesterol homeostasis.....	8
1.1.3.2 Adrenal cortex produced hormones	10
1.1.3.3 Medulla produced hormones	11
1.1.3.4 Function of adrenal produced hormones	12
1.1.4 Regulation of adrenal functions.....	15
1.1.4.1 Hypothalamus-pituitary-adrenal (HPA) axis	15
1.1.4.2 Renin-angiotensin-aldosterone system	16
1.1.4.3 Adrenal medulla and the sympathetic system.....	18
1.1.5 Sexual dimorphism of the adrenal gland	19
1.2 Adrenal cell lines.....	19
1.2.1 Rodent adrenocortical cell lines	20
1.2.1.1 The Y1 adrenal cell line	20
1.2.1.2 Other rodent cell lines.....	21
1.2.2 Human adrenocortical cell lines	22
1.2.2.1 The NCI-H295 cell line	22
1.2.2.2 Male adrenocortical cell lines	23
1.2.2.3 H295R cell.....	23
1.2.2.3.1 Receptors and responsiveness to stimulators	24
1.2.2.3.2 OECD test guideline No. 456: H295R steroidogenesis assay	25
1.2.3 Advantages and limitations of in vitro cell cultures v. in vivo animal study.....	26
1.3 Endocrine disrupting chemicals (EDCs)	27
1.3.1 Definition of EDCs	27
1.3.2 Presence of EDCs in human matrices	28
1.3.3 EDCs that affect the adrenal gland	29
1.4 Flame retardants	30
1.4.1 Polybrominated diphenol ethers (PBDEs).....	31
1.4.1.1 Physicochemical properties of PBDEs	31
1.4.1.2 Toxicity of PBDEs	33
1.4.1.3 Global regulation of PBDEs	34
1.4.2 Organophosphate esters (OPEs)	34
1.4.2.1 Physicochemical properties	35

1.4.2.2 Production and application	36
1.4.2.3 Routes of exposure	37
1.4.2.3.1 Levels in human matrices	37
1.4.2.4 Metabolism and elimination	38
1.4.2.5 Established health effects.....	38
1.4.2.6 Effect on the adrenal gland	39
1.4.2.7 Rationale and significance of studying chemical mixture	41
1.4.2.8 The Canadian house dust study	42
1.5 Formulation of the thesis project	42
CHAPTER 2	44
ABSTRACT	45
INTRODUCTION	46
MATERIALS AND METHODS	48
Chemicals	48
Cell cultures.....	48
High-content imaging	48
Benchmark concentration analyses	49
Administered equivalent dose analyses.....	50
ToxPi analyses	50
Measurement of basal and stimulated production of cortisol and aldosterone.....	51
Quantitative real-time PCR (qRT-PCR)	52
Statistical analyses.....	53
RESULTS	53
Cytotoxicity of OPEs.....	53
Effect of OPEs on the phenotypic characteristics of H295R cells	54
Reactive oxygen species	54
Mitochondria.....	54
Lysosomes.....	55
Lipid droplets.....	55
Potency ranking of OPEs.....	56
ToxPi analyses	57
Administered equivalent dose analyses.....	57
Effect of OPEs on the steroidogenic function of H295R cells	57
Effects of OPEs on the expression of key transcripts involved in steroidogenesis	58
DISCUSSION.....	60
REFERENCES	65
FIGURES	74
SUPPLEMENTAL MATERIALS.....	84
CONNECTING TEXT.....	93
CHAPTER 3.....	94
ABSTRACT	95
INTRODUCTION	96
MATERIALS AND METHODS	97
Organophosphate Ester House Dust Mixture	98
Cell Cultures	98
High-Content Imaging.....	98
Lipid Droplet Isolation	99
Lipidomic Profiling	100

Measurements of Basal and Stimulated Production of Steroid Hormones	101
Quantitative real-time PCR (qRT-PCR)	102
Statistical Analyses	103
RESULTS	104
Effects of the OPE Mixture on the Phenotypic Characteristics of H295R Cells	104
Effects of the OPE Mixture on H295R Cell Lipid Droplets.....	104
Effects of the OPE Mixture on H295R Cell Steroidogenesis.....	107
Effects of the OPE mixture on the expression of transcripts involved in cholesterol and steroid biosynthesis.....	108
DISCUSSION.....	109
REFERENCES	115
FIGURES	126
SUPPLEMENTAL MATERIALS.....	134
CONNECTING TEXT.....	149
CHAPTER 4.....	150
ABSTRACT	151
INTRODUCTION	152
MATERIALS AND METHODS	154
Organophosphate Ester House Dust Mixture	154
Animal Treatments	155
Tissue Collection	156
Histology	157
Serum Biochemistry	157
Hormone Measurements.....	158
RNA-seq and pathway analysis.....	158
Statistical Analyses	159
RESULTS	159
Effects of the OPE mixture on animal and adrenal weights.....	160
Serum biomarkers are affected by the OPE mixture	160
Effects of the OPE mixture on serum hormone levels	161
Effects of the OPE mixture on signaling pathways in the adrenal gland	161
DISCUSSION.....	164
REFERENCES	171
FIGURES	187
SUPPLEMENTAL MATERIALS.....	196
CHAPTER 5.....	220
5.1 Summary of findings	221
5.2 Common and cell specific effects of OPEs	222
5.3 Individual chemical vs mixture effects	225
5.3.1 Effects of the mixture across different cell lines	226
5.4 Composition of lipids altered by the OPE mixture	226
5.5 Complementary roles of in vitro and in vivo studies.....	229
5.6 Potential mechanisms of action of OPEs	230
5.7 In vitro prediction of toxicity: Are we there yet?.....	232

5.8 Future directions	233
5.9 Final conclusions.....	237
LIST OF ORIGINAL CONTRIBUTIONS	239
REFERENCE.....	241
COPYRIGHT INFORMATION AND LICENSING.....	286

LIST OF TABLES AND FIGURES

CHAPTER 1

Figure 1-1. The adrenal glands.

Figure 1-2. H&E staining showing the morphology of adrenal gland cells.

Figure 1-3. Sources of cholesterol used by the adrenal cells in the production of adrenal steroid.

Figure 1-4. The cholesterol biosynthesis pathway.

Figure 1-5. Adrenocortical steroidogenesis.

Figure 1-6. Simplified diagram of the sympathetic adrenal medullary axis and the hypothalamus-pituitary-adrenal (HPA) axis.

Figure 1-7. The renin-angiotensin-aldosterone system and the downstream targets.

Figure 1-8. Steroidogenic pathway in H295R cells.

Figure 1-9. General structure of PBDEs.

Figure 1-10. General structure of OPE.

Table 1-1. Summary of information on rodent adrenal cell lines.

CHAPTER 2

Figure 2-1. List of Chemicals Tested.

Figure 2-2. Effects of BDE-47 and OPEs on cell viability.

Figure 2-3. Effects of BDE-47 and OPEs on the phenotypic characteristics of H295R cells.

Figure 2-4. Benchmark concentration values of the test chemicals for all phenotypic endpoints.

Figure 2-5. Toxicological Prioritization Index analyses for chemical ranking.

Figure 2-6. Administered equivalent dose values of the test chemical for all phenotypic endpoints.

Figure 2-7. Effects of IPPP, TMPP, and TPHP on the steroid-producing functions of H295R cells.

Figure 2-8. Effects of IPPP, TMPP, and TPHP on the mRNA expression levels of the rate-limiting enzymes in cholesterol biosynthesis.

Figure 2-9. Effects of IPPP, TMPP, and TPHP on the mRNA expression of key steroidogenic enzymes.

Figure 2-10. Summary of the phenotypic and functional effects of OPEs on H295R human adrenal cells.

Table 2-S1. Cell-permeable fluorescent dyes and combinations used in high-content screening.

Table 2-S2. The steady-state concentration (C_{ss}) values for each chemical and the parameters used in high-throughput toxicokinetic analysis.

Figure 2-S1. Cytotoxicity of BDE-47 and OPEs in H295R cells.

Figure 2-S2. Effects of BDE-47 and OPEs on the phenotypic characteristics of H295R cells.

CHAPTER 3

Figure 3-1. Composition of the Canadian household dust based OPE mixture.

Figure 3-2. Effects of the OPE mixture on cell viability and total area of lipid droplets.

Figure 3-3. Multivariate analysis showing the degree of separation in lipid profiles between control, 1/300K, 1/100K, and 1/60K dilutions of the OPE mixture.

Figure 3-4. Significantly affected lipids for each mixture dilution.

Figure 3-5. Heatmap of the top 50 affected lipids.

Figure 3-6. Relative distribution of significantly altered lipids in each category and subclass.

Figure 3-7. Proposed lipid pathways disrupted by OPE mixture exposures.

Figure 3-8. Effects of the OPE mixture on the steroid-producing function of H295R cells.

Figure 3-9. Effects of the OPE mixture on the mRNA expression of key transcripts involved in cholesterol and steroid biosynthesis.

Table 3-S1. Relative concentrations of the individual OPEs in the OPE mixture at all dilutions tested.

Table 3-S2. Cell-permeable fluorescent dyes and combinations used in high-content screening.

Table 3-S3. Parameters used in lipidomic statistical analysis.

Table 3-S4. List of commonly affected lipids across the 3 OPE treatment groups.

Table 3-S5. Lipids displaying extra oxygen atom(s)

Table 3-S6. List of uniquely affected lipids across the 3 OPE treatment groups.

Figure 3-S1. Effects of the OPE mixture on the phenotypic characteristics of H295R cells.

Figure 3-S2. Venn diagram of statistically significant lipids from each exposure comparison and their overlap.

CHAPTER 4

Figure 4-1. Composition of the Canadian household dust based OPE mixture.

Figure 4-2. Effects of the OPE mixture on the weight of male and female adrenal glands.

Figure 4-3. Effects of the OPE mixture on the serum levels of glucose, triglycerides, total cholesterol, LDL cholesterol, and HDL cholesterol.

Figure 4-4. Effects of the OPE mixture on serum hormone levels.

Figure 4-5. Principal component analysis and heatmap of the overall expression profile of the adrenal gland exposed to the OPE mixture.

Figure 4-6. Differentially expressed genes in male treatment groups.

Figure 4-7. Top 10 canonical pathways in low, middle, and high OPE group identified by the Ingenuity Pathway Analyses in males.

Figure 4-8. Differentially expressed genes in female treatment groups.

Figure 4-9. Top 10 canonical pathways in low, middle, and high OPE group identified by the Ingenuity Pathway Analyses in females.

Table 4-S1. Scoring criteria for histology examination

Table 4-S2. Top 10 significantly upregulated or downregulated transcripts in male treatment groups.

Table 4-S3. Top 10 significantly upregulated or downregulated transcripts in female treatment groups.

Table 4-S4. Transcripts commonly affected across male treatment groups.

Table 4-S5. Transcripts commonly affected across female treatment groups.

Table 4-S6. Transcripts that are in the top 10 commonly affected pathways.

Figure 4-S1. Male and female percentage change in body weight following OPE exposure.

Figure 4-S2. Effects of the OPE mixture on adrenal gland morphology.

Figure 4-S3. Effect of OPE mixture exposure on the width of the zone in male and female adrenal glands.

Figure 4-S4. Serum biochemistry for male rats.

Figure 4-S5. Serum biochemistry for female rats.

Figure 4-S6. Top 5 uniquely affected pathways in each of the male treatment group identified by Ingenuity Pathway Analysis (IPA).

Figure 4-S7. Top 5 uniquely affected pathways in each of the female treatment group identified by Ingenuity Pathway Analysis (IPA).

LIST OF ABBREVIATIONS

ABC	ATP-binding cassette
ABCA1	ATP binding cassette subfamily A member 1
ABCG1	ATP binding cassette subfamily G member 1
ACTH	Adrenocorticotrophic hormone
AED	Administered equivalent doses
AGP	Adrenocortical primordium
AIC	Akaike information criterion
ANG II	Angiotensin II
AT1	Angiotensin II receptor type 1
AT2	Angiotensin II receptor type 2
ATCC	American Type Culture Collection
ATSDR	Agency for Toxic Substances and Disease Registry
BBOEP	Bis(2-butoxyethyl) phosphate
BCIPHIP	1-hydroxy-2-propyl bis(1-chloro-2-propyl) phosphate
BCIPP	Bis(1-chloro-2 propyl) phosphate
BDCIPP	Bis(1,3-dichloro-2-propyl) phosphate
BDE-47	2,2',4,4'-tetrabromodiphenyl ether
BEH-TEBP	Bis(2-ethylhexyl) 2,3,4,5-tetrabromophthalate
BFR	Brominated flame retardant
BMC	Benchmark concentration
BMCL	BMC lower bound
BMCU	BMC upper bound
BPA	Bisphenol A
BPF	Bisphenol F
cAMP	Cyclic adenosine monophosphate
CCPSA	Canada Consumer Product Safety Act
CE	Cholesterol ester
CEPA	Canadian Environmental Protection Act
CRH	Corticotropin-releasing hormone
CYP11A1	Cholesterol side-chain cleavage enzyme
CYP11B1	Steroid 11 β -hydroxylase
CYP11B2	Aldosterone synthase
CYP17,	Steroid 17-alpha-hydroxylase
CYP21	21-Hydroxylase
DBUP	Dibutyl phosphate
DEG	Differentially expressed genes
DG	Diglycerides
DHEA	Dehydroepiandrosterone
DHEAS	Dehydroepiandrosterone sulfate

DOC	Deoxycorticosterone
DPHP	Diphenyl phosphate
E2	17 β -estradiol
EDC	Endocrine-disrupting chemicals
EDSP	Endocrine Disruptor Screening Program
EDSTAC	Endocrine Disruptor Screening and Testing Advisory Committee
EHDPP	Ethylhexyl diphenyl phosphate
ELISA	Enzyme-linked immunosorbent assay
EPA	Environmental Protection Agency
FA	Fatty acids
GABA	Gamma-aminobutyric acid
GATA4	GATA-binding protein 4
GPCR	G-protein-coupled receptors
HDL	High-density lipoprotein
HMGCR	HMG-CoA reductase
HPA	Hypothalamus–pituitary–adrenal
HTTK	High-throughput toxicokinetics
INSIG	Insulin-induced gene
IPA	Ingenuity Pathway Analyses
IPPP	Isopropylated triphenyl phosphate
IVF	In vitro fertilization
IVIVE	In vitro to in vivo extrapolation
LDL	Low-density lipoprotein
LDLR	Low-density lipoprotein receptor
LXR	Liver X receptor
MOE	Margin of exposure
nCEH	Neutral cholesterol ester hydrolase
NOAEL	No observed adverse effect levels
NOEC	No observed effect concentrations
NR5A1	Steroidogenic factor 1
OECD	Organization for Economic Co-operation and Development
OPE	Organophosphate ester
P4	Progesterone
PBDE	Polybrominated diphenyl ethers
PCA	Principal component analysis
PCB	Polychlorinated biphenyls
PFAS	Perfluoroalkyl substances
PMOC	Persistent mobile organic compounds
PNMT	Phenylethanolamine-N-methyltransferase
POD	Points of departure

POP	Persistent organic pollutants
PPAR	Peroxisome proliferator activated receptor
SCAP	SREBP-cleavage activating protein
SF1,	Steroidogenic factor-1
SQLE	Squalene monooxygenase
SR-B1	Scavenger receptor B1
SREBP	Sterol regulatory element binding protein
SREBP2	Sterol regulatory element-binding protein 2
STAR	Steroidogenic acute regulatory
TBOEP	Tris(2-butoxyethyl) phosphate
TBP	Tributyl phosphate
TCEP	Tris(2-chloroethyl) phosphate
TCIPP	Tris(1-chloro-2-propyl) phosphate
TDCIPP	Tris(1,3-dichloro-2-propyl) phosphate
TDCIPPP	Tris(1,3-dichloro-2-propyl) phosphate
TEHP	Tris(ethylhexyl) phosphate
TG	Triglycerides
TMPP	Tris(methylphenyl) phosphate
TNBP	Tri-n-butyl phosphate
ToxCast	U.S.EPA Toxicity Forecaster
ToxPi	Toxicological Prioritization Index
TPHP	Triphenyl phosphate
TSPO	Translocator protein
UNEP	United Nations Environmental Programme
VMAT1	Vesicular monoamine transporter 1
WBC	White blood cell
WT1	Wilms tumor suppressor-1
3β-HSD	3 β -hydroxysteroid dehydrogenase

ACKNOWLEDGEMENTS

It is finally time to write the acknowledgements section. As I sat staring at the computer screen, trying to summarize my thoughts, I realized that no words could ever fully express how grateful I am to have had Dr. Barbara F. Hales as my supervisor. Every attempt seemed inadequate, and each word faded as I typed it. So, what I can say is simply: thank you. Your guidance throughout the years has been invaluable, and I could never have accomplished this without your support. I would also like to express my deepest gratitude to Dr. Bernard Robaire for taking me under his wing. You have been an integral part of this project, and your role has become essential. I am constantly amazed by how you have an answer to every question I ask. Learning from you has truly been an honor.

I am sincerely grateful to the members of my thesis advisory committee, Dr. Jason Tanny, Dr. Koren Mann, and Dr. Dusica Maysinger, for their insightful advice and suggestions during my studies. Thank you for encouraging me to explore the project from different perspectives and for helping to expand its scope.

A heartfelt thank you to every member of the Robaire and Hales labs, both past and present, for creating such a friendly and supportive environment. Special thanks to Elise Boivin-Ford, not only for being the reliable administrator of the lab, but also for being the "adult" we turn to when important decisions need to be made. I am also deeply grateful to Trang, who graciously let me tag along as I was learning cell culture and showed me all the helpful tricks. There is a cartoon I used to watch as a child, where one of the characters has magical powers and can pull whatever is needed out of his pocket. Whenever I needed something in the lab, I knew I could ask Trang, and she would somehow find it, as if the lab were her "magical pocket".

I would also like to take this opportunity to thank all of my friends, both from the lab and outside of it. Your support means the world to me. Knowing that I have people I can count on is

truly priceless, and I am so grateful to have you by my side. There are so many good memories I have shared with you guys, and I am excited for all the ones we will continue to make. A special thank you for all the cat photos you have sent, you always know how to brighten my day.

Lastly, I would like to express my deepest gratitude to my parents, Xiaomei Lang and Junfeng Li. Whenever I am with you, I know I can be a carefree child. You are the people who know me best in this world, and you have always made sure I know that I am loved. You have supported every decision I have made along the way, and your unwavering support has shaped me into the person I am today. To the feline members of the family, Maomao and Sesame, thank you for being just the right amount of mischievous to bring laughter to our home. I look forward to witnessing your roof-climbing adventures in person soon!

FORMAT OF THE THESIS

This thesis is manuscript based; it conforms to the guidelines for thesis preparation, as outlined by Graduate and Postdoctoral Studies at McGill University. The manuscripts are presented in the order in which they were published or submitted for publication. We retain the right to the manuscripts in this thesis according to the copyright agreements of the respective publishers, provided that this thesis is not published commercially or used for commercial purposes.

Chapter 1 begins with an introduction of the structure and the functional importance of the adrenal gland. This is followed by an overview of adrenal cell lines and a comparison between *in vivo* and *in vitro* models for studying the adrenals. The effects of endocrine disrupting chemicals on the adrenal gland are reviewed, with emphasis on two families of chemicals, polybrominated diphenol ethers and organophosphate esters. Finally, the importance of assessing environmentally relevant mixtures is discussed. The chapter ends with the rationale and objectives for the studies in this thesis. Chapter 2 is a published manuscript that incorporates high content screening and potency ranking approaches to identify responsible replacement chemicals and priorities chemicals for toxicological assessment. Chapter 3 is a published manuscript that describes the effects of environmentally relevant mixture of OPEs on the phenotype, function, and lipidome of the adrenal cells. Chapter 4 is a recently accepted manuscript that aims to assess the *in vivo* effect of the OPE mixture on the adrenal glands of Sprague Dawley rats. Chapter 5 is a general discussion of the findings in this thesis. References for the introduction and discussion are provided at the end of the thesis, while the references for Chapter 2 to 5 are included in their respective chapters. Bridging texts are included to connect the manuscripts in a logical progression.

CONTRIBUTION OF AUTHORS

CHAPTER 2

The Organophosphate Esters Used as Flame Retardants and Plasticizers affect H295R Adrenal Cell Phenotypes and Functions

Zixuan Li, Bernard Robaire, Barbara F Hales

The doctoral candidate was responsible for experimental design, data acquisition, data interpretation, and manuscript preparation for all experiments presented in this chapter. Marc A. Beal did high-throughput toxicokinetics modelling to calculate steady-state concentrations (C_{ss} values) of the test chemicals, which is used in the manuscript to calculate the administered equivalent doses. Bernard Robaire and Barbara F. Hales provided guidance in experimental design, data interpretation, and manuscript preparation.

CHAPTER 3

Impact of Exposure to a Mixture of Organophosphate Esters on Adrenal Cell Phenotype, Lipidome, and Function

Zixuan Li, Barbara F Hales, Bernard Robaire

The doctoral candidate was responsible for experimental design, data acquisition, data interpretation, and manuscript preparation for all experiments presented in this chapter. With exception of lipid profiling and quantification, which was done by The Metabolomics Innovation Centre (TMIC) equipment and services. Michael G. Wade formulated and prepared the mixture of organophosphate esters. Bernard Robaire and Barbara F. Hales provided guidance in experimental design, data interpretation, and manuscript preparation.

CHAPTER 4

Impact of Exposure to a Mixture of Organophosphate Esters on the Adrenal Glands of Sprague Dawley Rats

Zixuan Li, Barbara F Hales, Bernard Robaire

The doctoral candidate, Aimee Lee Katen, Abishankari Rajkumar, Trang Luu, Xiaotong Wang, and Dongwei Yu contributed towards animal monitoring, animal handling, and tissue collection.

The doctoral candidate contributed to the experimental design and was responsible for data acquisition, data interpretation, and manuscript preparation for all experiments presented in this chapter. Comprehensive cardiovascular panel analysis was provided by the pathology core at the Centre for Phenogenomics at the University of Toronto. The standard biochemistry panel was conducted at the Diagnostic and Research Support Service (DRSS) Laboratory of the Comparative Medicine Animal Research Centre at McGill University. RNA-Sequencing analyses and initial bioinformatics analyses were done by Novogene Corporation. Michael G. Wade formulated and prepared the mixture of organophosphate esters. Bernard Robaire and Barbara F. Hales provided guidance in experimental design, data interpretation, and manuscript preparation.

SOURCES OF FUNDING

These studies were funded by a Canadian Institutes of Health Research (CIHR) Institute for Population and Public Health team Grant (FRN IP3-150711), a Canadian Institutes of Health Research (CIHR) Project Grant FRN 156239, and McGill University. Z. L. is the recipient of training awards from McGill University and the Centre for Research in Reproduction and Development (CRRD). B.F.H. and B.R. are James McGill Professors.

CHAPTER 1 INTRODUCTION

1.1 The adrenal glands

The adrenal glands are small, triangular-shaped endocrine organs located at the top of each kidney. They play crucial roles in regulating various physiological processes through the secretion of hormones. The adrenal glands consist of two structurally and functionally distinct parts: the outer adrenal cortex and the inner adrenal medulla, which are encompassed within a common capsule (**Figure 1-1**). The cortex is responsible for the synthesis of glucocorticoid, mineralocorticoids, and androgens, which are essential in managing metabolism, blood pressure, and stress response. The adrenal medulla, on the other hand, produces catecholamines that help the body respond to stress, including the regulation of the fight-or-flight response. Dysfunctions of the adrenal glands can lead to various conditions, including Addison's disease, Cushing's syndrome, and hyperaldosteronism (Megha et al., 2022). These disorders underscore the critical role of the adrenal glands in the overall health and well-being of individuals, thereby emphasizing the need for further research and understanding of these vital organs.

1.1.1 Origin and development of the adrenal gland

Embryonic development and early postnatal growth provide a foundational context for understanding the mechanisms that govern adrenocortical zonation and homeostasis. Despite their structural and functional differences, the adrenal cortex, and non-germ cell components of the ovary and testis share a common origin known as the adrenocortical primordium (AGP) (reviewed in Pihlajoki et al., 2015). This structure is composed of coelomic epithelium-derived cells that co-express the transcription factor wilms tumor suppressor-1 (WT1), GATA-binding

protein 4 (GATA4), and steroidogenic factor-1 (SF1). As development proceeds, progenitors of the adrenal cortex and the gonad separate and activate different transcriptional programs. Adrenal progenitor cells migrate into the mesenchyme region, upregulating the expression of SF1 while downregulating the expression of WT1 and GATA4. In contrast, gonadal progenitor cells in the AGP maintain the expression of SF1, WT1, and GATA4 (Nicolaidis et al., 2023).

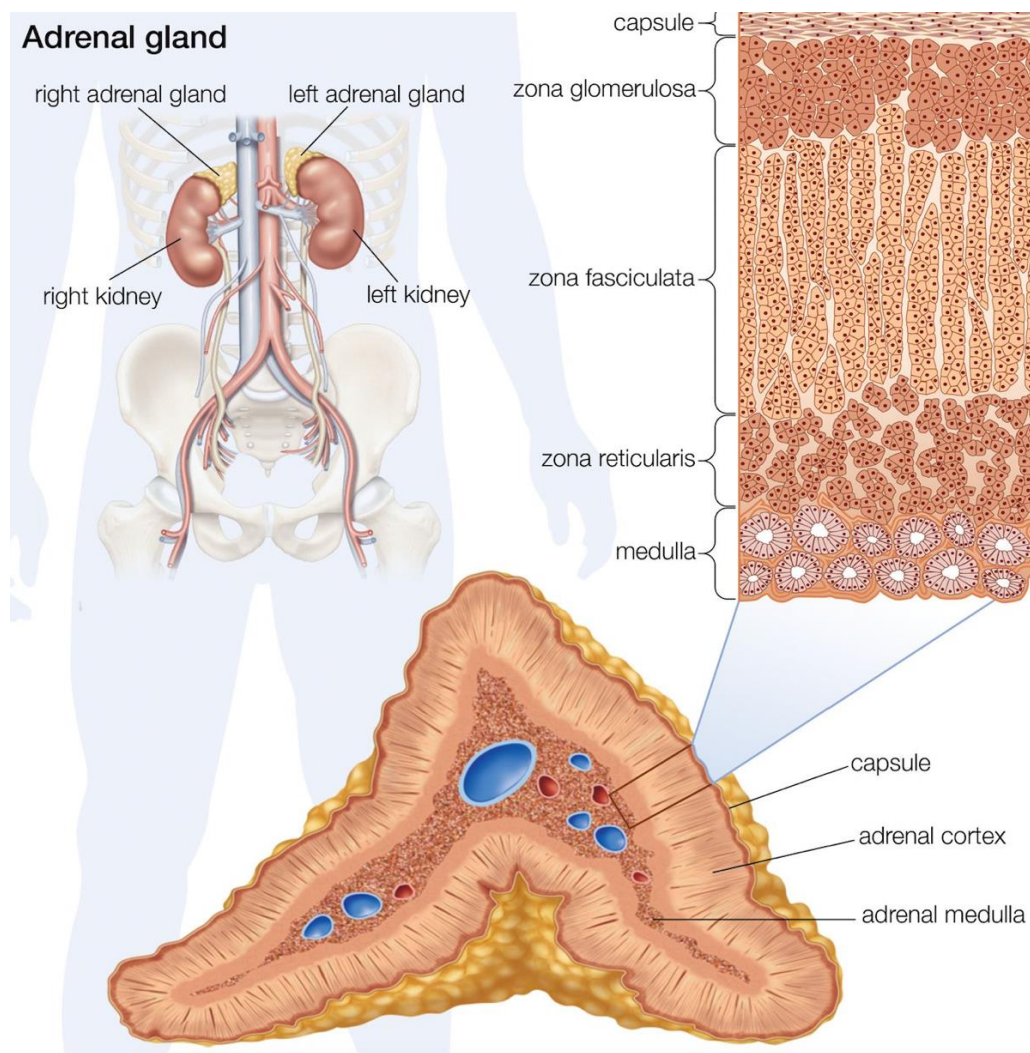


Figure 1-1. The adrenal glands. The relative location of the adrenal glands in the body is illustrated in the upper left panel. Below, a cross-sectional diagram of the adrenal gland and upper rights show an enlarged view of the cellular layers. Figure from Utiger, 2010.

The adrenal cortex and medulla have different developmental origins. The cortex is derived from AGP that originated from mesodermal tissue, whereas the medulla is ectodermal in origin and derived from neural crest. In evolutionary higher animals up to mammals, a closer relationship of the two parts is observed, in which the cortex encapsulates the medulla (reviewed in Xing et al., 2015). In rats, by embryonic day 13-14, distinct layers begin to emerge; the outer layer ultimately becomes the zona glomerulosa, followed by the zona fasciculata, while the inner layer differentiates into zona reticularis. By E14 to E16, the mesenchymal cells expressing the *Nr2f2* gene (encoding COUP transcription factor 2) aggregate around the developing adrenal gland to form the adrenal capsule. By E15, the adrenal medulla starts to develop as neural crest cells from the ectodermal tissue migrate to the developing adrenal gland and differentiate into chromaffin cells (Yamamoto and Arishima, 2004; Pankratz, 1931).

The adrenal cortex undergoes renewal throughout life thanks to the presence of progenitor cells (reviewed in Lyraki and Schedl., 2021). The impressive regenerative ability of the adrenal glands is demonstrated by experiments involving adrenal enucleation in rats. In these procedures, the gland is cut and compressed to expel the cortex. Remarkably, a new adrenal cortex forms from the residual capsule and nearby subcapsular cells within a few weeks (Greep and Deane, 1949). Renewal rates are sexually dimorphic in mice, with females displaying a threefold higher turnover rate than males (Grabek et al., 2019). This ongoing cellular turnover facilitates rapid remodeling of the adrenal cortex, allowing its different zones to temporarily expand, contract, or alter their biochemical properties in response to physiological demands or experimental interventions.

1.1.2 The morphology of the adrenal gland

The adult rat adrenal glands comprise two primary regions: the cortex and the medulla. Within the adrenal cortex, three concentrically arranged layers can be identified based on cellular arrangement and the configuration of cell cords. The outermost layer, known as the zona glomerulosa, features cells organized into arched loops or spherical structures. The middle layer, termed the zona fasciculata, is the widest and is characterized by large, lipid-rich cells arranged in long, radial cords. The innermost layer, the zona reticularis, is contiguous with the medulla and comprises intricately entwined cell cords. The medulla itself is composed of columnar cells organized into clusters situated centrally within the adrenal gland (**Figure 1-2**).

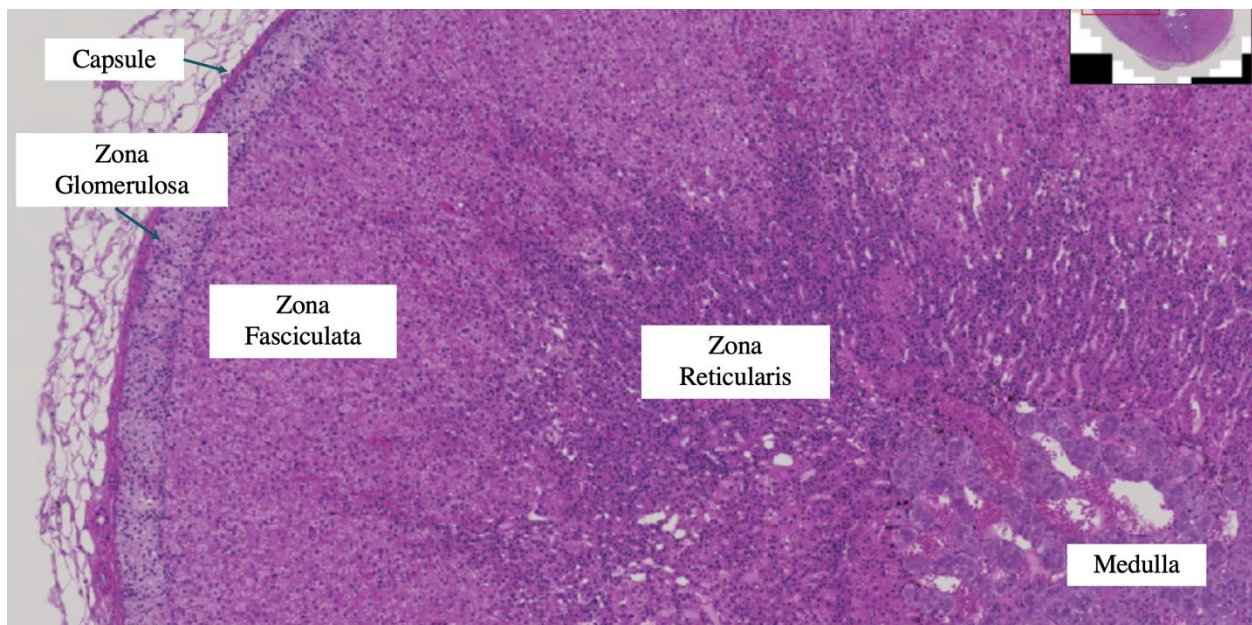


Figure 1-2. Hematoxylin and Eosin (H&E) staining showing the morphology of adrenal gland cells. Cross section of the adrenal gland from adult Sprague Dawley rat. Image captured using QuPath (v0.4.1; Bankhead et al., 2017).

In addition to adrenal cells, macrophages are present throughout the adrenal cortex. Aside from their phagocytic activity, these macrophages produce and secrete various cytokines,

including tumor necrosis factor beta (TNF- β), interleukin-1 (IL-1), and interleukin-6 (IL-6), as well as peptides such as vasoactive intestinal peptide (VIP), which interact with adrenal cells and modulate their functions. Lymphocytes are also distributed within the adrenal cortex and have been shown to produce substances resembling adrenocorticotrophic hormone (ACTH) (González-Hernández et al, 1994). Furthermore, studies indicate that immuno-endocrine interactions between lymphocytes and zona reticularis cells can stimulate the production of dehydroepiandrosterone (DHEA) (Wolkersdörfer et al., 1999).

The rat adrenal glands are among the most highly vascularized organs, receiving blood from 30 to 50 small arteries that originate from the aorta, renal arteries, and inferior phrenic arteries. Blood is directed into the subcapsular arteriolar plexus, from which it is subsequently distributed to the sinusoids and the capillaries that extend radially throughout the cortex. A direct blood supply to the medulla is maintained via shunt arterioles. Following its passage through the cortex and medulla, blood converges at the cortico-medullary junction and drains into the central adrenal vein, ultimately leading to the renal vein or directly into the inferior vena cava (reviewed in Vinson et al., 1985; Sparrow et al., 1987). This feature is crucial for efficient hormone production and release, as it ensures rapid delivery of precursors for steroid biosynthesis to the adrenal gland and rapid secretion of hormones into the bloodstream.

1.1.3 Adrenal steroidogenesis

The most important function of the adrenal gland is the production of steroid hormones, which occurs in all three layers of the adrenal cortex as well as in the adrenal medulla. This hormonal synthesis is regulated by distinct mechanisms tailored to the specific steroid being produced. Aldosterone, synthesized in the outermost layer of the adrenal, cortex i.e., the zona glomerulosa, is primarily influenced by the renin-angiotensin-aldosterone system and serum

potassium levels. The biosynthesis of corticosteroids in the zona fasciculata is predominantly regulated by ACTH. Adrenal androgens are produced in the zona reticularis, which is also under the regulation of ACTH (reviewed in Payne and Hales., 2004). The adrenal medulla serves as a link between the endocrine and sympathetic nervous systems; chromaffin cells in this region synthesize epinephrine (adrenaline) and, to a lesser extent, norepinephrine (noradrenaline). Norepinephrine acts as the neurotransmitter for the sympathetic division of the autonomic nervous system. Both norepinephrine and epinephrine are released into the circulation, where they exert their effects on distal tissues similar to other hormones (Boron and Boulpaep, 2017).

1.1.3.1 Cholesterol pathway

All steroids produced in the adrenal cortex are synthesized from a common precursor: cholesterol. Depending on the distinct zones of the adrenal gland, a series of enzymatic reactions facilitate the conversion of cholesterol into specific steroid hormones. Additionally, cholesterol is a crucial component of cell membranes, making up to 40% of their structure. It plays a key role in maintaining both their structural integrity and functional versatility (Cooper, 2000).

1.1.3.1.1 Source of cholesterol

Cholesterol can be acquired from multiple sources: extracellularly, intracellularly, or through *de novo* biosynthesis (**Figure 1-3**). The preferred sources of cholesterol vary by tissue type; this discussion focuses on the pathways utilized by the adrenal gland. Extracellular cholesterol can be imported into the cell via two primary pathways: the low-density lipoprotein (LDL) pathway and the scavenger receptor class B type I (SR-BI) pathway. In the adrenal gland, the LDL pathway plays a minor role in supplying cholesterol for steroidogenesis. Lipoproteins containing apolipoprotein B or E are internalized through the low-density lipoprotein receptor

(LDLR), with cholesterol subsequently released following hydrolysis by lysosomal acid lipase. In contrast, the SR-BI pathway serves as the primary source of cholesterol, mediating the uptake of high-density lipoprotein (HDL)-bound lipids. Cholesterol esterified from this source is de-esterified by the action of hormone-sensitive lipase (HSL), which accounts for nearly 90% of the cholesterol hydrolase activity in the adrenal gland. Intracellularly, cholesterol can be stored in esterified form within lipid droplets, with HSL facilitating its conversion to free cholesterol. Additionally, steroidogenic cells may utilize membrane-associated cholesterol as an alternative source (reviewed in Martinez-Arguelles and Papadopoulos, 2015).

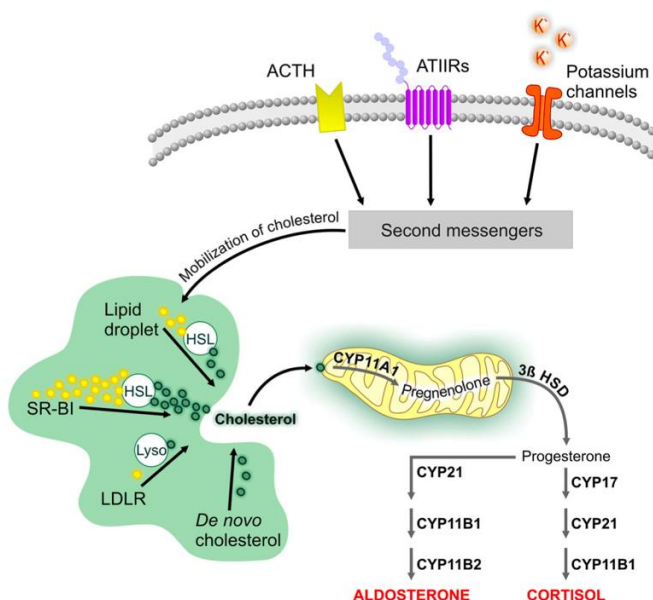


Figure 1-3. Sources of cholesterol used by the adrenal cells in the production of adrenal steroid. Cholesterol can be obtained from LDL and HDL lipid carriers, lipid droplets, or through *de novo* synthesis. Unesterified cholesterol is transported to the mitochondria, where its cleavage by CYP11A1 marks the first step in steroidogenesis. Tissue-specific expression within the various zones of the adrenal cortex facilitates the biosynthesis of aldosterone and cortisol. Figure from Martinez-Arguelles and Papadopoulos, 2015.

The *de novo* biosynthesis of cholesterol starts with the condensation of acetyl-CoA and acetoacetyl-CoA to produce 3-hydroxy-3-methylglutaryl-CoA (HMG-CoA), a reaction catalyzed by HMG-CoA synthase. This is followed by the conversion of HMG-CoA to mevalonate, mediated by HMG-CoA reductase, which represents the rate-limiting step in the pathway. Subsequently, mevalonate undergoes phosphorylation and decarboxylation to yield isoprenoid units, which then condense to form squalene. Once squalene is synthesized, the pathway diverges into two distinct routes: the Bloch pathway and the Kandutsch-Russell pathway. In rodents, the Bloch pathway is utilized exclusively in the testes and adrenal glands, while the skin and brain predominantly employ the modified Kandutsch-Russell pathway (**Figure 1-4**) (Mitsche et al., 2015).

1.1.3.1.2 Regulation of cholesterol homeostasis

Cholesterol homeostasis is tightly regulated through a complex interplay of synthesis, uptake, and efflux mechanisms. A key mediator of cholesterol biosynthesis is sterol regulatory element-binding protein 2 (SREBP2), which is synthesized in the endoplasmic reticulum (ER) and requires transport to the Golgi apparatus for activation. When cholesterol level in the ER is low, SREBP2 interacts with SREBP-cleavage activating protein (SCAP), allowing the SCAP-SREBP complex to exit the ER and anchor to the Golgi. There, SREBP2 is cleaved, resulting in the release of its active N-terminal domain, which then translocates to the nucleus to activate expression of transcripts related to cholesterol biosynthesis and uptake. Conversely, high level of cholesterol leads to the recruitment of insulin-induced gene (INSIG) protein to the SCAP-SREBP2 complex, preventing its transport and promoting the degradation of enzymes involved in cholesterol synthesis (reviewed in Horton et al., 2002).

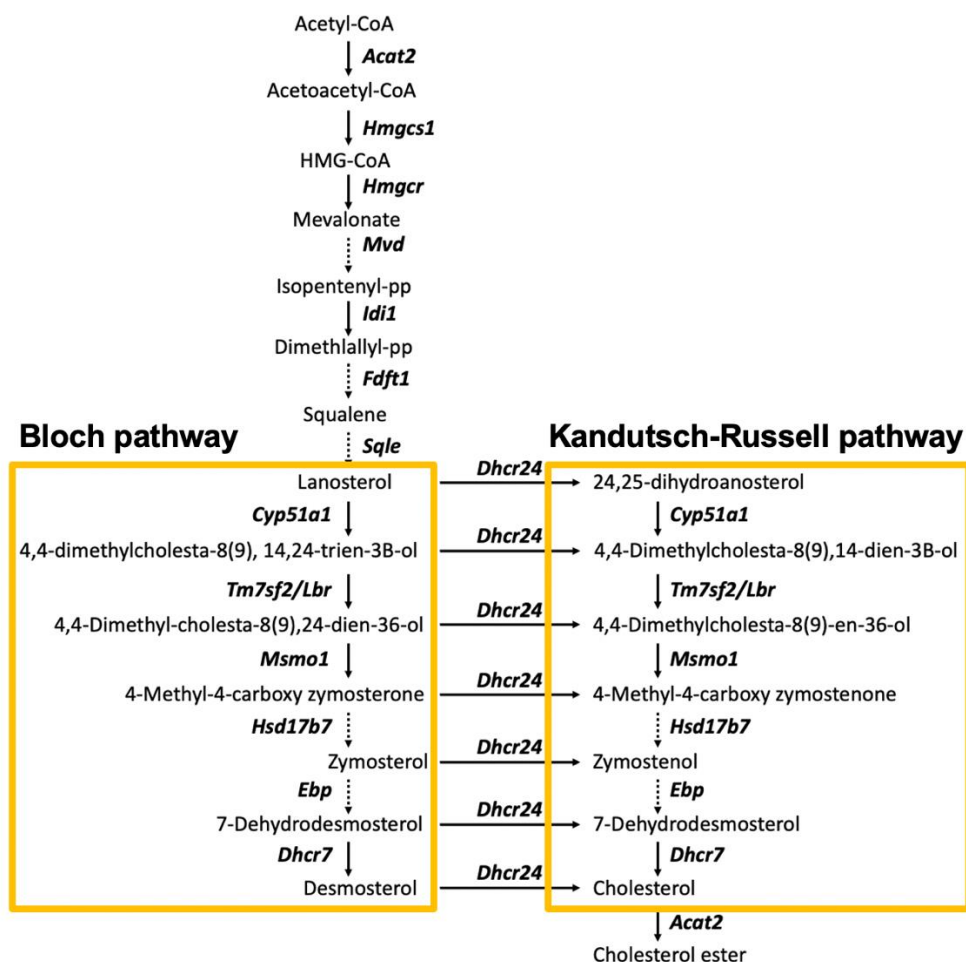


Figure 1-4. The cholesterol biosynthesis pathway. Two pathways that share common initial enzymatic reactions were illustrated, starting with the conversion of acetyl-CoA to HMG-CoA. HMGCR and SQLE are considered two rate-limiting enzymes of cholesterol biosynthesis.

Created with BioRender.

The accumulation of cholesterol also triggers the reverse cholesterol transport (RCT) system, which facilitates the export of cholesterol through various signaling pathways and transcription factors. Elevated cholesterol levels can lead to increased production of oxysterols, which, upon binding to the liver X receptor (LXR), stimulate the transcription of ATP-binding cassette (ABC) transporters, primarily ABCA1 and ABCG1. This promotes the efflux of

cholesterol to apolipoproteins, facilitating the formation of HDL particles (reviewed in Zhang et al., 2021).

1.1.3.2 Adrenal cortex produced hormones

Upon steroidogenic stimulation, cholesterol is first transported from the outer mitochondria membrane to the inner mitochondria membrane by a multimeric protein complex that is composed of steroidogenic acute regulatory (STAR) protein, translocator protein (TSPO), and other cofactors. Within the mitochondria, cholesterol is converted to pregnenolone by the enzyme CYP11A1. Pregnenolone then moves to the cytoplasm and undergo further enzymatic conversions. In zona glomerulosa, it is converted to progesterone by 3β -hydroxysteroid dehydrogenase (3β -HSD). Progesterone is subsequently hydroxylated to form deoxycorticosterone (DOC), which is then converted to corticosterone by CYP11B2. The same enzyme is also responsible for the conversion of corticosterone to aldosterone, which is the last step in the biosynthetic pathway (reviewed in Payne and Hales, 2004).

The production of cortisol in human happens in zona fasciculata, where pregnenolone is first converted to 17α -hydroxypregnenolone in the ER by the enzyme CYP17. In contrast, rodents lack this enzyme and convert pregnenolone to progesterone instead. Both 17α -hydroxypregnenolone and progesterone are subsequently converted to 11-deoxycortisol or 11-deoxycorticosterone in humans and rodents, respectively. The enzyme CYP11B2 catalyzes the final step of the production of cortisol in humans, whereas in rodents, corticosterone is produced. The human zona reticularis is reported to synthesize dehydroepiandrosterone (DHEA) via CYP17, which is then converted to androstenedione, testosterone, estrone, and 17β -estradiol (reviewed in Payne and Hales, 2004). Conversely, the absence of CYP17 in rodents limits their ability to produce androgens, resulting in negligible contributions to plasma levels of DHEA and

The diagram illustrates the biosynthesis of steroid hormones, starting from cholesterol and branching into three main pathways: mineralocorticoid, androgen, and glucocorticoid synthesis.

Mineralocorticoid Pathway (Adrenocortical zona glomerulosa):

- Cholesterol is converted to Pregnenolone by CYP11A.
- Pregnenolone is converted to Progesterone by 3β-HSD.
- Progesterone is converted to 11-Deoxycorticosterone by CYP21.
- 11-Deoxycorticosterone is converted to Corticosterone by CYP11B1.
- Corticosterone is converted to Aldosterone by CYP11B2.

Androgen Pathway:

- Pregnenolone is converted to 17α-Hydroxypregnenolone by CYP17.
- 17α-Hydroxypregnenolone is converted to 17α-Hydroxyprogesterone by 3β-HSD.
- 17α-Hydroxyprogesterone is converted to Androstenedione by CYP17.
- Androstenedione is converted to Testosterone by 17β-HSD.
- Testosterone is converted to Dihydrotestosterone by 5α-reductase.

Glucocorticoid Pathway (Adrenocortical zona fasciculata):

- 17α-Hydroxypregnenolone is converted to 11-Deoxycortisol by CYP21.
- 11-Deoxycortisol is converted to Cortisol by CYP11B1.
- Cortisol is converted to Androstenedione by CYP17.
- Androstenedione is converted to Estrone by CYP19.
- Estrone is converted to Estradiol by 17β-HSD.

(b)

Cholesterol

STAR
CYP11A1

Pregnenolone

HSD3B2

Progesterone

CYP21

Deoxycorticosterone

CYP11B2

Corticosterone

CYP11B2

Aldosterone

20 α HSD

20 α -Dihydroxypregnenolone

20 α -Dihydroxyprogesterone

11 β ,20 α -Dihydroxyprogesterone

CYP11B1

1.1.3.3 Medulla produced hormones

11

dopamine β -hydroxylase catalyzes the conversion of dopamine to norepinephrine, which is further converted to epinephrine by phenylethanolamine-N-methyltransferase (PNMT). Newly synthesized epinephrine is then taken up into the secretory granules, facilitated by VMAT1, with proton gradient maintenance by a vacuolar-type H-ATPase, allowing for the storage of both epinephrine and norepinephrine prior to secretion (Boron and Boulpaep, 2017).

1.1.3.4 Function of adrenal produced hormones

Aldosterone crosses cell membranes to bind to cytoplasmic mineralocorticoid receptors (MR), which then translocate to the nucleus to modulate mRNA transcription and protein synthesis. The affinity of MR for aldosterone can vary depending on its phosphorylation state; when phosphorylated, MR exhibits a lower affinity for aldosterone, thereby inhibiting its functional activity (Jiménez-Canino et al., 2016). The primary function of aldosterone is to act on the late distal tubule and collecting duct of nephrons in the kidney. In these regions, MR predominately remains in a non-phosphorylated state, allowing aldosterone to enhance the expression of sodium channels and sodium-potassium ATPase in the cell membrane. Sodium channels on the luminal side facilitate passive sodium influx due to a transepithelial potential difference of -50 mV, while the sodium-potassium ATPase actively transports sodium into the bloodstream and potassium into the cell. Additionally, potassium channels enable passive diffusion of potassium into the lumen when sodium enters the cell. This mechanism results in increased sodium absorption, which, in the presence of antidiuretic hormone (ADH), promotes water absorption and consequently raises blood osmolality, facilitating water flow down its concentration gradient. Thus, aldosterone affects blood pressure by regulating the sodium gradient in the nephron to either increase or decrease the water reabsorbed to contribute to the volume of the extracellular fluid (ECF) (Scott et al., 2023).

Cortisol, or corticosterone in rodents, is released in a diurnal circadian pattern. Cortisol levels are highest in the early morning, around 7–8 AM, and gradually decrease until midnight. Rodents have similar pattern, with peak levels of corticosteroids typically occur around 8 AM, while the lowest levels are observed between midnight and 4 AM. This release rhythm coordinates and optimizes metabolic responses that are predictable in relation to the environmental day, particularly to the sleep-wake cycle (reviewed in Oster et al., 2017). This hormone is essential for normal physiological functions. Additionally, any form of stress, physical or psychological, serves as an acute trigger for cortisol secretion. Cortisol plays a critical role in glucose metabolism, contributing to hyperglycemia; glucose is essential for providing energy to key organs, such as the brain and skeletal muscles during periods of stress, illness, or exercise. It enhances hyperglycemia by upregulating enzymes involved in gluconeogenesis and glycogenolysis while antagonizing the effect of insulin, resulting in decreased glucose uptake in cells. Furthermore, cortisol induces a catabolic state in muscles, leading to muscle breakdown and the mobilization of amino acids for gluconeogenesis. It also activates hormone-sensitive lipase in adipose tissue, increasing the availability of free fatty acids for beta-oxidation. The net effect of these processes includes decreased muscle mass, thinning skin, hyperglycemia, and lipodystrophy, which is characterized by fat redistribution to areas such as the neck and face (Chourpiliadis and Aeddula, 2023). In addition to its roles in metabolism, cortisol also acts on the immune system; it can lead to an overall increase in white blood cell (WBC) count by reducing neutrophil migration to tissues, inhibiting neutrophil apoptosis, and promoting the maturation of WBCs from the bone marrow, while simultaneously inducing apoptosis and sequestration of eosinophils (reviewed in Coutinho and Chapman, 2011).

Adrenal androgens (AAs), primarily secreted by the fetal adrenal zone and the zona reticularis of the adrenal cortex, include hormones such as dehydroepiandrosterone (DHEA),

dehydroepiandrosterone sulfate (DHEAS), androstenedione, androstenediol, and 11 β -hydroxyandrostenedione. DHEA and DHEAS are produced in larger quantities and serve as precursors for the peripheral conversion into more potent androgens, such as testosterone and estrogens. While adrenal androgens exhibit limited androgenic activity and do not significantly influence adults, they assume a more critical role during developmental stages. During puberty, adrenal androgens contribute to the emergence of secondary sexual characteristics in both sexes. In females, these hormones affect hair growth and libido, while in males, they facilitate muscle growth and the development of secondary sexual traits. Thus, the impact of adrenal androgens is particularly pronounced during periods of growth and sexual maturation, underscoring their importance in sexual differentiation and overall endocrine function (Antoniou et al., 2019).

The adrenal medulla synthesizes norepinephrine (noradrenaline) and epinephrine (adrenaline), which play a critical role in the "fight or flight" response. These catecholamines bind to α - and β -adrenergic receptors located in the central and peripheral nervous systems and on the membranes of smooth muscle cells, initiating an intracellular signaling cascade involving cyclic adenosine monophosphate (cAMP). This activation triggers a variety of physiological responses, including contraction of smooth and cardiac muscle, which results in vasoconstriction, increased blood pressure, elevated heart rate, and enhanced cardiac output, as well as increased blood flow to skeletal muscles. Moreover, their release promotes several metabolic processes, including enhanced sodium retention, elevated glucose levels through glycogenolysis, gluconeogenesis, and lipolysis. Additional effects include increased oxygen consumption and thermogenesis, reduced intestinal motility, and cutaneous vasoconstriction. Bronchiolar dilation also occurs to facilitate respiration, while behavioral activation manifests as heightened arousal, improved alertness, enhanced cognitive function, focused attention, and analgesia (reviewed in Paravati et al., 2022).

1.1.4 Regulation of adrenal functions

1.1.4.1 Hypothalamus-pituitary-adrenal (HPA) axis

The slow response to stress is mediated by the activation of the hypothalamic-pituitary-adrenal (HPA) axis, which begins with the release of corticotropin-releasing hormone (CRH) from the paraventricular nucleus of the hypothalamus (**Figure 1-6**). CRH interacts with two distinct receptors: CRH-R1, primarily responsible for stimulating ACTH release from the corticotropes of the anterior pituitary, and CRH-R2, predominantly located in peripheral tissues. Additionally, the CRH-binding protein (CRH-BP) has a higher binding affinity for CRH than the receptors themselves, playing a crucial role in regulating the bioavailability of CRH. CRH-BP binds 40% to 60% of CRH in the brain, and its expression increases in response to stress in a time-dependent manner, serving as a negative feedback mechanism that reduces CRH interaction with CRH-R1 (Behan et al., 1995; Behan et al., 1997).

Subsequent to the release of CRH, ACTH is secreted into the bloodstream, prompting the adrenal cortex to produce glucocorticoids, primarily cortisol in humans and corticosterone in rodents. The HPA axis is further regulated by pituitary adenylate cyclase-activating polypeptide (PACAP), which can enhance CRH production and modulate various levels of the axis while also influencing the autonomic stress response through increased catecholamine secretion (Stroth et al., 2011). In serum, approximately 80% of cortisol is bound to cortisol-binding globulin, with only the unbound fraction exerting biological activity (le Roux et al., 2003). High level of cortisol exerts a negative feedback effect on the HPA axis by inhibiting the release of both CRH and ACTH, thereby downregulating its own production and limiting the overall stress response. This feedback mechanism ensures that cortisol levels do not become excessively elevated, thus maintaining homeostasis within the body (Chourpiliadis and Aeddula, 2023).

1.1.4.2 Renin-angiotensin-aldosterone system

The renin-angiotensin-aldosterone system (RAAS) is activated by physiological stimuli such as low blood pressure or reduced serum sodium levels, leading to the secretion of renin from the juxtaglomerular cells of the kidneys. This initiates the cleavage of angiotensinogen into angiotensin I, which is subsequently converted to angiotensin II by angiotensin-converting enzyme (ACE) in the lungs. Angiotensin II stimulates the production of aldosterone by binding to angiotensin II receptors (AT₁R) located in the adrenal cortex. In turn, aldosterone acts on the aldosterone-sensitive distal nephron, which includes the late distal convoluted tubule, connecting tubule, and collecting duct system. (**Figure 1-7**) (Scott et al., 2023).

Although this nephron segment is responsible for only 6-10% of total sodium reabsorption, aldosterone is instrumental in modulating several critical physiological processes (reviewed in Palmer and Schnermann, 2015). It enhances sodium reabsorption, promotes water retention, facilitates potassium excretion, and regulates the excretion of hydrogen ions (H⁺) and bicarbonate (HCO₃⁻). Additionally, aldosterone promotes chloride reabsorption, adjusting its effects based on specific physiological conditions (reviewed in Wagner, 2014). Through these mechanisms, the RAAS plays a vital role in maintaining fluid and electrolyte balance, as well as regulating blood pressure.

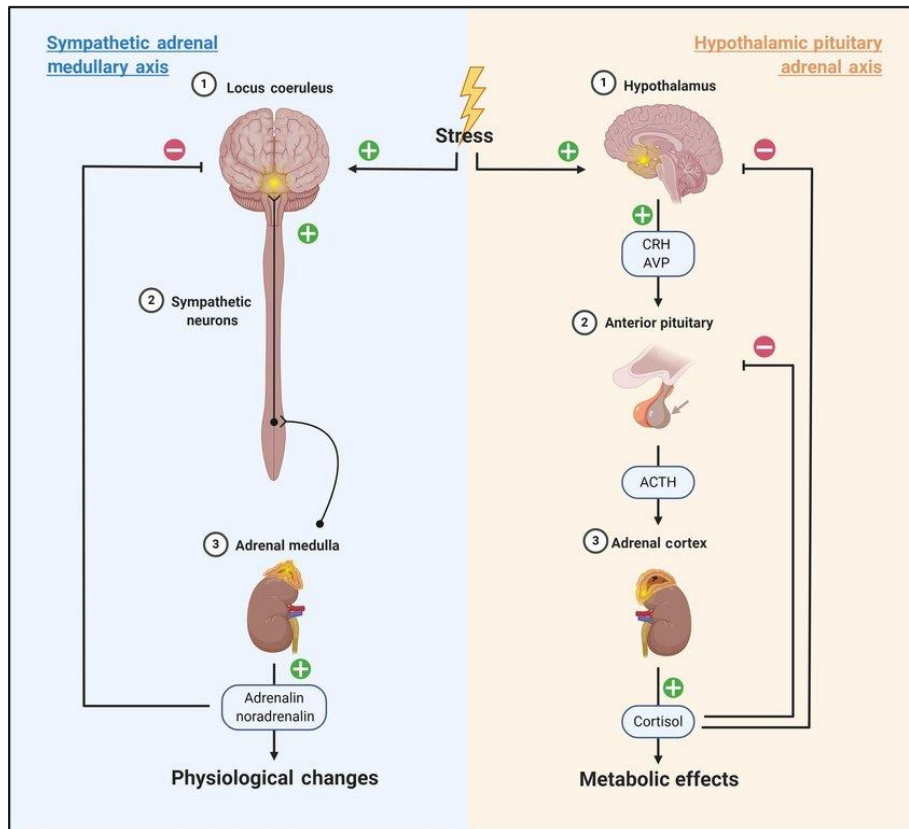


Figure 1-6. Simplified diagram of the sympathetic adrenal medullary axis (left) and the hypothalamus-pituitary-adrenal (HPA) axis (right). The sympathetic adrenal medullary axis represents the “acute” stress response pathway, whereas the HPA axis is activated when the stressor persists over an extended period. Figure from Carlton et al., 2021.

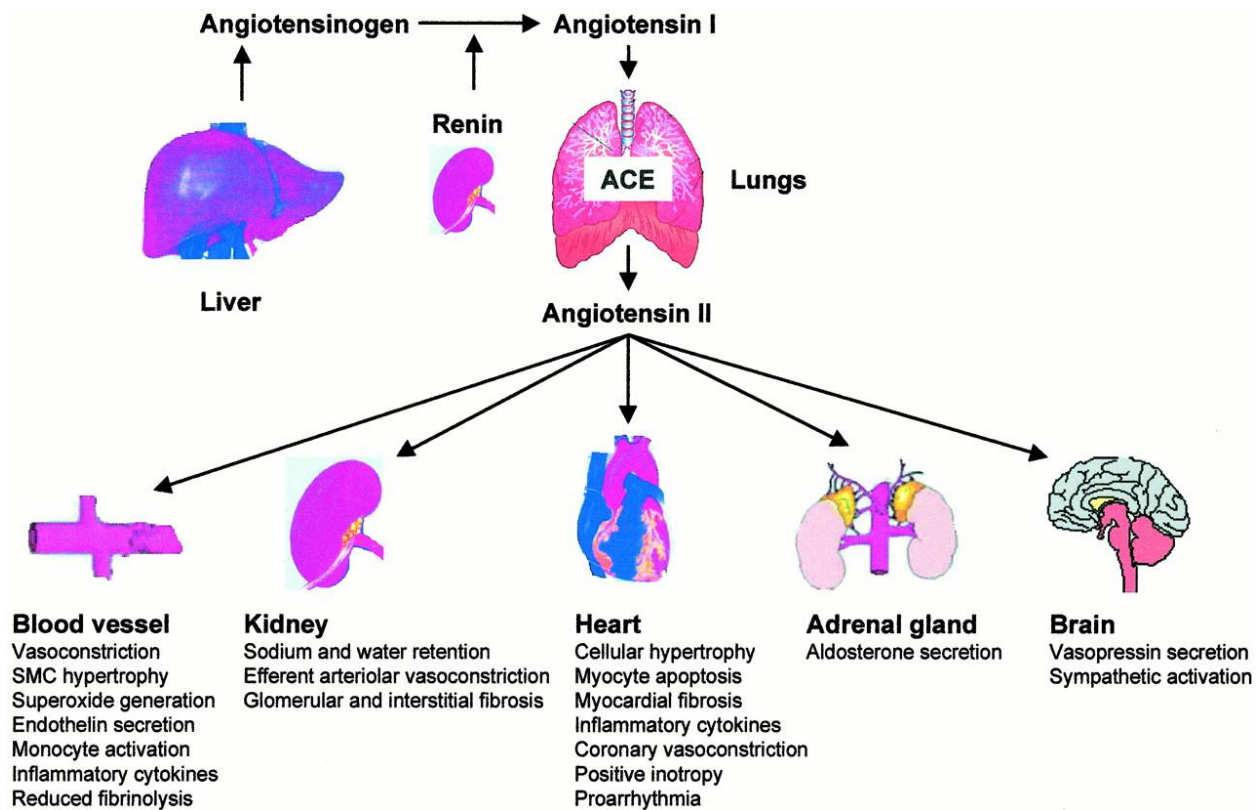


Figure 1-7. The renin-angiotensin-aldosterone system and the downstream targets. When there is a drop in blood pressure or fluid volume, RAAS is activated, leading to a series of coordinated actions that restore blood pressure to normal levels. Figure from Givertz, 2001.

1.1.4.3 Adrenal medulla and the sympathetic system

Immediate stressors or challenging situations trigger acute stress responses, activating the sympathetic division of the autonomic nervous system (**Figure 1-6**). This activation leads to the release of acetylcholine (ACh) from sympathetic splanchnic nerves, which binds to nicotinic receptors on chromaffin cells in the adrenal medulla. The binding of ACh facilitates the exocytosis of catecholamine-filled vesicles into the bloodstream.

Once released into circulation, catecholamines, including epinephrine and norepinephrine, interact with alpha and beta-adrenergic receptors—subtypes of G-protein-

coupled receptors (GPCRs) distinguished by their cellular localization. These adrenergic receptors activate intracellular signaling pathways, specifically cAMP and phosphoinositol second messenger systems. This signaling cascade mediates the sympathetic response by modulating the activity of ion channels and eliciting a range of physiological responses essential for managing acute stress (Paravati et al., 2022).

1.1.5 Sexual dimorphism of the adrenal gland

The adrenal gland in rodents demonstrates significant sexual dimorphism in both size and weight. Castration or androgen treatment can lead to either enlargement or reduction of the organ, respectively. This disparity is primarily attributable to a larger zona fasciculata in females, which is characterized by increased nuclear size, as well as a higher density of mitochondria and endoplasmic reticulum. Consequently, corticosterone production levels are elevated in females (Kitay, 1963). In contrast, the human male adrenal glands are heavier than females (Lam et al., 2001). Moreover, the adrenal cortex undergoes continuous renewal throughout life and has the capacity to regenerate following injury, supported by resident progenitor populations. In contrast, male adrenal glands exhibit a slower turnover rate, influenced by the suppressive effects of testicular androgens (Grabek et al., 2019). Gonadectomy studies further elucidate the transcriptional differences between sexes. Specifically, orchiectomized rats receiving testosterone replacement demonstrate enhanced expression of transcripts associated with lipid and cholesterol metabolism, while ovariectomized rats treated with estradiol show decreased expression of transcripts related to intracellular signaling pathways (Jopek et al., 2017).

1.2 Adrenal cell lines

To investigate the function of the adrenal glands, ongoing efforts are being made to develop *in vitro* cell models. These models include cell suspensions derived from adrenal tissues, primary cultures from normal adrenal glands and adrenal tumors (Gospodarowicz et al., 1977; O'Hare and Neville, 1973), and established cell lines originating from tumors (Rodriguez et al., 1997; Yasumura et al., 1966). The use of adrenal cell lines allows for the propagation of large numbers of functional cells, alleviating ethical concerns associated with animal sacrifice and the need of human tissue. This approach has significantly advanced our understanding of the fundamental mechanisms underlying adrenal function. The present discussion focuses on the widely used adrenal cell culture models, with particular emphasis on the specific cell line used in this study.

1.2.1 Rodent adrenocortical cell lines

1.2.1.1 The Y1 adrenal cell line

The Y1 adrenal cell line was derived from an adrenal tumor developed in mouse (Cohen et al., 1957). Buonassisi and colleagues successfully adapted this transplantable tumor for *in vitro* growth by alternately propagating dispersed tumor cells as monolayer cultures and as tumors in mice (Buonassisi et al., 1962). Among the clones derived from the mixed population of tumor cells, one was designated as Y1, which was subsequently deposited in the American Type Culture Collection (ATCC CCL-79) (Yasumura et al., 1966). In culture, Y1 cells primarily grow as flat, adherent cells characterized by polyhedral shapes. This morphology is maintained by a network of stress fibers and focal adhesions located near the cell surface (Cuprak et al., 1977; Mattson and Kowal, 1978; Voorhees et al., 1984; Yasumura et al., 1966). The stable growth and accessibility of the murine Y1 adrenocortical cell line have led to its widespread use as a model in murine adrenal cell culture studies.

In contrast to the normal rodent adrenal gland, which produces corticosterone as its major steroid product, Y1 cells produce 20-dihydroxyprogesterone and 11,20-dihydroxyprogesterone due to the lack of the CYP21 enzyme (Kowal and Fiedler, 1968; Pierson, 1967); these cells respond to ACTH but not to ANG II (**Table 1-1**) (Tian et al., 1996).

1.2.1.2 Other rodent cell lines

Several researchers have established immortalized adrenal cell lines from adrenal tumors in mice carrying the Simian Virus 40 T-antigen transgene (Compagnone et al., 1997; Mellon et al., 1994; Mukai et al., 2002). Mellon et al. (1994) utilized a human CYP11A promoter to selectively target T-antigen expression to the adrenal cortex, resulting in tumors in female mice that gave rise to cell lines primarily producing progesterone. These cell lines could be stimulated by 8-bromo-cAMP but were unresponsive to ACTH or ANG II. Another set of immortalized cell lines was created using a temperature-sensitive T-antigen transgene (Mukai et al., 2002), which displayed diverse steroidogenic profiles. The most notable advances were made by Ragazzon et al. (2006), who developed ATC1 and ATC7-L cell lines from transgenic mice that retained a complete zona fasciculata phenotype, demonstrating significant ACTH responsiveness and robust steroidogenic capacity. These cell lines are valuable for investigating steroidogenic gene regulation and the physiological mechanisms underlying glucocorticoid synthesis. Detailed characteristics of all cell lines described above can be found in **Table 1-1**.

Cell line	Steroids	Stimulants				Reference
	Produced	ACTH	K ⁺	ANG II	cAMP	
Y1	Progesterone metabolites	✓	×	×	✓	Yasumura et al., 1966

Mouse adrenal cell line: ATC1 and ATC7-L	Glucocorticoids	✓	ND	×	✓	Ragazzon et al., 2006
Immortalized mouse adrenal cell lines: AcA201, AcE60 and AcA101	Progesterone metabolites	×	×	×	✓	Mukai et al., 2002
Immortalized mouse adrenal cell lines: ST2, ST5-R, and ST5-L	Progesterone metabolites	×	ND	ND	✓	Mellon et al., 1994
Immortalized mouse adrenal cell line: ST5Lc	Progesterone metabolites Glucocorticoids	×	ND	ND	✓	Compagnone et al., 1997

Table 1-1. Summary of information on rodent adrenal cell lines. ND, not documented.

1.2.2 Human adrenocortical cell lines

One limitation of rodent adrenal cell lines in the study of adrenal steroidogenesis is their lack of the enzyme CYP17, which results in the exclusive production of corticosterone. To address this issue, several human adrenal cell lines have been developed, each exhibiting distinct characteristics regarding steroid production and responsiveness to steroidogenic stimuli.

1.2.2.1 The NCI-H295 cell line

The NCI-H295 cell line was established from a 48-year-old African American female with adrenocortical carcinoma (Gazdar et al., 1990). Initial attempts to culture NCI-H295 tumor cells in serum-containing medium were unsuccessful due to fibroblast overgrowth. However, the

culture was subsequently adapted to grow without the need for fibroblast growth factor, leading to the development of multiple substrains optimized for cell attachment and shorter cell cycle times. The H295R cell line emerged from this process. In comparison to the parent H295 cell line, H295R cells grow as an adherent monolayer and require only 2 days to double (reviewed in Rainey et al., 2004). The specific characteristics of the H295R cell line will be discussed in the following sections.

1.2.2.2 Male adrenocortical cell lines

There have been attempts to develop male adrenocortical cell lines, such as the ACT-1 cell line, isolated from a 62-year-old male patient initially diagnosed with left adrenocortical carcinoma, and the RL-251 cell line, derived from a 75-year-old male who presented with hypertension and fever. However, these cell lines exhibit limited adrenocortical functions, making them unsuitable for studying steroidogenesis (Ueno et al., 2001; Schteingart et al., 1993). Recently, a male adrenocortical cell line termed TVBF-7 was derived from a patient with adrenocortical carcinoma in progression following EDP-M (etoposide, doxorubicin, cisplatin, and mitotane) treatment. Compared to H295R cells, TVBF-7 cells demonstrate high levels of cortisol at baseline; however, they are unresponsive to stimulation by ACTH or forskolin, indicating autonomous cortisol secretion (Sigala et al., 2022). The development of human adrenocortical cell lines of male origin may facilitate the investigation of sex-specific effects of compounds on the adrenal gland in the future.

1.2.2.3 H295R cell

As one of the most widely used adrenal cell models, the H295R cell line represents a unique system for studying the phenotypic and functional characteristics of the adrenal glands.

H295R cells exhibit physiological characteristics similar to those of zonally undifferentiated human fetal adrenal cells and express genes encoding all key enzymes involved in the steroidogenic pathway (**Figure 1-8**) (Gazdar et al., 1990). The *in vivo* expression of these genes is tissue- and developmental stage-specific, with no single tissue or developmental stage typically expressing all genes associated with steroidogenesis (Hecker et al., 2006). Consequently, H295R cells possess the capacity to produce all steroid hormones found in the adult adrenal cortex and gonads, enabling assessments of the effects on corticosteroid, mineralocorticoid, and sex hormone synthesis.

1.2.2.3.1 Receptors and responsiveness to stimulators

Studies assessing the binding of radiolabeled ANG II to H295R cells, in the presence of antagonists for both AT1 and AT2 receptors, have demonstrated that H295R cells predominantly express AT1 receptors (Bird et al., 1993; Bird et al., 1994). Stimulation with ANG II through the AT1 receptor results in an increased production of aldosterone in H295R cells (Wu et al., 2001). Additionally, extracellular potassium (K^+) serves as a crucial physiological regulator of adrenal aldosterone production, elevating intracellular calcium levels in H295R cells and thereby activating aldosterone biosynthesis. Research has also indicated that K^+ stimulation promotes the production of both ANG I and ANG II, suggesting that these cells may serve as a valuable model for studying the renin-angiotensin system (Hilbers et al., 1999).

ACTH is the primary hormonal regulator of adrenal cortisol production; however, the H295R cell line exhibits only a mild response to ACTH. While ACTH treatment induces an acute increase in aldosterone synthesis, this effect cannot be sustained with long-term stimulation (Hanley et al., 1993). The limited response to ACTH may be attributed to the low expression levels of ACTH receptors in H295R cells (Mountjoy et al., 1994). Consequently, most

The diagram illustrates the biosynthesis of steroid hormones, starting from Cholesterol and branching into two main pathways: the mineralocorticoid pathway (left) and the androgen/estrogen pathway (right).

Mineralocorticoid Pathway (Left):

- Cholesterol is converted to Pregnenolone by CYP11A.
- Pregnenolone is converted to 17 α -OH Pregnenolone by CYP17.
- 17 α -OH Pregnenolone is converted to DHEA by CYP17.
- Pregnenolone is converted to Progesterone by 3 β -HSD.
- 17 α -OH Pregnenolone is converted to 17 α -OH Progesterone by 3 β -HSD.
- 17 α -OH Progesterone is converted to Androstenedione by CYP17.
- Progesterone is converted to 11-Deoxycorticosterone by CYP21.
- 17 α -OH Progesterone is converted to Deoxycortisol by CYP21.
- 11-Deoxycorticosterone is converted to Corticosterone by CYP11B1/B2.
- Deoxycortisol is converted to Cortisol by CYP11B1.
- Corticosterone is converted to Aldosterone by CYP11B2.

Androgen/Estrogen Pathway (Right):

- Androstenedione is converted to Testosterone by 17 β -HSD.
- Testosterone is converted to 17 β -estradiol by CYP19.
- Androstenedione is also converted to Estrone by CYP19.
- Testosterone is converted to Estrone by 17 β -HSD.
- Estrone is converted to 17 β -estradiol by 17 β -HSD.

1.2.2.3.2 OECD test guideline No. 456: H295R steroidogenesis assay

The U.S. Environmental Protection Agency Endocrine Disruptor Screening Program, along with the Organization for Economic Co-operation and Development (OECD), have recognized the H295R cell line as a valuable model for identifying endocrine-disrupting chemicals (EDCs). This cell line has the advantage of producing diverse steroids, including mineralocorticoids, glucocorticoids, progestins, androgens, and estrogens (Botteri Principato et al., 2018; Pinto et al., 2018; Haggard et al., 2019). Consequently, these cells have been validated

The U.S. Environmental Protection Agency Endocrine Disruptor Screening Program, along with the Organization for Economic Co-operation and Development (OECD), have recognized the H295R cell line as a valuable model for identifying endocrine-disrupting chemicals (EDCs). This cell line has the advantage of producing diverse steroids, including mineralocorticoids, glucocorticoids, progestins, androgens, and estrogens (Botteri Principato et al., 2018; Pinto et al., 2018; Haggard et al., 2019). Consequently, these cells have been validated

in accordance with established international testing guidelines and serve as a "Tier 1" screening tool for steroidogenesis in testing of EDCs.

Since the H295R steroidogenesis assay was only validated to detect testosterone (T) and 17 β -estradiol (E2), it has predominantly been used to predict chemical perturbations in T and E2 synthesis. Recently, the human adrenal H295R cell steroidogenesis assay was adapted to establish a high-throughput testing model, known as HT-H295R, as part of the ToxCast programs to rapidly prioritize and identify potential EDCs (Haggard et al., 2019). In the adapted assay, 13 steroid hormones produced by the cells will be measured using high-performance liquid chromatography followed by tandem mass spectrometry (HPLC-MS/MS), which will enable a broader understanding of the effects of chemicals on the steroid biosynthesis pathway (Karmaus et al., 2016; Haggard et al., 2019).

1.2.3 Advantages and limitations of *in vitro* cell cultures v. *in vivo* animal study

The *in vitro* cell culture system offers distinct advantages for toxicological studies including ease of handling, high reproducibility, and no requirement of animals. The controlled *in vitro* environment allows for precise manipulation of experimental conditions, permitting the direct assessment of the potential impact of a chemical on cell viability/cytotoxicity. This feature is crucial as it enables the differentiation between effects resulting from cytotoxicity and those arising from other endpoints, such as the direct interaction of chemicals with steroidogenic pathways, which would not be feasible in tissue explant systems composed of multiple cell types with varying sensitivities and functionalities. It has also been shown that data derived from *in vitro* assays correlate well with bioactivity predictions and frequently indicating effects at lower concentrations than those observed in *in vivo* studies, thus providing a predictive role in assessing the toxicity of chemicals (Friedman et al., 2019; Reardon et al., 2023). Moreover, the

rapid throughput of *in vitro* cultures supports high-throughput screening for chemical toxicity, thereby accelerating the identification of potentially harmful substances and facilitating the screening of candidates for ideal replacement chemicals.

Conversely, the use of *in vivo* studies provides a more comprehensive understanding of the systemic effects of chemicals, including interactions with other organ systems and the influence of metabolic pathways that are absent in cell cultures. *In vivo* studies account for the complexity of physiological processes, such as endocrine regulation and immune responses, which can significantly affect the outcomes of toxicological assessments. Moreover, the assessment of chemical effects on the entire organism can reveal potential behavioral, reproductive, and developmental impacts that may not be detectable *in vitro*. Thus, while the *in vitro* cells are valuable for targeted investigations into toxicity and mechanisms of action, they should be used in conjunction with *in vivo* models to provide a more comprehensive understanding of the potential toxic effects of chemicals.

1.3 Endocrine disrupting chemicals (EDCs)

1.3.1 Definition of EDCs

An endocrine disrupting chemical (EDCs) is defined by the US Environmental Protection Agency (EPA) (EDSTAC Report, 1998) as “an exogenous chemical substance or mixture that alters the structure or function(s) of the endocrine system and causes adverse effects at the level of the organism, its progeny, populations, or subpopulations of organisms, based on scientific principles, data, weight-of-evidence, and the precautionary principle”

1.3.2 Presence of EDCs in human matrices

EDCs are ubiquitously present in the environment. They can be found in a wide range of products including cosmetics, personal care items, pharmaceuticals, consumer goods, pesticides, and cleaning agents. The historical and ongoing use of EDCs has resulted in their detection across various environmental media, including food and human biological samples (reviewed in Yilmaz et al., 2020). Numerous global human biomonitoring studies have been conducted by various agencies to characterize the types of EDCs to which humans are exposed and to assess exposure levels (Health Canada, 2021a; Ospina et al., 2018; Govarts et al., 2023). These studies typically quantify chemical concentrations in body fluids such as urine and blood; however, EDCs have also been identified in other biological matrices, including breast milk (Cock et al., 2017; Kubwabo et al., 2013), hair and nails (Martín-Pozo et al., 2020; Robin et al., 2024), placenta (Leonetti et al., 2016), and adrenal glands (Fommei et al., 2017). Major families of identified EDCs include bisphenols, phthalates, perfluoroalkyl substances (PFASs), parabens, brominated and phosphorylated flame retardants, and organophosphate pesticides (European Parliament, 2019).

The lipophilic nature of most EDCs means that they bioaccumulate in the body. Some exceptions include bisphenols and organophosphate esters, that are rapidly metabolized, having half-lives ranging from hours to days (Thayer et al., 2015; Bui et al., 2017; Wang et al., 2020). Despite their relatively short half-lives, the widespread use of EDCs contributes to continuous human exposure to these chemicals. For example, data from biomonitoring studies conducted between 2013 and 2016 indicate that over 90% of children and adult tested have detectable levels of at least one family of EDCs in their urine or blood samples (European Parliament, 2019).

1.3.3 EDCs that affect the adrenal gland

The adrenal glands are among the most frequently targeted endocrine glands by environmental chemicals. Several families of EDCs have been shown to affect the adrenal glands. Bisphenols are prevalent in various products, including plastic bottles, baby bottles, thermal and currency paper, and coatings for food and beverage containers. Bisphenol A (BPA) and bisphenol F (BPF) have been shown to interact with mineralocorticoid and glucocorticoid receptors (Kojima et al., 2019; Liu et al., 2019; Grimaldi et al., 2019). BPA disrupts the expression of transcripts in the steroidogenic pathway (Medwid et al., 2019; Lin et al., 2021), alters serum corticosterone levels (Chen et al., 2014), and increases the thickness of the fasciculata zone in the adrenal cortex (Panagiotidou et al., 2014). Another group of EDCs, phthalates, has been found to decrease aldosterone production in adult Sprague Dawley rats by disrupting the expression levels of aldosterone receptors (Martinez-Arguelles et al., 2011). Additionally, alterations in blood pressure have been observed in male offspring exposed maternally to phthalates (Martinez-Arguelles et al., 2013), suggesting that the RAAS may be targeted by these chemicals.

It seems that there is a common trend for the effect of most EDCs on the adrenal glands. Disruptions in steroidogenic gene expression have also been reported following exposure to polychlorinated biphenyls (PCBs) (van den Dungen et al., 2015), per- and polyfluoroalkyl substances (PFAS) (van den Dungen et al., 2015), and organochlorines (Lund et al., 1988). It is perhaps not surprising that the production of cortisol and aldosterone is affected by these chemical families (Fommei et al., 2017; Salgado-Freiría et al., 2018; van den Dungen et al., 2015). Additionally, exposure to organochlorines has been linked to alterations in adrenal gland morphology and weight (Lund et al., 1988). Collectively, these findings suggest that the adrenal

glands are important targets of EDCs, and the implications of these effects for the pathogenesis of steroid- and adrenal-related disorders warrant further investigations.

1.4 Flame retardants

Flame retardants are man-made chemicals added to consumer products and building materials to inhibit the ignition and spread of fire. The use of flame retardants was primarily driven by the California flammability standard, Technical Bulletin 117 (TB 117), established in 1975. This standard mandates that polyurethane foam utilized in furniture must withstand a 12-second open flame test with minimal loss of foam, a requirement that is challenging to meet without the inclusion of chemical flame retardants (reviewed in van der Veen and de Boer, 2012; Stapleton et al., 2012). TB 117 was designed primarily to mitigate the risk of home fires ignited by small open flames, including those from candles, matches, and lighters. However, the effectiveness of flame retardants in enhancing fire safety remains a subject of debate. Concerns have been raised regarding the reliability of existing flammability tests, as these assessments often fail to accurately simulate the conditions of real fires. Additionally, furniture that incorporates flame retardants may emit a higher volume of toxic gases during a fire, thereby raising additional safety concerns (McKenna et al., 2018). Consequently, California adopted Technical Bulletin 117-2013 (TB 117-2013), which eliminated the open flame test and gave manufacturers the option of using smolder resistant fabrics or barriers that do not require flame retardants (State of California, 2013). Similarly, in Canada, compliance with flammability performance requirements set forth in the Canada Consumer Product Safety Act (CCPSA) for certain consumer products can be achieved without the use of flame-retardant chemicals (Government of Canada, 2021). While these policy changes have successfully reduced the use of

flame retardants in new products, their persistent presence in the environment, particularly in dust, suggests continued exposure risks (Rodgers et al., 2021).

The primary families of flame retardants include halogenated compounds (bromine and chlorine), phosphorus-based compounds, nitrogen-based compounds, and mineral-based substances (reviewed in van der Veen and de Boer, 2012). This project will focus on two major families: brominated and phosphorus flame retardants.

1.4.1 Polybrominated diphenol ethers (PBDEs)

Brominated flame retardants (BFRs) have been extensively used for decades, with polybrominated diphenyl ethers (PBDEs) being among the most heavily produced types (reviewed in Birnbaum and Staskal, 2004). PBDEs are commonly found in a variety of products, including furniture foam, plastics, textiles, electronics, and construction materials. As non-covalently bound additives, PBDEs have a tendency to leach from these products into the environment, leading to widespread human exposure. Individuals may encounter these compounds through various routes, including inhalation, ingestion, and dermal contact (reviewed in Maddela et al., 2020).

1.4.1.1 Physicochemical properties of PBDEs

PBDEs are a family of chemicals characterized by a common structural framework of brominated diphenyl ether, represented by the general chemical formula $C_{12}H_{(0-9)}Br_{(1-10)}O$. In this structure, any of the ten hydrogen atoms in the diphenyl ether moiety can be substituted with bromine, resulting in the formation of 209 possible congeners. Each PBDE congener is distinguished by the number of bromine atoms present and their specific positions within the molecule (**Figure 1-9**). PBDEs exist as mixtures of these distinct congeners, each possessing

unique molecular structures. Congeners that share the same number of bromine atoms are classified as homologs. The major types of commercial PBDE homologs include pentabromodiphenyl ether (pentaBDE), octabromodiphenyl ether (octaBDE), and decabromodiphenyl ether (decaBDE), with DecaBDE being the most widely used PBDE globally (ATSDR, 2004; EPA, 2009).

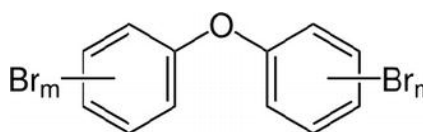


Figure 1-9. General structure of PBDEs.

PBDEs have been classified as persistent organic pollutants (POPs) under the Stockholm Convention due to their environmental persistence feature, capacity for long-range transport, potential for bioaccumulation, and toxicity to both humans and wildlife (Cequier et al., 2014). Variations in the degree of bromination significantly influence the physicochemical properties of PBDEs. Lower-brominated congeners tend to bioaccumulate more readily and exhibit greater environmental persistence compared to higher-brominated congeners, which are more likely to bind to sediment or soil particles (ATSDR, 2004). PBDEs are fat-soluble and hydrophobic (Hooper and McDonald, 2000). They are primarily detected in the adipose tissue (ATSDR, 2004). However, they have also been identified in other biological samples, including blood (Mazdai et al., 2003), breast milk (Marchitti et al., 2017), liver (Schecter et al., 2007), as well as in hair and nails (Zhao et al., 2020). The half-lives of PBDEs vary considerably, ranging from approximately 15 days for higher-brominated congeners to up to 4 years for lower-brominated congeners (Sjödén et al., 2020).

1.4.1.2 Toxicity of PBDEs

The majority of information regarding the toxicity of PBDEs and their metabolites is derived from animal studies; however, recent investigations have explored the associations between PBDE concentrations in human tissues, such as blood and breast milk, and various health outcomes. Research involving rats and mice has shown that ingestion of small amounts of lower-brominated PBDEs during early development leads to neurobehavioral changes (Dingemans et al., 2011; reviewed in Costa and Giordano, 2011) and reproductive system damage in adulthood (Kodavanti et al., 2010). Although altered neurobehavior has also been observed in animals exposed to decaBDE, this occurred at higher doses compared to lower-brominated congeners (ATSDR, 2004). Furthermore, studies involving adult rats and mice exposed to moderate amounts of lower-brominated PBDEs over short durations primarily indicated effects on thyroid and liver function (Meng et al., 2020; Casella et al., 2022; Bansal et al., 2014), while additional short-term studies suggested potential immune system impairment (Fair et al., 2012). Evidence from human studies indicates that PBDE exposure is associated with adverse effects on the nervous system (Vuong et al., 2017; Kiciński et al., 2012; Eriksson et al., 2002), reproductive health (Makey et al., 2016; Harley et al., 2010; reviewed in Hales and Robaire, 2020), and thyroid function (Gorini et al., 2018; Oulhote et al., 2016).

PBDEs have also been shown to affect the adrenal gland, although studies in this area are less abundant. Dungar et al. assessed the *in vitro* and *in vivo* effects of exposure to BDE-47 and found that both basal and stimulated aldosterone and cortisol levels were increased in HAC15 cells due to upregulation of enzymes involved in the corticosteroid synthesis pathway. Additionally, exposure to BDE-47 in Sprague Dawley rats resulted in increased adrenal gland weights and elevated plasma corticosterone levels (Dungar et al., 2021). Exposure to another PBDE, 4-bromodiphenyl ether (BDE-3), was associated with increased serum aldosterone and

corticosterone levels, mediated by the upregulation of *Cyp11b1*, *Cyp11b2*, *Scarb1*, *Star*, and *Nr5a1*, all of which are key components in the steroid and cholesterol biosynthesis pathways (Chen et al., 2019).

1.4.1.3 Global regulation of PBDEs

The ubiquitous persistence and bioaccumulative properties of PBDEs, as well as the above-mentioned adverse health concerns, have led to bans and voluntary phase-out of PBDEs worldwide since the early 2000s. For instance, the European Union (EU) has implemented legislation aimed at reducing or prohibiting the sale and use of specific brominated flame retardants (BFRs). Notably, in 2003, an EU directive banned the marketing of two commercial mixtures of PBDEs: PentaBDE and OctaBDE. In United States, while there are no federal restrictions on PBDEs, thirteen states have enacted legislation imposing limitations on their use or presence in specific commercial products (reviewed in Sharkey et al., 2020). In Canada, DecaBDE has been identified as a toxic substance under the Canadian Environmental Protection Act (CEPA) (Environment Canada, 2013). Moreover, the Prohibition of Certain Toxic Substances Regulations (PCTSR) was amended in 2022 to restrict the manufacture, use, sale, and import of PBDEs and products containing them (Government of Canada, 2020). Following the global phase-out of the use of PBDEs, studies have reported declining trend in the level of PBDEs in various environmental compartments, including air, surface water, sediment, fish, and bird eggs across Canada (Government of Canada, 2020).

1.4.2 Organophosphate esters (OPEs)

Organophosphorus compounds are characterized by a general structure that includes a phosphorus atom bonded to oxygen and carbon atoms ($S=P(OR)_3$). Initially developed in the

early 1930s as chemical warfare agents, such as nerve agents like sarin and VX, these compounds inhibit acetylcholinesterase, an enzyme crucial for the breakdown of the neurotransmitter acetylcholine. This inhibition results in the accumulation of acetylcholine, leading to prolonged stimulation of muscles and potentially fatal physiological effects (Robb et al., 2023). Following their military use, organophosphorus compounds gained prominence in agriculture as insecticides and herbicides, owing to their effectiveness and relatively rapid degradation in the environment. In the 1980s and 1990s, the chemical industry began to transition toward using organophosphate esters (OPEs) as flame retardants, particularly as alternatives to brominated flame retardants like PBDEs (Costa, 2018). Over the years, the production and consumption of OPEs have increased (Stapleton et al., 2012; reviewed in van der Veen and de Boer, 2012), leading to their detection in various environmental matrices (Struzina et al., 2022; He et al. 2018a; Percy et al., 2020) and human biological samples (Liu et al., 2015; Liu et al., 2016) at levels exceeding those of legacy PBDEs.

1.4.2.1 Physicochemical properties

OPEs can be classified as halogenated, aryl, or alkyl OPEs based on the nature of the substituents.

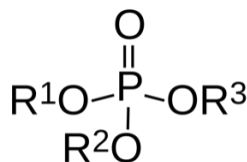


Figure 1-10. General structure of OPE.

The solubility of OPEs varies significantly, ranging from 0.36 to 5×10^5 mg/L, with solubility generally decreasing with increasing molecular weight and decreasing vapor pressure.

Most OPEs exhibit positive octanol-water partition coefficient ($\log K_{ow}$) values, indicating a greater lipophilicity than hydrophilicity (reviewed in Greaves and Letcher, 2017). Furthermore, the Henry's law constants for OPEs (which determine the amount of gas that dissolves in a liquid) exhibit a wide range of values, indicating a significant potential for migration and transformation across various environmental compartments. Notably, compared to polybrominated diphenyl ethers (PBDEs), OPEs—particularly chlorinated OPEs—are more soluble in water, making long-range transport via waterborne routes possible (reviewed in Van der Veen and De Boer, 2012).

1.4.2.2 Production and application

Following the phase-out of PBDEs, the global consumption of OPEs increased significantly, from 100,000 tons in 1992 to 1,050,000 tons in 2018 (reviewed in Greaves and Letcher, 2017). In addition to their roles as flame retardants, OPEs have been used as plasticizers, antifoaming agents, adhesives, and lubricants, meaning that their presence can be found from food packaging, toys, electronics to furniture and building materials (reviewed in Dou and Wang, 2023). The wide use of OPEs as the replacement chemical for PBDEs is based on the assumption that OPEs are less environmentally persistent, thereby posing a lower risk for widespread environmental distribution and exposure (Blum et al., 2019). However, multiple studies have indicated that the concentrations of OPEs have reached levels orders of magnitude higher in air and water across diverse environments, including urban areas and remote Arctic and Antarctic locations, than PBDEs during their peak usage (Rodgers et al., 2018; Ma et al., 2017). Consequently, OPEs have been identified as a class of equally concerning chemicals, categorized as persistent mobile organic compounds (PMOCs) (Blum et al., 2019).

1.4.2.3 Routes of exposure

Similar to PBDEs, OPEs are additives, meaning that they are not chemically bound to the products they have been added to, and are therefore susceptible to volatilization, abrasion, or dissolution (reviewed in Van der Veen and van der de Boer, 2012). As a result, OPEs are detected in indoor air, dust, water, and food. Inhalation, ingestion, hand-to-mouth contact, and dermal absorption are all important exposure routes for humans.

1.4.2.3.1 Levels in human matrices

Before the phase-out of PBDEs, levels of OPEs to which humans were exposed to were comparable to those of PBDEs in the 1990s. The increasing use of OPEs have led to greater human exposures, as evidenced by steadily rising urinary levels since the early 2000s (Hoffman et al., 2017). Since OPEs are used in food packing material, their presence has also been reported in butter, fish, and drinking water (Struzina et al., 2022; Bi et al., 2023; Sala et al., 2022; He et al., 2018b). On basis of the levels found in food, the estimated daily dietary intake for Σ OPEs ranges from 6 to 49 ng/kg bw (Poma et al., 2017).

Urinary levels of OPE metabolites have been frequently used as biomarkers for exposure assessment. These metabolites have been reported in the low to mid-nanomolar range, with diphenyl phosphate (DPHP)—a metabolite of multiple OPEs—alongside with 1-hydroxy-2-propyl bis(1-chloro-2-propyl) phosphate (BCIPHIP), a metabolite of TCIPP, and bis(1,3-dichloro-2-propyl) phosphate (BDCIPP), a metabolite of TDCIPP, frequently detected at higher concentrations than other urinary metabolites (Butt et al., 2016; Hammel et al., 2016). Furthermore, levels and profiles of human exposure to OPEs vary significantly by geographical region and individual behaviors, with children typically experiencing higher concentrations presumably due to their hand-to-mouth activities. According to exposure data from 12 countries,

the estimated daily intake of Σ OPEs from indoor dust ranges from 0.29 to 64.8 ng/kg per day for children and from 0.07 to 14.9 ng/kg per day for adults (Li et al., 2019).

1.4.2.4 Metabolism and elimination

Upon entering the body, most OPEs are readily metabolized into dialkyl or diaryl groups and various hydroxylation products through phase I metabolic processes (Van den Eede et al., 2013). This hydrolysis step is particularly crucial, as it significantly reduces the toxicity of OPEs. Some OPE metabolites may subsequently undergo conjugation with glutathione, glucuronic acid, or sulfate through phase II metabolic pathways (Ballesteros-Gómez et al., 2015; Van den Eede et al., 2013). Studies utilizing liver microsomes from human and crucian carp have demonstrated variations in the metabolism rates of different OPEs, indicating a structure- and species-dependent effect (Wang et al., 2020; Greaves et al., 2016; Hou et al., 2018; Van den Eede et al., 2015). Generally, OPEs are rapidly metabolized in the body, exhibiting relatively short half-lives ranging from hours to days (Geyer et al., 2004; Hoffman et al., 2014).

1.4.2.5 Established health effects

It is well established that organophosphate esters (OPEs) can induce neurotoxicity through non-cholinergic mechanisms of action. Specifically, they have been shown to inhibit gamma-aminobutyric acid (GABA) receptors, neuropathy target esterase, and voltage-dependent chloride channels (Lotti and Moretto, 2005; Casida, 2017). Multiple epidemiological studies have revealed that exposure to OPEs is associated with decreases in intelligence quotient (IQ) and working memory (Castorina et al., 2017). Additionally, prenatal exposure to OPEs has been linked to lower scores on fine motor assessments (Doherty et al., 2019a) and a higher risk of withdrawal symptoms, attention problems, and hyperactivity (Doherty et al., 2019b).

Furthermore, OPE exposure has been found to affect thyroid hormone production, which is critical for neurodevelopment (Demeneix, 2019; reviewed in Gore et al., 2014).

OPEs are also classified as EDCs. In women undergoing *in vitro* fertilization (IVF) treatment, urinary metabolites of OPEs have been correlated with poor treatment outcomes, including decreases in fertilization, implantation, clinical pregnancy, and live birth rates (Carignan et al., 2017). In men residing in the Greater Montreal area, exposure to various OPEs has been associated with altered sex hormone levels and compromised semen parameters (Siddique et al., 2022). *In vitro* studies have identified that OPEs can disrupt ovarian cell function by interfering with cholesterol and steroidogenic pathways (Wang et al., 2023a; Wang et al., 2024). Additionally, evidence of hepatotoxicity (Yu et al., 2024; Li et al., 2022), adverse effects on bone development (Yan and Hales, 2022), immune system impacts (Giles et al., 2024; Liao et al., 2023), and cardiovascular system disturbances (reviewed in Hu et al., 2022) have been reported. Notably, certain chlorinated OPEs, including tris(ethylhexyl) phosphate (TEHP) and tributyl phosphate (TBP), have been identified as carcinogenic (reviewed in Dou and Wang, 2023).

Despite these findings, few studies have investigated the effects of OPEs on the adrenal gland, one of the most important endocrine glands in the body. Furthermore, the specific mechanisms of action of OPEs on the adrenal glands remain largely unexplored. The following discussion will summarize what is currently known about effects of OPEs on the adrenal gland, including available *in vivo*, *in vitro*, and epidemiological studies.

1.4.2.6 Effect on the adrenal gland

Only a limited number of studies have investigated the effects of OPEs on the adrenal gland, and they focused on a small number of compounds. In a 13-week study examining

tris(methylphenyl) phosphate (TMPP), cytoplasmic vacuolization in the adrenal cortex, specifically in the zona glomerulosa and zona reticularis, was observed in both F344/N rats and B6C3F1 mice. Over a two-year exposure period, male mice exhibited a reduction in adrenal gland weights, while female mice demonstrated an increase. Additionally, cytoplasmic vacuolization and ceroid pigmentation were noted in the adrenal cortex of female mice (National Toxicology Program, 1994). Similarly, F344/N rats of both sexes showed increased adrenal gland weight, hypertrophy, and cholesteryl lipidosis in adrenocortical cells following exposure to TMPP (Latendresse et al., 1993, 1994, 1995). Another commonly studied OPE, isopropylated triphenyl phosphate (IPPP), was found to increase adrenal gland weights and induce the accumulation of lipid droplets in the zona fasciculata of the adrenal cortex in both sexes of Wistar rats (Wade et al., 2019). Furthermore, Akimoto et al. (2022) assessed the effects of neonatal exposure to tris(1,3-dichloro-2-propyl) phosphate (TDCIPP) on Wistar rats and reported increased adrenal gland weight in male adults.

In vitro studies have explored a broader range of OPEs. Using H295R cells, several OPEs were identified to affect the steroidogenic function of these cells by altering the expression of transcripts involved in steroidogenic pathways (Liu et al., 2012; Zhang et al., 2017). Additionally, OPEs and their metabolites exhibited antagonistic activity on both the mineralocorticoid and the glucocorticoid receptors (Zhang et al., 2017, 2020).

Few studies have reported human data of the effect of OPEs on the adrenal glands. Only one study assessed the association of the urinary levels of OPE metabolites with serum cortisol level and reported a positive correlation between levels of di-butyl phosphate (a metabolite of TPHP), bis(1-chloro-2-propyl) phosphate (a metabolite of TDCIPP), and bis(2-butoxyethyl) phosphate (a metabolite of TBOEP) and serum cortisol levels (Ji et al., 2021).

1.4.2.7 Rationale and significance of studying chemical mixtures

Toxicological studies have historically focused on the effects of individual chemical exposures. However, in real-world contexts, individuals rarely face exposure to single chemicals. Instead, exposure commonly occurs through a variety of sources, including diet, pharmaceuticals, air, and drinking water, where mixtures of both man-made and naturally occurring chemicals are present. Moreover, the interaction of these chemicals can be more complex than simple additive effects, as the mixture may show synergistic or antagonistic effects that can significantly alter their toxicity profiles. For instance, studies have demonstrated that exposure to chemical mixtures can induce endocrine disruptions even at concentrations below the no observed adverse effect levels (NOAELs) or no observed effect concentrations (NOECs) of individual members of a chemical family (Cavieres et al., 2002; Rajapakse et al., 2002; Welshons et al., 2003; Payne et al., 2000). While studying individual chemicals provides essential mechanistic insights and informs regulatory decisions for identifying safer alternatives, evaluating mixtures is crucial for a more physiologically relevant assessment of toxicity.

Studying the effects of chemical mixtures presents significant challenges. Individual exposure profiles can vary widely, making it impractical to evaluate every conceivable chemical combination and concentration in controlled studies. Some efforts have been made to address the health risks associated with combined exposures. For instance, chemicals with similar mechanisms of action or structural characteristics have been regulated as a group. However, this approach often overlooks real-world exposure scenarios and the varying potencies of different chemicals within the same group (Schmeisser et al., 2023).

There are also initiatives aimed at establishing guidelines for conducting health risk assessments of chemical mixtures. For chemicals that have a lack of established interactions, either assumed or demonstrated through experimental data, application of dose addition or

response addition approaches are used to calculate the safe dose. In cases where interactions are predicted, an Interaction-based Hazard Index (HI) method is used. This HI is designed to integrate interaction data from binary testing (US. EPA, 2000). However, several critical challenges remain. First, there is a scarcity of dose response data on many chemicals. Second, most existing studies focus on binary mixtures, which limits our understanding of the effects of more complex combinations. Finally, there is a lack of research on the chronic exposure to low concentrations of chemicals (Teuschler et al., 2002). Thus, high-throughput studies assessing environmental samples for chemical mixtures can produce valuable data on real-life exposure scenarios in a more efficient manner are needed. Such research can enhance our understanding of the complexities of chemical interactions and improve risk assessment frameworks.

1.4.2.8 The Canadian house dust study

Completed by Health Canada, the Canadian House Dust Study is a statistically representative national baseline study on chemical concentrations in dust sampled from urban households. The study utilized vacuum and wipe sampling methods to collect dust from 144 urban Canadian homes between 2007 and 2010 (Rasmussen et al., 2011; Rasmussen et al., 2013). From the study, 13 OPEs and their concentrations were identified in house dust (Fan et al., 2014; Kubwabo et al., 2021) and is used as the basis for composing an environmentally relevant mixture of OPEs to test mixture exposure effects on the adrenal glands in this project.

1.5 Formulation of the thesis project

In our daily lives, we are surrounded by synthetic chemicals. Exposure to these environmental pollutants can result in significant health issues, as evidenced by the legacy of polybrominated diphenyl ethers (PBDEs) flame retardants, which led to worldwide regulations

on their use. With PBDEs being phased out, organophosphate esters (OPEs) have become increasingly used as alternative flame retardants and plasticizers. Research indicates that OPEs may act as endocrine disrupting chemicals; however, there is limited understanding of their effects on the adrenal glands and the underlying mechanisms. This thesis aims to examine the toxicity of OPEs in adrenal glands through both *in vitro* and *in vivo* approaches, investigate the mechanism(s) driving these effects, and propose strategies for identifying safer alternatives to legacy compounds.

The objectives of this thesis are to:

- 1) Evaluate the effects of individual OPEs on the phenotype and function of adrenal cells
- 2) Assess the effects of an environmentally relevant OPE mixture on adrenal cells
- 3) Determine how an environmentally relevant mixture affects the adrenal glands of Sprague Dawley rats and the mechanism(s) involved

For aims 1 and 2, the H295R human adrenal cell line was used as an *in vitro* model to characterize the effects of OPEs on phenotypic and functional endpoints of the adrenal glands. The H295R cell line represents a unique *in vitro* system in that it has the ability to produce all of the steroid hormones found in the adult adrenal cortex and gonads. As discussed, it is also used in the standardized OECD screening assay for assessing the effect of chemicals on steroidogenesis. To identify safer replacements, a predominant PBDE congener, BDE-47, was used as a reference chemical in aim 1. Aim 3 incorporates an *in vivo* component into the project, allowing for the assessment of the metabolic effects of chemicals, sex differences, and the overall impact on the HPA axis.

CHAPTER 2

The Organophosphate Esters Used as Flame Retardants and Plasticizers affect H295R

Adrenal Cell Phenotypes and Functions

Zixuan Li, Bernard Robaire, Barbara F Hales

(Published: Endocrinology; July 31, 2023)

ABSTRACT

Adverse effects associated with exposure to brominated flame retardants have led to regulations for their use and their replacement with organophosphate esters (OPEs). However, little is known about the impact of OPEs on the adrenal, a vital endocrine gland. Here, we used a high-content screening approach to elucidate the effects of OPEs on H295R human adrenal cell phenotypic endpoints and function. The effects of 2,2',4,4'-tetrabromodiphenyl ether (BDE-47), a legacy brominated flame retardant, on H295R cell cytotoxicity, oxidative stress, mitochondria, lysosomes, and lipid droplets were compared to those of six OPEs. Most OPEs reduced oxidative stress, increased the numbers of mitochondria, decreased lysosomes, and increased lipid droplets. Two potency ranking approaches, the lowest benchmark concentration/administered equivalent dose methods and Toxicological Prioritization Index analyses, revealed that the triaryl-OPEs (IPPP, TMPP, and TPHP) and one non-triaryl OPE (TDCIPP) were more potent than BDE-47. The steroidogenic activity of adrenal cells in the presence or absence of forskolin, a steroidogenic stimulus, was determined after exposure to triaryl-OPEs. The basal production of cortisol and aldosterone was increased by IPPP but decreased by TPHP or TMPP exposure; the response to forskolin was not affected by these OPEs. All three triaryl OPEs altered the expression of rate-limiting enzymes involved in cholesterol and steroid biosynthesis; CYP11B1 and CYP11B2 were the most prominently affected targets. The OPE chemical-specific effects on cortisol and aldosterone production were best explained by alterations in STAR expression. Thus, the adrenal may be an important target for these endocrine disrupting chemicals.

INTRODUCTION

Flame retardants are chemicals added to consumer products and building materials to prevent the ignition or slow the spread of fire. The polybrominated diphenyl ether (PBDE) flame retardants were used extensively for decades; however, their persistence and bioaccumulative properties, as well as the associated toxicities, have led to regulations and/or voluntary phase-out of their use worldwide since the early 2000s (1). Organophosphate esters (OPEs) have emerged as major replacement flame retardants, in addition to their roles as additives in plasticizers, hydraulic fluids, and antifoaming agents (2, 3). Consequently, the production and volume of consumption of OPEs have increased (3-5). Like PBDEs, OPEs are not covalently bound to the materials to which they are added and can be readily released to the surrounding environment, leading to ubiquitous exposures. Indeed, OPEs have been detected in various environmental compartments and human matrices at levels that are higher in comparison to the legacy PBDEs (6-13).

Increased use of and exposure to OPEs have raised concerns regarding their potential adverse health effects. Authoritative bodies, such as Health Canada, the U.S. Environmental Protection Agency, and the European Chemicals Agency, have undertaken initiatives to identify and manage the risks associated with some OPEs (14-16). While ongoing assessments are being conducted, a growing body of evidence suggests that OPEs can act as endocrine disrupting chemicals. A study by Kojima et al. (17) revealed that several OPEs can act on human nuclear receptors as agonists or antagonists; these include the estrogen, androgen, and thyroid receptors. Some OPEs have also been associated with adverse effects on neurodevelopment (18-20), thyroid homeostasis (21, 22), and reproductive parameters (22-24) both in human populations and animal models. Furthermore, several OPEs, including those frequently detected in the environment, have demonstrated greater toxicity than the legacy PBDEs (25-27). Those findings suggest that exposure to some OPEs may pose a risk to the endocrine system and consequently have an impact on our overall health.

The adrenal gland is a vulnerable site for toxicological assault due to its high vascularity, the significant presence of enzymes from the cytochrome P450 (CYP) family, and ability to take up and store lipophilic compounds (28-30). However, only a few studies have assessed the effects of exposure to a limited number of OPEs on the adrenal gland. In animal models, exposure to tris(methylphenyl) phosphate (TMPP) affected adrenal gland weight and induced adrenal cortex vacuolization in mice and in rats (31-34). Adrenal gland weights were also increased in adult Wistar rats exposed to isopropylated triphenyl phosphate (IPPP) (35) or tris(1,3-dichloro-2-propyl) phosphate (TDCIPP) (36). *In vitro* studies using H295R adrenal cells have demonstrated that their steroidogenic function was affected by several OPEs, potentially by altering the genes involved in the steroidogenic pathways (37, 38). Moreover, OPEs and their primary metabolites were reported to have antagonistic activities on the mineralocorticoid receptor and/or glucocorticoid receptor (39, 40). Collectively, these studies provide compelling evidence that OPEs may target the adrenal gland, highlighting the need for further studies to understand the impact of OPE exposures on the adrenal gland and to elucidate the underlying mechanism(s) involved.

In the current study, we assessed the effects of OPEs on the phenotype and function of H295R human adrenal cells. H295R cells were selected for their ability to be stably maintained in culture, their expression of all the enzymes involved in the steroidogenic pathway, and the recommendation from OECD for their use as a test model for evaluating the effects of chemicals on steroidogenesis (41). We investigated the effects of six OPEs commonly found in Canadian house dust (42, 43) on various phenotypic cellular characteristics using high-content screening. A major PBDE congener, 2,2',4,4'-tetrabromodiphenyl ether (BDE-47), was used as a reference chemical. Based on the effects of OPEs on phenotypic endpoints, a combination of data analysis methods was used to determine potency rankings and to estimate the administered equivalent

doses (AED) in humans. Further, we examined the impact of the three most potent OPEs on the steroid-producing function of H295R cells and the potential underlying mechanism(s) involved in the action of OPEs on this adrenal cell function.

MATERIALS AND METHODS

Chemicals

Figure 1 provides a list of the chemicals tested. BDE-47, TBOEP, TMPP, TPHP, and TDCIPP were gifts from Dr. Nicole Kleinstreuer (National Toxicology Program Interagency Center for the Evaluation of Alternative Toxicological Methods). IPPP and TCIPP were kindly provided by Dr. Michael G. Wade (Health Canada). All chemicals were dissolved in dimethyl sulfoxide (Sigma-Aldrich, St. Louis, Missouri, USA).

Cell cultures

The H295R human adrenocortical carcinoma cells were purchased from ATCC (CRL-2128, Manassas, VA). H295R cells were cultured in phenol-red free DMEM/F-12 medium (Gibco, Burlington, Ontario, Canada), supplemented with Corning ITS+ Premix Universal Culture Supplement, Corning Nu-Serum Growth Medium Supplement, and 0.5% 100X penicillin-streptomycin (complete medium) (Wisent Bioproducts, Montreal, Quebec, Canada). Cells were cultured in Corning 75 cm² U-shape cell culture flask at 37 °C with 5% CO₂. The culture medium was renewed every two to three days.

High-content imaging

H295R cells were seeded in 96-well black PhenoPlates with optically clear flat-bottoms (Perkin

Elmer, Waltham, Massachusetts) pre-coated with 0.2% collagen 1 (3 mg/mL, rat tail) (Gibco, Burlington, Ontario, Canada) at a seeding density of 10,000 cells/well in 100 μ L of complete medium. Cells were given a 24 h acclimation period prior to chemical treatment and then exposed for 48 h to a vehicle control (0.5% DMSO) or each chemical (0.001, 0.01, 0.1, 1, 5, 10, 20, 50, or 100 μ M). All chemicals were dissolved in DMSO and stored at -20 $^{\circ}$ C. On the experimental day, the stock solutions were then diluted to the working concentration with complete medium. The final concentration of the solvent DMSO was 0.5%. To assess the effects of exposure on phenotypic characteristics following the chemical treatment period, cells were stained for 30 min with one of four different combinations of cell-permeable fluorescent dyes. Information on the cell-permeable fluorescent dyes, the combinations used, and their dilutions is provided in Supplementary Table 1 (44).

The Operetta High Content Imaging System (Perkin Elmer) with a non-confocal 40 x high-NA objective was used to read the plates for live cell imaging. For each well, 12 fields were screened; the images that were obtained were analyzed using the Columbus Image Data Storage and Analysis System (Perkin Elmer). The specific parameters assessed, and the detailed settings for each analysis, are provided in Supplementary Methods 1.1 (44).

Benchmark concentration analyses

BMD Express 2.2 (SciOne, Research Triangle Park, North Carolina) was used to derive the benchmark concentrations (BMCs) of the compounds for each phenotypic endpoint. The benchmark response, i.e., the pre-defined level of change from control, was set to 10% according to recommendations from the U.S. Environmental Protection Agency (45). These analytic procedures were described previously by Rajkumar et al. (26) and Wang et al. (27). In brief, BMC₁₀ values for cytotoxicity were derived using the PROAST 65.5 software package in R

console (v.3.6.2); for each phenotypic parameter, values were derived using the BMDEExpress 2.2 software. BMC₁₀ values were estimated based on the best-fit model with lowest Akaike information criterion (AIC) and were reported with the 95% confidence interval (reported as BMCL and BMCU limits). For data reliability purposes, the following exclusion criteria were used: the best-fit model should have a global goodness of fit p value > 0.1 and a BMCU/BMCL ratio < 40 (45).

Administered equivalent dose analyses

To estimate the administered equivalent doses (AEDs, mg/kg body weight/day), *in vitro* to *in vivo* extrapolation (IVIVE) modeling was done based on the BMCs and the steady-state concentrations (C_{ss}) for each compound. The C_{ss} values were modeled using the high-throughput toxicokinetics (HTTK) package (v1.10) in R. No additional parameters were required to model the C_{ss} for compounds that had input data: 1) that was available in the HTTK database (TPHP and TDCIPPP), 2) available from Health Canada (TMPP and TCIPP), or 3) that could be collected following the procedures used by Health Canada (BDE-47) (46). For other compounds, ADMET Predictor (version 10) was used for C_{ss} derivation. The C_{ss} value for each compound and the parameters and formula used in the IVIVE modeling are provided in Supplementary Table 2 (44). The following formula was used to derive the AED value for each compound (46):

$$\text{AED} = \frac{\text{BMC } (\mu\text{M}) \times 1 \text{ (mg/kg/day)}}{\text{C}_{\text{ss}} (\mu\text{M})}$$

ToxPi analyses

The Toxicological Priority Index (ToxPi) was used as a tool to rank chemicals based on their overall effects on the phenotypic endpoints (v.2.3; available at <https://toxpi.org>). Endpoints

assessed were cytotoxicity, Calcein intensity, oxidative stress, total mitochondria, active mitochondria, number of lysosomes, lysotracker red intensity, and total area of lipid droplets. Specifically, the BMC values for each endpoint were log transformed ($\text{Log}_{10}\text{BMC}$) and compared with the log-transformed BMC values of other chemicals. In order to reflect the potency of each chemical on the specific endpoint, they were then scaled between 0 and 1, with 0 being the chemicals inducing no effect and 1 being the most potent chemical. Using the scaled data, the software calculated unitless numbers, i.e., the ToxPi score, based on the potency of all the endpoints tested for that chemical (all endpoints were weighed equally). ToxPi analyses also generated chemical-specific pie charts with each slice representing a phenotypic endpoint; the area of the slice was proportional to the potency of the chemical for that parameter.

Measurement of basal and stimulated production of cortisol and aldosterone

H295R cells were seeded in 96 well plates pre-coated with 0.2% rat tail collagen 1 at a seeding density of 10,000 cells/well in 100 μL of complete medium for 24 h. The cells were then exposed to 200 μL complete medium containing a triaryl-OPE (IPPP, TMPP, or TPHP) at a concentration of 1 μM or 5 μM in the presence or absence of 10 μM forskolin (Sigma-Aldrich), a steroidogenic stimulus (41), for 48 h. At the end of the exposure period, cell culture media were pooled from duplicate wells (400 μL in total for each condition) and stored at -80°C until measurement. To assess the numbers of cells in each well, cells were stained with Hoechst 33342 for 30 min with no washing afterwards to prevent cell loss. Plates were then screened with the Operetta High Content Imaging System using a non-confocal 10 x high-NA objective; all fields were screened. The Columbus Image Data Storage and Analysis System was used to quantify the Hoechst-positive cell counts (Supplementary Methods 1.2) (44). Cortisol and aldosterone concentrations in the conditioned cell culture media were measured using commercial enzyme-linked

immunosorbent assay (ELISA) kits (Cayman Chemical Catalog # 500370, RRID: AB_2935793; Abcam Catalog # ab136933, RRID: AB_2895004, respectively) following the manufacturer's instructions. The SpectraMax Plus 384 microplate reader (Molecular Devices, San Jose, California, USA) was used to read the ELISA plates at a wavelength of 450 nm. The final concentrations were adjusted to the number of cells in each well and are presented as picograms per 1 million cells. The average intra-assay and inter-assay coefficients of variation were 7.2% and 10.7% for the cortisol assay; they were 4.5% and 13.9% for the aldosterone assay.

Quantitative real-time PCR (qRT-PCR)

H295R cells were seeded in 6 well plates pre-coated with collagen at a density of 300,000 cells/well in 1 mL of complete medium (seeding density was adjusted from the density used in the high-content screening experiments based on the surface area ratios of the well). Cells were acclimated for 24 h prior to exposure to a triaryl-OPE (IPPP, TMPP, or TPHP) at 1 μ M or 5 μ M for 48 h, in the presence or absence of 10 μ M forskolin (41). Total RNA was extracted using the RNeasy Plus Mini Kit (QIAGEN, Mississauga, Ontario, Canada) following the manufacturer's protocol. The concentration and purity of the extracted RNA were assessed using a NanoDrop 2000 spectrophotometer (ThermoFisher, Waltham, Massachusetts, USA).

All primers were obtained from QuantiTect Primer Assays (QIAGEN): HMG-CoA reductase (HMGCR, QT00004081), steroidogenic acute regulatory protein (STAR, QT00091959), steroidogenic factor 1 (NR5A1, QT00088018), cholesterol side-chain cleavage enzyme (CYP11A1, AT00040117), 11-beta-hydroxylase (CYP11B1, QT00028714), aldosterone synthase (CYP11B2, QT00076181), and glyceraldehyde 3-phosphate dehydrogenase (GAPDH, QT00079247). Samples were diluted to 2 ng/ μ L in RNase-free water. The working concentration was adjusted to 10 ng/ μ L for transcripts that had moderate to low expression levels in H295R

cells (CYP11B1 and CYP11B2). The Power SYBR Green RNA-to-CT 1-Step Kit (Applied Biosystems, Foster City, California) and the Viia7 Real-Time polymerase chain reaction (PCR) System (Applied Biosystems) were used to quantify transcript levels. Each 20 μ L reaction mix was composed of 0.16 μ L of reverse transcriptase, 2 μ L of primer, 2.84 μ L of RNase-free water, 10 μ L of SYBR Green Master Mix, and 5 μ L of RNA samples. PCR was conducted under following conditions: 48°C for 30 min, 95°C for 10 min, 40 cycles at 95°C for 15s, 55°C for 30s, and 72°C for 30s. Each reaction was done in triplicate; data were checked to identify and exclude outliers ($> 0.2 C_T$ values deviating from the average of the other two). The expression levels of transcripts were calculated based on the average of replicates and were normalized to the amount of the GAPDH transcripts. The QuantStudio Real Time PCR Software (version 1.3) was used for data analysis.

Statistical analyses

Data were analyzed using GraphPad Prism (version 9.4.1, GraphPad Software Inc., La Jolla, California). For high-content imaging data, Holm-Bonferroni-corrected 1-sample t test was used. For the nonlinear regression analysis, Log (inhibitor) versus response (3 parameters) model was used with the lowest response set as a constant equal to 0. For hormone production levels and mRNA transcript levels, 2-way ANOVA was used followed by the Dunnett's test. The minimum level of significance was $p < 0.05$. For qRT-PCR data, $p < 0.01$ was considered statistically significant. All experiments were repeated independently 5-6 times ($n = 5-6$).

RESULTS

Cytotoxicity of OPEs

Calcein positive Hoechst-stained nuclei were assessed as an indicator of cytotoxicity (Fig. 2A). IC_{50} values were calculated to compare the cytotoxicity among the test chemicals (Fig. 2B). BDE-47 (IC_{50} : 82.9 μ M) served as a reference legacy flame retardant. IPPP was the most cytotoxic OPE tested (IC_{50} : 8.0 μ M); cytotoxicity was observed at 5 μ M and very few live cells were observed at 100 μ M (Fig. 2A; Supplementary Fig. 1 (44)). TMPP, IPPP, and TPHP also demonstrated higher cytotoxicity than BDE-47. The cytotoxicity of TDCIPP (IC_{50} : 83.9 μ M) was comparable to that of BDE-47. TBOEP (IC_{50} : 220.6 μ M) only demonstrated cytotoxicity at the maximum concentration tested (100 μ M) and TCIPP did not demonstrate any cytotoxicity (Supplementary Fig. 1) (44). Notably, the OPEs that displayed higher cytotoxicity (TMPP, IPPP, and TPHP) than BDE-47 belonged to the triaryl-OPE group, sharing structural similarities characterized by the presence of three phenyl rings. Chemical concentrations that induced more than 30% cytotoxicity were excluded from the assessment of phenotypic endpoints.

Effect of OPEs on the phenotypic characteristics of H295R cells

Reactive oxygen species

CellROX staining intensity was assessed as an indicator of the production of reactive oxygen species. TMPP, TPHP, and TDCIPP all significantly decreased the level of CellROX staining (Fig. 3A). TMPP reduced CellROX staining to nearly 50% at 1 μ M and 5 μ M. Exposure to TPHP decreased CellROX staining only at one concentration, 10 μ M, whereas a wide variety of TDCIPP concentrations, starting as low as 0.1 μ M, decreased CellROX staining.

Mitochondria

The effects of OPEs on mitochondria were assessed using two fluorescent dyes. Mitotracker Green accumulates in the mitochondrial matrix regardless of the membrane potential and was

used to assess total numbers of mitochondria; Mitotracker Red accumulates only in active mitochondria (47). Exposure to TMPP (1 or 5 μ M), IPPP (5 μ M), or TPHP (0.1 to 20 μ M) induced minor increases (approximately 5-10%) in mitochondrial green intensity (Supplementary Fig. 2A) (44). The numbers of active mitochondria (Mitotracker red staining) were not affected by any of the chemicals tested (data not shown).

Lysosomes

Lysotracker Red, a dye that consists of a fluorophore linked to a weak base, becomes fluorescent once it is protonated and accumulates in an acidic environment. The intensity of this staining reflects the pH of lysosomes and thus can be used as an indicator of lysosome function (47, 48). Two parameters, lysosome numbers and lysosomal intensity, were assessed using this dye. Exposure to TMPP (10 μ M) or IPPP (5 μ M) decreased the numbers of lysosomes to 70% of control (Fig. 3B). Lysosome intensity was also decreased by BDE-47 and some OPEs (Supplementary Fig. 2B) (44). At 50 μ M, BDE-47 and TBOEP induced an approximately 30% decrease in Lysotracker red intensity; exposure to lower concentrations of TMPP (5 or 10 μ M) or IPPP (5 μ M) also induced a decrease (~10%) in lysosome intensity.

Lipid droplets

Nile Red, a dye that becomes fluorescent in a hydrophobic (lipid-rich) environment, was used to stain lipid droplets. Lipid droplets were not affected by exposure to BDE-47. However, exposure to all six OPEs increased the total area of lipid droplets in a concentration dependent manner (Fig. 3C). Exposure to TMPP (1 to 10 μ M) or IPPP (0.1 to 5 μ M) induced an up to 3-fold increase, whereas exposure to TPHP (10 or 20 μ M), TBOEP (5 to 50 μ M), TCIPP (5 to 100 μ M), or TDCIPP (5 to 50 μ M) induced a 1.2- to 1.5-fold increase in the area of lipid droplets.

Potency ranking of OPEs

Benchmark concentration analyses were done to calculate the concentrations of test chemicals that induced a 10% change from control, i.e., the BMC₁₀ values (Fig. 4). For each endpoint, BMC₁₀ values were determined only for chemicals that induced a significant change and passed the exclusion criteria. For cytotoxicity, the ranking of chemicals based on their BMC₁₀ values was very similar to that based on their IC₅₀ values: IPPP was the most potent OPE, and the triaryl-OPEs were more cytotoxic than BDE-47 or the nontriaryl-OPEs (Fig. 4).

The BMC₁₀ values for phenotypic endpoints were usually equivalent to or lower than the BMC₁₀ values associated with the induction of cytotoxicity. In comparison to BDE-47, OPEs affected more endpoints and their BMC₁₀ values were one to two orders of magnitude lower. TDCIPP had the lowest BMC₁₀ for oxidative stress (6.7 μ M). The BMC values for this endpoint for TMPP (BMC₁₀: 22.4 μ M) and TPHP (BMC₁₀: 22.9 μ M) were essentially the same. It was possible to calculate a BMC value for TMPP (BMC₁₀: 10.6 μ M) and IPPP (BMC₁₀: 3.2 μ M), but not for TPHP (poor model fit) for effects on the numbers of mitochondria. The BMC values for lysosomal intensity for TMPP (BMC₁₀: 3.6 μ M) and IPPP (BMC₁₀: 3.6 μ M) were considerably lower than those for BDE-47 (BMC₁₀: 41.3 μ M) or TBOEP (BMC₁₀: 88.3 μ M). The numbers of lysosomes were also affected by exposure to TMPP (BMC₁₀: 4.8 μ M) and IPPP (BMC₁₀: 1.9 μ M) at comparable BMC levels. The BMC values for a 10% increase in lipid droplets ranged between 0.2 μ M (IPPP) and 58.7 μ M (TCIPP), with IPPP being the most potent for this endpoint. The rank order of chemicals based on the lowest observed BMC₁₀ value, regardless of the endpoint, was: IPPP>TMPP>TPHP>TDCIPP>TBOEP>BDE-47>TCIPP.

ToxPi analyses

ToxPi analyses provide a strategy to rank chemicals based on their overall bioactivities; higher ToxPi scores indicate greater potency or toxicity. The ToxPi scores generated for each chemical, taking into consideration all the endpoints tested, are provided in Figure 5. Based on these ToxPi scores, the rank order of chemicals was: IPPP>TMPP>TPHP>TDCIPP>BDE-47>TBOEP>TCIPP.

Administered equivalent dose analyses

In vitro to *in vivo* modeling was done to relate the concentrations that induced an effect *in vitro* to *in vivo* exposure doses, i.e., the Administered Equivalent Dose (AED) (Fig. 6). The AED for IPPP was not calculated since this chemical had a high LogKow (octanol/water partition coefficient) value. BDE-47 was predicted to affect cell phenotypes at doses that ranged between 0.5-0.7 mg/kg bodyweight/day. In contrast, OPEs were predicted to affect these endpoints at doses as low as 0.0003 mg/kg bodyweight/day. The overall rank order of chemicals based on the lowest observed AED, regardless of the endpoint, was: TMPP>TPHP>TBOEP>TDCIPP>BDE-47>TCIPP. Aside from TBOEP, the overall ranking was very similar to the rank order determined by the lowest observed BMC₁₀ value approach.

Using three different ranking strategies, the triaryl-OPEs (TMPP, IPPP, and TPHP) were consistently ranked higher, suggesting that they are more potent than BDE-47 and the nontriaryl-OPEs. Thus, in the following assessment of the functional effect of OPEs, we selected the triaryl-OPEs to determine their effect on the steroidogenic function of H295R cells.

Effect of OPEs on the steroidogenic function of H295R cells

In order to evaluate the potential impact of OPEs on the steroidogenic capacity of H295R cells, we measured the levels of two key adrenal hormones, cortisol and aldosterone. The average basal level of cortisol produced by the cells was 1.5 pg/10⁶ cells (Fig. 7A). The presence of a steroidogenic stimulus, forskolin, increased the level of cortisol produced by the cells by approximately 9 times. A 48 h exposure to 5 μM IPPP doubled the amount of cortisol produced by the cells. However, exposure to either TMPP or TPHP decreased the concentration of cortisol by approximately 40%.

The baseline level of aldosterone produced by the cells was 100 pg/10⁶ cells (Fig. 7B); stimulation with forskolin increased this level by 3 times. Similar to the effect observed on cortisol production, exposure to IPPP (1 or 5 μM) induced an approximately 2.5-fold increase in the amount of aldosterone produced by the cells. TMPP had no effect on aldosterone production, whereas TPHP (1 μM) decreased the production of aldosterone by 26%. The production of cortisol or aldosterone in response to stimulation was not affected by any of the OPEs tested.

Effects of OPEs on the expression of key transcripts involved in steroidogenesis

We investigated the effects of OPEs on the expression of key transcripts involved in steroidogenesis under basal and stimulated conditions to determine whether the steroid-producing function of H295R cells was affected at this level. First, we assessed the expression of transcripts involved in the biosynthesis and transport of cholesterol, the precursor of all steroid hormones. The basal expression of HMGCR, the rate limiting enzyme in cholesterol biosynthesis, was slightly upregulated by all three OPEs (Fig. 8A). With forskolin stimulation, IPPP and TPHP induced an approximately 2-fold increase in HMGCR transcripts. The expression of STAR, a key protein involved in transporting cholesterol from the outer to inner mitochondria layer, closely correlated with the chemical-specific effects observed at the hormone

level (Fig. 8B). STAR expression was upregulated by IPPP but downregulated by TMPP and TPHP under both basal and stimulated conditions. NR5A1, an upstream regulator of the pathway, was affected only by IPPP and TMPP exposures (Fig. 8C). IPPP (5 μ M) induced a slight decrease in NR5A1 expression under both basal and stimulated conditions. TMPP (both 1 and 5 μ M) induced a decrease only under basal conditions.

We further assessed whether these three OPEs directly affect transcripts in the steroidogenic pathway (Fig. 9). CYP11A1, the rate limiting enzyme in steroid biosynthesis, was affected by exposure to either IPPP or TPHP, but only under stimulated conditions (Fig. 9A). Of note, the change in expression was similar to the effect observed on hormone levels. IPPP induced an increase the expression of CYP11A1, whereas a decrease was observed after exposure to TPHP. We then assessed effects on the expression of CYP11B1 and CYP11B2, the key enzymes responsible for the last step in the cortisol and aldosterone synthesis, respectively. IPPP induced a concentration dependent increase in basal and stimulated CYP11B1 expression (Fig. 9B). Notably, the increase under basal conditions was nearly 7-fold, in the range of the increase induced by forskolin stimulation. TMPP showed a trend towards an increase in the basal expression of CYP11B1 ($p = 0.05$). TPHP induced an approximately 2-fold increase in basal CYP11B1 expression; no effect was observed after stimulation. The largest increase in CYP11B2 expression was observed after exposure to IPPP (Fig. 9C); this concentration dependent increase was observed under both basal and stimulated conditions. Under basal conditions, there was a nearly 8-fold increase in cells exposed to 5 μ M IPPP. In the stimulated cells, the same IPPP concentration induced a \sim 2-fold increase. Exposure to TMPP led to a 3-fold increase in CYP11B2 expression under basal conditions. TPHP exposure led to a 2-fold increase in CYP11B2 expression under basal conditions and a 1.4-fold increase in stimulated cells.

DISCUSSION

In this study we demonstrated that OPEs affect H295R adrenal cell phenotypic parameters to a greater extent than BDE-47, a legacy brominated flame retardant. OPE exposures induced chemical-specific effects on adrenal cell steroidogenesis and, at the transcriptional level, on rate-limiting enzymes involved in cholesterol and steroid biosynthesis. To our knowledge, this is the first study to systematically compare the effects of OPEs on adrenal cell phenotypic characteristics and functional endpoints.

Few previous studies have tested the effects of OPEs on adrenal cells. Liu et al. (37) reported a 20% decrease in cell viability after the exposure of H295R cells to 30.7 μM of TPHP or 56.1 μM of TMPP. TMPP and TPHP were also among the more cytotoxic OPEs in another study with H295R cells in which they affected cell viability at concentrations an order of magnitude lower than those of TBOEP, TCIPP, or TDCIPP (39). This is also consistent with studies in other steroidogenic cells, such as the MA-10 Leydig cells, in which similar IC_{50} values (range between 10.3-27.5 μM , with IPPP being the most cytotoxic) were reported and all of the OPEs tested were more cytotoxic than BDE-47 (25). Furthermore, a structure-related effect was observed in KGN ovarian granulosa cells, where the triaryl-OPEs demonstrated higher potency in affecting steroid-producing activities compared to TBOEP (49). Interestingly, an association between the structures of the chemicals and their toxicity was also observed in KGN ovarian granulosa cells (27), in A549 lung epithelial cells (50), in HepG2 liver cells (51), and in CHO-K1 ovary cells (52); these data suggest that the cytotoxicity of OPEs may be related to their lipophilicity (Supplementary Table 2) (44).

The adrenal cell phenotypic parameters that were affected by OPEs include measures of reactive oxygen species, the numbers of mitochondria, lysosome numbers and their activity, and lipid droplet areas. These endpoints are key for the maintenance of normal cell functions. Oxidative stress levels were decreased in H295R cells after OPE exposures (Fig. 3A). Indeed,

the adrenal gland is well supplied with antioxidants that help to maintain redox homeostasis during steroidogenesis; these include enzymes such as glutathione peroxidases and superoxide dismutase (53). Interestingly, in silver carp larvae, TDCIPP, one of the OPEs that reduced oxidative stress levels in H295R cells, increased superoxide dismutase activity but decreased glutathione peroxidase (54). Further studies are required to assess the mechanisms by which some OPEs may decrease oxidative stress in adrenal cells. Mitochondria, the major site for the production of reactive oxygen species in cells, were also affected by some OPEs in H295R cells. Exposure to the three triaryl-OPEs induced a slight increase in the total number of mitochondria (Supplementary Fig. 2A) (44). A similar finding has been observed previously; in AML-12 liver cells, exposure to TPHP, TMPP, or TDCIPP increased the total area of mitochondria, reduced mitochondria network number, and depleted mitochondria membrane potentials (55).

In steroidogenic cells, lysosomes participate in the process of both the uptake of cholesterol from the circulation and the breakdown of lipid droplets to free the stored cholesterol which is the precursor for steroid hormone synthesis (56). A decrease in the number of lysosomes and potential disruption of lysosome function suggest that lipid homeostasis may be affected. Indeed, up to a 3-fold increase in the total area of lipid droplets was observed after OPE exposure (Fig. 3C). This is consistent with findings in KGN ovarian cells (27) and with the accumulation of lipids observed in *in vivo* experiments with mice or rats (31-35). In these animal studies, the accumulation of lipids in the adrenal gland was observed consistently in the cells of the zona glomerulosa and zona fasciculata. Those regions are actively involved in the biotransformation of cholesterol into cortisol (or corticosterone in mice or rats) and aldosterone. Moreover, Latendresse et al. (32) reported that TMPP could inhibit the activity of neutral cholesterol ester hydrolase (nCEH), an enzyme that catalyzes the conversion of stored cholesterol ester to free cholesterol. This action may lead to the buildup of cholesterol esters in the form of lipid droplets

in the adrenal gland.

We next undertook potency ranking analyses based on the phenotypic assessment data demonstrating that OPEs have differential effects on specific endpoints. The lowest BMC approach enabled the identification of chemicals that induced toxic effects on these endpoints at low concentrations. ToxPi analyses take into consideration the effects induced on all endpoints and provide an overall ranking of the chemicals. Both potency ranking approaches ranked the triaryl-OPEs as more potent than the non-triaryl chemicals. Our AED analyses predicted that the bioactive doses of OPEs range from 0.0003-2.96 mg/kg/day; importantly, these doses are much lower than those used in previous *in vivo* studies assessing the adrenal toxicity of OPEs, where the range was from 5-1700 mg/kg/day (31-36).

The three triaryl-OPEs with the highest potencies on phenotypic endpoints, IPPP, TMPP and TPHP, were selected to assess their impact on steroidogenesis in H295R cells. These OPEs showed chemical specific effects on the production of cortisol and aldosterone in the absence of forskolin stimulation. IPPP increased the secretion of cortisol whereas TMPP and TPHP decreased cortisol levels. Similarly, the aldosterone level was increased by IPPP, but decreased with TPHP exposures. Limited information is available in the literature on the effect of OPEs on cortisol and aldosterone levels. In a previous study with H295R cells, Zhang et al. (39) reported that TMPP (5 μ M) downregulated cortisol levels but had no effect on aldosterone; however, TPHP (5 μ M) increased the production of both cortisol and aldosterone. The effect of IPPP was not investigated and forskolin stimulation was not included in this study. In a human study (57), increased urinary OPE diester concentrations were associated with a 18%-41% increase in cortisol concentration in blood samples. Here, the OPE diesters included DPHP (a metabolite of IPPP and TPHP), BCIPP (a metabolite of TDCIPP), and BBOEP (a metabolite of TBOEP).

To identify the mechanism(s) responsible for the effects of OPEs on cortisol and

aldosterone production, we examined the effects of the three triaryl-OPEs at the transcriptional level. The expression level of HMGCR, the rate limiting enzyme in cholesterol biosynthesis, was upregulated by all three OPEs (Fig. 8A). In steroidogenic cells cholesterol is mainly stored as cholesterol esters in lipid droplets so an increase in the production of cholesterol may contribute to the increase in lipid droplets that we observed. STAR, which is involved in translocating cholesterol from the outer to inner mitochondrial membrane, may also play a role in regulating the adrenal production of hormones (58). We observed OPE-chemical specific effects on the expression of STAR under both basal and stimulated conditions (Fig. 8B). Previously, Zhang et al. (39) reported that TMPP increased HMGCR expression in H295R cells whereas exposure to TPHP decreased STAR expression. Next, we assessed the effects of OPE exposure on the expression of NR5A1, a key regulator of steroidogenesis in the adrenal, since SF-1, the product of this gene, has an essential role in regulating the expression of a number of steroidogenic genes, including CYP11B1 (59). The expression of NR5A1 was downregulated by both IPPP and TPHP, but the effect was small (Fig. 8C).

Exposure to IPPP or TPHP also impacted on the expression of the cytochromes P450 that catalyze critical steps in the biosynthesis of cortisol and aldosterone (CYP11A1, CYP11B1 and CYP11B2) (Fig. 9). The expression of CYP11B1 and CYP11B2, the transcripts that encode the final enzymes required for cortisol and aldosterone biosynthesis, were upregulated by all three triaryl-OPEs. It is also possible that OPEs affect the expression or activity of steroid hydroxylases by targeting other pathways. For example, the ACTH receptor and the angiotensin II receptor regulate the production of cortisol and aldosterone (60, 61); it remains to be elucidated whether OPEs affect the function of those two receptors. Moreover, the expression of CYP11B2 is suppressed by the PPAR γ receptor (62), which is a known target of TPHP (63). An upregulation of the level of CYP11B2 was also reported by Liu et al. (37) in H295R adrenal

cells. In another study that assessed the effect of nine OPEs on the steroidogenic pathway in H295R cells, TPHP and TMPP downregulated the expression of CYP11B1 after a 24 h exposure; CYP11B2 was not affected (39). This suggests that OPEs may induce different changes on transcription level of these genes at an earlier time point. Note that this study used a different cell culture medium and the cells were starved for 24 h before chemical treatment. These variations in experimental conditions may have contributed to the observed differences in downstream effects.

The H295R Steroidogenesis Assay has been incorporated into the Tier 1 Screening Battery of the United States Environmental Protection Agency (EPA) Endocrine Disruptor Screening Program (EDSP) (64). Our study expanded upon the H295R Steroidogenesis Assay and established a link between the impact of OPEs on steroidogenesis and the enzymatic activities of steroidogenic genes, along with the structural alterations observed in H295R cells. This connection provides valuable insights into the structure-function relationships underlying the action of OPEs. The possible targets of OPEs in the H295R human adrenal cells are presented schematically in Figure 10. Our findings demonstrate that OPEs affect the adrenal gland at both the structural and functional levels, leading to disruptions in the production of cortisol and aldosterone. Abnormal adrenal steroid production is associated with various diseases, including hypertension and metabolic syndrome, such as Addison's disease (adrenal steroid insufficiency) and primary aldosteronism (excess mineralocorticoid production). Consequently, our data provide compelling evidence for the endocrine-disrupting properties of OPEs and highlight the adrenal gland as an important target of OPE-induced effects.

REFERENCES

1. Sharkey M, Harrad S, Abdallah MAE, Drage DS, Berresheim H. Phasing-out of legacy brominated flame retardants: The UNEP Stockholm Convention and other legislative action worldwide. *Environ Int.* 2020;144:106041.
2. Stapleton HM, Sharma S, Getzinger G, Ferguson PL, Gabriel M, Webster TF, Blum A. Novel and High Volume Use Flame Retardants in US Couches Reflective of the 2005 PentaBDE Phase Out. *Environ Sci Technol.* 2012;46(24):13432-13439.
3. Veen I van der, Boer J de. Phosphorus flame retardants: Properties, production, environmental occurrence, toxicity and analysis. *Chemosphere.* 2012;88(10):1119-1153.
4. Hou R, Xu Y, Wang Z. Review of OPFRs in animals and humans: Absorption, bioaccumulation, metabolism, and internal exposure research. *Chemosphere.* 2016;153:78-90.
5. Greaves AK, Letcher RJ. A Review of Organophosphate Esters in the Environment from Biological Effects to Distribution and Fate. *B Environ Contam Tox.* 2017;98(1):2-7.
6. Struzina L, Castro MAP, Kubwabo C, Siddique S, Zhang G, Fan X, Tian L, Bayen S, Aneck-Hahn N, Bornman R, Chevrier J, Misunis M, Yargeau V. Occurrence of legacy and replacement plasticizers, bisphenols, and flame retardants in potable water in Montreal and South Africa. *Sci Total Environ.* 2022;840:156581.
7. Stapleton HM, Misenheimer J, Hoffman K, Webster TF. Flame retardant associations between children's handwipes and house dust. *Chemosphere.* 2014;116:54-60.
8. He C, Wang X, Thai P, Baduel C, Gallen C, Banks A, Bainton P, English K, Mueller JF. Organophosphate and brominated flame retardants in Australian indoor environments: Levels, sources, and preliminary assessment of human exposure. *Environ Pollut.* 2018;235:670-679.

9. Dirtu AC, Ali N, Eede NV den, Neels H, Covaci A. Country specific comparison for profile of chlorinated, brominated and phosphate organic contaminants in indoor dust. Case study for Eastern Romania, 2010. *Environ Int.* 2012;49:1-8.
10. Blum A, Behl M, Birnbaum LS, Diamond ML, Phillips A, Singla V, Sipes NS, Stapleton HM, Venier M. Organophosphate Ester Flame Retardants: Are They a Regrettable Substitution for Polybrominated Diphenyl Ethers? *Environ Sci Tech Let.* 2019;6(11):638-649.
11. Percy Z, Guardia MJL, Xu Y, Hale RC, Dietrich KN, Lanphear BP, Yolton K, Vuong AM, Cecil KM, Braun JM, Xie C, Chen A. Concentrations and loadings of organophosphate and replacement brominated flame retardants in house dust from the home study during the PBDE phase-out. *Chemosphere.* 2020;239:124701.
12. Liu LY, Salamova A, He K, Hites RA. Analysis of polybrominated diphenyl ethers and emerging halogenated and organophosphate flame retardants in human hair and nails. *J Chromatogr A.* 2015;1406:251-257.
13. Liu LY, He K, Hites RA, Salamova A. Hair and Nails as Noninvasive Biomarkers of Human Exposure to Brominated and Organophosphate Flame Retardants. *Environ Sci Technol.* 2016;50(6):3065-3073.
14. Health Canada. Summary of flame retardant assessments and management conducted under the Canadian Environmental Protection Act, 1999. Updated February 22, 2022. Accessed March 27, 2023. <https://www.canada.ca/en/environment-climate-change/services/evaluating-existing-substances/summary-flame-retardant-assessments-management-conducted-cepa.html>.
15. United States Environmental Protection Agency (U.S. EPA). Health and Safety Data Reporting: Addition of 20 High-Priority Substances and 30 Organohalogen Flame

Retardants. Updated October 11, 2022. Accessed March 23, 2023.

<https://www.epa.gov/chemicals-under-tsca/health-and-safety-data-reporting-addition-20-high-priority-substances-and-30>.

16. European chemical agency (ECHA). Regulatory strategy for flame retardants. Published March 2023. Accessed April 9, 2023.
https://echa.europa.eu/documents/10162/2082415/flame_retardants_strategy_en.pdf/9dd56b7e-4b62-e31b-712f-16cc51d0e724?t=1679045593845.
17. Kojima H, Takeuchi S, Itoh T, Iida M, Kobayashi S, Yoshida T. In vitro endocrine disruption potential of organophosphate flame retardants via human nuclear receptors. *Toxicology*. 2013;314(1),76-83.
18. Castorina R, Bradman A, Stapleton HM, Butt C, Avery D, Harley KG, Gunier RB, Holland N, Eskenazi B. Current-use flame retardants: Maternal exposure and neurodevelopment in children of the CHAMACOS cohort. *Chemosphere*. 2017;189:574-580.
19. Lipscomb ST, McClelland MM, MacDonald M, Cardenas A, Anderson KA, Kile ML. Cross-sectional study of social behaviors in preschool children and exposure to flame retardants. *Environ Health-uk*. 2017;16(1):23.
20. Pei Y, Peng J, Behl M, Sipes NS, Shockley KR, Rao MS, Tice RR, Zeng X. Comparative neurotoxicity screening in human iPSC-derived neural stem cells, neurons and astrocytes. *Brain Res*. 2016;1638(Pt A):57-73.
21. Fernie KJ, Palace V, Peters LE, Basu N, Letcher RJ, Karouna-Renier NK, Schultz SL, Lazarus RS, Rattner BA. Investigating endocrine and physiological parameters of captive American kestrels exposed by diet to selected organophosphate flame retardants. *Environ. Sci. Technol*. 2015;49,7448-7455.

22. Meeker JD, Stapleton HM. (2010). House dust concentrations of organophosphate flame retardants in relation to hormone levels and semen quality parameters. *Environ. Health Perspect.* 118(3),318-323.
23. Siddique S, Farhat I, Kubwabo C, Chan P, Goodyer CG, Robaire B, Chevrier J. Hales BF. Exposure of men living in the greater Montreal area to organophosphate esters: Association with hormonal balance and semen quality. *Environ. Int.* 2022;166,107402.
24. Luo K, Liu J, Wang Y, Aimuzi R, Luo F, Ao J, Zhang J. Associations between organophosphate esters and sex hormones among 6–19-year old children and adolescents in NHANES 2013–2014. *Environ Int.* 2020;136:105461.
25. Schang G, Robaire B, Hales BF. Organophosphate Flame Retardants Act as Endocrine-Disrupting Chemicals in MA-10 Mouse Tumor Leydig Cells. *Toxicol Sci.* 2016;150(2):499-509.
26. Rajkumar A, Luu T, Hales BF, Robaire B. High-content imaging analyses of the effects of bisphenols and organophosphate esters on TM4 mouse Sertoli cells. *Biol Reprod.* 2022;107(3):858-868.
27. Wang X, Luu T, Beal MA, Barton-Maclaren TS, Robaire B, Hales BF. The Effects of Organophosphate Esters Used as Flame Retardants and Plasticizers on Granulosa, Leydig, and Spermatogonial Cells Analyzed Using High-Content Imaging. *Toxicol Sci.* 2022;186(2):269-287.
28. Hinson JP, Raven PW. Effects of endocrine-disrupting chemicals on adrenal function. *Best Pract Res Cl En.* 2006;20(1):111-120.
29. Ribelin WE. The effects of drugs and chemicals upon the structure of the adrenal gland. *Fund Appl Toxicol.* 1984;4(1):105-119.
30. Lee S, Martinez–Arguelles D, Campioli E, Papadopoulos V. Fetal Exposure to Low

Levels of the Plasticizer DEHP Predisposes the Adult Male Adrenal Gland for Endocrine Disruption. *Endocrinology*. 2017;158(2):304-318.

31. National Toxicology Program. NTP Toxicology and Carcinogenesis Studies of Tricresyl Phosphate (CAS No. 1330-78-5) in F344/N Rats and B6C3F1 Mice (Gavage and Feed Studies). *Natl Toxicol Program Tech Rep Ser*. 1994;433:1-321.
32. Latendresse JR, Azhar S, Brooks CL, Capen CC. Pathogenesis of Cholesteryl Lipidosis of Adrenocortical and Ovarian Interstitial Cells in F344 Rats Caused by Tricresyl Phosphate and Butylated Triphenyl Phosphate. *Toxicol Appl Pharm*. 1993;122(2):281-289.
33. Latendresse JR, Brooks CL, Capen CC. Pathologic Effects of Butylated Triphenyl Phosphate-Based Hydraulic Fluid and Tricresyl Phosphate on the Adrenal Gland, Ovary, and Testis in the Fischer-344 Rat. *Toxicol Pathol*. 1994;22(4):341-352.
34. Latendresse JR, Brooks CL, Capen CC. Toxic Effects of Butylated Triphenyl Phosphate-based Hydraulic Fluid and Tricresyl Phosphate in Female F344 Rats. *Vet Pathol*. 1995;32(4):394-402.
35. Wade MG, Kawata A, Rigden M, Caldwell D, Holloway AC. Toxicity of Flame Retardant Isopropylated Triphenyl Phosphate: Liver, Adrenal, and Metabolic Effects. *Int J Toxicol*. 2019;38(4):279-290.
36. Akimoto T, Kobayashi S, Nakayama A, et al. Toxicological effects of Tris (1,3-dichloro-2-propyl) phosphate exposure in adult male rats differ depending on the history of exposure in the neonatal period. *J Appl Toxicol*. 2022;42(9):1503-1509.
37. Liu X, Ji K, Choi K. Endocrine disruption potentials of organophosphate flame retardants and related mechanisms in H295R and MVLN cell lines and in zebrafish. *Aquat Toxicol*. 2012;114-115:173-181.

38. Chang Y, Cui H, Jiang X, Li M. Comparative assessment of neurotoxicity impacts induced by alkyl tri-n-butyl phosphate and aromatic tricresyl phosphate in PC12 cells. *Environ Toxicol.* 2020;35(12):1326-1333.
39. Zhang Q, Wang J, Zhu J, Liu J, Zhao M. Potential Glucocorticoid and Mineralocorticoid Effects of Nine Organophosphate Flame Retardants. *Environ Sci Technol.* 2017;51(10):5803-5810.
40. Zhang Q, Yu C, Fu L, Gu S, Wang C. New Insights in the Endocrine Disrupting Effects of Three Primary Metabolites of Organophosphate Flame Retardants. *Environ Sci Technol.* 2020;54(7):4465-4474.
41. OECD. Test No. 456: H295R Steroidogenesis Assay: OECD Guidelines for the Testing of Chemicals. OECD Publishing. 2022;Section 4.
42. Fan X, Kubwabo C, Rasmussen PE, Wu F. Simultaneous determination of thirteen organophosphate esters in settled indoor house dust and a comparison between two sampling techniques. *Sci. Total Environ.* 2014;491–492:80-86.
43. Kubwabo C, Fan X, Katuri GP, Habibagahi A, Rasmussen PE. Occurrence of aryl and alkyl-aryl phosphates in Canadian house dust. *Emerg. Contam.* 2021;7:149-159.
44. Li Z, Robaire B, Hales BF. Supplementary data for The Organophosphate Esters Used as Flame Retardants and Plasticizers affect H295R Adrenal Cell Phenotypes and Functions. Published July 24, 2023. <https://doi.org/10.6084/m9.figshare.23672913.v1>
45. United States Environmental Protection Agency (U.S. EPA). Benchmark Dose Technical Guidance. Washington, DC 20460: Risk Assessment Forum, U.S. EPA Report EPA/100/R-12/001. Published June 2012. Accessed April 18, 2023. <https://www.epa.gov/risk/benchmark-dose-technical-guidance>.
46. Health Canada. Science Approach Document: Bioactivity Exposure Ratio: Application in

- Priority Setting and Risk Assessment. Published March 2021. Accessed April 18, 2023.
<https://www.canada.ca/en/environment-climate-change/services/evaluating-existing-substances/science-approach-document-bioactivity-exposure-ratio-application-priority-setting-risk-assessment.html>.
47. Iain DJ. Chapter 12: probes for organelles. In: Molecular Probes Handbook: A guide to fluorescent probes and labeling technologies. 11th ed. Life technologies Inc; 2010:495-543.
48. Chazotte B. Labeling lysosomes in live cells with LysoTracker. Cold Spring Harb. Protoc. 2011,pdb.prot5571.
49. Wang X, Lee E, Hales BF, Robaire B. Organophosphate Esters Disrupt Steroidogenesis in KGN Human Ovarian Granulosa Cells. Endocrinology. Published online 2023.
doi:10.1210/endocr/bqad089.
50. Yuan S, Zhu K, Ma M, Zhu X, Rao K, Wang Z. In vitro oxidative stress, mitochondrial impairment and G1 phase cell cycle arrest induced by alkyl-phosphorus-containing flame retardants. Chemosphere. 2020;248:126026.
51. Zhou Y, Liao H, Yin S, Wang P, Ye X, Zhang J. Aryl-, halogenated- and alkyl-organophosphate esters induced oxidative stress, endoplasmic reticulum stress and NLRP3 inflammasome activation in HepG2 cells. Environ Pollut. 2023;316(Pt 1):120559.
52. Huang C, Li N, Yuan S, Ji X, Ma M, Rao K, Wang Z. Aryl- and alkyl-phosphorus-containing flame retardants induced mitochondrial impairment and cell death in Chinese hamster ovary (CHO-k1) cells. Environ Pollut. 2017;230:775-786.
53. Prasad R, Kowalczyk JC, Meimaridou E, Storr HL, Metherell LA. Oxidative stress and adrenocortical insufficiency. J Endocrinol. 2014;221(3):R63-R73.
54. Yang H, Pu Y, Liu C, Gao L, Duan X, Liu S, Chen D, Zhong L, Li Y. Environmentally

relevant concentrations of tris (1,3-dichloro-2-propyl) phosphate induce growth inhibition and oxidative stress in silver carp (*Hypophthalmichthys molitrix*) larvae. *Ecotox Environ Safe*. 2022;241:113798.

55. Le Y, Shen H, Yang Z, Lu D, Wang C. Comprehensive analysis of organophosphorus flame retardant-induced mitochondrial abnormalities: Potential role in lipid accumulation. *Environ Pollut*. 2021;274:116541.
56. Mesmin B, Antonny B, Drin G. Insights into the mechanisms of sterol transport between organelles. *Cellular and molecular life sciences: CMLS*. 2013;70:3405-3421.
57. Ji Y, Yao Y, Duan Y, Zhao H, Hong Y, Cai Z, Sun H. Association between urinary organophosphate flame retardant diesters and steroid hormones: A metabolomic study on type 2 diabetes mellitus cases and controls. *Sci Total Environ*. 2021;756:143836.
58. Papadopoulos V, Miller WL. Role of mitochondria in steroidogenesis. *Best Pract Res Clin En*. 2012;26(6):771-790.
59. Bassett M, Zhang Y, Clyne C, White P, Rainey W. Differential regulation of aldosterone synthase and 11beta-hydroxylase transcription by steroidogenic factor-1. *J Mol Endocrinol*. 2002;28(2):125-135.
60. Nogueira EF, Rainey WE. Regulation of Aldosterone Synthase by Activator Transcription Factor/cAMP Response Element-Binding Protein Family Members. *Endocrinology*. 2010;151(3):1060-1070.
61. Gallo PN, Payet MD. Mechanism of action of ACTH: Beyond cAMP. *Microsc Res Tech*. 2003;61(3):275-287.
62. Uruno A, Matsuda K, Noguchi N, Yoshikawa T, Kudo M, Satoh F, Rainey WE, Hui XG, Akahira J ichi, Nakamura Y, Sasano H, Okamoto H, Ito S, Sugawara A. Peroxisome proliferator-activated receptor- γ suppresses CYP11B2 expression and aldosterone

production. J Mol Endocrinol. 2011;46(1):37-49.

63. Belcher SM, Cookman CJ, Patisaul HB, Stapleton HM. In vitro assessment of human nuclear hormone receptor activity and cytotoxicity of the flame retardant mixture FM 550 and its triarylphosphate and brominated components. Toxicol Lett. 2014;228(2):93-102.
64. United States Environmental Protection Agency (U.S. EPA). Endocrine Disruptor Screening Program (EDSP); Announcing the Availability of the Tier 1 Screening Battery and Related Test Guidelines. Published October 21, 2009. Accessed June 2, 2023.
<https://www.regulations.gov/document/EPA-HQ-OPPT-2008-0521-0001>.

FIGURES

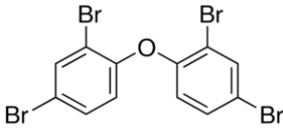
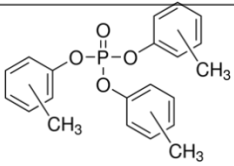
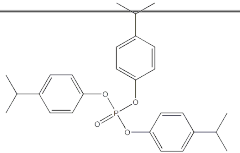
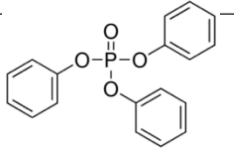
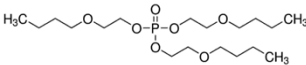
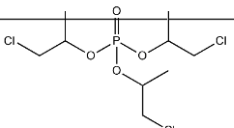
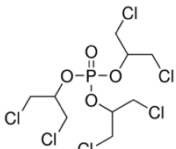
Chemical (acronym)	CAS No.	Structure	Supplier (Purity)
2,2',4,4'-tetrabromodiphenyl ether (BDE-47)	5436-43-1		Sigma-Aldrich (98.0%)
Tris(methylphenyl) phosphate (TMPP)	1330-78-5		Sigma-Aldrich (98.6%)
Isopropylated triphenyl phosphate (IPPP)	68937-41-7		NIEHS/NTP (N/A)
Triphenyl phosphate (TPHP)	115-86-6		Sigma-Aldrich (99.9%)
Tris(2-butoxyethyl) phosphate (TBOEP)	78-51-3		Sigma-Aldrich (93.6%)
Tris(1-chloro-2-propyl) phosphate (TCIPP)	13674-84-5		AK Scientific (90.0%)
Tris(1,3-dichloro-2-propyl) phosphate (TDCIPP)	13674-87-8		TCI America (95.9%)

Figure 2-1. List of Chemicals Tested.

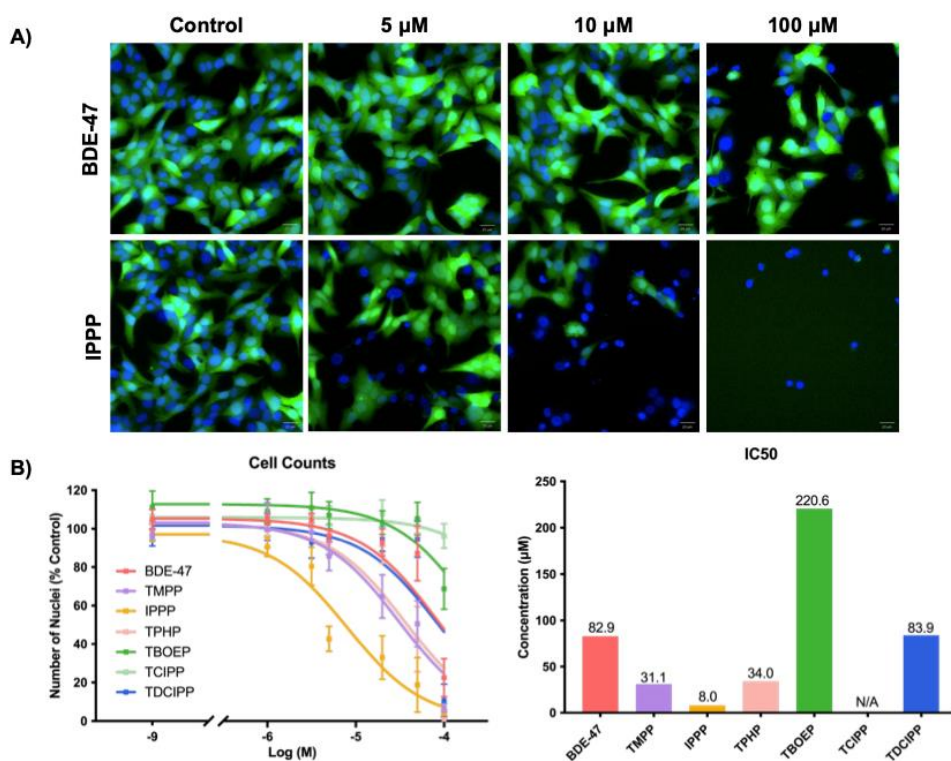


Figure 2-2. Effects of 2,2',4,4'-tetrabromodiphenyl ether (BDE-47) and organophosphate esters (OPEs) on cell viability. Cells were exposed to one of the chemicals for 48 h, followed by staining with Hoechst 33342 (blue, nuclei) and Calcein-AM (green, viable cells) fluorescent dyes. The numbers of viable cells were visualized and quantified with the Operetta High Content Imaging System (40 x magnification). A) Representative images of cells exposed to BDE-47 or IPPP at concentrations of 5 μ M, 10 μ M or 100 μ M. B) Nonlinear regression analyses were conducted to estimate the IC₅₀ values of the test chemicals. Data are shown as percentages relative to controls; values represent means \pm SEM; n = 6. Abbreviation: N/A, not available/applicable.

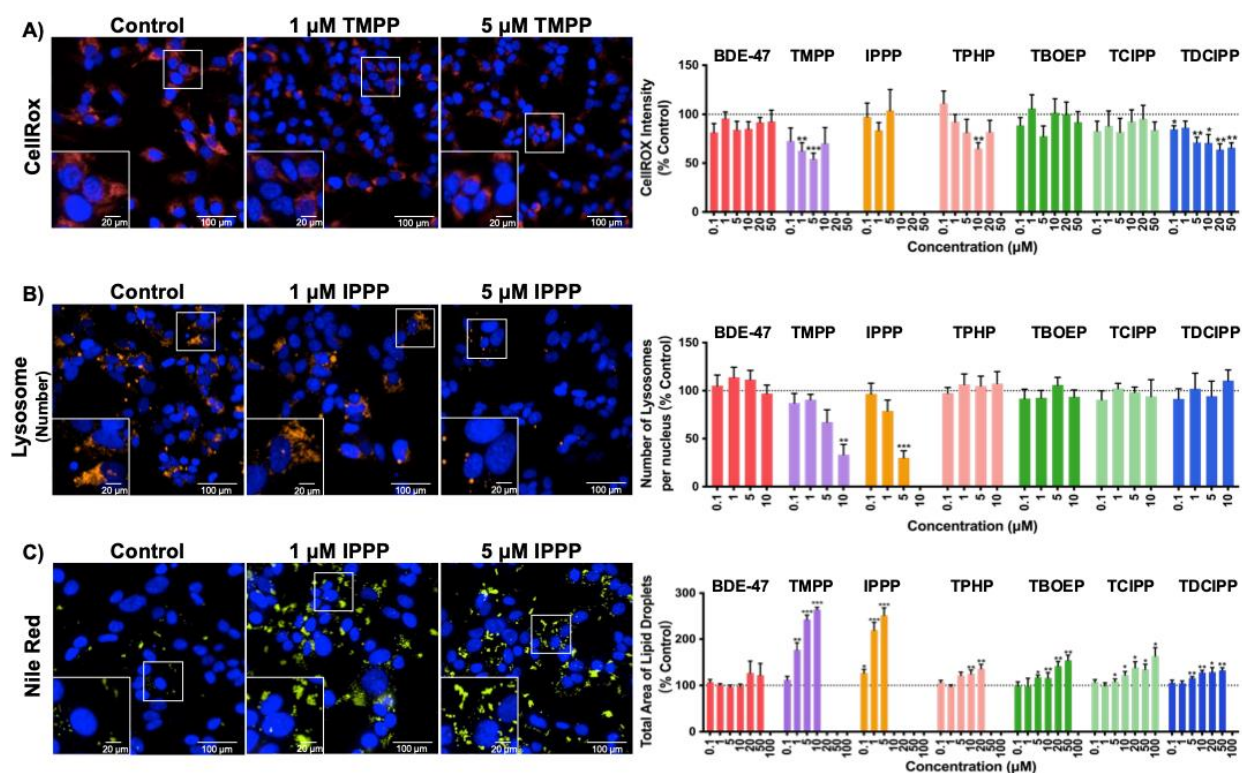


Figure 2-3. Effects of 2,2',4,4'-tetrabromodiphenyl ether (BDE-47) and organophosphate esters (OPEs) on the phenotypic characteristics of H295R cells. Cells were stained with: A) Hoechst 33342 (blue, nuclei) and CellROX (red, an indicator of oxidative stress); B) Hoechst 33342 (blue, nuclei) and Lysotracker Red (orange, lysosome numbers); C) Hoechst 33342 (blue, nuclei) and Nile Red (yellow, lipid droplets) fluorescent dyes and were visualized with the Operetta high content imaging system (40 x magnification). Data are shown as percentages relative to controls; values represent means \pm SEM; n = 6. *p<.05, **p<.01, and ***p<.001 compared to control. Concentrations that induced > 30% cytotoxicity were excluded from the analyses and were not shown.

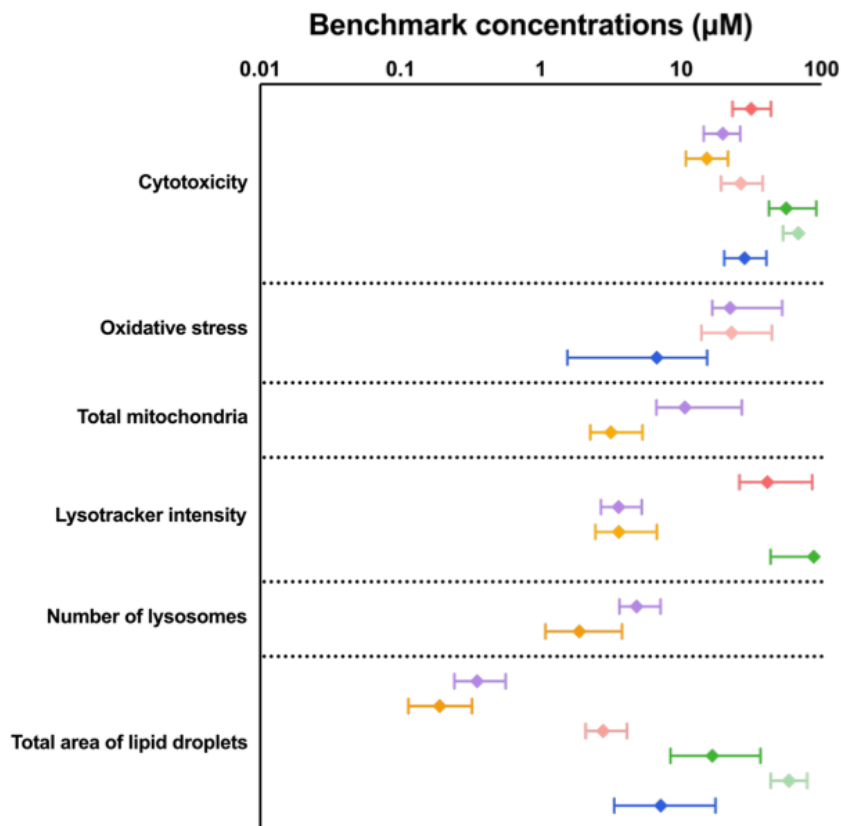


Figure 2-4. Benchmark concentration (BMC, μM) values of the test chemicals for all phenotypic endpoints. Data points represent BMC_{10} values (concentrations that induced a 10% change from control). Error bars represent means \pm upper and lower limits; $n = 6$. For each endpoint, chemicals that are not shown on the graph either had no effect on that endpoint or failed to generate a significant benchmark model.

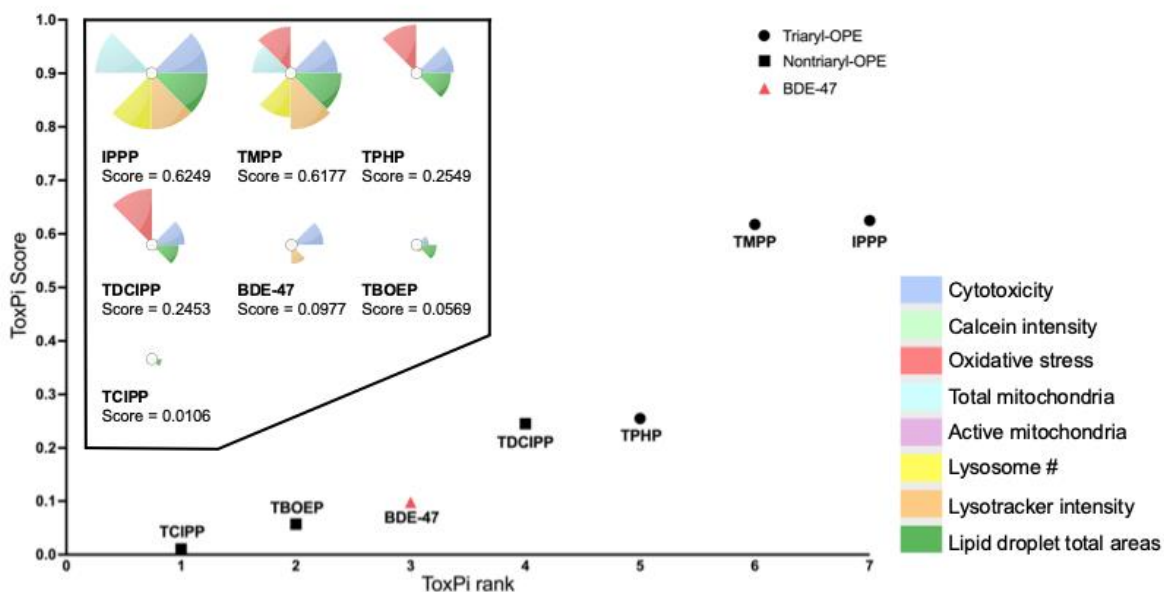


Figure 2-5. Toxicological Prioritization Index (ToxPi) analyses for chemical ranking. ToxPi profiles for each chemical and their ToxPi scores are displayed in the box. Eight endpoints were analyzed; endpoints were weighted equally. Different symbols were used to differentiate between chemicals with different structural characteristics: triaryl-OPE (circle), nontriaryl-OPE (square), BDE-47 (triangle). Ranking of chemicals was based on their overall bioactivities: chemicals with the highest ToxPi scores were considered the most potent and were ranked accordingly.

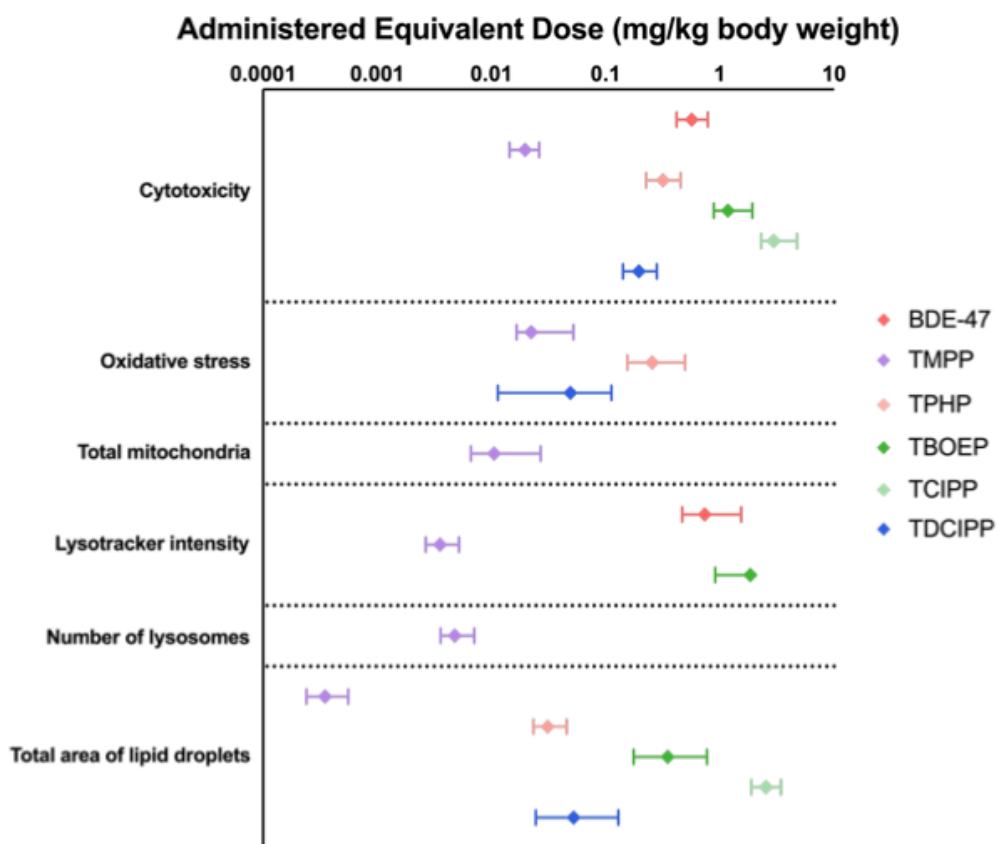


Figure 2-6. Administered equivalent dose (AED, mg/kg body weight) values of the test chemical for all phenotypic endpoints. Data are shown as means \pm upper and lower limits; $n = 6$. The AED values for IPPP were not calculated due to its high octanol/water partition coefficient (LogKow) and clearance values.

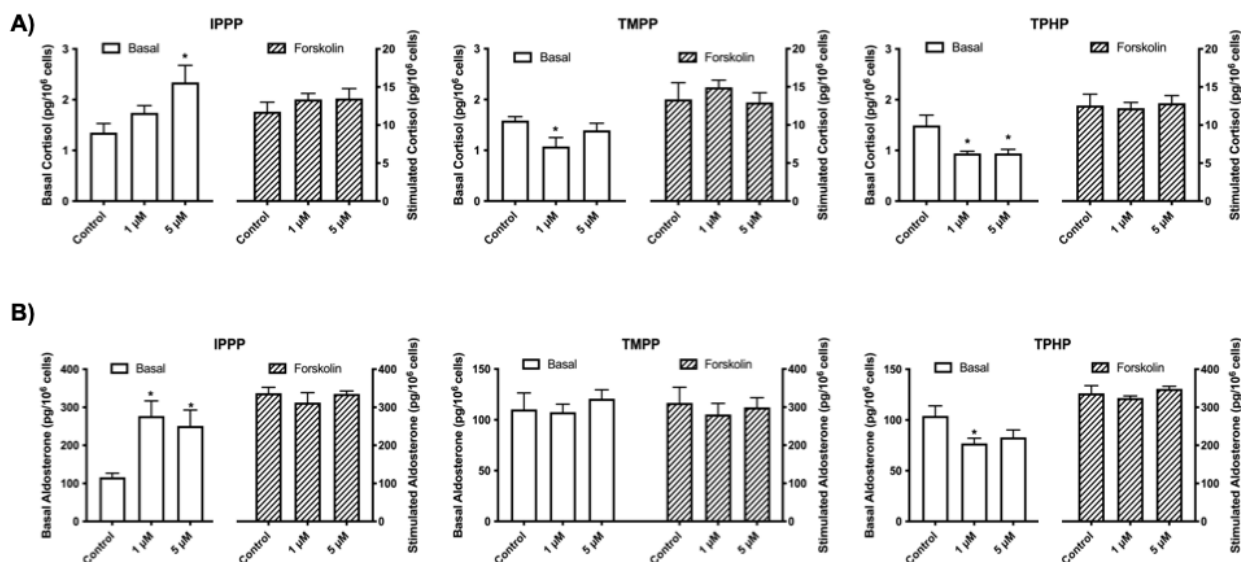


Figure 2-7. Effects of IPPP, TMPP, and TPHP on the steroid-producing functions of H295R cells. Cells were exposed to one of the chemicals at 1 μ M or 5 μ M for 48 h. A concentration of 10 μ M forskolin was used for the stimulated condition. Numbers of cells were quantified by Hoechst 33342 staining and high content imaging (20 x magnification). Bar graphs show basal (left Y axis, white bars) and stimulated (right Y axis, striped bars) production of cortisol A) and aldosterone B) levels. * $p < 0.05$ compared to control; values represent means \pm SEM; $n = 5$.

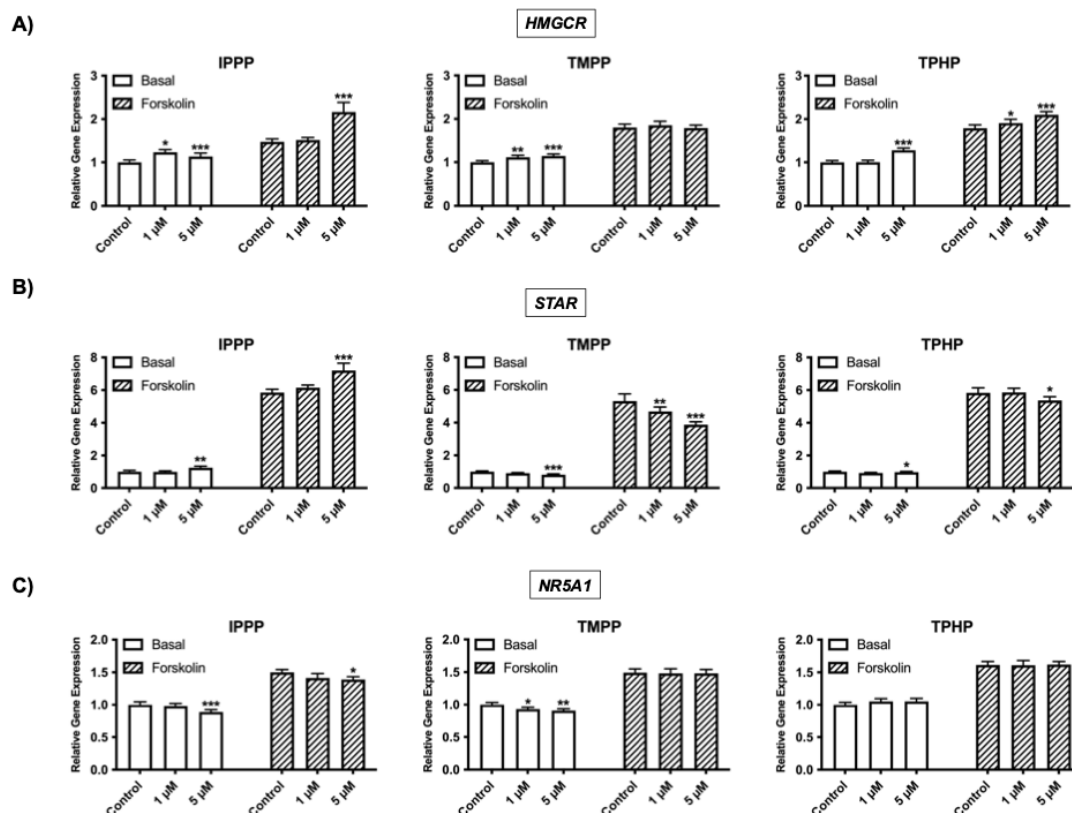


Figure 2-8. Effects of IPPP, TMPP, and TPHP on the mRNA expression levels of the rate-limiting enzymes in cholesterol biosynthesis: (A) HMGCR, a rate limiting enzyme in cholesterol synthesis; (B) STAR, a cholesterol transporter; and (C) NR5A1, an upstream regulator, in H295R cells under basal and stimulated conditions. Cells were exposed to one of the chemicals at 1 μ M or 5 μ M for 48 h. For the stimulated condition, a concentration of 10 μ M forskolin was used. Data represent means \pm 95% CI, n = 5. *p<0.01, **p<0.001, ***p<0.0001 compared to control.

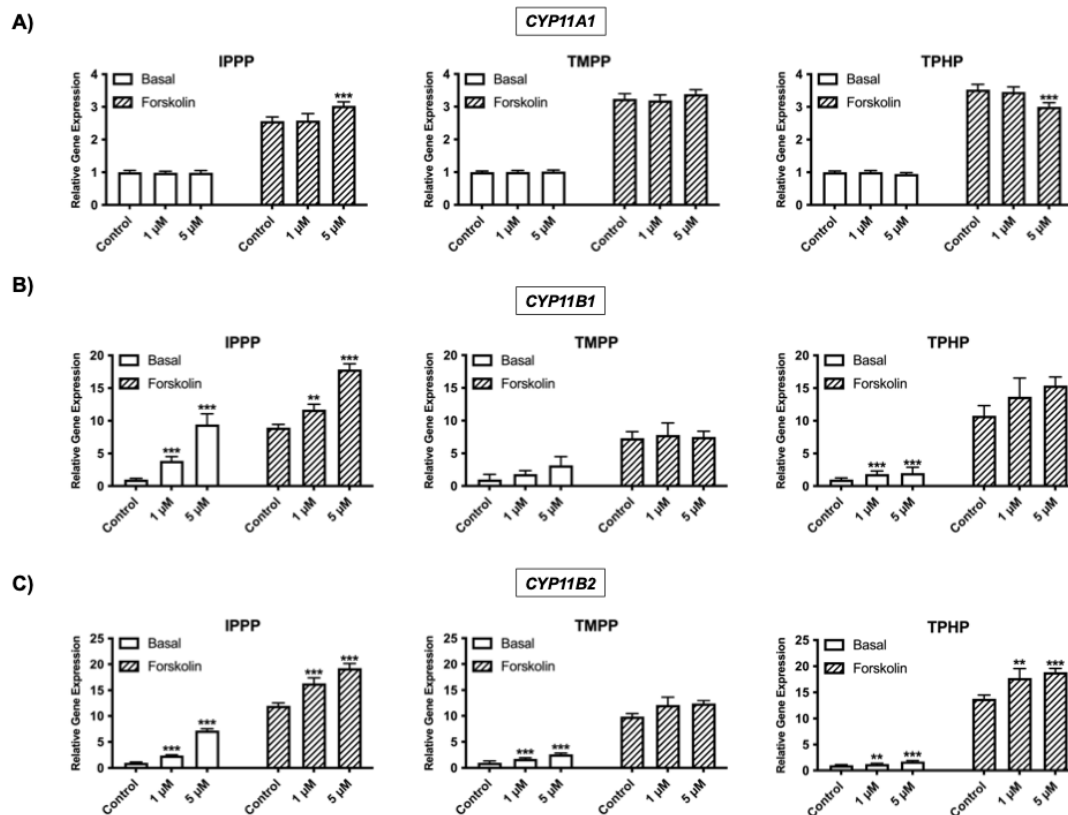
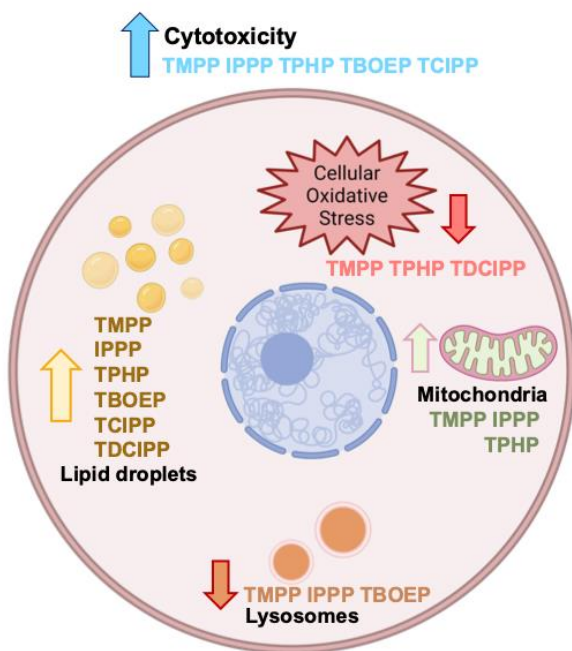


Figure 2-9. Effects of IPPP, TMPP, and TPHP on the mRNA expression of key steroidogenic enzymes: A: CYP11A1; B: CYP11B1; C: CYP11B2 in H295R cells under basal and stimulated conditions. Cells were exposed to one of the chemicals at 1 μ M or 5 μ M for 48 h. For the stimulated condition, a concentration of 10 μ M forskolin was used. Data represent means \pm 95% CI, n = 5. *p<0.01, **p<0.001, ***p<0.0001 compared to control.

A) Phenotype



B) Function

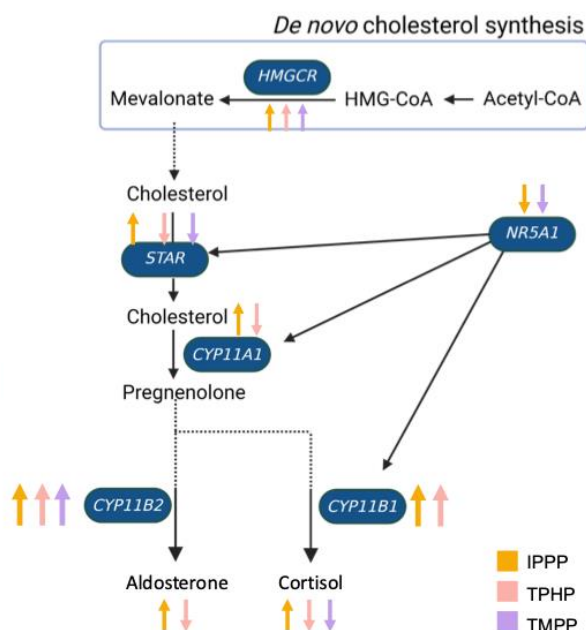


Figure 2-10. Summary of the A) phenotypic and B) functional effects of OPEs on H295R human adrenal cells. A) Exposure to most OPEs increased cytotoxicity, reduced oxidative stress levels, increased the numbers of mitochondria, decreased lysosome numbers and lysosomal intensity, and increased the area of lipid droplets. B) The three triaryl-OPEs targeted the steroidogenic pathway by affecting the expression of key enzymes involved in the rate-limiting steps in cholesterol and steroid biosynthesis, resulting in alterations in the levels of cortisol and aldosterone. A larger arrow suggests a greater effect size, indicating a more pronounced impact of OPEs on the endpoints. IPPP: yellow arrow; TPHP: pink arrow; TMPP: purple arrow. Created with BioRender.com.

SUPPLEMENTAL MATERIALS

Supplemental Method

Image acquisition and processing for high-content screening.

For all dye combinations: images were imported into the Columbus software for analysis. The setup was as follows: individual planes, advanced flatfield correction (basic if advanced was not available).

Combination 1: Hoechst 33342/Calcein-AM/Lysotracker Red

To identify nuclei: [Find nuclei] - channel Hoechst 33342, method C (common threshold = 0.2, area > 30 μm^2 , split coefficient = 7, individual threshold = 0.5, contrast > 0.1).

To assess the morphology and intensity of the nuclei: [Calculate morphology properties] - population: nuclei, region: nucleus, method: standard area (μm^2) and roundness; [Calculate intensity properties]: channel: Hoechst 33342, population: nuclei, region: nucleus; method standard, mean. To exclude outliers: [Select population] - population: nuclei, method: filter by property (filter F1 = intensity < 2000). To identify the cytoplasmic areas: [Find Cytoplasm] - channel: Calcein green, nuclei selected; method A (individual threshold = 0.15). To assess the intensity of the cytoplasmic area: [Calculate intensity properties (2)] - channel: Calcein green, population: nuclei selected, region: cytoplasm, method: standard (mean). To define the Calcein-positive viable cells: [Select Population (2)] - population: nuclei selected, method: filter by properties (filter F1 = intensity > 100). To identify lysosomes: [Find spots] - channel lysotracker red, region of interest (ROI) population: Nuclei selected, ROI region: cell, method A (relative spot intensity > 0.075, splitting coefficient = 1). To assess the morphology and intensity of the lysosomes: [Calculate morphology properties (2)] - population: nuclei selected, region: cell, method: standard (area (μm^2) and roundness); [Calculate intensity properties (3)]:

channel: lysotracker red, population: spots, region: spot maximum, method: standard (mean). To exclude outliers: [Select population (3)] - population: spots, method: filter by property (Filter F1, intensity < 10,000, filter F2 = spot area < 200 px²).

The outputs of combination 1 included: the number of nuclei, Calcein intensity, the Calcein-positive ratio (i.e., the number of Calcein-positive cells divided by the total number of selected nuclei), the number of lysosomes per cell, and the average intensity of Lysotracker Red staining.

Combination 2: Hoechst 33342/Mitotracker Green/Mitotracker Red/Cellmask

To identify nuclei: [Find nuclei] - channel Hoechst 33342, method C (common threshold = 0.2, area > 30 μm^2 , split coefficient = 7, individual threshold = 0.5, contrast > 0.1).

To assess the morphology and intensity of the nuclei: [Calculate morphology properties] - population: nuclei, region: nucleus, method: standard (area (μm^2) and roundness); [Calculate intensity properties] - channel: Hoechst 33342, population: nuclei, region: nucleus; method standard (mean). To exclude outliers: [Select population] - population: nuclei, method: filter by property (filter F1: intensity < 2000). To identify the cytoplasmic areas: [Find Cytoplasm] - channel: Cellmask Deep Red, nuclei selected, method: F (individual threshold = 0.15). To determine total mitochondria intensity: [Find Image Region] - channel: Mitotracker Green, ROI population: nuclei selected, ROI region: cell; method (common threshold = 0.35, split into objects, area > 0 px²). To assess the mean staining intensity of mitochondria: [Calculate Intensity Properties (2)] - channel: Mitotracker Green, population: mitogreen, region: mitochondria, method: standard (mean); [Calculate Intensity Properties (3)] - channel: Mitotracker Red, population: mitored, region: mitochondria, method: standard (mean). The outputs of combination

included: the number of nuclei, the average intensity of Mitotracker Green staining, the average intensity of Mitotracker Red staining, and the active to total mitochondria ratio (average intensity of Mitotracker Red/Mitotracker Green).

Combination 3: Hoechst 33342/Calcein-AM/CellROX

To identify nuclei: [Find nuclei] - channel Hoechst 33342, method C (common threshold = 0.2, area > 30 μm^2 , split coefficient = 7, individual threshold = 0.5, contrast > 0.1).

To assess the morphology and intensity of the nuclei: [Calculate morphology properties] - population: nuclei, region: nucleus, method: standard (area (μm^2) and roundness); [Calculate intensity properties] - channel: Hoechst 33342, population: nuclei, region: nucleus; method standard (mean). To exclude outliers: [Select population] - population: nuclei, method: filter by property (filter F1: intensity < 2000). To identify the cytoplasmic areas: [Find Cytoplasm] - channel: Calcein green, nuclei selected; method A (individual threshold = 0.15). To identify the cell surrounding areas (background staining): [Find Surrounding Region] - channel: Calcein green, population: nuclei selected, region: cell, method A (individual threshold = 0.15). To assess the intensity of CellROX in the cytoplasmic and the background regions: [Calculate Intensity Properties] - channel: CellROX, population: nuclei selected, region: cell or background, method standard (mean). To calculate the corrected CellROX intensity: subtract Intensity Background CellROX from Intensity Cell CellROX. The outputs of combination 3 included: the number of nuclei and the corrected intensity of CellROX staining.

Combination 4: Hoechst 33342/Nile Red/Cellmask

To identify nuclei: [Find nuclei] - channel Hoechst 33342, method C (common threshold = 0.2, area > 30 μm^2 , split coefficient = 7, individual threshold = 0.5, contrast > 0.1).

To assess the morphology and intensity of the nuclei: [Calculate morphology properties] - population: nuclei, region: nucleus, method: standard (area (μm^2) and roundness); [Calculate intensity properties] - channel: Hoechst 33342, population: nuclei, region: nucleus; method standard (mean). To exclude outliers: [Select population] - population: nuclei, method: filter by property (filter F1: intensity < 2000). To identify the cytoplasmic areas: [Find Cytoplasm] - channel: Cellmask Deep Red, nuclei selected, method: F (individual threshold = 0.15). To identify lipid droplets: [Find Spots] - channel: Nile Red, ROI population: nuclei selected, ROI region: cell; method A (relative spot intensity > 0.080, splitting coefficient = 1). The outputs of combination 4 included: the number of nuclei, the total area of lipid droplets per cells, and the average number of lipid droplets per cell.

Image acquisition and processing for Hoechst-positive cell counts.

The Operetta images were imported into Columbus software for analysis. The setup was as follows: individual planes, advanced flatfield correction (basic if advanced was not available). To identify nuclei: [Find nuclei] - channel Hoechst 33342, method M (diameter = 25 μm , splitting coefficient = 0.55, common threshold = 0.25). To assess the intensity of nucleus: [Calculate intensity properties] - channel: Hoechst 33342, population: nuclei, region: nucleus; method standard (mean). To identify and exclude outliers: [Select population] - population: nuclei, method: filter by property (filter F1: intensity < 5000).

List of supplemental tables and figures

Table 2-S1. Cell-permeable fluorescent dyes and combinations used in high-content screening.

Table 2-S2. The steady-state concentration (C_{ss}) values for each chemical and the parameters used in high-throughput toxicokinetic analysis.

Figure 2-S1. Cytotoxicity of BDE-47 and OPEs in H295R cells.

Figure 2-S2. Effects of BDE-47 and OPEs on the phenotypic characteristics of H295R cells.

Dye (Cat#)	Staining	Dilution	Comb1	Comb2	Comb3	Comb4
Hoechst 33342 (R37165)	Nuclei	1:2000	✓	✓	✓	✓
Calcein-AM (C1430)	Cytoplasm (Cell viability)	1:1000	✓		✓	
LysoTracker Red DND-99 (L7528)	Lysosomes	1:6000	✓			
MitoTracker Green FM (M7514)	Total mitochondria	1:2000		✓		
MitoTracker Red CM- H2XRos (M7513)	Active mitochondria	1:2500		✓		
CellROX Deep Red (C10422)	Reactive oxygen species (oxidative stress)	1:2500			✓	
CellMask Deep Red (C10046)	Plasma membrane	1:1000		✓		✓
Nile Red (N1142)	Lipid droplets	1:100				✓

Table 2-S1. Cell-permeable fluorescent dyes and combinations used in high-content screening.

Phenol-red free DMEM/F-12 (incomplete medium) was used to prepare dye combinations 1, 2, and 3; 2% (w/v) polyvinylpyrrolidone was used to prepare combination 4. For combinations 1, 3, and 4, 100 μ M of the exposure medium was removed before adding 50 μ M of the corresponding dye solution. For combination 2, all exposure medium (200 μ M) was removed before adding 150 μ M of the corresponding dye solution; this was done to minimize the interaction between serum and MitoTracker Green dye. After the 30 min staining period, all dye solutions were removed, and cells were washed once with 200 μ M of the incomplete medium. For live cell imaging, 100 μ M incomplete medium was added to each well. Comb: combination; w/v: weight/volume percent.

Acronyms	Cas#	LogKow	M.W.	Human.Clint	Human.Funbound.plasma	C _{ss}
BDE-47	5436-43-1	6.81	485.795	2.230921	0.0187	55.8
TMPP	1330-78-5	5.11	368.4	2.99254	0.0004	1008
IPPP ^{1,2}	68937-41-7	9.4	452.5	138.4571	0.023353	N/A
TPHP ¹	115-86-6	4.589	326.3	26.44	0.002852	89.67
TBOEP ¹	78-51-3	3.749	398.5	6.860755	0.24436	47.66
TCIPP	13674-84-5	2.592	327.6	1.925409	0.1434	23.15
TDCIPP ¹	13674-87-8	3.65	430.9	5.092	0.01078	136.3

Table 2-S2. The steady-state concentration (C_{ss}) values for each chemical and the parameters used in high-throughput toxicokinetic analysis.

N/A: non-available/applicable; LogKow: octanol/water partition coefficients; M.W.: molecular weight; Clint: intrinsic clearance; Funbound.plasma: fraction unbound in the plasma protein.

¹ Chemicals that are already in the HTTK database.

² Chemicals that have high LogKow and clearance values.

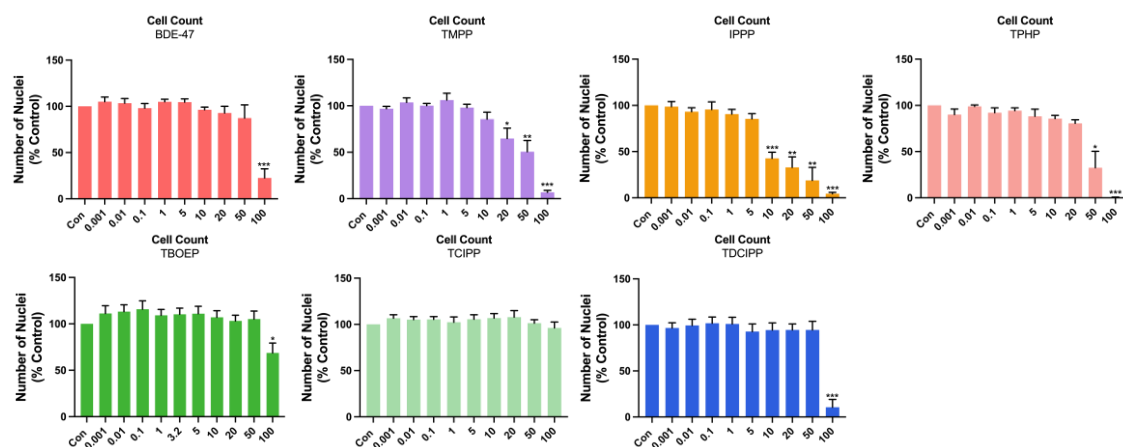


Figure 2-S1. Cytotoxicity of BDE-47 and OPEs in H295R cells. Cells were stained with Hoechst 33342 (blue, nuclei) and were visualized with the Operetta High Content Imaging System (40 x magnification). Data are shown as percentages relative to controls; values represent means \pm SEM; n = 6. *p<0.05, **p<0.01, and ***p<0.001 compared to control.

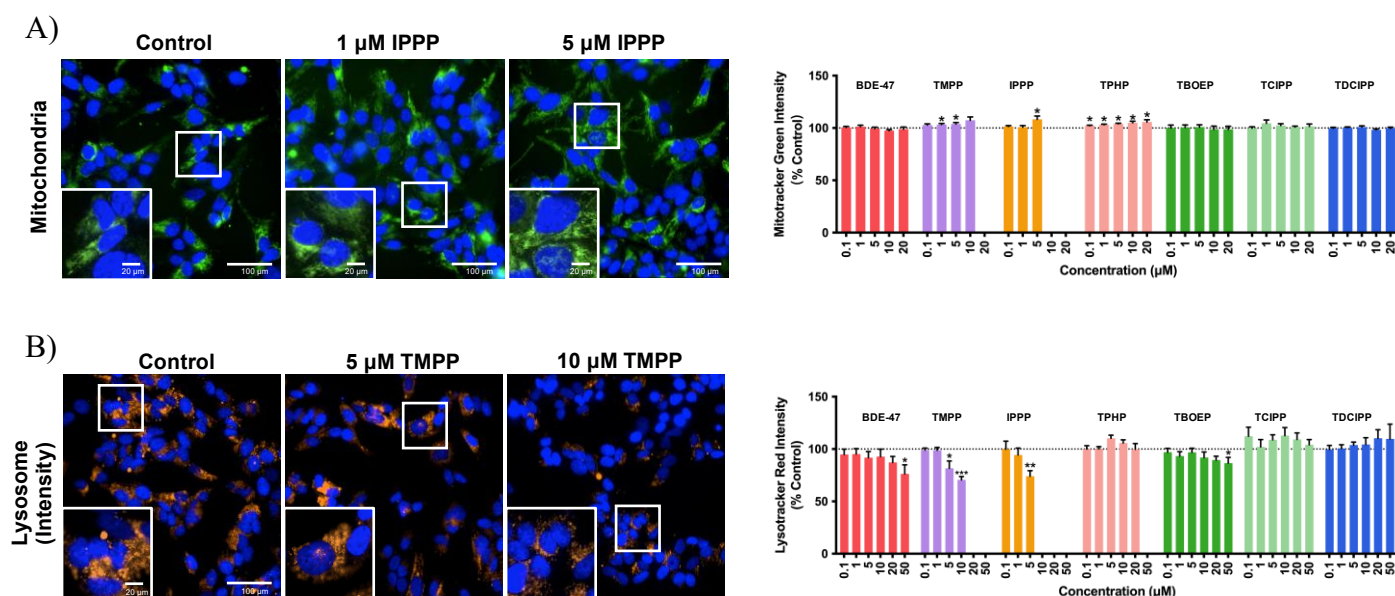


Figure 2-S2. Effects of BDE-47 and OPEs on the phenotypic characteristics of H295R cells.

Cells were stained with: A) Hoechst 33342 (blue, nuclei) and Mitotracker Green (green, total mitochondria); or B) Hoechst 33342 (blue, nuclei) and LysoTracker Red (orange, lysosomal intensity) fluorescent dyes and were visualized with the Operetta high content imaging system (40 x magnification). Data are shown as percentages relative to controls; values represent means \pm SEM; n = 6. *p<0.05, **p<0.01, and ***p<0.001 compared to control. Concentrations that induced > 30% cytotoxicity were excluded from the analyses and were not shown.

CONNECTING TEXT

In chapter two, we showed that exposure to individual OPEs that are commonly detected in the environment affected the phenotypes and functions of H295R adrenal cells. Using benchmark modeling and Toxicological Prioritization Index (ToxPi) analyses, we found that OPEs with three phenol rings (triaryl-OPEs) are more potent than legacy PBDEs. In contrast, non-triaryl OPEs may serve as potential safer alternatives. However, our findings also revealed that the effect of individual OPEs can vary considerably and sometimes produce contrasting outcomes. Given that real-world exposure typically involves complex mixtures of OPEs, evaluating individual chemicals in isolation, without considering their combined effects, may lead to inaccurate risk assessments for human health.

The focus of chapter three is to assess the effects of an environmentally relevant mixture of OPEs on H295R adrenal cells. This mixture was formulated to reflect the OPE profile found in dust samples collected as part of the Canadian House Dust Study. We first assessed the phenotypic alterations in H295R cells upon exposure to the mixture through high content screening. Lipid droplets emerged as a prominent phenotypic change, prompting further lipidomic analysis to explore how the mixture affects the composition of lipid droplets. Additionally, we examined the effects of the mixture on the functional capacity of H295R cells in producing steroid hormones and investigated potential underlying mechanism(s) by analyzing alterations in transcripts involved in the cholesterol biosynthesis and steroidogenic pathways.

CHAPTER 3

Impact of Exposure to a Mixture of Organophosphate Esters on Adrenal Cell Phenotype, Lipidome, and Function

Zixuan Li, Barbara F Hales, Bernard Robaire

(Published: Endocrinology; February 20, 2024)

ABSTRACT

Organophosphate esters (OPEs) are used primarily as flame retardants and plasticizers. Previously, we reported that adrenal cells are important targets of individual OPEs. However, real life exposures are to complex mixtures of these chemicals. To address this, we exposed H295R human adrenal cells to varying dilutions (1/1000K to 1/3K) of a Canadian household dust based OPE mixture for 48 h and evaluated effects on phenotypic, lipidomic, and functional parameters. Using a high-content screening approach, we assessed phenotypic markers at mixture concentrations at which there was greater than 70% cell survival; the most striking effect of the OPE mixture was a 2.5-fold increase in the total area of lipid droplets. We then determined the response of specific lipid species to OPE exposures with novel, non-targeted lipidomic analysis of isolated lipid droplets. These data revealed that house dust OPEs induced concentration-dependent alterations in the composition of lipid droplets, particularly affecting the triglyceride, diglyceride, phosphatidylcholine, and cholesterol ester subclasses. The steroid producing function of adrenal cells in the presence or absence of a steroidogenic stimulus, forskolin, was determined. While the production of 17 β -estradiol remained unaffected, a slight decrease in testosterone production was observed after stimulation. Conversely, a 2-fold increase in both basal and stimulated cortisol and aldosterone production was observed. Thus, exposure to a house dust based mixture of OPEs exerts endocrine-disrupting effects on adrenal cells, highlighting the importance of assessing the effects of environmentally relevant mixtures.

INTRODUCTION

Organophosphate esters (OPEs) are human-made chemicals that are used as flame retardants, plasticizers, hydraulic fluids, and coatings for electronic devices in a wide range of commercial and industrial products (1, 2). Since OPEs are additives, and thus is not chemically bound in products, they can be released readily into the surrounding environment via volatilization, abrasion, or dissolution (1, 3, 4). The concentrations of OPEs in dust samples provide critical information about the potential for exposure to OPEs as a consequence of dust inhalation, ingestion, or dermal contact (5-8). OPEs have been detected in dust worldwide (8-10); up to 13 OPEs were detected in Canadian household dust at levels ranging from 5 to 57,700 ng/g (11, 12). Due to the prevalence of exposures, urinary concentrations of OPEs have increased drastically in samples collected in the United States between 2002 and 2015 (13).

Exposures to OPEs have been associated with adverse outcomes in reproduction (14-17), development (18-22), and thyroid homeostasis (23-26). However, commercially available flame retardants are often mixtures. For instance, Firemaster® 550, a proprietary flame retardant mixture, contains 2 brominated compounds, 2-ethylhexyl-2,3,4,5-tetrabromobenzoate (EH-TBB) and bis(2-ethylhexyl) 2,3,4,5-tetrabromophthalate (BEH-TEBP), and 2 OPEs, triphenyl phosphate (TPHP) and isopropylated triphenolphosphate (IPPP) (1, 27). The few experimental studies that have assessed the effects of mixtures have focused primarily on Firemaster® 550. Exposure to this mixture has been associated with alterations in neurodevelopment, metabolism, behavior, and adipogenesis (28-34). Recently, Witchey et al (35) reported lipid dysregulation in the neonatal cortex tissue of rats exposed to Firemaster® 550; this effect was sex specific and attributed largely to the OPE components in the mixture.

The adrenal gland produces a variety of hormones that play a vital role in regulating blood pressure, metabolism, and the response to stress (36). Steroid hormones synthesized in the

adrenal include glucocorticoids, mineralocorticoids, androgens and estrogens. Improper functioning of the adrenal gland in producing steroid hormones in conditions such as Addison's disease, where insufficient cortisol is produced, may have life-threatening consequences (37). In a previous study with H295R adrenal cells we identified the adrenal gland as an important target of OPEs (38). Depending on the endpoint examined, individual OPEs had differential, and sometimes contrasting, effects on these cells. However, a consistent finding was that all six of the OPEs tested increased the total area of lipid droplets (38). Exposure to IPPP doubled the amount of cortisol produced under basal conditions, yet both TPHP and tris(methylphenyl) phosphate (TMPP) decreased cortisol production. Since the effects of exposures to mixtures are more complex than simple additivity (39, 40) and real-world exposures are to mixtures (11, 12, 41), there is a need to assess the possibly adverse effects of exposure to environmentally relevant OPE mixtures.

The objective of this study was to determine how a Canadian household dust based OPE mixture affects the phenotype, lipid composition, and steroid production of H295R cells. We are particularly interested in lipids as they have crucial roles in signal transduction, as cellular energy sources, and as structural components (42). In adrenal cells, lipid droplets also act as reservoirs of the cholesterol esters that are essential for steroid hormone synthesis (43, 44). We have employed novel, in-depth, lipidomic analysis in conjunction with a comprehensive evaluation of cell phenotypes and function to identify the effects of an environmentally relevant OPE mixture in adrenal cells.

MATERIALS AND METHODS

Organophosphate Ester House Dust Mixture

The OPE house dust mixture, prepared by Dr. Michael G. Wade (Health Canada), contained the 13 OPEs that were detected in over 85% of house dust samples collected from 144 urban Canadian homes between 2007 and 2010 (Fig. 1; (11, 12)). The relative proportion of each OPE in this mixture is based on their 95th percentile values from these samples. A list of the dilutions used in this study, and their equivalent concentrations in the culture medium, is provided in Table S1 (45). At the lowest dilution tested in this study (1/1000K), the added level of OPEs is comparable to the urine level of OPEs detected in men living in the greater Montreal area (14). The undiluted OPE mixture contained 0.888 mg/μL of OPEs; this is the equivalent of 5.005 g of house dust.

Cell Cultures

The H295R human adrenocortical carcinoma cells were purchased from ATCC (CRL-2128, Manassas, VA). The passage numbers of the H295R cells used in this study did not exceed 10. The cell line tested negative for mycoplasma contamination using the MycoAlert[®] Mycoplasma Detection Kit from Lonza (Rockland, Maine, USA). Cells were cultured in Corning 75 cm² U-shaped cell culture flask at 37 °C with 5% CO₂ in 12 mL phenol-red free DMEM/F-12 medium (Gibco, Burlington, Ontario, Canada). The culture medium was supplemented with Corning ITS+ Premix Universal Culture Supplement, Corning Nu-Serum Growth Medium Supplement, and 0.5% 100X penicillin-streptomycin (Wisent Bioproducts, Montreal, Quebec, Canada). Culture medium was renewed every 2 to 3 days.

High-Content Imaging

H295R cells were seeded (10,000 cells/well) in 96-well black PhenoPlates with optically clear flat-bottoms (Perkin Elmer, Waltham, Massachusetts) that were pre-coated with 0.2% collagen 1 (3 mg/mL, rat tail) (Gibco, Burlington, Ontario, Canada). To ensure optimal cell adhesion, there was a 24 h acclimation period prior to chemical treatments. Subsequently, the cells were exposed to either vehicle control (0.5% DMSO) or one of the mixture dilutions (1/1000K, 1/300K, 1/100K, 1/75K, 1/60K, 1/45K, 1/30K, 1/10K, or 1/3K) for 48 h. On the experimental day, the stock solutions were diluted with medium to the working concentration. DMSO was added to each of the dilutions to maintain a final concentration of 0.5% DMSO in all treatment groups. To assess the effects of the OPE mixture on cell phenotypes, H295R cells were stained with 1 of 4 different combinations of cell-permeable fluorescent dyes for 30 min. Further details regarding the cell-permeable fluorescent dyes, including the combinations used and their respective dilutions, can be found in Table S2 (45).

Live cell imaging was conducted using the Operetta high content imaging system (Perkin Elmer) equipped with a non-confocal 40 x high-NA objective. Twelve fields were screened per well. The acquired images were analyzed using the Columbus Image Data Storage and Analysis System (Perkin Elmer). Detailed information on the specific parameters assessed and the settings used for each analysis are provided in Supplementary Methods 1.1 (45).

Lipid Droplet Isolation

H295R cells were seeded in Corning 175 cm² U-shaped cell culture flask at a seeding density of 10,000,000 cells/flask (adjusted to ensure that enough lipid droplets were collected for lipidomic analysis). Following a 24 h acclimation period, cells were exposed to the OPE mixture at one of three different dilutions: 1/300K, 1/100K, or 1/60K. At the end of the 48 h chemical exposure period, lipid droplets were isolated from the cells using a lipid droplet isolation kit (Cell Biolabs,

San Diego, California, USA; Catalog # MET-5011) according to the manufacturer's protocol.

The extracted lipid droplets were then stored at -80°C until further analysis. Samples were sent to the Metabolomics Innovation Center (TMIC; Edmonton, Alberta, Canada) at the University of Alberta for lipidomic analysis.

Lipidomic Profiling

Non-targeted, high-sensitivity lipidomic analysis of lipid droplets was conducted using nanoLC-MS as detailed by Buzatto et al (46). The lipid extraction procedure was based on a modified Folch liquid-liquid protocol. In brief, 90 µL of each sample was vortexed with 1.1 µL of an internal standard solution and 479 µL of methanol, followed by extraction with 960 µL of dichloromethane. A clean-up step was conducted using 270 µL of water. The samples were then allowed to equilibrate at room temperature for 10 mins and centrifuged at 16,000 g for 10 mins at 4°C. The organic layer was collected and dried with a nitrogen blowdown evaporator. The dried samples were resuspended in 4.6 µL of NovaMT MixB, and the mixture was diluted with 40.4 µL of NovaMT MixA (Nova Medical Testing Inc., Edmonton, Alberta, Canada).

A pooled mixture containing all samples was prepared for quality control. Lipids were identified and quantified using the LC-MS technique. This analysis was performed in both positive and negative ion modes with injection duplicates using the Dionex UltiMate 3000 UHPLC instrument (ThermoFisher Scientific) linked to a Bruker Maxis II QTOF Mass Spectrometer (Bruker Corporation). A three-tier ID approach based on the MS/MS identification (Tiers 1 and 2) and MS match (Tier 3) was used for lipid identification. Tier 1 identification included lipids with MS/MS scores greater than or equal to 500, precursor m/z error smaller than or equal to 20.0 ppm and 5.0 mDa. Tier 2 included lipids with MS/MS scores smaller than 500, while the remaining criteria stayed the same. Features not identified in tiers 1 and 2 were

searched in the LipidMaps database (<http://www.lipidmaps.org>) for putative identification by mass match with an m/z error smaller than or equal to 20.0 ppm and 5.0 mDa (tier 3). Lipid identification followed the guidelines established by the Lipidomics Standards Initiative (<https://lipidomics-standards-initiative.org>). Additional information regarding the parameters used for data processing and normalization can be found in Supplemental Methods section 1.2 (45). The identified lipids were class-matched to the most similar internal standard.

Measurements of Basal and Stimulated Production of Steroid Hormones

H295R cells were seeded in 96 well plates pre-coated with 0.2% rat tail collagen 1 at a seeding density of 10,000 cells/well and were allowed to adhere for 24 h. The cells were then exposed for 48 h to 200 μ L culture medium containing the OPE mixture at one of four different dilutions (1/1000K, 1/100K, 1/60K, or 1/30K) in the presence or absence of 10 μ M forskolin (Sigma-Aldrich), a steroidogenic stimulus (47). At the end of the exposure period, culture media from duplicate wells (400 μ L in total for each condition) were pooled and stored at -80°C until further analysis. Hoechst 33342 was used to stain cell nuclei; cells were stained for 30 min with no washing afterwards to prevent cell loss. Plates were then screened with the Operetta high content imaging system (all fields were screened; 10 x magnification). The Columbus Image Data Storage and Analysis System was used to quantify Hoechst-positive cell counts (Supplementary Methods 1.3 (45)).

To assess the effects of the OPE mixture on the steroid hormone producing function of the cells, enzyme-linked immunosorbent assay (ELISA) kits were used to measure the levels of 17 β -estradiol, testosterone, aldosterone and cortisol [17 β -estradiol: Tecan (IBL) Catalog # RE52041, RRID:AB_2934323; Testosterone: IBL-America Catalog # IB79106, RRID: AB_2814981; Aldosterone: Abcam Catalog # ab136933, RRID: AB_2895004; Cortisol: Cayman

Chemical Catalog # 500370, RRID: AB_2935793)] in accordance with the manufacturers' instructions. The SpectraMax Plus 384 microplate reader (Molecular Devices, San Jose, California, USA) was used to read the ELISA plates at a wavelength of 450 nm. The final concentrations were normalized to the number of cells in each well and are presented as picograms or nanograms per 1 million cells. The average intra-assay and inter-assay coefficients of variation were 3.2% and 11.3% for the 17 β -estradiol assay; 4.5% and 10.2% for the testosterone assay; 3.5% and 12.0% for the aldosterone assay; and 4.8% and 14.2% for the cortisol assay.

Quantitative real-time PCR (qRT-PCR)

H295R cells were seeded in 24 well plates pre-coated with collagen at a density of 60,000 cells/well in 1 mL of complete medium (seeding density was adjusted based on the surface area ratios of the well). Cells were acclimated for 24 h prior to exposure to the OPE mixture at 1/1000K, 1/100K, 1/60K, or 1/30K for 48 h, in the presence or absence of 10 μ M forskolin (47). Total RNA was extracted using the RNeasy Plus Mini Kit (QIAGEN, Mississauga, Ontario, Canada) following the manufacturer's protocol. A NanoDrop 2000 spectrophotometer (ThermoFisher, Waltham, Massachusetts, USA) was used to assess the concentration and purity of the extracted RNA.

All primers were obtained from QuantiTect Primer Assays (QIAGEN): HMG-CoA reductase (HMGCR, QT00004081), steroidogenic acute regulatory protein (STAR, QT00091959), 11-beta-hydroxylase (CYP11B1, QT00028714), aldosterone synthase (CYP11B2, QT00076181), and glyceraldehyde 3-phosphate dehydrogenase (GAPDH, QT00079247). Total RNA was diluted to a working concentration of 2 ng/ μ L in RNase-free water. For transcripts that had moderate to low expression levels, the concentration was adjusted to 10 ng/ μ L (CYP11B1

and CYP11B2). The Power SYBR Green RNA-to-CT 1-Step Kit (Applied Biosystems, Foster City, California) and the Viia7 Real-Time polymerase chain reaction (PCR) System (Applied Biosystems) were used to quantify transcript levels. Each reaction mix (20 μ L) was composed of 0.16 μ L of reverse transcriptase, 2 μ L of primer, 2.84 μ L of RNase-free water, 10 μ L of SYBR Green Master Mix, and 5 μ L of RNA samples. The following condition was used for PCR experiments: 48°C for 30 min, 95°C for 10 min, 40 cycles at 95°C for 15s, 55°C for 30s, and 72°C for 30s. Each reaction was done in triplicate; outliers ($> 0.2 C_T$ values deviating from the average of the other two) were checked and excluded. The expression levels of transcripts were calculated based on the average of replicates. Averaged expression levels were normalized to the amount of the GAPDH transcripts. The QuantStudio Real Time PCR Software (version 1.3) was used for data analysis.

Statistical Analyses

Data were analyzed using GraphPad Prism (version 9.4.1, GraphPad Software Inc., La Jolla, California). For high-content imaging data, Holm-Bonferroni-corrected 1-sample t test was used. For hormone production levels, 2-way ANOVA was used followed by the Dunnett's test. High-content screening experiments were repeated independently 10 times ($n = 10$). For hormone measurements and lipidomic analyses, experiments were repeated independently 5 times ($n = 5$). The minimal level of significance was $p < 0.05$. For qRT-PCR data, $p < 0.01$ was considered statistically significant.

The peak-paired data from lipidomic analyses were uploaded to MetaboAnalyst 5.0 (<https://www.metaboanalyst.ca>) for multivariate statistical analysis. The parameters used are shown in Table S3 (45).

RESULTS

Effects of the OPE Mixture on the Phenotypic Characteristics of H295R Cells

Cytotoxicity of the OPE mixture was assessed using Calcein-AM, a nonfluorescent cell-permeant dye that is converted to green-fluorescent Calcein in live cells. The numbers of Calcein positive, Hoechst-stained nuclei were quantified and compared to control (Fig. 2A). OPE mixture dilutions ranging from 1/1000K to 1/30K did not induce significant cell death. More than 30% cell death was observed at 1/10K or 1/3K; thus, these dilutions were excluded from subsequent phenotypic assessments.

Nile Red is a dye that fluoresces in lipid-rich environments. Nile Red stained lipid droplets, shown in the representative figures as yellow dots, were clustered in the cytoplasm of cells (Fig. 2B). The total areas of lipid droplets were increased by OPE mixture exposures in a concentration dependent manner. At 1/300K, the level of lipid droplets was increased by 1.5-fold; it was further upregulated to 2.5-fold at 1/30K, the highest non-cytotoxic dilution.

No significant alterations were observed in other phenotypic endpoints, including the levels of reactive oxygen species, lysosomal function, numbers of lysosomes, and the numbers of total and active mitochondria (Fig. S1 (45)).

Effects of the OPE Mixture on H295R Cell Lipid Droplets

Lipidomic analysis was done to assess the specific lipid species affected by the OPE mixture. Using the 3-tier lipid identification method, based on the lipid MS/MS match scores and the precursor m/z errors, a total of 599 lipids were identified with high confidence in tier 1, 68 lipids were identified with high confidence in tier 2, and 2900 lipids were putatively identified in tier 3.

The degree of separation in the lipidome profiles between the control and the three OPE mixture treatment groups is visualized in Fig. 3A in a partial least-squares discriminant analysis (PLS-DA) 2D score plot. All treatment groups were fully separated from the control, indicating that exposure to the OPE mixture had a profound impact on lipid composition. There was a slight overlay between treatment groups, suggesting that there were some commonalities in the affected lipid profiles. Indeed, the Venn diagram showed that 6 lipids were commonly affected by all 3 treatment groups; there were 7 to 16 affected lipids shared between any two treatment groups (Table S4; Fig S2 (45)). The top 15 lipids that drive the separation observed in the PLS-DA plot are identified in the Variable Importance in Projection (VIP) score graph (Fig. 3B). Notably, lipids from the sphingolipids group displayed the highest VIP scores, accounting for 1/3 of the top 15 VIP lipids. Additionally, other lipids driving the OPE mixture induced shifts in lipid compositions were from the glycerophospholipids, glycerolipids, sterol lipids, and fatty acyl groups.

Exposure to the 1/300K dilution OPE mixture significantly altered the levels of 62 lipids (Fig. 4A); among these, 20 lipids were downregulated and 42 lipids were upregulated. Similarly, exposure to the 1/100K dilution OPE mixture resulted in alterations in the same number of lipids, with an equivalent distribution of significantly up- and down-regulated lipids. The highest non-cytotoxic OPE dilution tested (1/60K) affected a total of 70 lipids; unlike the 1/300K dilution, the majority of these affected lipids were downregulated (50 lipids). The top 10 affected lipids in all treatment groups, ranked by fold change (5 in the downregulated and 5 in the upregulated category), along with their respective lipid subclasses, are labeled in the volcano plots presented in Fig. 4B-D. Of note, half of the most affected lipids belong to the glycerolipids category. The remaining most affected lipids originated from various categories, including fatty acyls, sphingolipids, sterol lipids, glycerophospholipids, and polyketides. Moreover, 56.7% of the

significantly affected lipids were oxidized, suggesting a possible correlation between exposure to the OPE mixture and lipid oxidation. A list of the lipids displaying extra oxygen atom(s) in their structures is provided in Table S5 (45).

A heatmap showing the top 50 affected lipids, along with their respective categories, provides an overview of the significantly affected lipids (Fig. 5). OPE exposures at different dilutions showed distinct patterns compared to the controls in terms of the specific lipids affected. For example, at the 1/100K dilution of the OPE mixture, several lipids from the diglyceride group (DG) were significantly upregulated, whereas no significant alterations in other treatment groups were observed. This distinction is also apparent in the Venn diagram, in which lipids affected by a single treatment constitute more than half of the total affected lipids (Table S6; Fig. S2 (45)).

We next analyzed the relative distribution of significantly affected lipids in each lipid category (Fig. 6A). Glycerolipids represented 24% of the affected lipids at the 1/300K dilution; this percentage increased to 43% at the highest concentration of the OPE mixture tested. While a relatively lower percentage of lipids from the sterol lipid group were affected at the 1/300K dilution, exposure to the 1/60K OPE mixture concentration doubled the number of affected lipids from this group (from 5% to 10%). The proportions of the affected lipids in the sphingolipids and glycerophospholipids groups were comparable, with approximately 20% of the affected lipids attributed to each of the treatment groups. The numbers of lipids affected in the sphingolipids group remained relatively stable across treatment groups, whereas exposure to the highest concentration of the OPE mixture affected fewer glycerophospholipids. Lipids from the fatty acyl group showed a notable response to the OPE mixture. At the lowest OPE dilution (1/300K), 19% of the affected lipids were from the fatty acyl group; only 4% from this group were affected with increasing concentrations. The last two groups of lipids constituted the

smallest proportion of significantly affected lipids. Polyketides initially accounted for 10% of the affected lipids (1/300K OPE mixture) but this was reduced to only 1% at the 1/60K dilution. Prenol lipids represented an even smaller percentage and were affected (2%) only at the 1/300K dilution.

A further analysis of the subclass distribution of the most altered lipids identified the lipid species that were most impacted. In the glycerolipids group, the most affected lipids were diglycerides (DG) and triglycerides (TG) (Fig. 6B). Within the sterol lipids group, 2 subclasses of affected lipids were identified, the cholesterol esters (CE) and sterol lipids (ST) (Fig. 6C); the number of cholesterol ester lipids affected was elevated after exposure to the 1/60K OPE mixture. In the sphingolipid category, 8 subclasses of lipids were identified; a similar number of affected lipids were present across the treatment groups (Fig. 6D). More lipids from the fatty acyls group [fatty acids (FA), nitrogenated fatty acids (NA), and N-acyl ethanolamines (NAE)] were affected at lower OPE concentrations (Fig. 6E); however, some lipids [N-acyl ethanolamines (NAE), N-acyl amines (NAT), and wax esters (WE)] were affected primarily at the 1/60K dilution. Among the glycerophospholipids, phosphatidylcholine (PC) accounted for an average of 70% of the affected lipids at both the 1/300K and 1/100K dilutions (Fig. 6F). A proposed disrupted lipid pathway with affected lipid species and their categories is provided in Fig. 7.

Effects of the OPE Mixture on H295R Cell Steroidogenesis

Since steroidogenesis is a major function of the adrenal, the effects of exposure to the OPE mixture on the ability of H295R cells to produce 17β -estradiol and testosterone (predominantly gonadal hormones) and aldosterone and cortisol (key adrenal hormones) under basal and stimulated conditions were analyzed (47).

The average basal production of 17β -estradiol was 0.5 ng/ 10^6 cells (Fig. 8A). In the presence of stimulation with forskolin, the level of 17β -estradiol produced was increased approximately 7-fold. Exposure to the OPE mixture did not affect basal or stimulated 17β -estradiol production. The production of testosterone was not affected by OPE exposure under basal conditions (Fig. 8B). Forskolin stimulation increased testosterone production from 6.3 ng/ 10^6 cells to 9.0 ng/ 10^6 cells; exposure to the 1/60K or 1/30K OPE mixture dilutions decreased forskolin stimulated testosterone production by approximately 19%.

The baseline production of aldosterone was 130 pg/ 10^6 cells; forskolin stimulation induced a 3-fold increase in aldosterone production (Fig. 8C). Exposure to the OPE mixture strongly upregulated both basal and stimulated production of aldosterone by approximately 2-fold. OPE exposure also increased H295R cell production of both basal and stimulated cortisol (Fig. 8D). The average basal level of cortisol produced was 2.2 pg/ 10^6 cells; production was increased by 1.6 times after exposure to 1/100K of the OPE mixture. In forskolin stimulated cells, cortisol production was increased to an average level of 14.1 pg/ 10^6 cells; an approximately 2-fold increase was observed after exposure to OPEs at the 1/1000K, 1/100K, and 1/60K dilutions.

Effects of the OPE mixture on the expression of transcripts involved in cholesterol and steroid biosynthesis

We further assessed whether exposure to the OPE mixture affects the steroidogenic ability of H295R cells at the transcriptional level. First, we measured the mRNA level of HMGCR, the enzyme responsible for the rate limiting step in cholesterol biosynthesis (Fig. 9A). Under basal conditions, the OPE mixture at 1/1000K, 1/100K, or 1/60K dilutions induced a slight increase in the level of HMGCR expression. Treatment with the OPE mixture under stimulated conditions

induced a 11% increase only at the 1/1000K dilution. The expression level of STAR, a cholesterol transporter, was downregulated at 1/30K of the OPE mixture at both the basal and stimulated levels (Fig. 9B). The expression levels of two key transcripts responsible for the last steps in the biosynthesis of cortisol (CYP11B1) and aldosterone (CYP11B2) were assessed. A 2-fold increase in the level of CYP11B1 was observed at the 1/100K dilution; it reached 4.5-fold with exposure to 1/60K of the OPE mixture (Fig. 9C). With forskolin stimulation, an approximately 22% increase was observed with exposure to 1/1000K or 1/100K of the OPE mixture. At 1/60K, the expression level of CYP11B1 was upregulated by 46% compared to control. Similarly, exposure to the OPE mixture upregulated the level of CYP11B2 (Fig. 9D). Under basal conditions, OPE mixture induced an up to 3-fold increase; a nearly 2-fold increase was observed under stimulated conditions.

DISCUSSION

This is the first demonstration that a household dust based mixture of OPEs affects adrenal cells. Exposure to this OPE mixture, at dilutions as low as 1/300K, induced an accumulation of lipid droplets in adrenal cells and altered the secretion of both basal and stimulated adrenal steroids. A closer look at the lipid species revealed that this OPE mixture dysregulates both the quantity of lipid droplets and their lipid composition.

Previous studies have provided evidence that exposure to individual OPEs may affect the adrenal. In animal studies, neonatal exposure to tris(1,3-dichloro-2-propyl) phosphate (TDCIPP) significantly increased the weight of the adrenal gland in adult male rats (48). Exposure to TMPP or IPPP has been associated with adrenal cortex vacuolization (49-54). Tris(2-butoxyethyl) phosphate (TBOEP), the major component of the OPE mixture, was shown to affect the transcription profiles of genes in the hypothalamus–pituitary–adrenal (HPA) axis in zebrafish

(55). In adrenal cells, exposure to tri-n-butyl phosphate (TNBP) or TMPP decreased cell viability (56). Moreover, exposure to TCEP, TCIPP, TDCIPP, TBOEP, TPHP, or TMPP altered the ability of adrenal cells to synthesize steroid hormones by dysregulating the transcription of genes in the steroidogenic pathway (57).

Our high content screening strategy enabled the identification of lipid droplet accumulation as the most prominent phenotypic target affected by a house dust based OPE mixture (Fig. 2). Interestingly, increases in lipid droplets after OPE exposures have been observed in various cell types, suggesting that this may be a common mechanism of action of OPEs in different organs (31, 32, 58-60). Previously, we reported that exposure to 6 of the individual OPEs present in this mixture induced an increase in the lipid droplet areas in H295R cells. However, in contrast to the effects of individual OPEs, the OPE mixture did not affect oxidative stress, mitochondria, or lysosomes. An accumulation of lipids was also reported in the rat adrenal gland after exposure to TMPP, one of the components in the OPE mixture (51). The lipidomics data revealed that the major lipid categories contributing to the increased area of lipid droplets induced by the OPE mixture were glycerolipids and sphingolipids (Fig 5). The sterol lipids were affected to a lesser extent. An upregulation in the level of ST was identified in the lipidomics analysis; this was most marked at the 1/300K dilution (Fig. 5). Indeed, exposure to the OPE mixture increased the expression of HMGCR, the rate-limiting enzyme in cholesterol biosynthesis (Fig. 9A). An increase in HMGCR enzyme activity may contribute to the production of cholesterol.

Previous studies have shown that lipid droplets are composed of a hydrophobic core of neutral lipids surrounded by a phospholipid membrane monolayer (42). The neutral core contains mostly triglycerides (TG), from the glycerolipids category, and cholesterol esters (CE), from the sterol lipids category. The phospholipid membrane of lipid droplets is enriched with

phosphatidylcholine (PC), from the glycerophospholipids category (61). Using LC–MS methodology, we identified 3570 lipid species with high sensitivity. Traditional lipidomic analysis typically narrows down to focus on a limited selection of lipid classes in order to simplify the complex lipidome in biological samples. By not limiting ourselves to a specific lipid category, we have shown that our house dust based OPE mixture significantly altered a total of 142 lipids that belong to 7 lipid categories (Fig. S2 (45); Fig. 6). To the best of our knowledge, comprehensive non-targeted lipidomics analysis has been described previously for only one of the steroidogenic tissues, the MA-10 mouse Leydig cells (62, 63, 64). At the functional resting state of these Leydig cells, the main types of neutral lipids were TG (97.1%), followed by 2.0% CE (62). In the current study, TGs and DGs, were also two of the most prominently affected lipid classes (Fig. 6). Effects of OPEs on these two lipids have been characterized previously in liver cells (65, 66). Ethylhexyl diphenyl phosphate (EHDPHP), one of the components in our OPE mixture, significantly increased TG levels and the ratio between TG and DG produced by HepG2 spheroids (65). Increased intracellular levels of TG have also been reported in HepG2 cells after exposure to other components of our OPE mixture; these include tris(2-chloroethyl) phosphate (TCEP), tris(1-chloro-2-propyl) phosphate (TCIPP) and TDCIPP (66). In animal models, exposure to TPHP has been associated with serum hypertriglyceridemia as a consequence of inhibition of carboxylesterase 1G, a gene coding for the enzyme responsible for fatty acyl metabolism (67).

Exposure to all 3 dilutions of the OPE mixture significantly downregulated the level of cholesterol esters in adrenal cells; at increasing concentrations more lipids from the cholesterol ester subclass were affected (Fig. 4; Fig. 6). Cholesterol esters play important roles in steroid-secreting cells as they are the stored form of cholesterol, the precursor for all steroid hormones (68). A downregulation of the levels of cholesterol ester was observed in HepG2 cells after

exposure to 10 μ M of EHDPHP (65); these investigators also observed a decrease in the level of total cholesterol when they analyzed the total lipidome. In contrast, exposure to TMPP was reported to upregulate the level of cholesterol esters in the adrenal glands of F344 rats; this effect was attributed to disruption in the process by which the cholesterol esters stored in lipid droplets are converted to free cholesterol (51).

The subclass of lipids most affected by the OPE mixture in the glycerophospholipids category was phosphatidylcholine (PC), the main component of lipid droplet membranes (Fig. 6). PC was upregulated by the OPE mixture, especially at the 1/300K dilution. A decreased level of PC was reported in murine macrophage cells after exposure to TPHP; this was accompanied by downregulation of the expression of lysophosphatidylcholine acyltransferase 3 (Lpcat3) (69). Exposure to the OPE mixture also increased ceramide (Cer) and hexosyl ceramides (HexCer) (Fig. 4). Interestingly, a previous study reported that the levels of these two lipids were downregulated in liver cells after EHDPHP exposure (65), suggesting that there are chemical and cell line specific effects on this category of lipids.

Prenol lipids and polyketides were also affected by the OPE mixtures, although to a lesser extent (Fig. 6). Prenol lipids, more specifically the isoprenoids that were affected by the OPE mixture, serve as precursors and intermediates in the synthesis of sterol lipids (70). Several OPEs, including IPPP, TPHP, TMPP, TBOEP, and TDCIPP, have been reported to affect isoprenoid biosynthesis by targeting the rate limiting enzyme HMG-CoA reductase (HMGCR) and the master regulator of the pathway, sterol regulatory element binding protein (SREBP) (38, 66, 71, 72). The functional importance and the effects of OPEs on polyketides remains largely unknown; however, some polyketides appear to serve primarily as means of chemical defense for cells (73).

Few studies have assessed the effect of mixtures on the lipidome. In Wistar rats, exposure

to Firemaster® 550 affected ceramides (Cer), sphingomyelins (SM), and triglycerides (TG) in the neonatal cortex (35). In preadipocytes and murine 3T3-L1 preadipocytes, Firemaster® 550 targeted the peroxisome proliferator activated receptor (PPAR γ) and liver X receptor (LXR) (31, 32). These two receptors are important regulators of triglyceride, fatty acids, and cholesterol ester homeostasis (74-77); disruptions in their functions may explain the changes in the levels of lipid species we have observed.

It is perhaps not surprising that the effects of our house dust OPE mixture on the adrenal cell lipidome are accompanied by effects on steroidogenesis. This OPE mixture significantly decreased testosterone production but increased the levels of aldosterone and cortisol (Fig. 8). Luo et al. (78) reported that the decreased concentrations of testosterone in urine samples collected from 6-19-year-old children and adolescents were associated with increased levels of dibutyl phosphate (DBUP), a metabolite of tri-n-butyl phosphate (TNBP), and of dibutyl phosphate (DPHP), a metabolite of IPPP and TPHP. Increased urinary levels of DPHP, bis(1-chloro-2 propyl) phosphate (BCIPP) (a metabolite of TDCIPP), and bis(2-butoxyethyl) phosphate (BBOEP) (a metabolite of TBOEP) were also associated with an increase in serum cortisol levels (79). Limited human data are available on the effects of OPE exposures on aldosterone levels. However, Zhang et al. (80) reported an increase in aldosterone production in H295R cells exposed to 5 μ M TPHP.

The mechanism(s) behind the observed increase in the area of lipid droplets and disruptions in the hormone production levels were examined by assessing the effect of the OPE mixture on the expression level of key transcripts involved in cholesterol and steroid biosynthesis (Fig. 9). In line with the increased level of ST reported in the lipidomics analysis, the level of HMGCR was upregulated by the OPE mixture (Fig 9A). Similarly, exposure to the OPE mixture strongly upregulated the levels of CYP11B1 and CYP11B2 (Fig. 9C; Fig 9D). This

effect could contribute to the increased levels of cortisol and aldosterone observed. In contrast, the level of STAR was downregulated by the OPE mixture at the highest dilution tested (Fig 9B). It was reported that in STAR knockout mouse MA-10 Leydig cells, the composition of lipid droplets was altered (64). Thus, it is possible that changes in STAR expression contribute to the observed disruptions in lipid compositions. Previously, we investigated the effects of 3 OPEs present in the OPE mixture, IPPP, TMPP, and TPHP, and reported similar results of these chemicals on the levels of HMGCR, CYP11B1, and CYP11B2 (38). However, exposure to the mixture downregulated STAR expression, whereas it was upregulated by IPPP and downregulated by TMPP or TPHP exposures. Thus, assessing the effect of environmentally relevant the mixtures is imperative, as relying on evaluating individual chemicals provides only a partial representation of effects.

Our data provide compelling evidence that the adrenal gland is an important endpoint to consider in assessing the effects of OPEs. Furthermore, it is important to assess the impact of environmentally relevant mixtures. Together, our studies demonstrate that exposure to a house dust based OPE mixture disrupts human adrenal cell lipid homeostasis and steroid production.

REFERENCES

1. van der Veen I, de Boer J. Phosphorus flame retardants: properties, production, environmental occurrence, toxicity and analysis. *Chemosphere*. 2012;88(10):1119-1153.
2. Agency for Toxic Substances and Disease Registry (ATSDR). U.S. Department of Health and Human Services. Public Health Service: Toxicological Profile for Phosphate Ester Flame Retardants. Published September 2012. Accessed September 19, 2023. <https://www.atsdr.cdc.gov/toxprofiles/tp202.pdf>
3. Wei GL, Li DQ, Zhuo MN, Liao YS, Xie ZY, Guo TL, Li JJ, Zhang SY, Liang ZQ. Organophosphorus flame retardants and plasticizers: sources, occurrence, toxicity and human exposure. *Environ Pollut*. 2015;196:29-46.
4. Rauert C, Lazarov B, Harrad S, Covaci A, Stranger M. A review of chamber experiments for determining specific emission rates and investigating migration pathways of flame retardants. *Atmos Environ*. 2014;82:44-55.
5. Blum A, Behl M, Birnbaum LS, Diamond ML, Phillips A, Singla V, et al. Organophosphate Ester Flame Retardants: Are They a Regrettable Substitution for Polybrominated Diphenyl Ethers? *Environ Sci Tech Let*. 2019;6(11):638-649.
6. Hou M, Fang J, Shi Y, Tang S, Dong H, Liu Y, et al. Exposure to organophosphate esters in elderly people: Relationships of OPE body burdens with indoor air and dust concentrations and food consumption. *Environ Int*. 2021a;157:106803.
7. Hou M, Shi Y, Na G, Cai Y. A review of organophosphate esters in indoor dust, air, hand wipes and silicone wristbands: Implications for human exposure. *Environ Int*. 2021b;146:106261.
8. Li W, Wang Y, Asimakopoulou AG, Covaci A, Gevao B, Johnson-Restrepo B, Kumosani TA, Malarvannan G, Moon HB, Nakata H, Sinha RK, Tran TM, Kannan K.

- Organophosphate esters in indoor dust from 12 countries: Concentrations, composition profiles, and human exposure. *Environ Int.* 2019;133(Pt A):105178.
9. Abdallah MA, Covaci A. Organophosphate flame retardants in indoor dust from Egypt: implications for human exposure. *Environ Sci Technol.* 2014;48(9):4782-9.
 10. Langer S, Fredricsson M, Weschler CJ, Bekö G, Strandberg B, Remberger M, Toftum J, Clausen G. Organophosphate esters in dust samples collected from Danish homes and daycare centers. *Chemosphere.* 2016;154:559-566.
 11. Fan X, Kubwabo C, Rasmussen PE, Wu F. Simultaneous determination of thirteen organophosphate esters in settled indoor house dust and a comparison between two sampling techniques. *Sci Total Environ.* 2014;491-492:80-6.
 12. Kubwabo C, Fan X, Katuri GP, Habibagahi A, Rasmussen PE. Occurrence of aryl and alkyl-aryl phosphates in Canadian house dust. *Emerg Contam.* 2021;7:149-159.
 13. Hoffman K, Butt CM, Webster TF, Preston EV, Hammel SC, Makey C, Lorenzo AM, Cooper EM, Carignan C, Meeker JD, Hauser R, Soubry A, Murphy SK, Price TM, Hoyo C, Mendelsohn E, Congleton J, Daniels JL, Stapleton HM. Temporal Trends in Exposure to Organophosphate Flame Retardants in the United States. *Environ Sci Technol Lett.* 2017;4(3):112-118.
 14. Siddique S, Farhat I, Kubwabo C, et al. Exposure of men living in the greater Montreal area to organophosphate esters: association with hormonal balance and semen quality. *Environ Int.* 2022;166:107402.
 15. Carignan CC, Mínguez-Alarcón L, Butt CM, Williams PL, Meeker JD, Stapleton HM, Toth TL, Ford JB, Hauser R; EARTH Study Team. Urinary Concentrations of Organophosphate Flame Retardant Metabolites and Pregnancy Outcomes among Women Undergoing in Vitro Fertilization. *Environ Health Perspect.* 2017;125(8):087018.

16. Meeker JD, Stapleton HM. House dust concentrations of organophosphate flame retardants in relation to hormone levels and semen quality parameters. *Environ Health Perspect.* 2010;118(3): 318-323.
17. Zhu Y, Ma X, Su G, Yu L, Letcher RJ, Hou J, Yu H, Giesy JP, Liu C. Environmentally Relevant Concentrations of the Flame Retardant Tris(1,3-dichloro-2-propyl) Phosphate Inhibit Growth of Female Zebrafish and Decrease Fecundity. *Environ Sci Technol.* 2015;49(24):14579-87.
18. Castorina R, Bradman A, Stapleton HM, Butt C, Avery D, Harley KG, Gunier RB, Holland N, Eskenazi B. Current-use flame retardants: Maternal exposure and neurodevelopment in children of the CHAMACOS cohort. *Chemosphere.* 2017;189:574-580.
19. Doherty BT, Hoffman K, Keil AP, Engel SM, Stapleton HM, Goldman BD, Olshan AF, Daniels JL. Prenatal exposure to organophosphate esters and cognitive development in young children in the Pregnancy, Infection, and Nutrition Study. *Environ Res.* 2019;169:33-40.
20. Wang H, Wang P, Li Q, Li J, Zhang L, Shi H, Li J, Zhang Y. Prenatal Exposure of Organophosphate Esters and Its Trimester-Specific and Gender-Specific Effects on Fetal Growth. *Environ Sci Technol.* 2022;56(23):17018-17028.
21. Yan H, Hales BF. Exposure to tert-Butylphenyl Diphenyl Phosphate, an Organophosphate Ester Flame Retardant and Plasticizer, Alters Hedgehog Signaling in Murine Limb Bud Cultures. *Toxicol Sci.* 2020;178(2):251-263.
22. Yan H, Hales BF. Effects of Organophosphate Ester Flame Retardants on Endochondral Ossification in Ex Vivo Murine Limb Bud Cultures. *Toxicol Sci.* 2019;168(2):420-429.

23. Yao Y, Li M, Pan L, Duan Y, Duan X, Li Y, Sun H. Exposure to organophosphate ester flame retardants and plasticizers during pregnancy: Thyroid endocrine disruption and mediation role of oxidative stress. *Environ Int.* 2021;146:106215.
24. Liu X, Cai Y, Wang Y, Xu S, Ji K, Choi K. Effects of tris(1,3-dichloro-2-propyl) phosphate (TDCPP) and triphenyl phosphate (TPP) on sex-dependent alterations of thyroid hormones in adult zebrafish. *Ecotoxicol Environ Saf.* 2019;170:25-32.
25. Percy Z, Vuong AM, Xu Y, Xie C, Ospina M, Calafat AM, Hoofnagle A, Lanphear BP, Braun JM, Cecil KM, Dietrich KN, Yolton K, Chen A. Maternal Urinary Organophosphate Esters and Alterations in Maternal and Neonatal Thyroid Hormones. *Am J Epidemiol.* 2021;190(9):1793-1802.
26. Fernie KJ, Palace V, Peters LE, Basu N, Letcher RJ, Karouna-Renier NK, Schultz SL, Lazarus RS, Rattner BA. Investigating endocrine and physiological parameters of captive American kestrels exposed by diet to selected organophosphate flame retardants. *Environ Sci Technol.* 2015;49(12):7448-55.
27. Stapleton HM, Misenheimer J, Hoffman K, Webster TF. Flame retardant associations between children's handwipes and house dust. *Chemosphere.* 2014;116:54-60.
28. Bailey JM, Levin ED. Neurotoxicity of FireMaster 550® in zebrafish (*Danio rerio*): Chronic developmental and acute adolescent exposures. *Neurotoxicol Teratol.* 2015;52(Pt B):210-9.
29. Patisaul HB, Roberts SC, Mabrey N, McCaffrey KA, Gear RB, Braun J, Belcher SM, Stapleton HM. Accumulation and endocrine disrupting effects of the flame retardant mixture Firemaster® 550 in rats: an exploratory assessment. *J Biochem Mol Toxicol.* 2013;27(2):124-36.

30. Rock KD, Horman B, Phillips AL, McRitchie SL, Watson S, Deese-Spruill J, Jima D, Sumner S, Stapleton HM, Patisaul HB. EDC IMPACT: Molecular effects of developmental FM 550 exposure in Wistar rat placenta and fetal forebrain. *Endocr Connect.* 2018;7(2):305-324.
31. Tung EWY, Ahmed S, Peshdary V, Atlas E. Firemaster® 550 and its components isopropylated triphenyl phosphate and triphenyl phosphate enhance adipogenesis and transcriptional activity of peroxisome proliferator activated receptor (Ppar γ) on the adipocyte protein 2 (aP2) promoter. *PLoS One.* 2017a;12(4):e0175855.
32. Tung EWY, Peshdary V, Gagné R, Rowan-Carroll A, Yauk CL, Boudreau A, Atlas E. Adipogenic Effects and Gene Expression Profiling of Firemaster® 550 Components in Human Primary Preadipocytes. *Environ Health Perspect.* 2017b;125(9):097013.
33. Pillai HK, Fang M, Beglov D, Kozakov D, Vajda S, Stapleton HM, Webster TF, Schlezinger JJ. Ligand binding and activation of PPAR γ by Firemaster® 550: effects on adipogenesis and osteogenesis in vitro. *Environ Health Perspect.* 2014;122(11):1225
34. Baldwin KR, Phillips AL, Horman B, Arambula SE, Rebuli ME, Stapleton HM, Patisaul HB. Sex Specific Placental Accumulation and Behavioral Effects of Developmental Firemaster 550 Exposure in Wistar Rats. *Sci Rep.* 2017;7(1):7118.
35. Witchey SK, Doyle MG, Fredenburg JD, St Armour G, Horman B, Odenkirk MT, Aylor DL, Baker ES, Patisaul HB. Impacts of Gestational FireMaster 550 (FM 550) Exposure on the Neonatal Cortex are Sex Specific and Largely Attributable to the Organophosphate Esters. *Neuroendocrinology.* 2022;10.1159/000526959.
36. Rosol TJ, Yarrington JT, Latendresse J, Capen CC. Adrenal gland: structure, function, and mechanisms of toxicity. *Toxicol Pathol.* 2001;29(1):41-8.

37. Burton C, Cottrell E, Edwards J. Addison's disease: identification and management in primary care. *Br J Gen Pract.* 2015;65(638):488-90.
38. Li Z, Robaire B, Hales BF. The Organophosphate Esters Used as Flame Retardants and Plasticizers Affect H295R Adrenal Cell Phenotypes and Functions. *Endocrinology.* 2023;164(9):bqad119.
39. Silva E, Rajapakse N, Kortenkamp A. Something from "nothing"--eight weak estrogenic chemicals combined at concentrations below NOECs produce significant mixture effects. *Environ Sci Technol.* 2002;36(8):1751-6.
40. Rajapakse N, Silva E, Kortenkamp A. Combining xenoestrogens at levels below individual no-observed-effect concentrations dramatically enhances steroid hormone action. *Environ Health Perspect.* 2002;110(9):917-21.
41. Chen Y, Liu Q, Ma J, Yang S, Wu Y, An Y. A review on organophosphate flame retardants in indoor dust from China: Implications for human exposure. *Chemosphere.* 2020;260:127633.
42. Olzmann JA, Carvalho P. Dynamics and functions of lipid droplets. *Nat Rev Mol Cell Biol.* 2019;20(3):137-155.
43. Boyd GS, McNamara B, Suckling KE, Tocher DR. Cholesterol metabolism in the adrenal cortex. *J Steroid Biochem.* 1983;19(1C):1017-27.
44. Hu J, Zhang Z, Shen WJ, Azhar S. Cellular cholesterol delivery, intracellular processing and utilization for biosynthesis of steroid hormones. *Nutr Metab.* 2010;7:47.
45. Li Z, Hales BF, Robaire B. Supplementary data for Impact of Exposure to an Environmentally Relevant Mixture of Organophosphate Esters on Adrenal Cell Phenotype, Lipidome, and Function. Deposited November 13, 2023.
10.6084/m9.figshare.24550468

46. Buzatto ZA, Kwon BK, Li L. Development of a NanoLC-MS workflow for high-sensitivity global lipidomic analysis. *Anal Chim Acta*. 2020;1139:88-99.
47. OECD. Test No. 456: H295R Steroidogenesis Assay: OECD Guidelines for the Testing of Chemicals. OECD Publishing. 2022; Section 4.
48. Akimoto T, Kobayashi S, Nakayama A, Isobe A, Abe K, Hatakeyama T, Ohta R, Yanagisawa R, Koike E, Suzuki N, Kawaguchi M. Toxicological effects of Tris (1,3-dichloro-2-propyl) phosphate exposure in adult male rats differ depending on the history of exposure in the neonatal period. *J Appl Toxicol*. 2022;42(9):1503-1509.
49. Chapin RE, George JD, Lamb JC 4th. Reproductive toxicity of tricresyl phosphate in a continuous breeding protocol in Swiss (CD-1) mice. *Fundam Appl Toxicol*. 1988;10(2):344-54.
50. National Toxicology Program. NTP Toxicology and carcinogenesis studies of tricresyl phosphate (CAS No. 1330-78-5) in F344/ N rats and B6C3F1 mice (gavage and feed studies). *Natl. Toxicol. Program. Tech. Rep. Ser.* 1994; 433: 1-321.
51. Latendresse JR, Azhar S, Brooks CL, Capen CC. Pathogenesis of cholesteryl lipidosis of adrenocortical and ovarian interstitial cells in F344 rats caused by tricresyl phosphate and butylated triphenyl phosphate. *Toxicol Appl Pharmacol*. 1993;122(2):281-9.
52. Latendresse JR, Brooks CL, Capen CC. Pathologic effects of butylated triphenyl phosphate-based hydraulic fluid and tricresyl phosphate on the adrenal gland, ovary, and testis in the Fischer-344 rat. *Toxicol Pathol*. 1994;22(4):341-52.
53. Latendresse JR, Brooks CL, Capen CC. Toxic effects of butylated triphenyl phosphate-based hydraulic fluid and tricresyl phosphate in female F344 rats. *Vet Pathol*. 1995;32(4):394-402.

54. Wade MG, Kawata A, Rigden M, Caldwell D, Holloway AC. Toxicity of Flame Retardant Isopropylated Triphenyl Phosphate: Liver, Adrenal, and Metabolic Effects. *Int J Toxicol*. 2019;38(4):279-290.
55. Ma Z, Tang S, Su G, Miao Y, Liu H, Xie Y, Giesy JP, Saunders DM, Hecker M, Yu H. Effects of tris (2-butoxyethyl) phosphate (TBOEP) on endocrine axes during development of early life stages of zebrafish (*Danio rerio*). *Chemosphere*. 2016;144:1920-7.
56. Chang Y, Cui H, Jiang X, Li M. Comparative assessment of neurotoxicity impacts induced by alkyl tri-n-butyl phosphate and aromatic tricresyl phosphate in PC12 cells. *Environ Toxicol*. 2020;35(12):1326-1333.
57. Liu X, Ji K, Choi K. Endocrine disruption potentials of organophosphate flame retardants and related mechanisms in H295R and MVLN cell lines and in zebrafish. *Aquat Toxicol*. 2012;114-115:173-81.
58. Wang X, Luu T, Beal MA, Barton-Maclaren TS, Robaire B, Hales BF. The Effects of Organophosphate Esters Used as Flame Retardants and Plasticizers on Granulosa, Leydig, and Spermatogonial Cells Analyzed Using High-Content Imaging. *Toxicol Sci*. 2022;186(2):269-287.
59. Rajkumar A, Luu T, Hales BF, Robaire B. High-content imaging analyses of the effects of bisphenols and organophosphate esters on TM4 mouse Sertoli cells. *Biol Reprod*. 2022;107(3):858-868.
60. Negi CK, Bajard L, Kohoutek J, Blaha L. An adverse outcome pathway based in vitro characterization of novel flame retardants-induced hepatic steatosis. *Environ Pollut*. 2021; 289:117855.

61. Koganti PP, Tu LN, Selvaraj V. Functional metabolite reserves and lipid homeostasis revealed by the MA-10 Leydig cell metabolome. *PNAS Nexus*. 2022;1(4):pgac215.
62. Venugopal S, Galano M, Chan R, Sanyal E, Issop L, Lee S, Taylor L, Kaur P, Daly E, Papadopoulos V. Dynamic Remodeling of Membranes and Their Lipids during Acute Hormone-Induced Steroidogenesis in MA-10 Mouse Leydig Tumor Cells. *Int. J. Mol. Sci.* 2021;22(5):2554.
63. Galano M, Li Y, Li L, Sottas C, Papadopoulos V. Role of Constitutive STAR in Leydig Cells. *Int. J. Mol. Sci.* 2021;22(4):2021.
64. Bartz R, Li WH, Venables B, Zehmer JK, Roth MR, Welti R, Anderson RG, Liu P, Chapman KD. Lipidomics reveals that adiposomes store ether lipids and mediate phospholipid traffic. *J Lipid Res.* 2007;48(4):837-47.
65. Negi CK, Gadara D, Kohoutek J, Bajard L, Spáčil Z, Blaha L. Replacement Flame-Retardant 2-Ethylhexyldiphenyl Phosphate (EHDPP) Disrupts Hepatic Lipidome: Evidence from Human 3D Hepatospheroid Cell Culture. *Environ Sci Technol.* 2023;57(5):2006-2018.
66. Hao Z, Zhang Z, Lu D, Ding B, Shu L, Zhang Q, Wang C. Organophosphorus Flame Retardants Impair Intracellular Lipid Metabolic Function in Human Hepatocellular Cells. *Chem Res Toxicol.* 2019;32(6):1250-1258.
67. Morris PJ, Medina-Cleghorn D, Heslin A, King SM, Orr J, Mulvihill MM, Krauss RM, Nomura DK. Organophosphorus flame retardants inhibit specific liver carboxylesterases and cause serum hypertriglyceridemia. *ACS Chem Biol.* 2014;9(5):1097-103.
68. Miller WL, Auchus RJ. The molecular biology, biochemistry, and physiology of human steroidogenesis and its disorders. *Endocr Rev.* 2011;32(1):81-151.

69. Hu W, Kang Q, Zhang C, Ma H, Xu C, Wan Y, Hu J. Triphenyl phosphate modulated saturation of phospholipids: Induction of endoplasmic reticulum stress and inflammation. *Environ Pollut.* 2020;263(Pt A):114474.
70. Holstein SA, Hohl RJ. Isoprenoids: remarkable diversity of form and function. *Lipids.* 2004;39(4):293-309.
71. Wang X, Lee E, Hales BF, Robaire B. Organophosphate Esters Disrupt Steroidogenesis in KGN Human Ovarian Granulosa Cells. *Endocrinology.* 2023;164(7):bqad089.
72. An J, Jiang J, Tang W, Zhong Y, Ren G, Shang Y, Yu Z. Lipid metabolic disturbance induced by triphenyl phosphate and hydroxy metabolite in HepG2 cells. *Ecotoxicol Environ Saf.* 2023;262:115160.
73. Pfeifer BA, Khosla C. Biosynthesis of polyketides in heterologous hosts. *Microbiol Mol Biol Rev.* 2001;65(1):106-18.
74. Patel MB, Oza NA, Anand IS, Deshpande SS, Patel CN. Liver x receptor: a novel therapeutic target. *Indian J Pharm Sci.* 2008 Mar-Apr;70(2):135-44.
75. Heckmann BL, Zhang X, Saarinen AM, Schoiswohl G, Kershaw EE, Zechner R, Liu J. Liver X receptor α mediates hepatic triglyceride accumulation through upregulation of G0/G1 Switch Gene 2 expression. *JCI Insight.* 2017;2(4):e88735.
76. Colin S, Briand O, Touche V, Wouters K, Baron M, Pattou F, Hanf R, Tailleux A, Chinetti G, Staels B, Lestavel S. Activation of intestinal peroxisome proliferator-activated receptor- α increases high-density lipoprotein production. *Eur Heart J.* 2013;34(32):2566-74.
77. Kershaw EE, Schupp M, Guan HP, Gardner NP, Lazar MA, Flier JS. PPARgamma regulates adipose triglyceride lipase in adipocytes in vitro and in vivo. *Am J Physiol Endocrinol Metab.* 2007;293(6):E1736-45.

78. Luo K, Liu J, Wang Y, Aimuzi R, Luo F, Ao J, Zhang J. Associations between organophosphate esters and sex hormones among 6-19-year old children and adolescents in NHANES 2013-2014. *Environ Int.* 2020;136:105461.
79. Ji Y, Yao Y, Duan Y, Zhao H, Hong Y, Cai Z, Sun H. Association between urinary organophosphate flame retardant diesters and steroid hormones: A metabolomic study on type 2 diabetes mellitus cases and controls. *Sci Total Environ.* 2021;756:143836.
80. Zhang Q, Wang J, Zhu J, Liu J, Zhao M. Potential Glucocorticoid and Mineralocorticoid Effects of Nine Organophosphate Flame Retardants. *Environ Sci Technol.* 2017;51(10):5803-5810.

FIGURES

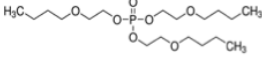
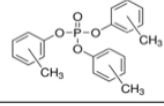
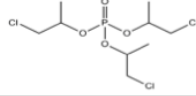
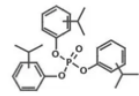
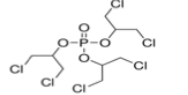
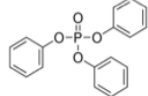
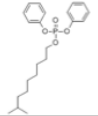
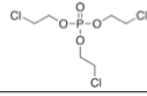
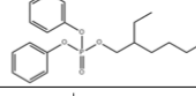
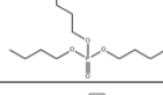
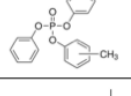
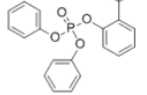
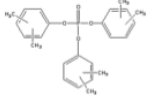
Chemical (acronym)	CAS No.	% Wt	Structure	Supplier
Tris(2-butoxyethyl) phosphate (TBOEP)	78-51-3	59.07%		Sigma-Aldrich
Tris(methylphenyl) phosphate (TMPP)	1330-78-5	8.44%		Alpha Aesar
Tris(1-chloro-2-propyl) phosphate (TCIPP)	13674-84-5	7.31%		AK Scientific
Isopropylated triphenyl phosphate (IPPP)	68937-41-7	5.62%		NIEHS/NTP
Tris(1,3-dichloro-2-propyl) phosphate (TDCIPP)	13674-87-8	5.06%		TCI America
Triphenyl phosphate (TPHP)	115-86-6	5.01%		Sigma-Aldrich
Isodecyl diphenyl phosphate (IDDPHP)	29761-21-5	4.27%		Scientific Polymer Products
Tris(2-chloroethyl) phosphate (TCEP)	115-96-8	2.48%		Sigma-Aldrich
Ethylhexyl diphenyl phosphate (EHDPHP)	1241-94-7	1.18%		AK Scientific
Tri-n-butyl phosphate (TNBP)	126-73-8	0.79%		Sigma-Aldrich
Cresyl diphenyl phosphate (CDPP)	26444-49-5	0.48%		Alpha Aesar
tert-Butylphenyl diphenyl phosphate (BPDP)	56803-37-3	0.19%		Scientific Polymer Products
Trixylyl phosphate (TXP)	25155-23-1	0.11%		CHEMOS

Figure 3-1. Composition of the Canadian household dust based OPE mixture.

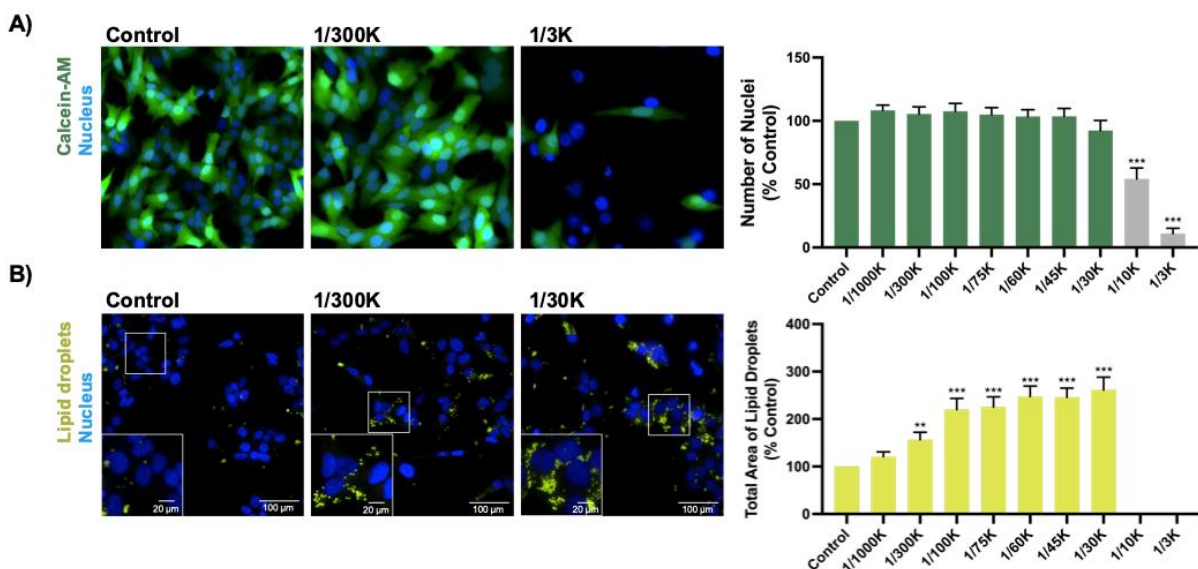


Figure 3-2. Effects of the organophosphate ester (OPE) mixture on (A) cell viability and (B) total area of lipid droplets. Cells were exposed to the OPE mixture for 48 h, followed by staining with (A) Hoechst 33342 (blue, nuclei) and Calcein-AM (green, viable cells) or (B) Hoechst 33342 (blue, nuclei) and Nile Red (yellow, lipid droplets) fluorescent dyes and were visualized with the Operetta high content imaging system (40 x magnification). Data are shown as percentages relative to controls; values represent means \pm SEM; n = 10. * $p < .05$, ** $p < .01$, and *** $p < .001$ compared to control. Concentrations that induced $> 30\%$ cytotoxicity were excluded from the analyses and were not shown for the lipid droplets endpoint.

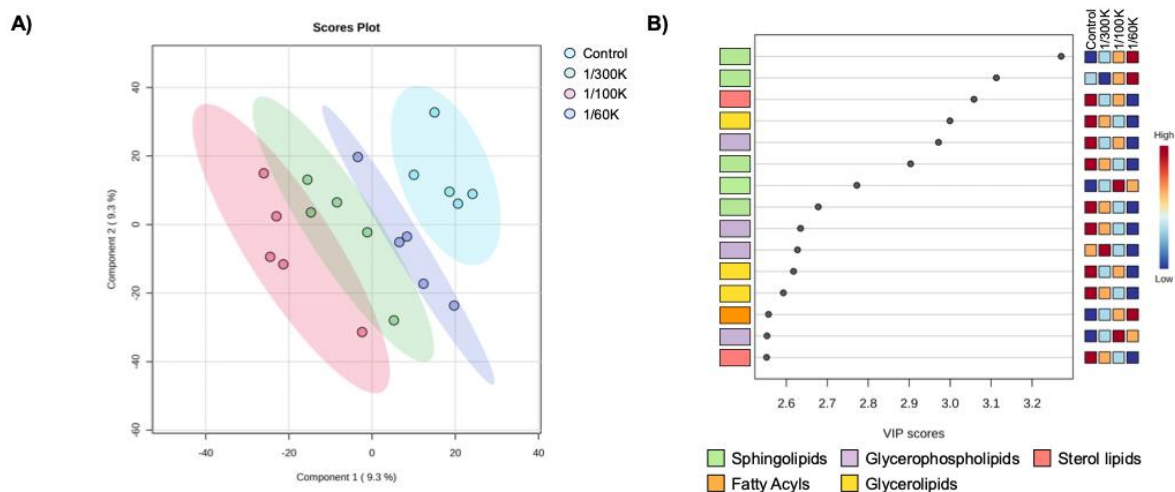


Figure 3-3. Multivariate analysis showing the degree of separation in lipid profiles between control, 1/300K, 1/100K, and 1/60K dilutions of the OPE mixture. (A) Differences in effects at mixture dilutions are visualized in a supervised PLS-DA plot. (B) PLS-DA Variable importance in projection (VIP) scores of the 15 most important lipids. Lipid category identification is indicated by the box on the left; each color represents a different lipid category.

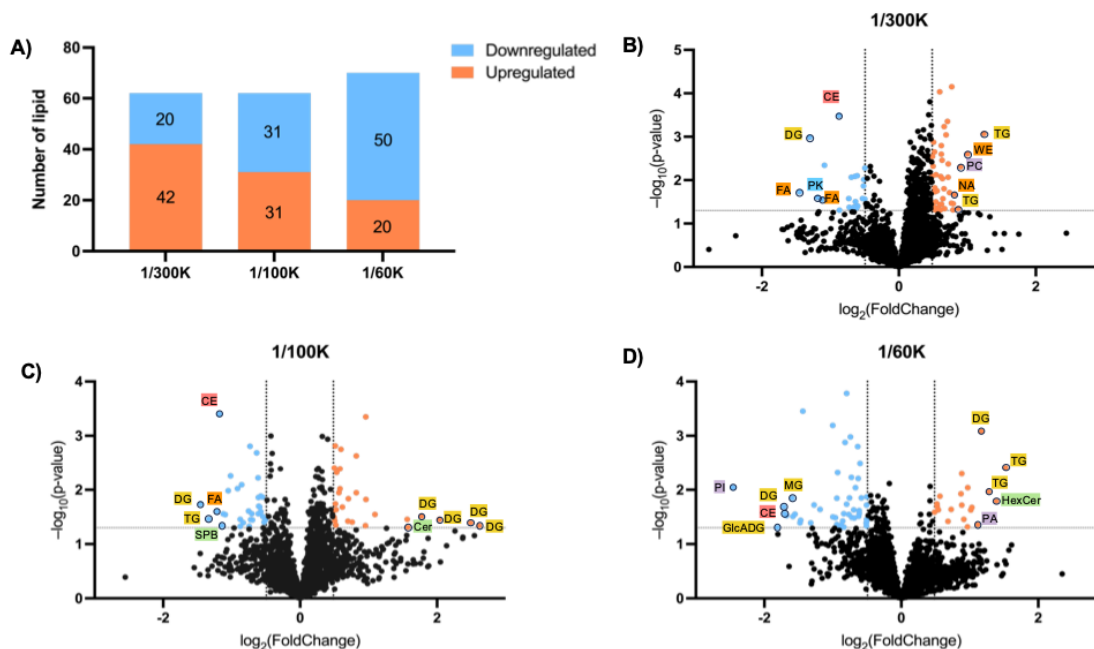


Figure 3-4. (A) Numbers of significantly affected lipids for each mixture dilution. (B) Volcano plot showing significantly altered lipids induced by exposure to a 1/300K dilution of the OPE mixture. (C) Lipids altered after exposure to 1/100K. (D) Lipids altered by the 1/60K dilution of the OPE mixture. Mixture exposures were for 48 h and are compared with control. Dashed gray lines indicate the cutoffs used (Fold change > 1.4 or < 0.71 and p-value < 0.05). Based on these cutoffs, blue dots indicate downregulated lipids and orange dots indicate upregulated lipids. For each dilution, the top 5 affected lipids in both the upregulated and downregulated group were highlighted by their subclass and category.

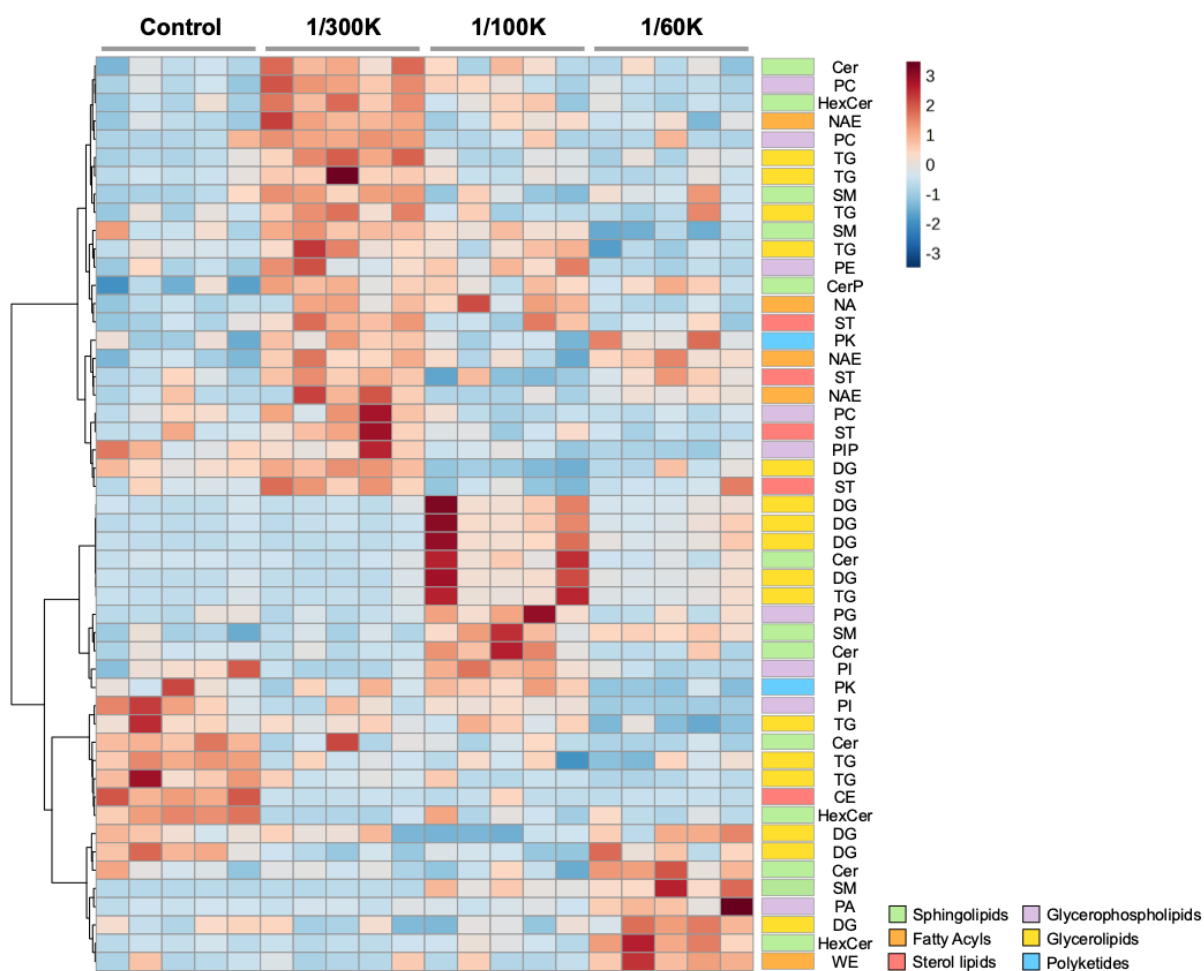


Figure 3-5. Heatmap of the top 50 affected lipids. Blue color indicates that lipids were downregulated; red color indicates upregulation. Lipids were labeled individually with their subclasses; lipid category were indicated by the box in colors.

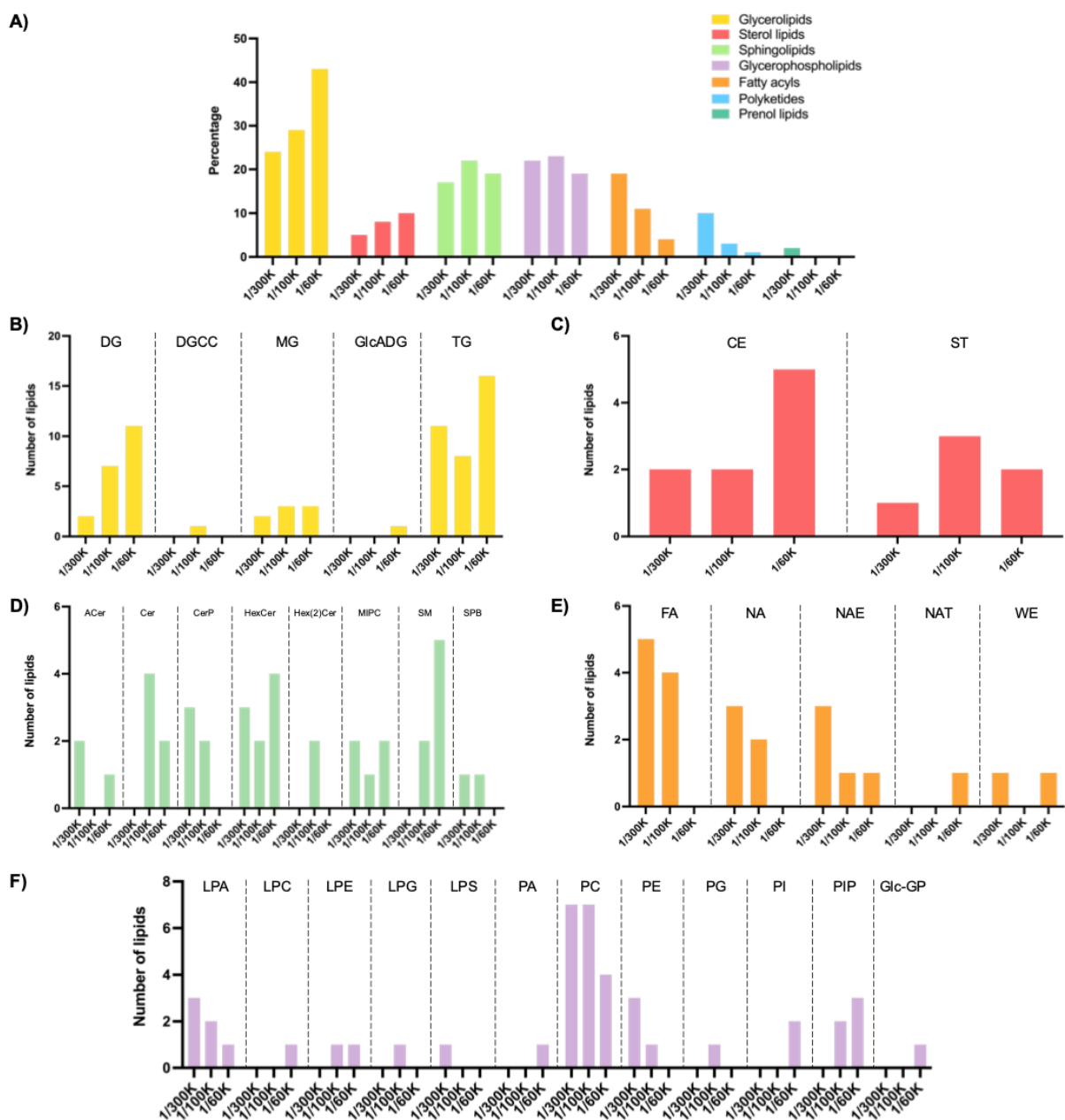


Figure 3-6. Relative distribution of significantly altered lipids in each category (A) and subclass (B–F). Color coding represents lipids that are from the same category: glycerolipids (yellow); sterol lipids (red); spingolipids (green); glycerophospholipids (purple); fatty acyls (orange); polyketides (blue); prenol lipids (teal).

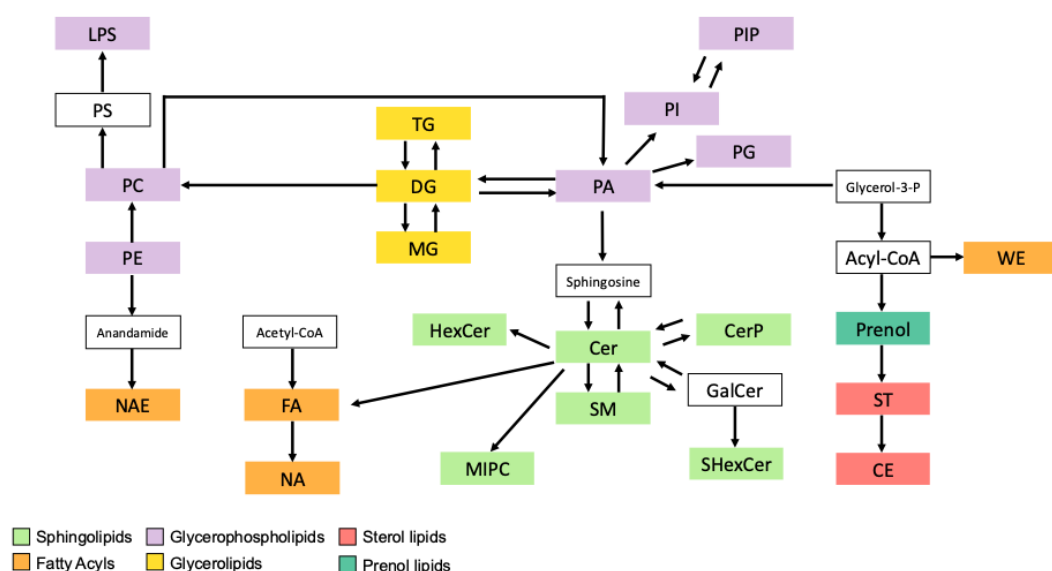


Figure 3-7. Proposed lipid pathways disrupted by OPE mixture exposures. Colored boxes highlight lipids affected by the OPE mixture; lipids in white boxes were not affected in the current study. Color coding represents lipids from the same category. Abbreviations for lipid subclasses: ceramide (Cer); sphingomyelin (SM); ceramide 1-phosphates (CerP); hexosyl ceramides (HexCer); sulfoglycosphingolipids (SHexCer); galactosylceramide (GalCer); ceramide phosphoinositols (MIPC); phosphatidic acids (PA); phosphatidylinositol (PI); phosphatidylglycerols (PG); glycerophosphoinositol monophosphates (PIP); phosphatidylcholine (PC); phosphatidylethanolamines (PE); phosphatidylserines (PS); lysophosphatidylserines (LPS); n-acyl ethanolamines (NAE); nitrogenated fatty acids (NA); fatty acids (FA); wax esters and diesters (WE); monoacylglycerols (MG); diglyceride (DG); triglycerides (TG); sterol lipids (ST); and cholesterol (CE).

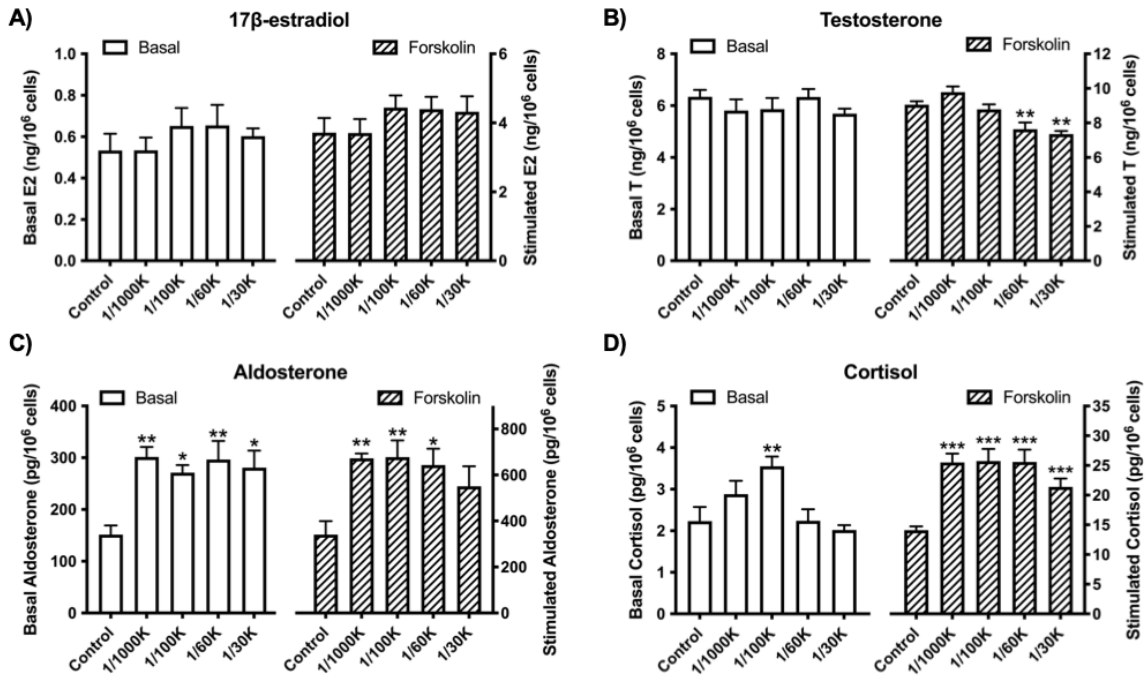


Figure 3-8. Effects of the OPE mixture on the steroid-producing function of H295R cells. Cells were exposed for 48 h. For the stimulated condition, a concentration of 10 μ M forskolin was used. Number of cells were quantified by Hoechst 33342 staining and high content imaging (10 x magnification). Bar graphs show basal (left Y axis, white bars) and stimulated (right Y axis, striped bars) production of (A) 17 β -estradiol, (B) testosterone, (C) aldosterone, and (D) cortisol levels. * p <.05, ** p <.01, and *** p <.001 compared to control; values represent means \pm SEM; n = 5.

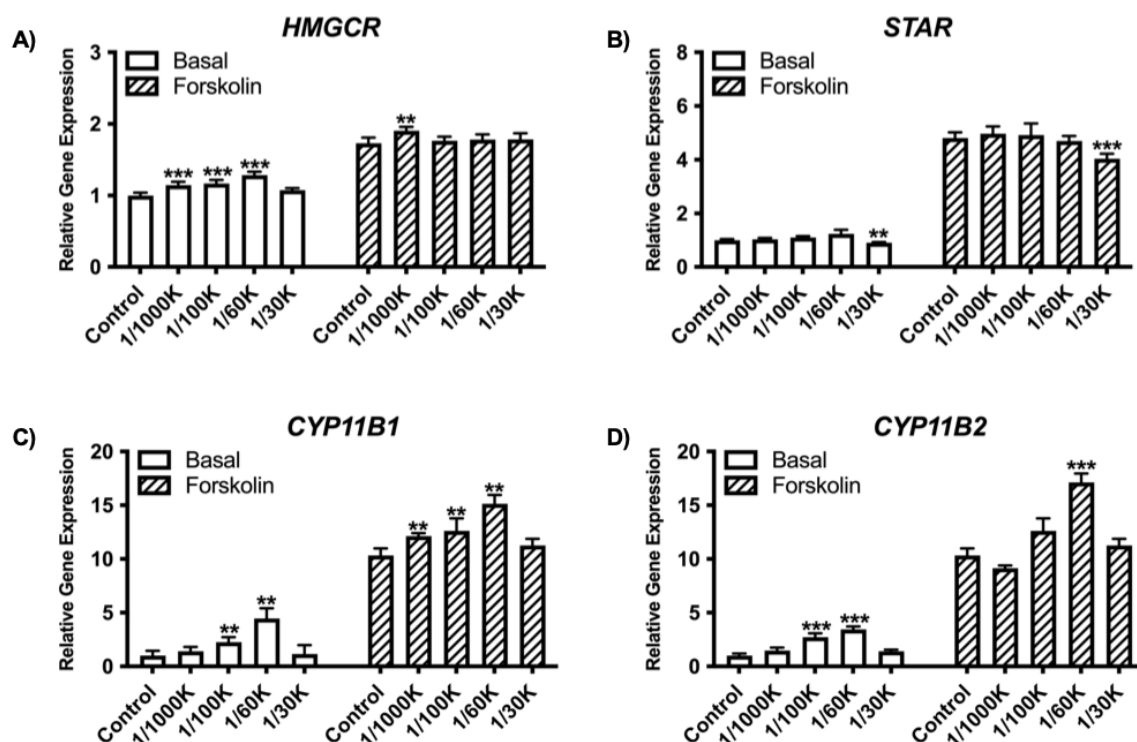


Figure 3-9. Effects of the OPE mixture on the mRNA expression of key transcripts involved in cholesterol and steroid biosynthesis: A: HMGCR; B: STAR; C: CYP11B1; D: CYP11B2 in H295R cells under basal and stimulated conditions. Cells were exposed for 48 h. For the stimulated condition, a concentration of 10 μ M forskolin was used. Data represent means \pm 95% CI, n = 5. *p<0.01, **p<0.001, ***p<0.0001 compared to control.

SUPPLEMENTAL MATERIALS

Supplemental Methods

Image acquisition and processing for high-content screening.

For all dye combinations: images were imported into the Columbus software for analysis.

The setup was as follows: individual planes, advanced flatfield correction (basic if advanced was not available).

Combination 1: Hoechst 33342/Calcein-AM/Lysotracker Red

To identify nuclei: [Find nuclei] - channel Hoechst 33342, method C (common threshold = 0.2, area > 30 μm^2 , split coefficient = 7, individual threshold = 0.5, contrast > 0.1).

To assess the morphology and intensity of the nuclei: [Calculate morphology properties] - population: nuclei, region: nucleus, method: standard area (μm^2) and roundness;

[Calculate intensity properties]: channel: Hoechst 33342, population: nuclei, region:

nucleus; method standard, mean. To exclude outliers: [Select population] - population:

nuclei, method: filter by property (filter F1 = intensity < 2000). To identify the

cytoplasmic areas: [Find Cytoplasm] - channel: Calcein green, nuclei selected; method A

(individual threshold = 0.15). To assess the intensity of the cytoplasmic area: [Calculate

intensity properties (2)] - channel: Calcein green, population: nuclei selected, region:

cytoplasm, method: standard (mean). To define the Calcein-positive viable cells: [Select

Population (2)] - population: nuclei selected, method: filter by properties (filter F1 =

intensity > 100). To identify lysosomes: [Find spots] - channel lysotracker red, region of

interest (ROI) population: Nuclei selected, ROI region: cell, method A (relative spot

intensity > 0.075, splitting coefficient = 1). To assess the morphology and intensity of the

lysosomes: [Calculate morphology properties (2)] - population: nuclei selected, region:

cell, method: standard (area (μm^2) and roundness); [Calculate intensity properties (3)]:

channel: lysotracker red, population: spots, region: spot maximum, method: standard

(mean). To exclude outliers: [Select population (3)] - population: spots, method: filter by

property (Filter F1, intensity < 10,000, filter F2 = spot area < 200 px^2).

The outputs of combination 1 included: the number of nuclei, Calcein intensity, the

Calcein-positive ratio (i.e., the number of Calcein-positive cells divided by the total

number of selected nuclei), the number of lysosomes per cell, and the average intensity of Lysotracker Red staining.

Combination 2: Hoechst 33342/Mitotracker Green/Mitotracker Red/Cellmask

To identify nuclei: [Find nuclei] - channel Hoechst 33342, method C (common threshold = 0.2, area > 30 μm^2 , split coefficient = 7, individual threshold = 0.5, contrast > 0.1).

To assess the morphology and intensity of the nuclei: [Calculate morphology properties] - population: nuclei, region: nucleus, method: standard (area (μm^2) and roundness);

[Calculate intensity properties] - channel: Hoechst 33342, population: nuclei, region: nucleus; method standard (mean). To exclude outliers: [Select population] - population: nuclei, method: filter by property (filter F1: intensity < 2000). To identify the cytoplasmic areas: [Find Cytoplasm] - channel: Cellmask Deep Red, nuclei selected, method: F

(individual threshold = 0.15). To determine total mitochondria intensity: [Find Image Region] - channel: Mitotracker Green, ROI population: nuclei selected, ROI region: cell;

method (common threshold = 0.35, split into objects, area > 0 px^2). To assess the mean staining intensity of mitochondria: [Calculate Intensity Properties (2)] - channel:

Mitotracker Green, population: mitogreen, region: mitochondria, method: standard

(mean); [Calculate Intensity Properties (3)] - channel: Mitotracker Red, population:

mitored, region: mitochondria, method: standard (mean). The outputs of combination 2

included: the number of nuclei, the average intensity of Mitotracker Green staining, the

average intensity of Mitotracker Red staining, and the active to total mitochondria ratio

(average intensity of Mitotracker Red/Mitotracker Green).

Combination 3: Hoechst 33342/Calcein-AM/CellROX

To identify nuclei: [Find nuclei] - channel Hoechst 33342, method C (common threshold = 0.2, area > 30 μm^2 , split coefficient = 7, individual threshold = 0.5, contrast > 0.1).

To assess the morphology and intensity of the nuclei: [Calculate morphology properties] - population: nuclei, region: nucleus, method: standard (area (μm^2) and roundness);

[Calculate intensity properties] - channel: Hoechst 33342, population: nuclei, region: nucleus; method standard (mean). To exclude outliers: [Select population] - population: nuclei, method: filter by property (filter F1: intensity < 2000). To identify the cytoplasmic areas: [Find Cytoplasm] - channel: Calcein green, nuclei selected; method A (individual threshold = 0.15). To identify the cell surrounding areas (background staining): [Find Surrounding Region] - channel: Calcein green, population: nuclei selected, region: cell, method A (individual threshold = 0.15). To assess the intensity of CellROX in the cytoplasmic and the background regions: [Calculate Intensity Properties] - channel: CellROX, population: nuclei selected, region: cell or background, method standard (mean). To calculate the corrected CellROX intensity: subtract Intensity Background CellROX from Intensity Cell CellROX. The outputs of combination 3 included: the number of nuclei and the corrected intensity of CellROX staining.

Combination 4: Hoechst 33342/Nile Red/Cellmask

To identify nuclei: [Find nuclei] - channel Hoechst 33342, method C (common threshold = 0.2, area > 30 μm^2 , split coefficient = 7, individual threshold = 0.5, contrast > 0.1).

To assess the morphology and intensity of the nuclei: [Calculate morphology properties] - population: nuclei, region: nucleus, method: standard (area (μm^2) and roundness);

[Calculate intensity properties] - channel: Hoechst 33342, population: nuclei, region: nucleus; method standard (mean). To exclude outliers: [Select population] - population: nuclei, method: filter by property (filter F1: intensity < 2000). To identify the cytoplasmic

areas: [Find Cytoplasm] - channel: Cellmask Deep Red, nuclei selected, method: F (individual threshold = 0.15). To identify lipid droplets: [Find Spots] - channel: Nile Red, ROI population: nuclei selected, ROI region: cell; method A (relative spot intensity > 0.080, splitting coefficient = 1). The outputs of combination 4 included: the number of nuclei, the total area of lipid droplets per cells, and the average number of lipid droplets per cell.

Data processing and normalization for lipidomic analysis.

LC-MS data were independently processed in positive and negative ionization. Lipid features were extracted and aligned using NovaMT LipidScreener. The detected features in positive and negative ionization from each sample experiment were combined. Missing values were substituted by (1) the median intensity of the sample group for features detected in at least 75% of injections within the group; (2) the minimum intensity within the group for features detected in at least 50% of injections; or (3) the global minimum for all sample and QC injections for features detected in less than 50% of injections within the group. The parameters used in data processing are shown below:

Intensity Threshold	2000 cts
Signal-to-Noise ratio (S/N) threshold	10
Minimum Peak Length	6 spectra
Retention Time Tolerance	5 seconds
m/z Tolerance	20.0 ppm for peak picking, 25.0 ppm for alignment
Feature Filtering	Detection for $\geq 80\%$ of injections in at least one sample group or QCs

A three-tier identification approach based on MS/MS spectral similarity, retention time and accurate mass match was employed for lipid identification. A nine-tier filtering and

scoring approach embedded in NovaMT LipidScreener was employed to restrict the number of matches and select the best identification. The parameters used for identification are described below.

Tier 1 (MS/MS identification)	MS/MS match score ≥ 500 ; precursor m/z error ≤ 20.0 ppm and 5.0 mDa
Tier 2 (MS/MS identification)	MS/MS match score < 500 ; precursor m/z error ≤ 20.0 ppm and 5.0 mDa
Tier 3 (MS match)	Mass match with m/z error ≤ 20.0 ppm and 5.0 mDa

Data normalization were performed by using a set of 15 deuterated internal standards belonging to different lipid classes (NovaMT LipidRep Internal Standard Basic Mix for Serum/Plasma). The positively and putatively identified lipids were matched to one of the 15 internal standards according to lipid class similarity and expected retention time range for each class. Intensity ratios, i.e., intensity of each lipid divided by intensity of the matched internal standard, were calculated for normalization and statistical analysis.

Image acquisition and processing for Hoechst-positive cell counts.

The Operetta images were imported into Columbus software for analysis. The setup was as follows: individual planes, advanced flatfield correction (basic if advanced was not available). To identify nuclei: [Find nuclei] - channel Hoechst 33342, method M (diameter = 25 μ m, splitting coefficient = 0.55, common threshold = 0.25). To assess the intensity of nucleus: [Calculate intensity properties] - channel: Hoechst 33342, population: nuclei, region: nucleus; method standard (mean). To identify and exclude outliers: [Select population] - population: nuclei, method: filter by property (filter F1: intensity < 4500).

List of supplemental tables and figures

Table 3-S1. Relative concentrations of the individual OPEs in the OPE mixture at all dilutions tested.

Table 3-S2. Cell-permeable fluorescent dyes and combinations used in high-content screening.

Table 3-S3. Parameters used in lipidomic statistical analysis.

Table 3-S4. List of commonly affected lipids across the 3 OPE treatment groups.

Table 3-S5. Lipids displaying extra oxygen atom(s)

Table 3-S6. List of uniquely affected lipids across the 3 OPE treatment groups.

Figure 3-S1. Effects of the OPE mixture on the phenotypic characteristics of H295R cells.

Figure 3-S2. Venn diagram of statistically significant lipids from each exposure comparison and their overlap.

Chemical	1/1000K (μM)	1/300K (μM)	1/100K (μM)	1/75K (μM)	1/60K (μM)	1/45K (μM)	1/30K (μM)	1/10K (μM)	1/3K (μM)
Tris(2-butoxyethyl) phosphate (TBOEP)	1.32	4.39	13.16	17.55	21.94	29.25	43.87	131.62	438.74
Tris(methylphenyl) phosphate (TMPP)	0.20	0.68	2.03	2.72	3.39	4.52	6.78	20.34	67.81
Tris(1-chloro-2-propyl) phosphate (TCIPP)	0.20	0.66	1.98	2.64	3.30	4.40	6.60	19.81	66.05
Isopropylated triphenyl phosphate (IPPP)	0.11	0.37	1.10	1.47	1.84	2.45	3.68	11.03	36.76
Tris(1,3-dichloro-2-propyl) phosphate (TDCIPP)	0.10	0.35	1.04	1.39	1.74	2.32	3.48	10.43	34.76
Triphenyl phosphate (TPHP)	0.14	0.45	1.36	1.82	2.27	3.03	4.54	13.63	45.45
Isodecyl diphenyl phosphate (IDDPHP)	0.10	0.32	0.97	1.29	1.62	2.16	3.24	9.71	32.37
Tris(2-chloroethyl) phosphate (TCEP)	0.08	0.26	0.77	1.03	1.29	1.71	2.57	7.71	25.71
Ethylhexyl diphenyl phosphate (EHDPHP)	0.03	0.10	0.29	0.39	0.48	0.64	0.96	2.89	9.64
Tri-n-butyl phosphate (TNBP)	0.03	0.09	0.26	0.35	0.44	0.59	0.88	2.63	8.78
Cresyl diphenyl phosphate (CDPP)	0.01	0.04	0.13	0.17	0.21	0.28	0.42	1.25	4.17
tert-Butylphenyl diphenyl phosphate (BPDP)	<0.01	0.01	0.04	0.06	0.07	0.10	0.15	0.44	1.47
Trixylyl phosphate (TXP)	<0.01	<0.01	0.02	0.03	0.04	0.05	0.08	0.24	0.79

Table 3-S1. Relative concentrations of the individual OPEs in the OPE mixture at all dilutions tested.

Dye (Cat#)	Staining	Dilution	Comb1	Comb2	Comb3	Comb4
Hoechst 33342 (R37165)	Nuclei	1:2000	✓	✓	✓	✓
Calcein-AM (C1430)	Cytoplasm (Cell viability)	1:1000	✓		✓	
LysoTracker Red DND-99 (L7528)	Lysosomes	1:6000	✓			
MitoTracker Green FM (M7514)	Total mitochondria	1:2000		✓		
MitoTracker Red CM- H2XRos (M7513)	Active mitochondria	1:2500		✓		
CellROX Deep Red (C10422)	Reactive oxygen species (oxidative stress)	1:2500			✓	
CellMask Deep Red (C10046)	Plasma membrane	1:1000		✓		✓
Nile Red (N1142)	Lipid droplets	1:100				✓

Table 3-S2. Cell-permeable fluorescent dyes and combinations used in high-content screening.

Phenol-red free DMEM/F-12 (incomplete medium) was used to prepare dye combinations 1, 2, and 3; 2% (w/v) polyvinylpyrrolidone was used to prepare combination 4. For combinations 1, 3, and 4, 100 μ M of the exposure medium was removed before adding 50 μ M of the corresponding dye solution. For combination 2, all exposure medium (200 μ M) was removed before adding 150 μ M of the corresponding dye solution; this was done to minimize the interaction between serum and MitoTracker Green dye. After the 30 min staining period, all dye solutions were removed, and cells were washed once with 200 μ M of the incomplete medium. For live cell imaging, 100 μ M incomplete medium was added to each well. Comb: combination; w/v: weight/volume percent.

	Multivariate Analysis
Data filtering and clean up	RSD >30% for QC samples; low RSD (near-constant values) between samples
Sample normalization	Internal standards, median
Data scaling	Autoscaling
Data transformation	None

Table 3-S3. Parameters used in lipidomic statistical analysis.

Lipids commonly affected by all 3 treatment groups:

Sphingolipids	Glycerolipids	Fatty acyls	Glycerophospholipids	Polyketides	Prenol lipids	Sterol lipids
HexCer 31:0;O3	TG 45:1;O3		PC O-14:0 LPA 10:0;O	PK 20:7;O5		CE 16:0

Lipids commonly affected by 1/300K and 1/100K dilutions of the OPE mixture:

Sphingolipids	Glycerolipids	Fatty acyls	Glycerophospholipids	Polyketides	Prenol lipids	Sterol lipids
CerP 40:2;O2 CerP 43:4;O2	DG 34:0 TG 34:1;O2 TG O-8:0_18:0_22:6	FA 27:2;O3 FA 26:2;O3 FA 24:1;O2 NA 40:2;O4;N	PE O-34:5			

Lipids commonly affected by 1/300K and 1/60K dilutions of the OPE mixture:

Sphingolipids	Glycerolipids	Fatty acyls	Glycerophospholipids	Polyketides	Prenol lipids	Sterol lipids
MIPC 53:4;O4 ACer 58:4;O2	TG 54:2 TG O-8:0_16:1_22:6 MGDG O-8:0_12:0	NAE 18:0;O3	PC 8:0_28:5			

Lipids commonly affected by 1/100K and 1/60K dilutions of the OPE mixture:

Sphingolipids	Glycerolipids	Fatty acyls	Glycerophospholipids	Polyketides	Prenol lipids	Sterol lipids
HexCer 35:2;O3 SM 36:3;O2 SM 46:1;O2 Cer 38:0;O3	DG 43:8;O TG 38:6;O2 DG 12:0_44:1 DG 16:0_32:1 DG 16:0_36:1 DG 16:1_36:1		PC 31:0 PC O-34:0 PIP 34:4;O PIP 35:8;O LPE O-19:0;O			ST 27:4;O

Table 3-S4. List of commonly affected lipids across the 3 OPE treatment groups.

Sphingolipids	Glycerolipids	Fatty acyls	Glycerophospholipids	Polyketides	Prenol lipids	Sterol lipids
13751ACer 58:4;O2	5699DG 28:1;O2	70135FA 24:1;O2	21192Glc-GP 40:1;O	3220PK 20:7;O5	1568PR 37:10;O3	575ST 20:5;O6
20394Cer 34:6;O3	16604DG 43:8;O	19934FA 26:1;O2	799LPA 10:0;O	3903PK 20:7;O5		n 15657.0ST 22:0;O8
18018Cer 38:0;O3	9474DG 49:2;O2	763FA 26:2;O3	15LPA 10:0;O	1450PK 20:7;O5		68994ST 25:3;O2
16153Cer 41:2;O2	70288DG 51:3;O2	920FA 27:2;O3	69944LPA 10:0;O	69706PK 20:7;O5		1350ST 26:4;O3
17944Cer 42:2;O2	21733DG dO-40:0;O	485NA 23:2;O2;N3	14098LPE O-19:0;O	2506PK 20:7;O5		15736ST 27:4;O
18666Cer 53:0;O4	9395DG O-39:0;O	1594NA 40:2;O4;N	73689PIP3 34:4;O	48753PK 20:7;O5		15655ST 28:0;O2
5225CerP 40:2;O2	14521TG 34:1;O2	11089NA 41:2;O5;N	57267PIP3 35:8;O	3271PK 20:7;O5		14781ST 51:6;O7
16762CerP 43:4;O2	14762TG 36:1;O2	1691NAE 11:1;O		10589PK 32:10;O5;N2		
22696Hex2Cer 30:2;O2	14362TG 38:6;O2	2392NAE 17:2;O3		67987PK 42:13;O24		
7264Hex2Cer 51:4;O2	15091TG 42:1;O3	10986NAE 18:0;O3				
3008HexCer 29:2;O5	14780TG 44:6;O2	22294NAT 21:2;O2				
n 6605.0HexCer 29:5;O3	8045TG 45:1;O3	2740NAT 28:2;O3				
5209HexCer 31:0;O3	17111TG 45:3;O	19399NAT 32:7;O3				
5223HexCer 34:2;O2	11359TG 48:11;O2					
14699HexCer 35:2;O3	68053TG 50:6;O2					
7956HexCer 41:0;O4	12304TG 51:9;O2					
13295HexCer 48:3;O2	18204TG 59:4;O					
72658HexCer 51:1;O4	9541TG 80:1;O					
48762MIPC 38:1;O5						
4155MIPC 53:4;O4						
4300MIPC 54:6;O3						
57218SM 14:0;O2/22:0						
16490SM 32:6;O4						
16338SM 32:6;O5						
4967SM 36:3;O2						
8814SM 42:4;O2						
23188SM 46:1;O2						
555SPB 20:1;O2						
45653SPB 22:0;20						
61539SL 12:1;O/12:1;O						

Table 3-S5. Lipids displaying extra oxygen atom(s)

Lipids only affected by the 1/300K dilution of the OPE mixture:

Sphingolipids	Glycerolipids	Fatty acyls	Glycerophospholipids	Polyketides	Prenol lipids	Sterol lipids
SM 42:4;O2 HexCer 51:1;O4 SM 12:1;O/12:1;O SPB 20:1;O2 HexCer 29:2;O5 HexCer 34:2;O2 HexCer 48:3;O2	TG 42:1;O3 TG 36:1;O2 TG O-70:12 TG 51:9;O2 DG 36:1 TG 44:6;O2 DG dO-40:0;O	NAT 32:7;O3 WE 34:3 NA 23:2;O2;N3 NAE 17:2;O3 NAE 28:2 NAT 21:2;O2	PC O-37:0 LPI 33:2 PC dO-37:0 LPI 23:0 PE O-36:4 LPS 31:5 PC O-36:5	PK 42:13;O24 PK 32:10;O5;N2	PR 37:10;O3 PR 40:15	ST 22:0;O8 ST 51:6;O7 ST 25:3;O2

Lipids only affected by the 1/100K dilution of the OPE mixture:

Sphingolipids	Glycerolipids	Fatty acyls	Glycerophospholipids	Polyketides	Prenol lipids	Sterol lipids
SPB 22:0;2O MIPC 54:6;O3 Cer 53:0;O4 Cer 34:6;O3 Hex2Cer 51:4;O2 Cer 41:2;O2 Hex2Cer 30:2;O2	TG O-8:0_22:0_22:6 TG 32:0 TG 33:0 DGCC 8:0_32:3 MG 34:1 DG 28:1;O2 MG O-8:0_10:0 TG 48:11;O2 MG O-13:0_28:2	FA 26:1;O2 NAE 11:1;O NA 41:2;O5;N	PC 8:0_28:2 PC 9:0_26:5 LPG O-33:1 PG O-58:9 PC O-21:1 PC 67:1			ST 26:4;O3 ST 20:5;O6 CE 10:2

Lipids only affected by the 1/60K dilution of the OPE mixture:

Sphingolipids	Glycerolipids	Fatty acyls	Glycerophospholipids	Polyketides	Prenol lipids	Sterol lipids
HexCer 29:5;O3 HexCer 41:0;O4 ST 28:0;O2;GlcA SM 32:6;O4 Cer 42:2;O2 SM 14:0;O2/22:0 SM 32:6;O5 DG 49:2;O2 MIPC 38:1;O5	GlcADG 12:0_16:0_14:0 MG O-10:0_28:2 DG 43:2 TG O-16:0_16:0_18:1 TG 18:2_19:0_21:3 DG 51:3;O2 TG 59:4;O TG 80:1;O TG 39:5 TG 11:0_16:0_17:0 TG 50:6;O2 DG O-39:0;O TG 50:3 DG O-36:6 MG 2:0_22:1 TG 14:2_22:0_22:1 TG O-16:0_16:1_18:1 TG 18:0_19:1_21:5 DG O-35:7 TG 45:3;O	NAT 28:2;O3 WE 19:0	PI O-40:0 PI O-38:0 PIP 39:10 LPC 32:1 PA 38:1 Glc-GP 40:1;O			CE 22:3 CE 14:0 CE 20:4 CE 22:4

Table 3-S6. List of uniquely affected lipids across the 3 OPE treatment groups.

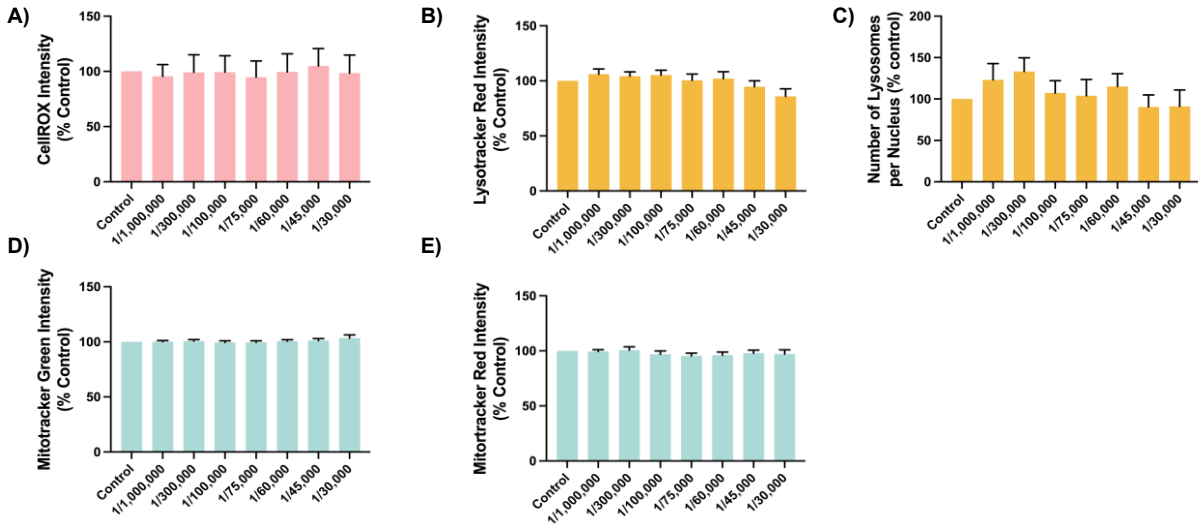


Figure 3-S1. Effects of the OPE mixture on the phenotypic characteristics of H295R cells. A) oxidative stress levels; B) lysotracker red intensity; C) lysosome numbers; D) total mitochondria; and E) active mitochondria. Cells were exposed to the OPE mixture for 48 h, followed by staining with fluorescent dyes and were visualized with the Operetta high content imaging system (40 x magnification). Data are shown as percentages relative to controls; values represent means \pm SEM; n = 10. Concentrations that induced > 30% cytotoxicity were excluded from the analyses.

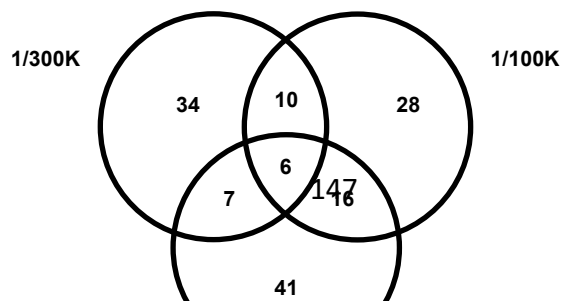


Figure 3-S2. Venn diagram of statistically significant lipids from each exposure comparison and their overlap. Venn diagram showing common and unique significantly affected lipids in the 3 treatment groups. Overall, 6 lipids were commonly affected in all treatment groups. 34 lipids were unique to the 1/300K group; 28 lipids were unique to the 1/100K group; and 41 lipids were unique to the 1/60K group.

CONNECTING TEXT

The previous chapters compared the effects of OPEs to those of legacy PBDEs and elucidated the impact of an environmentally relevant mixture of OPEs on adrenal cells. At the cellular level, we observed that disruption in lipid homeostasis is a sensitive response to exposure to either the individual OPEs or the mixture. To further assess the potential impact of OPEs on the hypothalamic-pituitary-adrenal (HPA) axis, an effect that can only be studied in intact animals, we next investigated the *in vivo* effects of the OPE mixture. Given the limited metabolic capacity of the H295R cell line, the animal study also allowed us to capture any effects induced by OPEs that may be metabolized within the body.

Chapter four describes a study aimed at investigating the impact of an environmentally relevant mixture of OPEs on the adrenal glands of Sprague Dawley rats. To assess whether OPEs exert sex specific effect, we exposed both adult male and female Sprague Dawley rats to either a vehicle or one of the three doses of the OPE mixture (0.048, 1.6, or 48 mg/kg bw/day) for 70-72 days via diet. We assessed the weight, histology, and function of the adrenal gland following exposure to the OPE mixture. The activity of the HPA axis was evaluated by measuring levels of ACTH and renin in serum. Further, to examine the molecular mechanism(s) of action of the mixture, we did RNA sequencing analysis and elucidated the affected pathways in both male and female rats.

CHAPTER 4
Impact of Exposure to a Mixture of Organophosphate Esters on the Adrenal Glands of
Sprague Dawley Rats

Zixuan Li, Barbara F Hales, Bernard Robaire,

(Accepted: Toxicological Sciences; November 27, 2024)

ABSTRACT

There is growing evidence that organophosphate esters (OPEs) can act as endocrine-disrupting chemicals. However, only a few studies have assessed the effects of OPE exposure on one of the most important endocrine glands in the body, the adrenal gland. Our aim was to test the effects of a mixture of OPEs detected in Canadian house dust on adrenal function in Sprague Dawley rats. Adult male and female rats ($n = 15$ per treatment group) were administered either a vehicle or an OPE mixture (0.048, 1.6, or 48 mg/kg bw/day) for 70-72 days via their diet. With OPE exposure, adrenal glands from male adult rats were reduced in weight, while those of female rats showed an increase in weight. This led us to investigate whether OPEs induce sex-specific effects on adrenal gland function and the mechanisms involved. Serum levels of two adrenal hormones, aldosterone and corticosterone, were decreased only in male serum samples. Serum levels of renin and adrenocorticotrophic hormone (ACTH), which regulate aldosterone and corticosterone synthesis, respectively, were assessed. Exposure to the OPE mixture decreased renin levels only in males. Serum biochemistry analysis revealed that triglycerides and LDL cholesterol levels were increased in males. Transcriptomic analysis revealed that the top affected pathways in male adrenal glands from all three treatment groups were related to potassium channels, which play a role in regulating aldosterone and corticosterone levels. The most affected pathways in female adrenal glands were related to cholesterol biosynthesis and immune functions. These results show that an environmentally relevant mixture of OPEs affects adrenal function and that these effects are sex specific.

INTRODUCTION

Organophosphate esters (OPEs) are extensively used as flame retardants and plasticizers in various products including furniture, baby toys, electronics, textiles, and building materials (Wei et al., 2015; van der Veen and de Boer, 2012). Since OPEs are not covalently bonded to the polymers, they gradually volatilize into the air and subsequently settle into dust. This process creates multiple exposure pathways for individuals, including ingestion, inhalation, dermal contact, and dietary intake of contaminated dust (van der Veen and de Boer, 2012; Hou et al., 2021; Agency for Toxic Substances and Disease Registry, 2012). Among the indoor exposure pathways, ingestion of dust is the major source of human exposure to OPEs (Kim et al., 2019). Consequently, OPE metabolites are detectable in the urine samples of nearly 100% of adults and children in the United States, Europe, China, and Australia (Cequier et al., 2015; He et al., 2018a; Hoffman et al., 2017; Ospina et al., 2018; Sun et al., 2018). Moreover, OPEs have been identified in other human matrices, such as blood (reviewed by Chokwe et al., 2020; Hou et al., 2022), breast milk (Ma et al., 2019), hair, and nails (Liu et al., 2016; He et al., 2018b).

Exposure to OPEs is associated with various adverse health effects, including neurotoxicity (Doherty et al., 2019; Patisaul et al., 2021), developmental and reproductive toxicity (reviewed by Hales and Robaire, 2020; Siddique et al., 2022; Carignan et al., 2017; Meeker et al., 2010), carcinogenicity (Blum et al., 2019), and endocrine disruption (Hu et al., 2022; Rosenmai et al., 2021; Yao et al., 2021). The concurrent use of multiple OPEs raises concerns about the potential health risks of OPE mixtures. Studies in both humans and rodent models indicate that exposure to mixtures of OPEs can affect multiple organs, including bone (Macari et al., 2020; Pillai et al., 2014; Yan and Hales., 2021), liver (Aluru et al., 2021; Witchey et al., 2020), brain (Baldwin et al., 2017; Gillera et al., 2020; Marinello et al., 2022; Newell et al., 2023; Rock et al., 2020; Wiersielis et al., 2020; Witchey et al., 2023), ovary (Wang et al.,

2024), and adipose tissue (Pillai et al., 2014, Tung et al., 2017a; Tung et al., 2017b). Exposure to one of the most extensively studied mixtures, Firemaster 550, has demonstrated endocrine-disrupting potential, resulting in weight gain and early onset of puberty in rats at environmentally relevant levels (Patisaul et al., 2013). Despite these findings, research on the impact of OPEs on the adrenal gland, one of the most critical endocrine glands in the body, remains limited.

The adrenal gland produces hormones that regulate several vital functions, including metabolism, blood pressure, and the stress response (Rosol et al., 2001). Loss of adrenal function, as seen in adrenal insufficiency, can be life-threatening (Burton et al., 2015). The adrenal glands are among the endocrine tissues most frequently affected by chemicals (Ribelin et al., 1984). For instance, the off-target effects of etomidate have led to fatalities due to the unrecognized inhibition of steroidogenic enzymes involved in cortisol and aldosterone synthesis (Wagner et al., 1984). Despite the critical roles of the adrenal glands, they are often overlooked in toxicological studies, which have primarily focused on reproductive and developmental endpoints (Cockburn et al., 1999). To date, only a few studies have examined the effects of OPEs on the adrenal glands, and these studies have tested a very limited number of OPEs. *In vivo* studies have focused on the effects of three OPEs: tris(methylphenyl) phosphate (TMPP), isopropylated triphenyl phosphate (IPPP), and tris(1,3-dichloro-2-propyl) phosphate (TDCIPP). Only studies using TMPP assessed both male and female subjects, finding that adrenal gland weight and the adrenal cortex were affected in both sexes (National Toxicology Program, 1994; Latendresse et al., 1994; Latendresse et al., 1993; Latendresse et al., 1995). In contrast, studies using IPPP and TDCIPP tested only male rats (Wade et al., 2019; Akimoto et al., 2022). None of these studies explored the mechanisms of action of OPEs.

In vitro studies using human H295R adrenal cortical cells and PC12 rat adrenal cells have investigated a broader range of OPEs. These studies found that OPEs could induce cytotoxicity

(Chang et al., 2020) and alter the production of steroid hormones, specifically testosterone and 17 β -estradiol, by affecting enzymes in the steroidogenic pathway (Liu et al., 2012). Using human H295R adrenal cells, we previously demonstrated that exposure to commonly used OPEs affects both the phenotype and function of these cells (Li et al., 2023). Given the contrasting effects observed with individual OPEs on cortisol and aldosterone production levels, we assessed the impact of an environmentally relevant mixture of OPEs to better mimic real-world exposure scenarios. This mixture induced accumulation of lipid droplets as a primary target and affected the steroid hormone production levels in the cells (Li et al., 2024). This body of evidence underscores the necessity of including the adrenal glands in toxicological evaluations.

The goal of this study was to assess the impact of a Canadian household dust-derived mixture of OPEs on adrenal gland function in Sprague Dawley rats. This research represents the first *in vivo* assessment of real-world OPE exposure effects on the whole adrenal gland of both sexes. We assessed adrenal gland weight, histology, and function following exposure to the OPE mixture. Furthermore, we examined the molecular mechanisms underlying these effects by elucidating affected pathways in both male and female rats using RNA sequencing.

MATERIALS AND METHODS

Organophosphate Ester House Dust Mixture

The OPE house dust mixture, which contains 13 OPEs detected in over 85% of house dust samples collected from 144 urban Canadian homes between 2007 and 2010, was formulated by Dr. Michael G. Wade (Health Canada) (Figure 1; (Fan et al., 2014; Kubwabo et al., 2021)). The relative proportion of each OPE in this mixture is based on their 95th percentile values from these samples.

Diets were prepared fresh every month and fed to the animals no later than one month after preparation. To maximize the homogeneous distribution of the OPE mixture with the diet, the mixture was added to the mixing bowl containing powdered AIN-93G diet in a stepwise manner (Reeves, 1997). The combined diet, at the desired mixture concentration, was mixed with 8% (by weight) deionized water, pelleted, and dried at room temperature for 20h. Each diet was labeled with a date of preparation and a color code. The identity of the diet dose was revealed only after all in life handling and related data were collected and analyzed. The diets were formulated to deliver mixture doses of 0.048, 1.6, or 48 mg/kg body weight/day. This estimation is based on a daily food consumption rate for rats of 80 g/kg body weight/day and accounts for assumptions regarding dust ingestion rates (100 mg/day) for children (16.5 kg body weight), as well as the scaling of dose from humans to rodents based on body surface area (1:6.3 human to rat) rather than body weight. The low dose was selected to reflect a human-relevant exposure level, based on the estimated daily intake of Σ OPE from indoor dust in the United States in 2018 (Kim et al., 2019). The highest dose was chosen to represent a level at which some effects would be expected, based on observed changes in the adrenals of male rats treated with the individual OPE, IPPP, at 70 mg/kg body weight per day for 90 days (Wade et al., 2019). This dose also incorporates a 'safety factor' to address the significant variability in OPE dust concentrations. For example, the median TDCIPP concentration in dust was 1,506 ng/g, with a range spanning from 181 to 2,140,000 ng/g (Castorina et al., 2017).

Animal Treatments

72 days old male Sprague Dawley rats and 70 days old female Sprague Dawley rats were obtained from Charles River (St-Constant, QC, Canada) and maintained on a 12-hour light:12-hour dark cycle at the McIntyre Animal Resources Centre (McGill University, Montreal, QC,

Canada). Food and water were provided ad libitum. All animal studies followed the principles and procedures outlined in the Guide to the Care and Use of Experimental Animals prepared by the Canadian Council on Animal Care (McGill Animal Research Centre protocol 2018-7997). Rats were allowed to acclimatize for one week before being randomly assigned ($n = 15$ per group) to either the control group or one of the three OPE mixture treatment groups (0.048, 1.6, or 48 mg/kg bw/day). All researchers were blinded to the treatment groups for the entirety of the study. Animals and their food were weighed once a week to determine food consumption. Male rats were exposed for 70 days, which is sufficient to complete a full cycle of spermatogenesis and epididymal sperm maturation. Female rats were initially exposed for 30 days, the time required for ovarian follicles to progress from the primordial to the preovulatory stage. Following this, females were mated with males from the same dosage group and continuously exposed to either control or OPE-containing diets during gestation and lactation, until the pups were weaned on postnatal day 21.

Tissue Collection

Male rats ($n = 10$ per group) were euthanized under isoflurane anesthesia by exsanguination via cardiac puncture. Adrenal glands were collected, weighed, and snap-frozen in liquid nitrogen for further analysis. The remaining rats ($n = 5$ per group) were euthanized by fixation with Modified Davidson's solution via retrograde perfusion through the abdominal aorta. Procedures were conducted following standard guidelines (Parasuraman et al., 2010; Latendresse et al., 2002). Fixed adrenal glands were then post-fixed for 24 hours, dehydrated, and stored in a 4°C cold room until further analysis. Female rats ($n = 15$ per group) were euthanized under isoflurane anesthesia by exsanguination via cardiac puncture. Adrenal glands were collected, weighed, and snap-frozen in liquid nitrogen ($n = 10$). The remaining adrenal glands ($n = 5$ per group) were

fixed and stored in a 4°C cold room until further analysis.

Whole blood was transferred to Vacutainer SST tubes (BD Biosciences Canada, Mississauga, ON), allowed to clot for 30 minutes at room temperature, and then centrifuged at $2000 \times g$ for 10 minutes at 4°C for serum collection. For plasma collection, whole blood was transferred to Vacutainer EDTA tubes (BD Biosciences Canada, Mississauga, ON) and then centrifuged at $2000 \times g$ for 10 minutes at 4°C. Sera and plasma were aliquoted and stored at -80°C until further analysis.

Histology

Fixed adrenal glands were paraffin-embedded, serially sectioned at 5 µm thickness, and stained with hematoxylin and eosin. The stained slides were scanned using the AxioScan.Z1 microscope slide scanner (Zeiss Canada, Toronto, ON) and digitized. Digitized adrenal sections were examined blindly, considering key parameters such as adrenal hypertrophy, hemosiderin, lipid droplets, hyperplasia, apoptosis, and the width of blood sinusoids. Based on the severity of the examined parameters, a score from 0 to 5 was assigned, with 0 representing the absence of pathology. The scoring criteria are provided in Supplementary Table 1. The thickness of total cortex and that of zona glomerulosa, zona fasciculata, and zona reticularis were measured using QuPath (v0.4.1; Bankhead et al., 2017). Specifically, the length parallel to the adrenal radius of these areas was measured in five different sections per adrenal and the average value was used in final calculation of zone thickness.

Serum Biochemistry

Serum samples were sent to the Center for Phenogenomics (TCP, Toronto, ON, Canada) for a

comprehensive cardiovascular panel analysis, which included total cholesterol, HDL cholesterol, LDL cholesterol, triglycerides, and glucose. The standard biochemistry panel was conducted at the Diagnostic and Research Support Service (DRSS) Laboratory of the Comparative Medicine Animal Research Centre, McGill University (Montreal, QC, Canada).

Hormone Measurements

To assess the effects of the OPE mixture on the steroid hormone producing function of the adrenal gland, enzyme-linked immunosorbent assay (ELISA) kits were used to measure the levels of aldosterone, corticosterone, ACTH, and renin [Aldosterone: Abcam Catalog # ab136933, RRID: AB_2895004; Corticosterone: Arbor assays Catalog # K014-H1/H5, RRID: AB_2877626); ACTH: Abcam Catalog # ab263880, RRID: AB_2910221; Renin: Invitrogen Catalog # ERA52RB, RRID: AB_3661832] in accordance with the manufacturers' instructions. The detection limit for the assay kits were: aldosterone 4.7 pg/mL, corticosterone 0.0175 ng/mL, ACTH 6.0 pg/mL, and renin 30.0 pg/m. The SpectraMax Plus 384 microplate reader (Molecular Devices, San Jose, California, USA) was used to read the ELISA plates at a wavelength of 450 nm. Aldosterone and corticosterone levels have been adjusted for cross reactivity. The intra-assay and inter-assay coefficients of variation for female samples were 4.5% and 14.2% for the aldosterone assay; 4.6% and 14.8% for the corticosterone assay, 4.9% and 15.0% for the ACTH assay, and 4.5% and 14.4% for the renin assay. For males, they were 3.4% and 13.8% for the aldosterone assay; 3.6% and 13.4% for the corticosterone assay; 4.9% and 14.8% for the ACTH assay, and 3.5% and 13.5% for the Renin assay.

RNA-seq and pathway analysis

Adrenal glands were homogenized, and total RNA was isolated using the RNeasy Plus Mini Kit (Qiagen, Mississauga, ON, Canada). The integrity of the extracted RNA was assessed using the RNA 6000 Nano Kit (Agilent Technologies, Mississauga, ON, Canada) on the 2100 Bioanalyzer System (Agilent Technologies, Mississauga, ON, Canada). Paired-end sequencing (150 bp) was conducted at Novogene Corporation (Sacramento, California, USA) using their NovaSeq 6000 Sequencing System (Illumina, San Diego, California, USA). RNA-seq data have been uploaded to GEO (number pending). Differentially expressed genes (DEGs) were identified using the DESeq2 R package (version 1.20.0) ($p < 0.05$). Transcripts differentially expressed by more than 1.5-fold were then further analyzed using Ingenuity Pathway Analysis (IPA 2024; Qiagen, Valencia, California, USA) software.

Statistical Analyses

Data were analyzed using GraphPad Prism (version 9.4.1, GraphPad Software Inc., La Jolla, California, USA). One-way ANOVA followed by Dunnett's test was used to compare adrenal gland weight, plasma biochemistry data, and hormone levels. Adrenal gland weight and hormone measurements were obtained from 10 animals per experimental group, with four groups for males and four groups for females. These included a control group and three groups exposed to different OPE doses for each sex. Plasma biochemistry and RNA sequencing analysis were done for 5 animals from each treatment group. For all experiments, the minimum level of significance was taken as $p < 0.05$.

RESULTS

Effects of the OPE mixture on animal and adrenal weights

Weekly weights and food consumption were monitored throughout the treatment. No changes in body weight or food consumption were observed with OPE exposure in either the male or female treatment groups when compared with the control group (Supplementary Figure 1). As expected from the literature (Piao et al., 2013), the male adrenal glands weighed less than those of the female adrenal glands at the control level (Figure 2). Starting with the lowest OPE treatment group, the male adrenal gland showed a reduction in weight (Figure 2A). In contrast, the female adrenal glands showed a trend of increase in weight, with high OPE treatment group showing statistical significance (Figure 2B). The distinct sex differences observed in adrenal gland weight in response to OPE exposure led us to further investigate whether the function of the adrenal gland was affected. Histological examination did not reveal any apparent changes in the adrenal gland (Supplementary Figure 2). Apart from the decrease observed in the female fasciculata zone, exposure to the mixture did not induce alterations in the width of other zones (Supplementary Figure 3).

Serum biomarkers are affected by the OPE mixture

Serum samples were collected at the time of euthanasia and analyzed for biomarkers associated with pathogenesis (Supplementary Figure 4 and 5). OPE treatment did not result in any significant change in most biomarkers, indicating markers of liver or kidney function, muscle damage, and serum electrolyte levels. However, markers for lipid homeostasis were affected by the OPE mixture. Exposure to the high level of OPE mixture nearly doubled the levels of triglycerides and LDL cholesterol in male serum samples (Figure 3B and 3D). The same exposure level also induced a trend towards increased HDL cholesterol concentration in males ($p = 0.06$) (Figure 3E). For females, the only observed change was at the low exposure level, where

a trend towards increased total cholesterol ($p = 0.07$) was noted (Figure 3C).

Effects of the OPE mixture on serum hormone levels

The average baseline level of serum aldosterone in males was 550.5 pg/ml (Figure 4A), while that in females was much lower at 208.2 pg/ml (Figure 4B). In the male adrenal gland, exposure to the OPE mixture resulted in a downregulation of aldosterone levels in all three treatment groups, with the resulting levels similar to the baseline level observed in females, around 200 pg/ml (Figure 4A). No significant effect in aldosterone levels was observed in the female treatment groups (Figure 4B). The average baseline level of renin is similar in males (510.8 pg/ml) and females (505.6 pg/ml) (Figure 4C and 4D). In males, a concentration dependent decrease in the level of renin was observed, with the high OPE group significantly reduced the level to 356.8 pg/ml (Figure 4C). In females, however, exposure to OPEs resulted in a trend of increase in the level of renin ($p = 0.08$) (Figure 4D).

The baseline level of serum corticosterone in males (377.6 ng/ml) was approximately three times higher than in females (140.3 ng/ml) (Figure 4E and 4F). In the high OPE treatment group, the level of corticosterone in males were reduced to half of the control level (Figure 4E). No effect was observed in the females (Figure 4F). ACTH regulates the level of corticosterone produced by the adrenal gland. While OPE exposure did not significantly affect ACTH levels in either male or female rats, a similar trend was observed in ACTH levels compared to corticosterone levels (Figure 4G and 4H).

Effects of the OPE mixture on signaling pathways in the adrenal gland

RNA sequencing was done to determine the transcriptomic changes induced by the OPE mixture

in the adrenal gland. Principal component analysis (PCA) plot revealed the extensive degree of separation in the transcriptomic profile of male and female adrenal glands (Figure 5A). OPE treatment resulted in significant alterations in the overall transcriptomic profiles of both male and female adrenal glands, as evidenced by the clear separation between control and the three OPE-treated groups. The heatmap analysis further revealed distinct expression patterns; at the control level, male and female adrenal glands exhibited remarkably different expression profiles (Figure 5B). Compared to controls, OPE treatment induced changes in gene expression, with different sets of targeted transcripts affected in male and female adrenal glands (Supplementary Table 2 and 3). This prompted further investigation into the specific transcripts and pathways impacted by the treatment.

For the male adrenal gland, a total of 674 differentially expressed genes (DEGs) were identified, with 381 transcripts downregulated and 293 being upregulated by at least 1.5-fold in the low OPE treatment group (Figure 6A). Fewer transcripts were altered in total in the middle OPE treatment group, with a similar number of transcripts downregulated (230 transcripts) or upregulated (225 transcripts). In the high OPE treatment group, 480 transcripts were affected, with somewhat more transcripts downregulated (255 transcripts) than upregulated (225 transcripts). More transcripts were specifically targeted by each treatment group than those commonly affected across groups as shown in the Venn diagram (Figure 6B). The top affected pathways in each of the uniquely affected gene sets for three treatment groups were identified using IPA. At the low OPE exposure level, pathways related to inflammation and adrenal gland development were affected (Supplementary Figure 6A). With increasing OPE concentrations, pathways related to cancer, WNT signaling, and neurotransmitter receptors were targeted (Supplementary Figure 6B and C). Among the transcripts commonly affected, 44 out of 52 could be identified with specific functions (Figure 6C and Supplementary Table 4). Nearly half of the

commonly affected transcripts are associated with the immune pathway, the apoptosis pathway, or have functions related to the adrenal gland. The remaining transcripts are related to lipid metabolism, the cell cycle, cell-cell interactions, or serve as transporters or receptors.

Analysis of the DEGs in male adrenal glands using IPA revealed the top affected canonical pathways in all three treatment groups (Figure 7A-C). There were insufficient data in the Ingenuity Knowledge Base to predict whether several pathways, such as leukotriene biosynthesis, prostanoid biosynthesis, and cysteine biosynthesis/homocysteine degradation, are activated or inhibited. Overall, the majority of the affected pathways were predicted to be inhibited. The only commonly impacted pathway across all three treatment groups was potassium channels. Based on known activity patterns in the Ingenuity Knowledge Base, this pathway was predicted to be activated at all three OPE exposure levels. Potassium channels play a role in the biosynthesis of aldosterone and corticosterone. When activated, as shown in Figure 7D and Supplementary Table 6, and using expression changes in low OPE treatment group as an example, more potassium will be exported out of the cell, leading to a decrease in the downstream production of corticosterone (in fasciculata cells) or aldosterone (in glomerulosa cells).

The number of DEGs in the female adrenal gland indicated that more transcripts were affected in the low and high OPE treatment groups comparing to the control (Figure 8A). In the low OPE group, 729 transcripts were affected, with 383 downregulated and 346 upregulated. The high OPE treatment group affected the greatest number of transcripts (803 in total); downregulated transcripts again accounted for a smaller number (358), while the remaining transcripts were upregulated (445). The Venn diagram showed a similar pattern to that observed in the male adrenal gland: there were more transcripts individually affected by each treatment group compared to those commonly affected across groups (Figure 8B). The low OPE treatment

group affected pathways related to adrenal cell movement, steroid hormone receptors, and inhibited ferroptosis (Supplementary Figure 7A). In the middle OPE treatment group, the WNT signaling pathway and pathways related to adrenal development and differentiation were targeted (Supplementary Figure 7B). The highest exposure condition targeted cancer-related pathways, autophagy, and immune pathways (Supplementary Figure 7C). Analysis of the commonly affected transcripts revealed that those involved in steroidogenesis were only affected in the female treatment groups (Figure 8C and Supplementary Table 5).

There are more overlaps in the top affected pathways across the three treatment groups in female adrenal glands. Analysis using IPA revealed an enrichment for canonical pathways related to cholesterol biosynthesis and the immune system (Figure 9A-C). Cholesterol biosynthesis was predicted to be strongly activated in all treatment groups. The LXR/RXR pathway, an important regulator of cholesterol homeostasis, was predicted to be inhibited at low OPE group but activated at the middle and high exposure levels. The predicted activation of the SREBF pathway will, in turn, promote the transcription of transcripts involved in cholesterol biosynthesis. Two immune-related pathways, interferon alpha/beta signaling and the role of hypercytokinemia/hyperchemokines in the pathogenesis of influenza, were predicted to be inhibited. The commonly affected pathways and the expression pattern of affected transcripts in the low OPE treatment group are shown in Figure 9D and Supplementary Table 6.

DISCUSSION

The adrenal glands produce hormones that regulate diverse essential functions, ranging from stress responses to metabolism, blood pressure, and circadian rhythms. Our study reveals that exposure to an environmentally relevant mixture of OPEs had sex-specific effects on the weight and function of the adrenal glands in Sprague Dawley rats. To our knowledge, this is the first

time a household dust based OPE mixture that closely resembles human exposure has been characterized for its effects on the adrenal gland. Importantly, this is also one of the few times that both male and female adrenal glands have been assessed for the toxicological impact of endocrine disrupting chemicals.

The first indication of an effect on the adrenal gland is a change in organ weight. Exposure to individual OPEs has been shown to affect the weight of the adrenal gland. In a 2-year feeding study, male and female F344/N rats were exposed to TMPP at various doses. At 3 months, the adrenal glands of female rats receiving 15 mg/kg of TMPP were reported to be significantly heavier (National Toxicology Program, 1994). The same study also utilized the B6C3F1 mouse model, and at 15 months, the adrenal glands of female mice receiving 27 mg/kg TMPP were significantly heavier, whereas the adrenal glands of male mice receiving 37 mg/kg of TMPP were lighter (National Toxicology Program, 1994). This trend is similar to what we observed with Sprague Dawley rats exposed to the OPE mixture, where the adrenal glands of females increased in weight, while those of males decreased (Figure 2). In studies assessing short-term exposure effects, female F344 rats exposed to 0.4 g/kg TMPP for 40 days showed heavier adrenal glands compared to controls (Latendresse et al., 1993). However, the effects of other OPEs have varied. Exposure to IPPP induced a dose-dependent increase in adrenal gland weights in both sexes of Wistar rats (Wade et al., 2019). Although only male Wistar rats were assessed, exposure to TDCIPP also resulted in an increase in the weight of the adrenal gland (Akimoto et al., 2022). The variability in observed effects depending on the OPEs assessed highlights the importance of evaluating mixtures that reflect human exposure patterns.

Lipid homeostasis appears to be a sensitive molecular event targeted by OPE exposures. Previously, we showed that the same OPE mixture induced lipid accumulation and altered the composition of lipid droplets in female H295R adrenal cells after a 48h exposure period (Li et

al., 2024). Among the affected lipids, triglycerides were significantly altered. Serum lipid levels provide insight into the net effect of OPEs on lipids. In our study, serum lipid levels in male rats were notably more affected than in females. Specifically, triglycerides and LDL cholesterol levels increased in the highest exposure group. In contrast, females exhibited a trend of increased total cholesterol level only (Figure 3). Alterations in serum lipid levels have been reported in other models. For example, exposure to TPHP has been associated with elevated triglyceride and total cholesterol levels in adult zebrafish (Du et al., 2016). Similarly, exposure to IPPP resulted in increased total and HDL cholesterol levels in both sexes of Wistar rats (Wade et al., 2019). Additionally, the metabolite of TDCIPP was positively associated with increased total cholesterol and LDL cholesterol levels in Canadian women (Siddique et al., 2020). Indeed, higher levels of OPEs have been associated with increased risk of cardiovascular disease, with TPHP proposed as a major driver (Guo et al., 2022; Zhang et al., 2024). In the rat adrenal gland, no significant change in lipid droplets was observed. It is possible that accumulation of lipid droplets serves as an acute response of the cells exposed to the OPE mixture *in vitro*, but that at the tissue level, it was brought back to homeostatic state over longer periods of time.

The adrenal cortex, responsible for producing aldosterone and corticosterone, serves as the final effector organ in the hypothalamic-pituitary-adrenal (HPA) axis. In our study, we observed that exposure to the OPE mixture significantly reduced both aldosterone and corticosterone levels in male rats, with aldosterone level being the more significantly affected (Figure 4). It is not surprising that aldosterone levels were more affected compared to corticosterone levels, as the glomerulosa zone, which produces aldosterone, is the outermost layer of the adrenal gland and is thus the first to be impacted by chemical exposures (Rosol et al., 2001). The adrenal cortex undergoes continual renewal throughout life, and the function of the female adrenal cortex in steroid hormone production might remain less affected due to its

naturally faster turnover rate (Greep and Deane, 1949). Notably, corticosterone also influences bone metabolism by inducing apoptosis in osteoblasts and osteocytes while prolonging the lifespan of osteoclasts (reviewed by Mitra, 2011). The same OPE mixture was found to suppress endochondral ossification in murine limb bud cultures (Han and Hales, 2021). Therefore, alterations in corticosterone levels may contribute to the adverse effects on bone formation. Previously, we found that exposure to the same OPE mixture increased aldosterone and cortisol levels in adrenal H295R cells derived from female patients by disrupting the expression of enzymes in the steroidogenic pathway (Li et al., 2024). Limited human data are available on the effects of OPE exposures on aldosterone and cortisol levels. One study indicates that increased urinary levels of di-butyl phosphate (a metabolite of TPHP), bis(1-chloro-2-propyl) phosphate (a metabolite of TDCIPP), and bis(2-butoxyethyl) phosphate (a metabolite of TBOEP) are associated with increased serum cortisol levels (Ji et al., 2021).

To assess whether the observed changes in aldosterone and corticosterone levels reflected alterations in hormones upstream in the pathway, we evaluated the levels of renin and ACTH. Renin, released by the kidneys in response to low blood pressure, converts angiotensinogen into angiotensin I, which is then transformed into angiotensin II. Angiotensin II stimulates the adrenal glands to release aldosterone, promoting sodium reabsorption and increasing blood volume and pressure (Lavoie and Sigmund, 2003). The decrease in the level of renin produced by the kidneys suggests that it may partly contribute to the decreased aldosterone levels observed in males. This also indicates that kidney might be one of the targets of OPEs. It has been reported that urinary metabolites of OPEs in humans are positively associated with chronic kidney disease (Kang et al., 2019). ACTH is a peptide hormone synthesized and secreted by the anterior pituitary gland in response to corticotropin-releasing hormone (CRH) from the hypothalamus. ACTH binds to melanocortin 2 receptors on the adrenal cortex, leading to the production of corticosterone

(Smith and Vale, 2006). Although the levels of ACTH were not significantly affected in either male or female rats, we did notice that the trend in the level of ACTH after exposure to the OPE mixture was similar to the effect seen in corticosterone levels, suggesting that OPEs may affect the HPA axis both locally at the adrenal glands and at the pituitary level. Further investigations are needed to examine the effects of OPEs on the renin-angiotensin-aldosterone system and the HPA axis to elucidate the precise mechanism(s) by which OPEs operates.

The RNA sequencing analysis revealed the potential mechanisms of action of the OPE mixture. First, we observed that the overall transcriptomic profiles of the female and male adrenal glands differ at the control level (Figure 5). Differences in adrenal transcriptomic profiles between sexes have been documented previously. For instance, in a gonadectomy study, orchiectomized rats with testosterone replacement exhibited stimulation of transcripts associated with lipid and cholesterol metabolism, whereas ovariectomized rats with estradiol replacement showed inhibition of transcripts involved in intracellular signaling pathways (Jopek et al., 2017). With OPE exposure, the pathways disrupted in male adrenal glands exhibit a distinctly different profile compared to those in females. To elucidate the mechanisms of action of OPEs, we first investigated the commonly affected pathways in males across treatment groups. Potassium channels emerged as the only consistently affected pathway (Figure 7). Notably, circulating levels of K^+ are major regulators of aldosterone and, to a lesser extent, corticosterone synthesis. Alterations in extracellular K^+ concentrations lead to significant changes in the membrane potential of zona glomerulosa and zona fasciculata cells, which are controlled by multiple potassium channels (Guagliardo et al., 2012; Bandulik et al., 2015; Bandulik et al., 2019). In our dataset, the expression of several potassium channels was upregulated, potentially causing depolarization of the cell membrane and resulting in decreased levels of aldosterone and corticosterone produced. This finding may partly explain the reduced levels of aldosterone and

corticosterone observed in male rats.

In female adrenal glands, a broader range of pathways were significantly affected. Key pathways impacted include cholesterol biosynthesis, lipid regulation, and the immune system (Figure 9). Cholesterol biosynthesis has been identified as a common target of OPEs. Previous studies have demonstrated that exposure to either the OPE mixture (Li et al., 2024) or individual OPEs (Li et al., 2023) results in the accumulation of lipid droplets in H295R adrenal cells. Analysis of these droplets revealed that sterol lipids were among the most significantly upregulated lipid categories. Correspondingly, the transcript for the enzyme responsible for the rate-limiting step in cholesterol biosynthesis, *Hmgcr*, was also upregulated (Li et al., 2024). Additionally, activation of the SREBF pathway led to the upregulation of transcripts involved in cholesterol biosynthesis, contributing to elevated cholesterol levels. Lipid homeostasis has been consistently identified as one of the most perturbed pathways affected by OPEs across various *in vivo* and *in vitro* studies, including those involving ovarian cells (Wang et al., 2023), hepatocytes (Shen et al., 2019; Wang et al., 2020; Yu et al., 2024), macrophages (Giles et al., 2024), murine limb buds (Han and Hales, 2021), and zebrafish brains (Yan et al., 2022). Lipid homeostasis is also regulated by the LXR pathway. Our findings align with previous observations, which reported pathway inhibition following exposure to the same OPE mixture in murine limb buds (Han and Hales, 2021), and to TPHP and 2-ethylhexyl diphenyl phosphate (EHDPHP) in macrophages, where these exposures induced a foam cell phenotype by inhibiting cholesterol efflux (Hu et al., 2019). At higher exposure levels, the observed pathway activation might be due to feedback mechanisms, where increased levels of cholesterol stimulate the activation of the pathway to facilitate cholesterol export. Furthermore, pathways related to immune functions in the female adrenal glands were generally found to be inhibited. Evidence suggests that organophosphate pesticides have immunosuppressive effects (Mitra et al., 2019). Several OPEs

used as flame retardants and plasticizers have also been positively correlated with the prevalence of immune-related diseases in Japanese households (Araki et al., 2014). The same mixture as the one used in this study also altered the expression of phagocytic receptors in macrophage cells, which are key players in the immune response (Giles et al., 2024). Additionally, exposure to components of this mixture, such as tris(2-butoxyethyl) phosphate (TBOEP), tris(1-chloro-2-propyl) phosphate (TCIPP), and tris(2-chloroethyl) phosphate (TCEP), has been reported to alter the expression of genes related to immune functions in the HepG2 human hepatocellular carcinoma cell line (Krivoshiev et al., 2018a; Krivoshiev et al., 2018b).

The inclusion of three doses allowed us to compare exposure effects at different levels. For both male and female rats, the low dose affected a greater number of transcripts (Figure 6A and 8A). In fact, in low dose treatment group, the affected transcripts had consistent changes in the direction of their expression level, making a stronger prediction of the affected pathways (Figure 7A and 9A). It is also noteworthy that higher concentrations of these chemicals were associated with the activation of additional pathways related to cancer development (Supplementary Figure 6C and 7C), suggesting an elevated risk associated with higher exposure levels.

Our study provides novel evidence that exposure to a household dust-based OPE mixture adversely affects both lipid homeostasis and adrenal gland function. Transcriptomic analysis further revealed that these effects occur through sex-specific mechanisms: in males the primary affected pathway involves potassium channels, while in females disruptions in lipid homeostasis and immune functions are most affected. However, we acknowledge that human exposure patterns vary depending on geographical location, individual behaviors, and socio-economic factors. The exposure profile tested here may not be fully representative of the entire population. Additionally, since rodents lack the enzyme CYP17 and have different steroidogenic pathways

(van Weerden et al., 1992), the translation of these findings into human effects must be done with caution.

Together, these findings highlight the importance of evaluating the toxicological impacts of environmentally relevant mixtures in both sexes. Furthermore, since every step in the steroid biosynthetic pathway, from the ACTH receptor and cholesterol transport to critical CYP and hydroxysteroid dehydrogenase enzymes involved in steroid synthesis, is known to be targeted by over 70 compounds (Harvey and Everett, 2003; Harvey et al., 2007; Harvey et al., 2009), including OPEs, the adrenal gland should be considered a crucial endpoint in toxicological assessments.

REFERENCES

Agency for Toxic Substances and Disease Registry (ATSDR). (2012). U.S. Department of Health and Human Services. Public Health Service: Toxicological Profile for Phosphate Ester Flame Retardants. Published September 2012. Accessed July 13, 2024.

<https://www.atsdr.cdc.gov/toxprofiles/tp202.pdf>

Akimoto, T., Kobayashi, S., Nakayama, A., et al. (2022). Toxicological effects of Tris (1,3-dichloro-2-propyl) phosphate exposure in adult male rats differ depending on the history of exposure in the neonatal period. *J. Appl. Toxicol.* **42**, 1503-1509.

Aluru, N.G., Hallanger, I., McMonagle, H., Harju, M. (2021). Hepatic Gene Expression Profiling of Atlantic Cod (*Gadus morhua*) Liver after Exposure to Organophosphate Flame Retardants Revealed Altered Cholesterol Biosynthesis and Lipid Metabolism. *Environ. Toxicol. Chem.* **40**, 1639-1648.

Araki, A., Saito, I., Kanazawa, A., Morimoto, K., Nakayama, K., Shibata, E., Tanaka, M., Takigawa, T., Yoshimura, T., Chikara, H. et al. (2014). Phosphorus flame retardants in indoor dust and their relation to asthma and allergies of inhabitants. *Indoor Air*. **24**, 3-15.

Baldwin, K.R., Phillips, A.L., Horman, B., et al. (2017). Sex Specific Placental Accumulation and Behavioral Effects of Developmental Firemaster 550 Exposure in Wistar Rats. *Sci Rep*. **7**, 7118.

Bandulik, S., Tauber, P., Lalli, E., Barhanin, J., Warth, R. (2015). Two-pore domain potassium channels in the adrenal cortex. *Pflugers. Arch*. **467**, 1027-1042.

Bandulik, S., Barhanin, J., Warth, R. (2019). Potassium channels in adrenocortical cells. *Current Opinion in Endocrine and Metabolic Research*. **8**, 1-8.

Bankhead, P., Loughrey, M. B., Fernández, J. A., Dombrowski, Y., McArt, D. G., Dunne, P. D., McQuaid, S., Gray, R. T., Murray, L. J., Coleman, H. G., James, J. A., Salto-Tellez, M., Hamilton, P. W. (2017). QuPath: Open source software for digital pathology image analysis. *Sci. Rep*. **7**, 16878.

Blum, A., Behl, M., Birnbaum, L.S., Diamond, M.L., Phillips, A., Singla, V., et al. (2019). Organophosphate Ester Flame Retardants: Are They a Regrettable Substitution for Polybrominated Diphenyl Ethers? *Environ. Sci. Tech. Let*. **6**, 638-649.

Burton, C., Cottrell, E., Edwards, J. (2015). Addison's disease: identification and management in primary care. *Br. J. Gen. Pract*. **65**, 488-490.

Carignan, C.C., Mínguez-Alarcón, L., Butt, C.M., Williams, P.L., Meeker, J.D., Stapleton, H.M., Toth, T.L., Ford, J.B., Hauser, R. (2017). EARTH Study Team. Urinary Concentrations of Organophosphate Flame Retardant Metabolites and Pregnancy Outcomes among Women Undergoing in Vitro Fertilization. *Environ. Health. Perspect.* **125**, 087018.

Castorina, R., Butt, C., Stapleton, H. M., Avery, D., Harley, K. G., Holland, N., Eskenazi, B., & Bradman, A. (2017). Flame retardants and their metabolites in the homes and urine of pregnant women residing in California (the CHAMACOS cohort). *Chemosphere.* **179**, 159–166.

Cequier, E., Sakhi, A.K., Marcé, R.M., Becher, G., Thomsen, C. (2015). Human exposure pathways to organophosphate triesters — A biomonitoring study of mother-child pairs. *Environ Int.* **75**, 159–165.

Chang, Y., Cui, H., Jiang, X., Li, M. (2020). Comparative assessment of neurotoxicity impacts induced by alkyl tri-n-butyl phosphate and aromatic tricresyl phosphate in PC12 cells. *Environ. Toxicol.* **35**, 1326-1333.

Chokwe, T.B., Abafe, O.A., Mbelu, S.P., Okonkwo, J.O., Sibali, L.L. (2020). A review of sources, fate, levels, toxicity, exposure and transformations of organophosphorus flame-retardants and plasticizers in the environment. *Emerg. Contam.* **6**, 345-366.

Cockburn, A., and Leist, K-H. (1999). Current and regulatory trends in endocrine and hormonal toxicology, in: P.W. Harvey, K.C. Rush, A. Cockburn (Eds.). *Endocrine and Hormonal Toxicology*, Wiley, Chichester, pp. 507–534.

Doherty, B.T., Hoffman, K., Keil, A.P, et al. (2019). Prenatal exposure to organophosphate esters and cognitive development in young children in the Pregnancy, Infection, and Nutrition Study. *Environ. Res.* **169**, 33-40.

Du, Z., Zhang, Y., Wang, G., Peng, J., Wang, Z., Gao, S. (2016). TPHP exposure disturbs carbohydrate metabolism, lipid metabolism, and the DNA damage repair system in zebrafish liver. *Sci. Rep.* **6**, 1-10.

Fan, X., Kubwabo, C., Rasmussen, P.E., Wu, F. (2014). Simultaneous determination of thirteen organophosphate esters in settled indoor house dust and a comparison between two sampling techniques. *Sci. Total. Environ.* **491**, 80-86.

Giles, B.H., Kukolj, N., Mann, K.K., Robaire, B. (2024). Phenotypic and Functional Outcomes in Macrophages Exposed to an Environmentally Relevant Mixture of Organophosphate Esters in Vitro. *Environ. Health. Perspect.* **132**, 87002.

Gillera, S.E.A., Marinello, W.P., Horman, B.M., et al. (2020). Sex-specific effects of perinatal FireMaster® 550 (FM 550) exposure on socioemotional behavior in prairie voles. *Neurotoxicol. Teratol.* **79**, 106840.

Greep, R.O., and Deane, H.W. (1949). Histological, cytochemical and physiological observations on the regeneration of the rat's adrenal gland following enucleation. *Endocrinology*. **45**, 42–56.

Guagliardo, N.A., Yao, J., Hu, C., Schertz, E.M., Tyson, D.A., Carey, R.M., Bayliss, D.A., Barrett, P.Q. (2012). TASK-3 channel deletion in mice recapitulates low-renin essential hypertension. *Hypertens.* **59**, 999-1005.

Guo, X., Wu, B., Xia, W., Gao, J., Xie, P., Feng, L., Sun, C., Liang, M., Ding, X., Zhao, D., Ma, S., Liu, H., Lowe, S., Bentley, R., Huang, C., Qu, G., Sun, Y. (2022). Association of organophosphate ester exposure with cardiovascular disease among US adults: Cross-sectional findings from the 2011–2018 National Health and Nutrition Examination Survey. *Chemosphere*. **308**, 126428.

Hales, B.F., and Robaire, B. (2020). Effects of brominated and organophosphate ester flame retardants on male reproduction. *Andrology*. **8**, 915-923.

Harvey, P.W., and Everett, D. (2003). The adrenal cortex and steroidogenesis as cellular and molecular targets for toxicity: critical omissions from regulatory endocrine disrupter screening strategies for human health. *J. Appl. Toxicol.* **23**, 81–87.

Harvey, P.W., Everett, D.J., Springall, C.J. (2007). Adrenal toxicology: a strategy for assessment of functional toxicity to the adrenal cortex and steroidogenesis. *J. Appl. Toxicol.* **27**, 103–115.

Harvey, P.W., Everett, D.J., Springall, C.J. (2009). Adrenal toxicology: molecular targets, endocrine mechanisms, hormonal interactions, assessment models and species differences in toxicity in: P.W. Harvey, D.J. Everett, C.J. Springall (Eds.). *Adrenal Toxicology*, Informa Healthcare, New York, pp. 3–35.

He, C., English, K., Baduel, C., Thai, P., Jagals, P., Ware, R.S., Li, Y., Wang, X., Sly, P.D., Mueller, J.F. (2018a). Concentrations of organophosphate flame retardants and plasticizers in urine from young children in Queensland, Australia and associations with environmental and behavioural factors. *Environ. Res.* **164**, 262-270.

He, M.J., Lu, J.F., Ma, J.Y., Wang, H., Du, X.F. (2018b). Organophosphate esters and phthalate esters in human hair from rural and urban areas, Chongqing, China: Concentrations, composition profiles and sources in comparison to street dust. *Environ. Pollut.* **237**, 143-153.

Hoffman, K., Butt, C.M., Webster, T.F., Preston, E.V., Hammel, S.C., Makey, C., Lorenzo, A.M., Cooper, E.M., Carignan, C., Meeker, J.D., Hauser, R., Soubry, A., Murphy, S.K., Price, T.M., Hoyo, C., Mendelsohn, E., Congleton, J., Daniels, J.L., Stapleton, H.M. (2017). Temporal Trends in Exposure to Organophosphate Flame Retardants in the United States. *Environ. Sci. Technol.* **4**, 112–118.

Hou, M., Shi, Y., Na, G., Cai, Y. (2021). A review of organophosphate esters in indoor dust, air, hand wipes and silicone wristbands: Implications for human exposure. *Environ. Int.* **146**, 106261.

Hou, M., Shi, Y., Jin, Q., Cai, Y. (2022). Organophosphate esters and their metabolites in paired human whole blood, serum, and urine as biomarkers of exposure. *Environ. Int.* **164**, 107269.

Hu, W., Jia, Y., Kang, Q., Peng, H., Ma, H., Zhang, S., Hiromori, Y., Kimura, T., Nakanishi, T., Zheng, L., et al. (2019). Screening of house dust from Chinese homes for chemicals with liver x receptors binding activities and characterization of atherosclerotic activity using an in vitro macrophage cell line and ApoE^{-/-} mice. *Environ. Health. Persp.* **127**, 117003.

Hu, W., Gao, P., Wang, L., Hu, J. (2022). Endocrine disrupting toxicity of aryl organophosphate esters and mode of action. *Crit. Rev. Eem. Sci. Tec.* **53**,1–18.

Ji, Y., Yao, Y., Duan, Y, et al. (2021). Association between urinary organophosphate flame retardant diesters and steroid hormones: a metabolomic study on type 2 diabetes mellitus cases and controls. *Sci. Total. Environ.* **756**, 143836.

Jopek, K., Celichowski, P., Szyszka, M., et al. (2017). Transcriptome Profile of Rat Adrenal Evoked by Gonadectomy and Testosterone or Estradiol Replacement. *Front. Endocrinol.* **8**, 26.

Kang, H., Lee, J., Lee, J. P., & Choi, K. (2019). Urinary metabolites of organophosphate esters (OPEs) are associated with chronic kidney disease in the general US population, NHANES 2013-2014. *Environ. Int.* **131**, 105034.

Kim, U. J., Wang, Y., Li, W., and Kannan, K. (2019). Occurrence of and human exposure to organophosphate flame retardants/plasticizers in indoor air and dust from various microenvironments in the United States. *Environ. Int.* **125**, 342–349.

Krivoshiev, B.V., Beemster, G., Sprangers, K., Cuypers, B., Laukens, K., Blust, R., Husson, S.J. (2018a). Toxicogenomics of the flame retardant tris (2-butoxyethyl)phosphate in HepG2 cells using RNA-seq. *Toxicol. In Vitro.* **46**, 178–188.

Krivoshiev, B.V., Beemster, G., Sprangers, K., Blust, R., Husson, S.J. (2018b). A toxicogenomics approach to screen chlorinated flame retardants tris(2-chloroethyl) phosphate and tris(2-chloroisopropyl) phosphate for potential health effects. *J. Appl. Toxicol.* **38**, 459–470.

Kubwabo, C., Fan, X., Katuri, G.P., Habibagahi, A., Rasmussen, P.E. (2021). Occurrence of aryl and alkyl-aryl phosphates in Canadian house dust. *Emerg. Contam.* **7**, 149-159.

Latendresse, J.R., Azhar, S., Brooks, C.L., Capen, C.C. (1993). Pathogenesis of Cholesteryl Lipidosis of Adrenocortical and Ovarian Interstitial Cells in F344 Rats Caused by Tricresyl Phosphate and Butylated Triphenyl Phosphate. *Toxicol. Appl. Pharm.* **122**, 281-289.

Latendresse, J.R., Brooks, C.L., Capen, C.C. (1994). Pathologic Effects of Butylated Triphenyl Phosphate-Based Hydraulic Fluid and Tricresyl Phosphate on the Adrenal Gland, Ovary, and Testis in the Fischer-344 Rat. *Toxicol. Pathol.* **22**, 341-352.

Latendresse, J.R., Brooks, C.L., Capen, C.C. (1995). Toxic Effects of Butylated Triphenyl Phosphate-based Hydraulic Fluid and Tricresyl Phosphate in Female F344 Rats. *Vet. Pathol.* **32**, 394-402.

Latendresse, J. R., Warbritton, A. R., Jonassen, H., & Creasy, D. M. (2002). Fixation of testes and eyes using a modified Davidson's fluid: comparison with Bouin's fluid and conventional Davidson's fluid. *Toxicologic pathology.* **30**, 524–533.

Lavoie, L.J and Sigmund, D.C. (2003). Minireview: Overview of the Renin-Angiotensin System—An Endocrine and Paracrine System. *Endocrinology.* **144**, 2179–2183.

Li, Z., Robaire, B., Hales, B.F. (2023). The organophosphate esters used as flame retardants and plasticizers affect H295R adrenal cell phenotypes and functions. *Endocrinology.* **164**, bqad119.

Li, Z., Hales, B.F., Robaire, B. (2024). Impact of Exposure to a Mixture of Organophosphate Esters on Adrenal Cell Phenotype, Lipidome, and Function. *Endocrinology.* **165**, bqae024.

Liu, X., Ji, K., Choi, K. (2012). Endocrine disruption potentials of organophosphate flame retardants and related mechanisms in H295R and MVLN cell lines and in zebrafish. *Aquat. Toxicol.* **114**, 173-181.

Liu, L.Y., He, K., Hites, R.A., Salamova, A. (2016). Hair and Nails as Noninvasive Biomarkers of Human Exposure to Brominated and Organophosphate Flame Retardants. *Environ. Sci. Technol.* **50**, 3065-3073.

Ma, J., Zhu, H., Kannan, K. (2019). Organophosphorus Flame Retardants and Plasticizers in Breast Milk from the United States. *Environ. Sci. Technol. Lett.* **6**, 525-531.

Macari, S., Rock, K.D., Santos, M.S., et al. (2020). Developmental Exposure to the Flame Retardant Mixture Firemaster 550 Compromises Adult Bone Integrity in Male but not Female Rats. *Int. J. Mol. Sci.* **21**, 2553.

Marinello, W.P., Gillera, S.E.A., Fanning, M.J., et al. (2022). Effects of developmental exposure to FireMaster® 550 (FM 550) on microglia density, reactivity and morphology in a prosocial animal model. *Neurotoxicology.* **91**, 140-154.

Meeker, J.D., and Stapleton, H.M. (2010). House dust concentrations of organophosphate flame retardants in relation to hormone levels and semen quality parameters. *Environ. Health. Perspect.* **118**, 318-323.

Mitra, R. (2011). Adverse effects of corticosteroids on bone metabolism: a review. *PM R.* **2013**, 466-471.

Mitra, A., Sarkar, M., Chatterjee, C. (2019). Modulation of immune response by organophosphate pesticides: Mammals as potential model. *Proc Zool Soc.* **72**, 13-24.

National Toxicology Program. NTP Toxicology and Carcinogenesis Studies of Tricresyl Phosphate (CAS No. 1330-78-5) in F344/N Rats and B6C3F1 Mice (Gavage and Feed Studies). (1994). Natl. Toxicol. Program. Tech. Rep. Ser. **433**, 1-321.

Newell, A.J., Kapps, V.A., Cai, Y., et al. (2023). Maternal organophosphate flame retardant exposure alters the developing mesencephalic dopamine system in fetal rat. *Toxicol. Sci.* **191**, 357-373.

Ospina, M., Jayatilaka, N.K., Wong, L.Y., Restrepo, P., Calafat, A.M. (2018). Exposure to organophosphate flame retardant chemicals in the U.S. general population: Data from the 2013–2014 National Health and Nutrition Examination Survey. *Environ. Int.* **110**, 32–41.

Parasuraman, S., Raveendran, R., & Kesavan, R. (2010). Blood sample collection in small laboratory animals. *Journal of pharmacology & pharmacotherapeutics.* **1**, 87–93.

Patisaul, H.B., Roberts, S.C., Mabrey, N., et al. (2013). Accumulation and endocrine disrupting effects of the flame retardant mixture Firemaster® 550 in rats: an exploratory assessment. *J. Biochem. Mol. Toxicol.* **27**, 124-136.

Patisaul, H.B., Behl, M., Birnbaum, L.S., et al. (2021). Beyond Cholinesterase Inhibition: Developmental Neurotoxicity of Organophosphate Ester Flame Retardants and Plasticizers. *Environ. Health. Perspect.* **129**, 105001.

Piao, Y., Liu, Y., Xie, X. (2013). Change Trends of Organ Weight Background Data in Sprague Dawley Rats at Different Ages. *J. Toxicol. Pathol.* **26**, 29-34.

Pillai, H.K., Fang, M., Beglov, D., et al. (2014). Ligand binding and activation of PPAR γ by Firemaster® 550: effects on adipogenesis and osteogenesis in vitro. *Environ. Health. Perspect.* **122**, 1225-1232.

Reeves P. G. (1997). Components of the AIN-93 diets as improvements in the AIN-76A diet. *J. Nutr.* **127**, 838S–841S.

Ribelin, W.E. (1984). The effects of drugs and chemicals upon the structure of the adrenal gland. *Fundam. Appl. Toxicol.* **4**, 105-119.

Rock, K.D., Armour, G., Horman, B., et al. (2020). Effects of Prenatal Exposure to a Mixture of Organophosphate Flame Retardants on Placental Gene Expression and Serotonergic Innervation in the Fetal Rat Brain. *Toxicol. Sci.* **176**, 203-223.

Rosenmai, A.K., Winge, S.B., Möller, M., et al. (2021). Organophosphate ester flame retardants have antiandrogenic potential and affect other endocrine related endpoints in vitro and in silico. *Chemosphere.* **263**, 127703.

Rosol, T.J., Yarrington, J.T., Latendresse, J., Capen, C.C. (2001). Adrenal Gland: Structure, Function, and Mechanisms of Toxicity. *Toxicol. Pathol.* **29**, 41–48.

Shen, J., Zhang, Y., Yu, N., Crump, D., Li, J., Su, H., Letcher, R.J., Su, G. (2019).

Organophosphate ester, 2-ethylhexyl diphenyl phosphate (EHDPP), elicits cytotoxic and transcriptomic effects in chicken embryonic hepatocytes and its biotransformation profile compared to humans. *Environ. Sci. Technol.* **53**, 2151–2160.

Siddique, S., Harris, S.A., Kosarac, I., Latifovic, L., Kubwabo, C. (2020). Urinary metabolites of organophosphate esters in women and their relationship with serum lipids: An exploratory analysis. *Environ. Pollut.* **263**, 114110.

Siddique, S., Farhat, I., Kubwabo, C., et al. (2022). Exposure of men living in the greater Montreal area to organophosphate esters: association with hormonal balance and semen quality. *Environ. Int.* **166**, 107402.

Smith, S. M., and Vale, W. W. (2006). The role of the hypothalamic-pituitary-adrenal axis in neuroendocrine responses to stress. *Dialogues in clinical neuroscience.* **8**, 383–395.

Sun, Y., Gong, X., Lin, W, et al. (2018). Metabolites of organophosphate ester flame retardants in urine from Shanghai, China. *Environ. Res.* **164**, 507-515.

Tung, E.W.Y., Ahmed, S., Peshdary, V., Atlas, E.. (2017a). Firemaster® 550 and its components isopropylated triphenyl phosphate and triphenyl phosphate enhance adipogenesis and transcriptional activity of peroxisome proliferator activated receptor (Ppar γ) on the adipocyte protein 2 (aP2) promoter. *PLoS One.* **12**, e0175855.

Tung, E.W.Y., Peshdary, V., Gagné, R., et al. (2017b). Adipogenic effects and gene expression profiling of firemaster® 550 components in human primary preadipocytes. *Environ. Health. Perspect.* **125**, 097013.

van der Veen, I., and de Boer, J. (2012) Phosphorus flame retardants: properties, production, environmental occurrence, toxicity and analysis. *Chemosphere.* **88**, 1119-1153.

van Weerden, W.M., Bierings, H.G., van Steenbrugge, G.J., de Jong, F.H., and Schröder, F.H. (1992). Adrenal glands of mouse and rat do not synthesize androgens. *Life sciences.* **50**, 857–861.

Wade, M.G., Kawata, A., Rigden, M., Caldwell, D., Holloway, A.C. (2019). Toxicity of Flame Retardant Isopropylated Triphenyl Phosphate: Liver, Adrenal, and Metabolic Effects. *Int. J. Toxicol.* **38**, 279-290.

Wagner, R.L., White, P.F., Kan, P.B., Rosenthal, M.H., Feldman, D. (1984). Inhibition of adrenal steroidogenesis by the anesthetic etomidate. *N. Engl. J. Med.* **310**, 1415-1421.

Wang, X., Li, F., Liu, J., Ji, C., Wu, H. (2020). Transcriptomic, proteomic and metabolomic profiling unravel the mechanisms of hepatotoxicity pathway induced by triphenyl phosphate (TPP). *Ecotoxicol. Environ. Saf.* **205**, 111126.

Wang, X., Rowan-Carroll, A., Meier, M.J., et al. (2023). Toxicological Mechanisms and Potencies of Organophosphate Esters in KGN Human Ovarian Granulosa Cells as Revealed by High-throughput Transcriptomics. *Toxicol. Sci.* **197**, 170–185.

Wang, X., Rowan-Carroll, A., Meier, M.J., Yauk, C.L., Wade, M.G., Robaire, B., Hales, B.F. (2024). House dust-derived mixtures of organophosphate esters alter the phenotype, function, transcriptome, and lipidome of KGN human ovarian granulosa cells. *Tox. Sci.* **200**, 95–113.

Wei, G.L., Li, D.Q., Zhuo, M.N., Liao, Y.S., Xie, Z.Y., Guo, T.L., Li, J.J., Zhang, S.Y., Liang, Z.Q. (2015). Organophosphorus flame retardants and plasticizers: sources, occurrence, toxicity and human exposure. *Environ. Pollut.* **196**, 29-46.

Wiersielis, K.R., Adams, S., Yasrebi, A., Conde, K., Roepke, T.A. (2020). Maternal exposure to organophosphate flame retardants alters locomotor and anxiety-like behavior in male and female adult offspring. *Horm. Behav.* **122**, 104759.

Witchey, S.K., Samara, L., Horman, B.M., Stapleton, H.M., Patisaul, H.B. (2020). Perinatal exposure to FireMaster® 550 (FM550), brominated or organophosphate flame retardants produces sex and compound specific effects on adult Wistar rat socioemotional behavior. *Horm. Behav.* **126**, 104853.

Witchey, S.K., Doyle, M.G., Fredenburg, J.D., et al. (2023). Impacts of Gestational FireMaster 550 Exposure on the Neonatal Cortex Are Sex Specific and Largely Attributable to the Organophosphate Esters. *Neuroendocrinology.* **113**, 1262-1282.

Yan, H., and Hales, B.F. (2021). Effects of an Environmentally Relevant Mixture of Organophosphate Esters Derived From House Dust on Endochondral Ossification in Murine Limb Bud Cultures. *Toxicol. Sci.* **180**, 62-75.

Yan, Z., Feng, C., Jin, X., Wang, F., Liu, C., Li, N., Qiao, Y., Bai, Y., Wu, F., Giesy, J.P. (2022). Organophosphate esters cause thyroid dysfunction via multiple signaling pathways in zebrafish brain. *Environ. Sci. Ecotechnol.* **12**, 100198.

Yao, Y., Li, M., Pan, L., et al. (2021). Exposure to organophosphate ester flame retardants and plasticizers during pregnancy: Thyroid endocrine disruption and mediation role of oxidative stress. *Environ. Int.* **146**, 106215.

Yu, D., Hales, B.F., Robaire, B. (2024). Organophosphate ester flame retardants and plasticizers affect the phenotype and function of HepG2 liver cells. *Toxicol. Sci.* **199**, 261-275.

Zhang, D., Liu, X., Tu, J., Xiao, Q., Han, L., Fu, J., Bian, J., Zhang, R., Chen, J., Shao, Y., Lu, S. (2024). Mediating Role of Glucose-Lipid Metabolism in the Association between the Increased Risk of Coronary Heart Disease and Exposure to Organophosphate Esters, Phthalates, and Polycyclic Aromatic Hydrocarbon. *Environment & Health.* **2**, 170-179.

FIGURES

Name	Acronym	CAS No.	Supplier	% by weight	Dose received (Mean) (mg/kg bw/day)		
					Low	Middle	High
Tris(2-butoxyethyl) phosphate	TBOEP	78-51-3	Sigma-Aldrich	59.07	0.01719	0.57170	17.14237
Tris(methylphenyl) phosphate	TMPP	1330-78-5	Alpha Aesar	8.44	0.00246	0.08168	2.44932
Tris(1-chloro-2-propyl) phosphate	TCIPP	13674-84-5	AK Scientific	7.31	0.00213	0.07075	2.12139
Isopropylated triphenyl phosphate	IPPP	68937-41-7	NIEHS / NTP	5.62	0.00164	0.05439	1.63095
Tris(1,3-dichloro-2-propyl) phosphate	TDCIPP	13674-87-8	TCI America	5.06	0.00147	0.04897	1.46843
Triphenyl phosphate	TPHP	115-86-6	Sigma-Aldrich	5.01	0.00146	0.04849	1.45392
Isodecyl diphenyl phosphate	IDDPHP	29761-21-5	Scientific Polymer Products	4.27	0.00124	0.04133	1.23917
Tris(2-chloroethyl) phosphate	TCEP	115-96-8	Sigma-Aldrich	2.48	0.00072	0.02400	0.71971
Ethylhexyl diphenyl phosphate	EHDPHP	1241-94-7	AK Scientific	1.18	0.00034	0.01142	0.34244
Tri-n-butyl phosphate	TNBP	126-73-8	Sigma-Aldrich	0.79	0.00023	0.00765	0.22926
Cresyl diphenyl phosphate	CDPP	26444-49-5	Alpha Aesar	0.48	0.00014	0.00465	0.13930
Tert-butylphenyl diphenyl phosphate	BPDP	56803-37-3	Scientific Polymer Products	0.19	0.00006	0.00184	0.05514
Trixylyl phosphate	TXP	25155-23-1	CHEMOS	0.11	0.00003	0.00106	0.03192
Total Mixture Dose (Mean) (mg/kg bw/day)					0.029	0.968	29.020

Figure 4-1. Composition of the Canadian household dust based OPE mixture. Bodyweight and food weight were recorded weekly for each rat. Using these values, the average food consumption was calculated, along with the resulting proportion of the individual OPEs and the overall mixture received by the animals (mg/kg bw/day) for each dose.

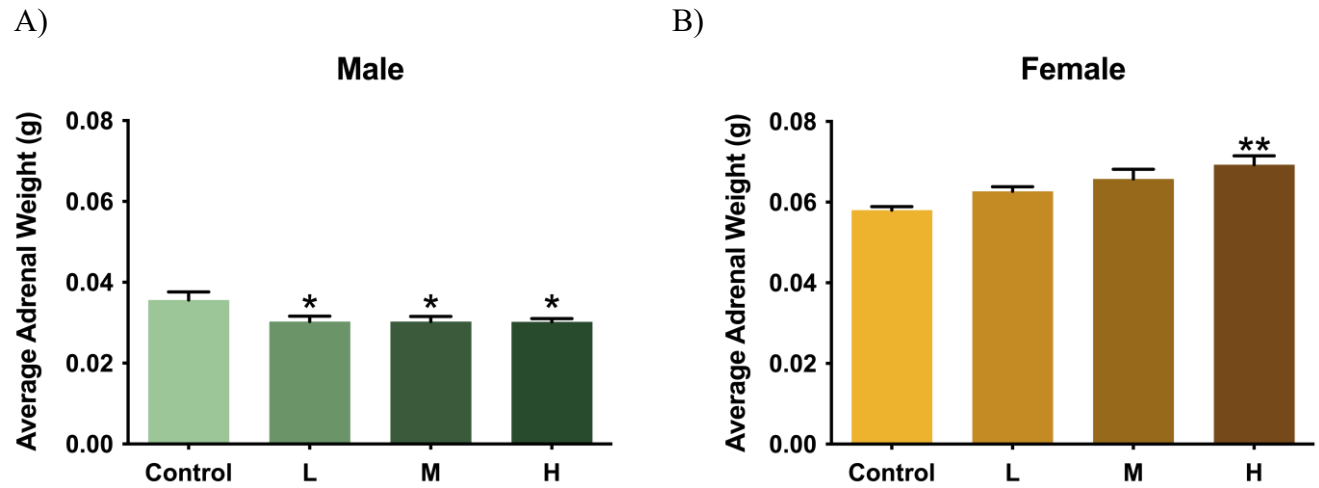


Figure 4-2. Effects of the OPE mixture on the weight of (A) male and (B) female adrenal glands.

* $P < .05$ and ** $P < .01$ compared with control; values represent means \pm SEM; $n = 8-10$.

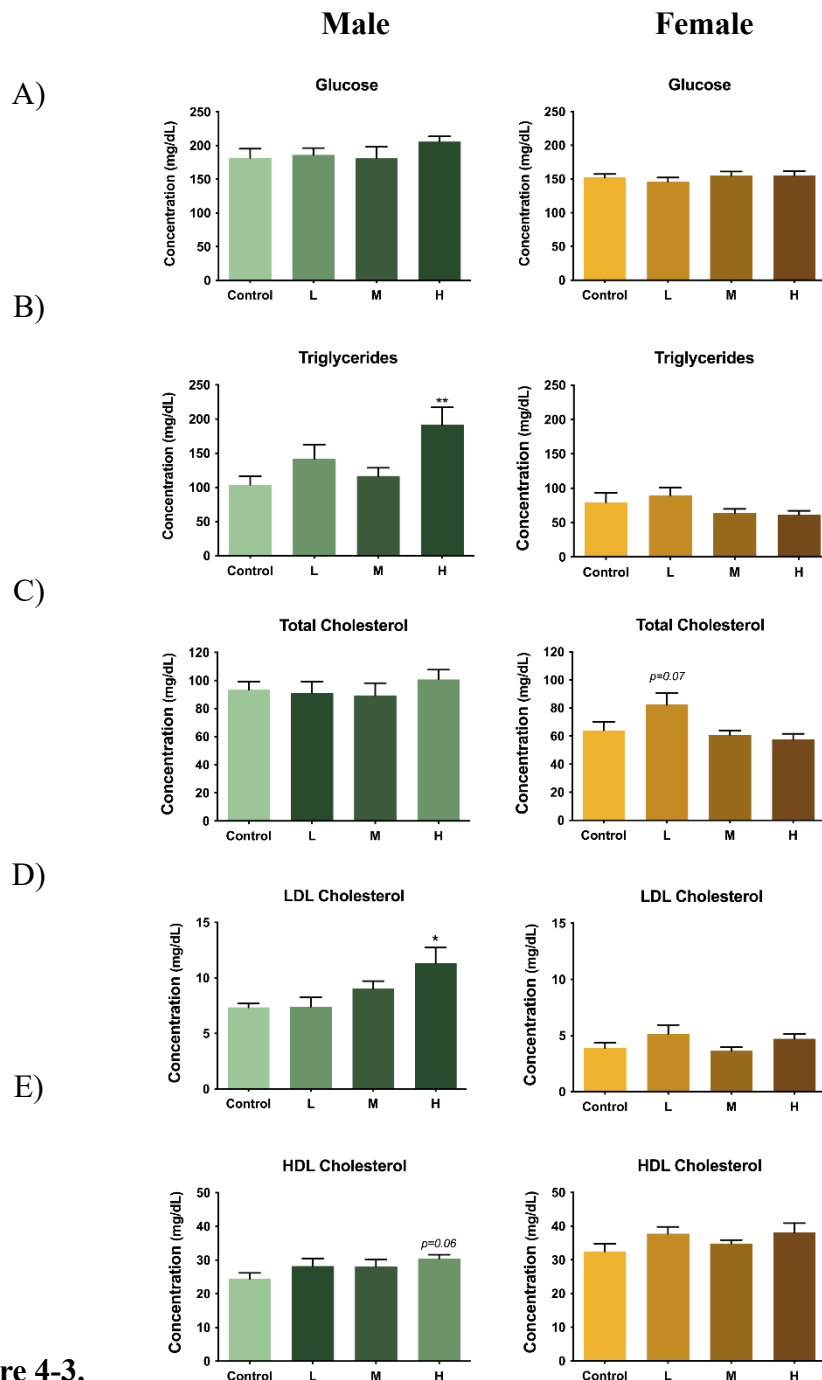


Figure 4-3.

Effects of the OPE

mixture on the serum level of glucose (A), triglycerides (B), total cholesterol (C), LDL cholesterol (D), and HDL cholesterol (E) concentrations in male (green) and female (yellow) treatment groups. * $P < .05$ and ** $P < .01$ compared with control; values represent means \pm SEM; $n = 5$.

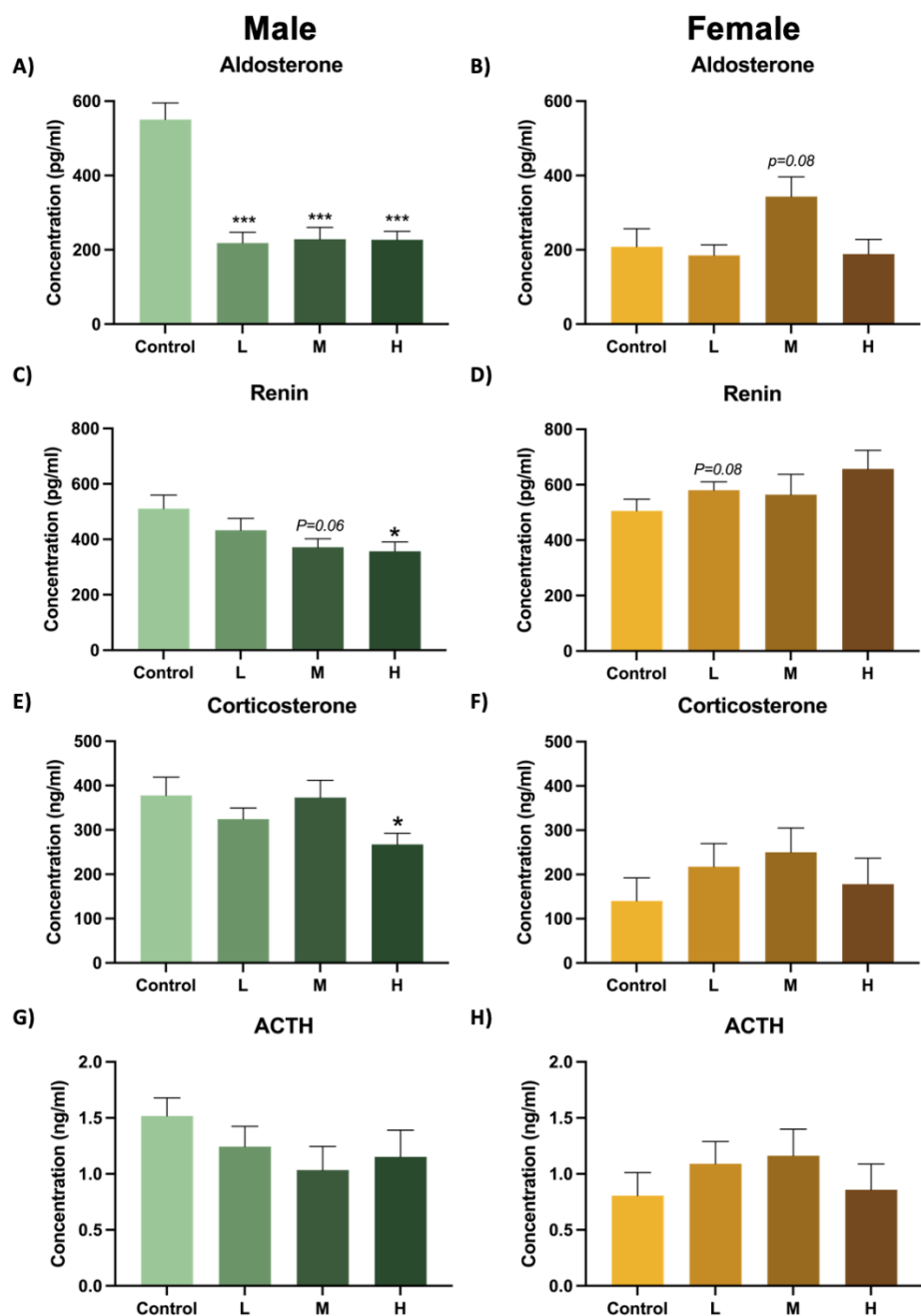


Figure 4-4. Effects of the OPE mixture on serum hormone levels. Serum levels of aldosterone (A and B), renin (C and D), corticosterone (E and F) and ACTH (G and H) in male (green) and female (yellow) Sprague Dawley rats were measured. * $P < .05$ and *** $P < .001$ compared with control; values represent means \pm SEM; $n = 5-10$.

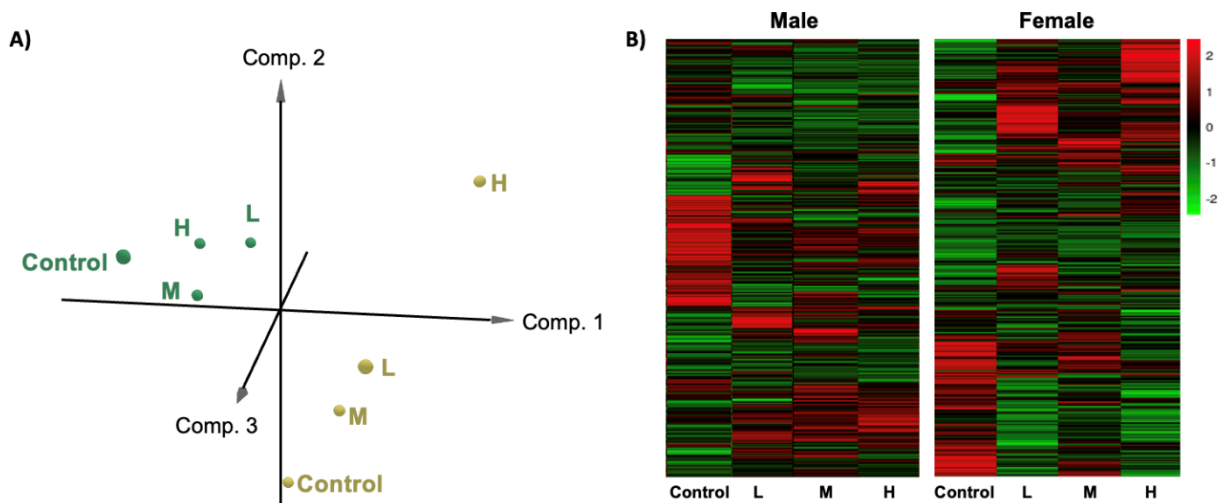


Figure 4-5. Principal component analysis (PCA) and heatmap of the overall expression profile of the adrenal gland exposed to the OPE mixture. (A) PCA plot showing the degree of separation in the transcriptomic profiles between the male and female OPE treatment groups. (B) Heatmap showing the transcriptomic profiles of the adrenal glands. Red indicates upregulation, green indicates downregulation. $n = 5$.

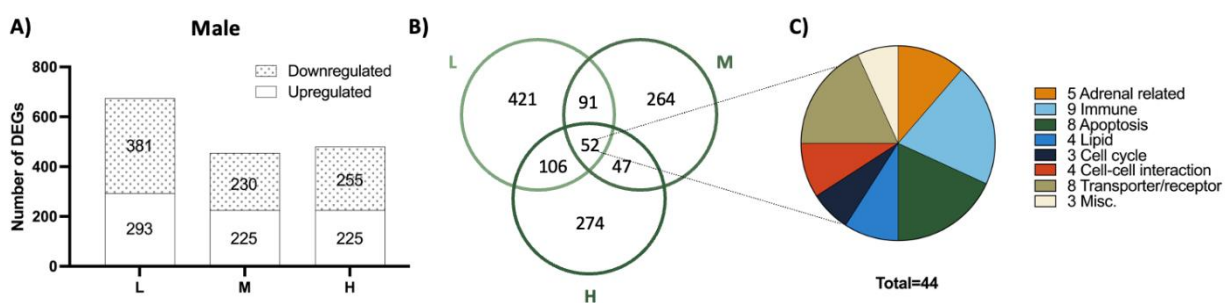


Figure 4-6. Differentially expressed genes (DEGs) in male treatment groups. (A) Numbers of significantly downregulated or upregulated transcripts (fold changes > 1.5 and p-values < 0.05). (B) Venn diagram showing the numbers of unique DEGs specific to each treatment, as well as the DEGs shared among the treatments. (C) DEGs commonly affected in male treatment groups and their related functions. 44 out of 52 were identified with known functions. $n = 5$.

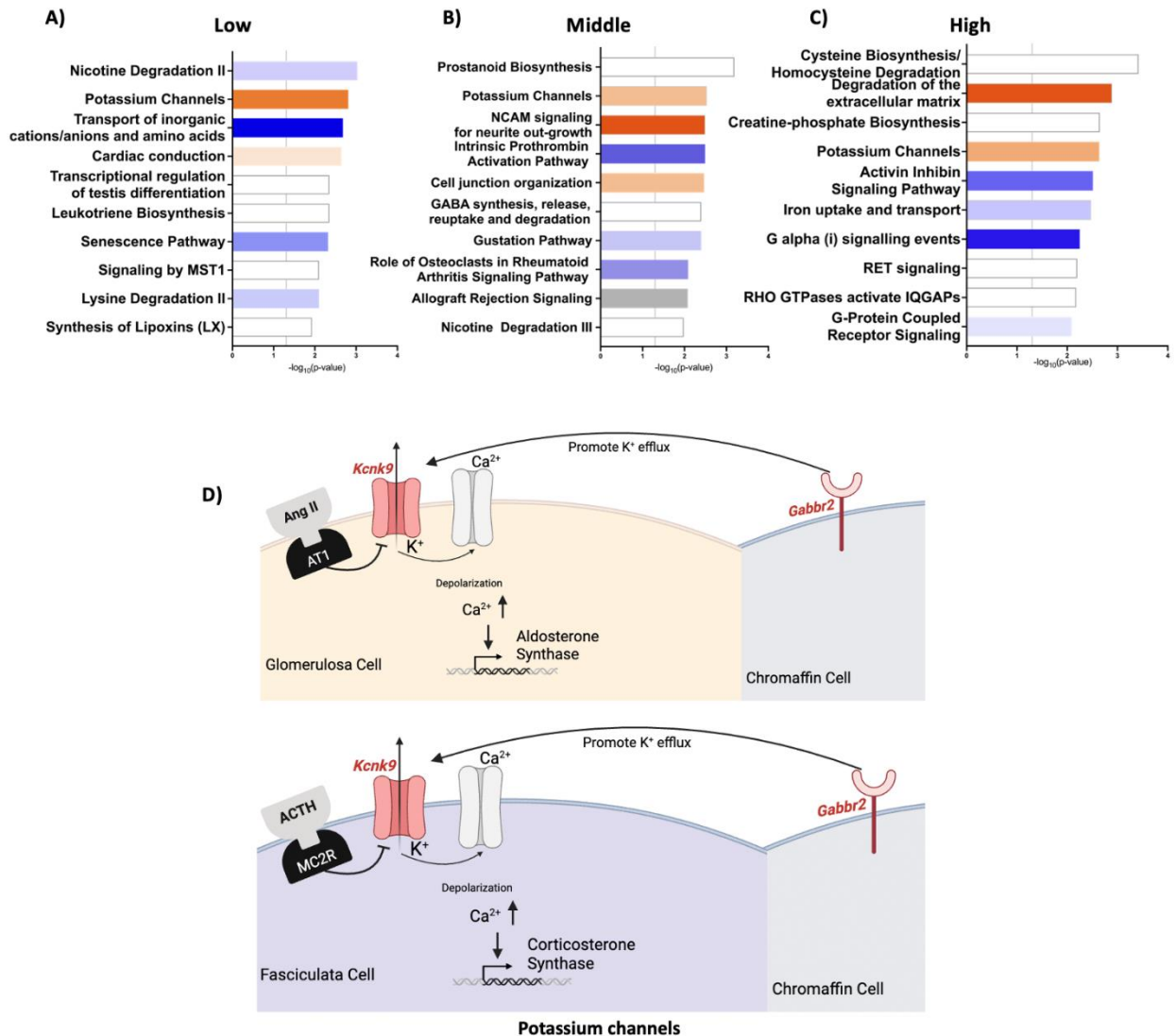


Figure 4-7. Top 10 canonical pathways in (A) low, (B) middle, and (C) high OPE group identified by the Ingenuity Pathway Analyses (IPA). Orange indicates pathway activation; blue indicates pathway inhibition; white indicates that insufficient DEGs (< 4) were associated with the pathway; grey indicates unknown direction of change of pathway activity. (D) Pathway diagram showing the commonly affected pathway(s). The expression changes represent transcripts affected in the low OPE treatment group. Red indicates upregulation of the expression level of the transcript, blue indicates downregulation. n = 5. Created with BioRender.com

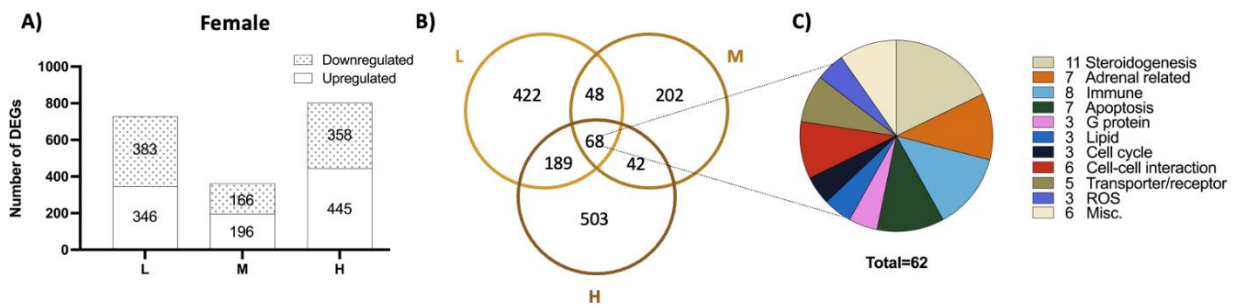


Figure 4-8. Differentially expressed genes (DEGs) in female treatment groups. (A) Numbers of significantly downregulated or upregulated transcripts (fold changes > 1.5 and p-values < 0.05). (B) Venn diagram showing the numbers of unique DEGs specific to each treatment, as well as the DEGs shared among the treatments. (C) DEGs commonly affected in female treatment groups and their related functions. 62 out of 68 transcripts were identified with known functions. n = 5.

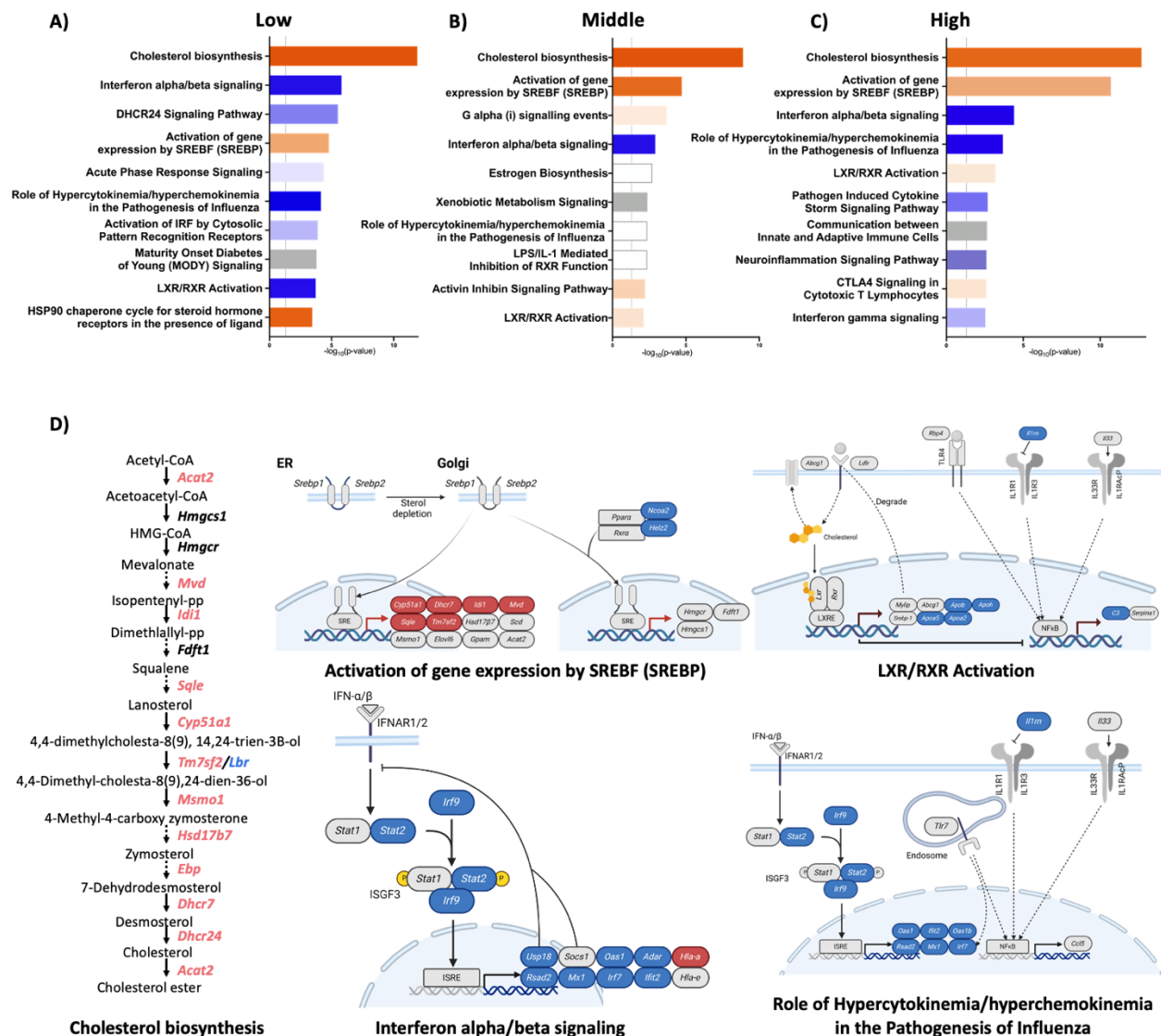


Figure 4-9. Top 10 canonical pathways in (A) low, (B) middle, and (C) high OPE group identified by the Ingenuity Pathway Analyses (IPA). Orange indicates pathway activation; blue indicates pathway inhibition; white indicates that insufficient DEGs (< 4) were associated with the pathway; grey indicates unknown direction of change of pathway activity. (D) Pathway diagram showing the commonly affected pathway(s). The expression changes represent transcripts affected in the low OPE treatment group. Red indicates upregulation of the expression level of the transcript, blue indicates downregulation. n = 5. Created with BioRender.com

SUPPLEMENTAL MATERIALS

List of supplemental tables and figures

Table 4-S1. Scoring criteria for histology examination

Table 4-S2. Top 10 significantly upregulated or downregulated transcripts in male treatment groups.

Table 4-S3. Top 10 significantly upregulated or downregulated transcripts in female treatment groups.

Table 4-S4. Transcripts commonly affected across male treatment groups.

Table 4-S5. Transcripts commonly affected across female treatment groups.

Table 4-S6. Transcripts that are in the top 10 commonly affected pathways.

Figure 4-S1. Male and female percentage change in body weight following OPE exposure.

Figure 4-S2. Effects of the OPE mixture on adrenal gland morphology.

Figure 4-S3. Effect of OPE mixture exposure on the width of the zone in male and female adrenal glands.

Figure 4-S4. Serum biochemistry for male rats.

Figure 4-S5. Serum biochemistry for female rats.

Figure 4-S6. Top 5 uniquely affected pathways in each of the male treatment group identified by Ingenuity Pathway Analysis (IPA).

Figure 4-S7. Top 5 uniquely affected pathways in each of the female treatment group identified by Ingenuity Pathway Analysis (IPA).

Table 4-S1. Scoring criteria for histology examination

	Lipofuscin	Lipid droplets	Sinusoids	Hemosiderin	Hypertrophy	Pyknosis
0	Non observed	No or few obvious droplets in cortical cells within the layer	No gap	Non observed	Non observed	Non observed
1	Single cell	Few round, discrete droplets	Hairline gap	Minimal hemosiderin deposition, localized to a few scattered areas	Slight increase in cell size observed	Few cells show condensation of chromatin with nuclei appearing slightly shrunken and darker
2	Multiple cells containing	Multiple round droplets per cell throughout tissue	< half cell width	Mild hemosiderin deposition, with small foci of staining in the tissue.	Moderate enlargement of adrenal cells present	A moderate number of cells show condensed chromatin with a more noticeable decrease in nuclear size and darker staining
3	Multiple cells visible in at least 1/100X field or multiple cells with area or roughly half of cytoplasm	Same as above but with many droplets and with frequent cells containing corona of droplets around nucleus. Maybe a foamy cell	Half cell width	Visible in several areas but not widespread.	Clearly enlarged cells with noticeable changes in the tissue, but the overall architecture remains intact	Pronounced nuclear condensation and dark, irregular-shaped nuclei
4	Regions of section with many fields with 3-5 cells per field	Foamy cells or clusters of foamy cells scattered through layer	Full cell width	Marked hemosiderin deposition, evident in multiple regions of the tissue.	Substantial enlargement of adrenal cells and more pronounced architectural changes	Many cells showing shrunken and darkly condensed nuclei. Some nuclei may be fragmented.

5	Lipofuscin containing cells distributed extensively throughout layer	Extensive foamy cells. Tissue notably hypertrophied.	N/A	Extensive hemosiderin deposition, with almost all tissue areas showing significant staining.	Extensive enlargement and distortion of adrenal glands, with possible disorganization of tissue structure	Almost all cells in the field showing severe nuclear condensation or fragmentation
---	--	--	-----	--	---	--

Table 4-S2: Top 10 significantly upregulated or downregulated transcripts in male treatment groups.

A) Low OPE treatment group upregulated

ID	Symbol	Name	Change in expression level	Log₂(FC)	p-value
ENSRNOG00000014414	Qrfpr	Pyroglutamylated RFamide Peptide Receptor	1982.3	0.6	3.70E-02
ENSRNOG00000028266	Lrrc55	Leucine rich repeat containing 55	1362.9	0.8	1.40E-03
ENSRNOG00000010640	Agtr1b	Angiotensin II receptor, type 1b	1126.6	0.8	7.00E-04
ENSRNOG00000009265	Kcnk9	Potassium two pore domain channel subfamily K member 9	928.9	0.6	3.00E-02
ENSRNOG00000003510	Fmo2	Flavin containing dimethylaniline monooxygenase 2	859.6	0.7	1.60E-04
ENSRNOG00000050006	Agtr2	Angiotensin II receptor type 2	706.2	0.7	1.40E-03
ENSRNOG00000017911	Tcaf1	TRPM8 channel associated factor 1	689.8	0.7	1.50E-03
ENSRNOG00000001499	Mia	Melanoma inhibitory activity	618.3	1.2	6.20E-08
ENSRNOG00000007600	Igsf1	Immunoglobulin superfamily member 1	607.9	0.7	8.00E-04
ENSRNOG00000016675	Kcnn2	Potassium calcium-activated channel subfamily N member 2	598.6	0.7	3.80E-03

B) Low OPE treatment group downregulated

ID	Symbol	Name	Change in expression level	Log₂(FC)	p-value
ENSRNOG00000007765	Frzb	Frizzled related protein	-11387.6	-0.7	3.40E-04
ENSRNOG00000007607	Nr4a1	Nuclear receptor subfamily 4 group A member 1	-8606.1	-2.1	3.60E-03
ENSRNOG00000005964	Nr4a3	Nuclear receptor subfamily 4 group A member 3	-7581.6	-2.6	7.50E-03
ENSRNOG000000042838	Junb	Transcription Factor AP-1 Subunit JunB	-7514.6	-2.4	5.60E-04
ENSRNOG000000056596	Alas1	5'-aminolevulinate synthase 1	-7146.2	-1.2	3.20E-02
ENSRNOG00000014456	Coq10b	Coenzyme Q10B	-6380.1	-1.4	2.30E-02
ENSRNOG00000006931	Eepd1	Endonuclease/Exonuclease/Phosphatase Family Domain Containing 1	-5950.5	-0.7	1.20E-02
ENSRNOG00000004284	Btg1	BTG anti-proliferation factor 1	-5469.4	-1.3	1.10E-02
ENSRNOG000000058646	Zfp361l	ZFP36 ring finger protein like 1	-5464.7	-0.8	1.60E-03
ENSRNOG00000000805	Gja1	Gap junction protein alpha 1	-4703.9	-0.7	1.90E-03

C) Middle OPE treatment group upregulated

ID	Symbol	Name	Change in expression level	Log ₂ (FC)	p-value
ENSRNOG00000054757	Adcy6	Adenylate cyclase 6	683.3	0.6	1.77E-04
ENSRNOG00000029510	Plxnb1	Plexin B1	536.5	0.6	5.84E-03
ENSRNOG00000001499	Mia	Melanoma inhibitory activity	394.8	0.8	4.30E-05
ENSRNOG000000014124	Nod2	Nucleotide binding oligomerization domain containing 2	372.1	0.6	1.72E-02
ENSRNOG00000048248	AABR07000699.1	Uncharacterized	340.8	3.3	5.99E-03
ENSRNOG000000012991	Adgra2	Adhesion G protein-coupled receptor A2	315.7	0.6	1.01E-03
ENSRNOG000000010977	Igfbp6	Insulin like growth factor binding protein 6	306.0	0.6	1.39E-02
ENSRNOG00000005580	Itgb4	Integrin subunit beta 4	292.9	0.9	5.58E-03
ENSRNOG000000020401	Adcy4	Adenylate cyclase 4	284.2	0.6	1.58E-04
ENSRNOG000000043304	Apcdd1	APC down-regulated 1	278.0	0.8	4.29E-03

D) Middle OPE treatment group downregulated

ID	Symbol	Name	Change in expression level	Log ₂ (FC)	p-value
ENSRNOG00000007765	Frzb	Frizzled related protein	-11584.0	-0.7	1.81E-03
ENSRNOG000000014856	Etnk1	Ethanolamine kinase 1	-2757.5	-0.6	1.12E-02
ENSRNOG000000018257	Hpx	Hemopexin	-2528.5	-1.5	1.34E-09
ENSRNOG000000056940	Cited2	Cbp/P300 interacting transactivator with Glu/Asp rich carboxy-terminal domain 2	-1829.4	-0.8	7.77E-03
ENSRNOG000000013663	Tmem86a	Transmembrane protein 86A	-1475.6	-0.8	1.32E-02
ENSRNOG000000011150	Arsb	Arylsulfatase B	-1349.3	-0.6	2.64E-02
ENSRNOG000000010602	Birc2	Baculoviral IAP repeat containing 2	-1332.3	-0.6	3.41E-02
ENSRNOG000000001647	Ets2	ETS proto-oncogene 2, transcription factor	-1175.7	-0.7	3.35E-03
ENSRNOG000000016587	Ninjl	Ninjurin 1	-1043.4	-0.7	2.67E-03
ENSRNOG000000029651	Rdh16	Retinol dehydrogenase 16	-968.0	-0.6	8.97E-07

E) High OPE treatment group upregulated

ID	Symbol	Name	Change in expression level	Log ₂ (FC)	p-value
ENSRNOG00000043451	Spp1	Secreted Phosphoprotein 1	16498.3	1.9	7.75E-03
ENSRNOG00000014414	Qrfpr	Pyroglutamylated RFamide peptide receptor	2145.7	0.6	1.96E-02
ENSRNOG00000009265	Kcnk9	Potassium two pore domain channel subfamily K member 9	1823.2	1.0	1.11E-02
ENSRNOG00000003510	Fmo2	Flavin containing dimethylaniline monooxygenase 2	827.4	0.7	5.32E-04
ENSRNOG00000017911	Tcaf1	TRPM8 channel associated factor 1	564.8	0.6	1.04E-02
ENSRNOG00000000886	Caln1	Calneuron 1	459.8	0.6	1.14E-02
ENSRNOG00000012791	Ajuba	LIM Domain-Containing Protein Ajuba	451.0	0.6	4.02E-02
ENSRNOG00000045967	AABR07064061.1	Uncharacterized	345.7	1.4	8.06E-07
ENSRNOG00000027606	Neurl1b	Neuralized E3 ubiquitin protein ligase 1B	303.7	0.7	1.82E-02
ENSRNOG00000016119	Fzd7	Frizzled class receptor 7	294.5	0.7	1.11E-03

F) High OPE treatment group downregulated

ID	Symbol	Name	Change in expression level	Log ₂ (FC)	p-value
ENSRNOG00000014900	Crem	cAMP responsive element modulator	-8184.2	-1.5	3.79E-02
ENSRNOG00000005964	Nr4a3	Nuclear receptor subfamily 4 group A member 3	-7593.0	-2.4	8.09E-03
ENSRNOG00000006859	Insig1	Insulin induced gene 1	-5731.1	-1.4	2.04E-02
ENSRNOG000000058646	Zfp361l	ZFP36 ring finger protein like 1	-4674.9	-0.6	2.71E-02
ENSRNOG000000008487	Amotl2	Angiomotin Like 2	-3882.0	-1.3	3.46E-02
ENSRNOG000000025608	Lrat	Lecithin Retinol Acyltransferase	-3479.6	-0.6	1.92E-02
ENSRNOG00000014338	Slc25a25	Solute carrier family 25 member 25	-3275.5	-1.7	6.08E-03
ENSRNOG00000016552	Hmgcs1	3-hydroxy-3-methylglutaryl-CoA synthase 1	-3116.2	-1.6	4.77E-03
ENSRNOG000000004091	Cwc25	CWC25 Spliceosome Associated Protein Homolog	-2986.5	-2.5	8.65E-03
ENSRNOG000000005600	Nr4a2	Nuclear receptor subfamily 4 group A member 2	-2922.6	-2.8	4.81E-03

Table 4-S3: Top 10 significantly upregulated or downregulated transcripts in female treatment groups.

A) Low OPE treatment group upregulated

ID	Symbol	Name	Change in expression level	Log ₂ (FC)	p-value
ENSRNOG00000031979	Mt-atp6	Mitochondrially encoded ATP synthase 6	262969.7	0.6	4.14E-03
ENSRNOG00000030371	Mt-co2	Mitochondrially Encoded Cytochrome C Oxidase II	235140.0	0.7	2.53E-03
ENSRNOG00000008074	Cyp11a1	Cytochrome P450 Family 11 Subfamily A Member 1	73775.4	0.6	8.70E-03
ENSRNOG00000040287	Cyp1b1	Cytochrome P450 family 1 subfamily B member 1	53755.1	0.8	6.78E-03
ENSRNOG00000000981	Scarb1	Scavenger receptor class B member 1	37729.0	0.9	3.85E-02
ENSRNOG00000009734	Akr1b8	Aldo-keto reductase family 1, member B8	33640.9	1.3	5.41E-05
ENSRNOG00000029707	Mt-nd4	Mitochondrially encoded NADH dehydrogenase 4	32949.2	1.0	1.18E-04
ENSRNOG00000033615	Mt-nd3	Mitochondrially encoded NADH dehydrogenase 3	29778.8	0.7	1.35E-03
ENSRNOG00000029042	Mt-nd6	Mitochondrially encoded NADH dehydrogenase 6	29042.7	0.7	9.72E-04
ENSRNOG00000012123	Fdx1	Ferredoxin 1	21258.5	0.7	1.52E-02

B) Low OPE treatment group downregulated

ID	Symbol	Name	Change in expression level	Log ₂ (FC)	p-value
ENSRNOG00000056493	Mybpc1	Myosin binding protein C1	-6024.1	-0.7	1.27E-03
ENSRNOG00000026605	Ifi2712b	Interferon, alpha-inducible protein 27 like 2B	-2392.8	-0.6	1.52E-02
ENSRNOG00000016326	Cx3cl1	C-X3-C motif chemokine ligand 1	-1864.7	-0.7	7.11E-05
ENSRNOG00000010643	Kank2	KN motif and ankyrin repeat domains 2	-1364.0	-0.7	1.52E-03
ENSRNOG00000029658	Rnf213	Ring finger protein 213	-1280.8	-0.8	3.79E-03
ENSRNOG00000021027	Dbp	D-box binding PAR bZIP transcription factor	-1192.1	-0.6	4.21E-02
ENSRNOG00000001963	Mx2	MX Dynamin Like GTPase 2	-1096.7	-1.6	4.35E-03
ENSRNOG00000021719	Slfn5	Schlafen family member 5	-1044.2	-0.6	2.57E-03
ENSRNOG00000029386	RT1-N2	RT1 class Ib, locus N2	-969.3	-1.3	5.69E-05
ENSRNOG00000011977	Sema5a	Semaphorin 5A	-953.8	-0.6	2.83E-02

C) Middle OPE treatment group upregulated

ID	Symbol	Name	Change in expression level	Log ₂ (FC)	p-value
ENSRNOG00000009734	Akr1b8	Aldo-keto reductase family 1, member B8	13948.7	0.7	1.54E-02

ENSRNOG00000012786	Pgrmc1	Progesterone receptor membrane component 1	8666.4	0.6	2.82E-02
ENSRNOG00000053577	Gramd1b	GRAM domain containing 1B	3383.8	0.8	2.68E-03
ENSRNOG00000006859	Insig1	Insulin induced gene 1	1607.8	1.1	3.73E-04
ENSRNOG00000001229	Col18a1	Collagen type XVIII alpha 1 chain	1581.5	0.9	2.98E-03
ENSRNOG00000014414	Qrfpr	Pyroglutamylated RFamide peptide receptor	1490.3	0.6	3.04E-02
ENSRNOG00000008709	Arhgap32	Rho GTPase activating protein 32	1241.8	0.6	4.40E-02
ENSRNOG00000003510	Fmo2	Flavin containing dimethylaniline monooxygenase 2	1085.4	0.8	5.50E-04
ENSRNOG00000003969	Fam20a	FAM20A golgi associated secretory pathway pseudokinase	666.2	0.8	1.79E-02
ENSRNOG00000007234	Cyp51	Sterol 14 α -Demethylase Cytochrome P450	613.7	0.6	5.28E-03

D) Middle OPE treatment group downregulated

ID	Symbol	Name	Change in expression level	Log ₂ (FC)	p-value
ENSRNOG00000037607	Rplp2	Ribosomal protein lateral stalk subunit P2	-876.4	-3.4	1.09E-03
ENSRNOG00000012847	Scgb1c1	Secretoglobulin Family 1C Member 1	-716.1	-1.1	4.63E-02
ENSRNOG00000016678	Angptl2	Angiopoietin like 2	-615.8	-0.8	2.35E-03
ENSRNOG00000048248	AABR07000699.1	Uncharacterized	-425.8	-6.0	8.58E-13
ENSRNOG00000017676	Plvap	Plasmalemma vesicle associated protein	-325.1	-0.6	1.54E-02
ENSRNOG00000047225	Tma7	Translation Machinery Associated 7	-254.3	-3.6	6.59E-04
ENSRNOG00000032327	Pdia5	Protein disulfide isomerase family A member 5	-234.8	-0.9	6.98E-05
ENSRNOG00000013215	Dctd	Deoxycytidylate Deaminase	-233.1	-1.0	8.17E-04
ENSRNOG00000032401	H3f3a3	H3.3 histone A like 3	-224.0	-1.1	7.70E-03
ENSRNOG00000045829	Thbs1	Thrombospondin 1	-203.8	-1.0	1.04E-03

E) High OPE treatment group upregulated

ID	Symbol	Name	Change in expression level	Log ₂ (FC)	p-value
ENSRNOG00000030371	Mt-co2	Mitochondrially encoded cytochrome C oxidase II	177930.9	0.6	7.00E-03

ENSRNOG00000040287	Cyp1b1	Cytochrome P450 family 1 subfamily B member 1	67460.3	1.0	4.00E-03
ENSRNOG00000009875	Akr1b7	Aldo-keto reductase family 1, member B7	49935.6	0.6	6.00E-03
ENSRNOG00000015052	Star	Steroidogenic acute regulatory protein	41711.3	0.8	5.00E-03
ENSRNOG00000000981	Scarb1	Scavenger receptor class B member 1	33453.1	0.9	1.20E-02
ENSRNOG00000009734	Akr1b8	Aldo-keto reductase family 1, member B8	27271.2	1.2	0.00E+00
ENSRNOG00000043866	AY172581.24	Uncharacterized	14879.4	1.2	2.90E-02
ENSRNOG00000012786	Pgrmc1	Progesterone receptor membrane component 1	13921.3	1.0	2.00E-03
ENSRNOG00000030478	AY172581.9	Uncharacterized	10971.0	0.7	2.80E-02
ENSRNOG00000007765	Frzb	Frizzled related protein	7944.7	1.1	4.30E-02

F) High OPE treatment group downregulated

ID	Symbol	Name	Change in expression level	Log ₂ (FC)	p-value
ENSRNOG00000013552	Scd1	Stearoyl-CoA desaturase	-7578.7	-2.4	1.60E-02
ENSRNOG00000056493	Mybpc1	Myosin binding protein C1	-5023.1	-0.6	2.00E-02
ENSRNOG00000045636	Fasn	Fatty acid synthase	-4580.2	-1.8	5.00E-03
ENSRNOG00000009715	Me1	Malic enzyme 1	-3225.6	-0.9	1.00E-03
ENSRNOG00000003259	C1qtnf1	C1q and TNF related 1	-3012.9	-0.7	6.00E-03
ENSRNOG00000026605	Ifi2712b	Interferon, alpha-inducible protein 27 like 2B	-2692.6	-0.8	3.30E-02
ENSRNOG00000013166	Wnt4	Wnt family member 4	-2347.9	-0.9	7.00E-03
ENSRNOG00000057569	Ahnak	AHNAK Nucleoprotein	-2278.4	-0.6	1.10E-02
ENSRNOG00000016326	Cx3cl1	C-X3-C motif chemokine ligand 1	-1743.4	-0.7	1.00E-03
ENSRNOG00000056228	Atp10a	ATPase phospholipid transporting 10A	-1578.5	-0.7	1.50E-02

Table 4-S4: Transcripts commonly affected across male treatment groups, part 1.

Category	ID	Symbol	Name	Log ₂ (FC) Low OPE	Log ₂ (FC) Middle OPE	Log ₂ (FC) High OPE
Adrenal related	ENSRNO G0000000 9437	Ewsr1	EWS RNA binding protein 1	-1.61	-1.46	-1.24
	ENSRNO G0000001 1202	St8sia4	ST8 alpha-N-acetyl- neuraminide alpha- 2,8-sialyltransferase 4	1.00	0.75	1.28
	ENSRNO G0000003 6828	Chma4	Cholinergic receptor nicotinic alpha 4 subunit	1.16	0.86	1.21
	ENSRNO G0000001 0158	Pde1b	Phosphodiesterase 1B	0.62	0.59	0.68
	ENSRNO G0000001 9128	Magel2	MAGE family member L2	-1.00	-1.30	-0.69
Immune	ENSRNO G0000004 9422	Fcgr2a	Fc gamma receptor IIa	-3.98	-2.89	-1.98
	ENSRNO G0000001 0634	Megf11	Multiple EGF like domains 11	-1.69	-1.42	-1.02
	ENSRNO G0000005 8555	Nkrf	NF-Kappa-B- repressing factor	-4.14	-0.93	-1.02
	ENSRNO G0000000 8615	Mal2	T cell differentiation protein 2	-0.60	-1.10	-0.74
	ENSRNO G0000002 9582	Lrch2	Leucine rich repeats and calponin homology domain containing 2	1.10	0.74	0.86
	ENSRNO G0000002 9749	Pabpc4l	Poly(A) binding protein cytoplasmic 4 like	2.35	1.79	2.19
	ENSRNO G0000001 6394	Wdr77	WD repeat domain 77	2.47	2.19	2.80
	ENSRNO G0000001 5550	Ptgds	Prostaglandin D2 synthase	4.33	3.53	3.49
	ENSRNO G0000000 5720	Spic	Spi-C transcription factor	3.01	2.76	3.53
	ENSRNO G0000001 3250	Pdcd5	Programmed cell death 5	-4.33	-3.80	-4.64
Apoptosis	ENSRNO G0000001 9822	Gadd45b	Growth arrest and DNA damage inducible beta	-0.83	-0.81	-0.81
	ENSRNO G0000001 0602	Birc2	baculoviral IAP repeat containing 2	-0.79	-0.59	-0.67
	ENSRNO G0000000 3496	Tbc1d9	TBC1 domain family member 9	-0.68	-0.99	-0.85
	ENSRNO G0000000 0795	Rt1-n3	RT1 class Ib, locus N3	0.65	0.90	0.75
	ENSRNO G0000005 8938	Camkv	CaM kinase like vesicle associated	1.00	0.91	0.74
	ENSRNO G0000002 1507	Luzp2	Leucine zipper protein 2	1.34	1.05	1.41
	ENSRNO G0000001 2988	Lix1	Limb and CNS expressed 1	1.82	1.38	1.61
	ENSRNO G0000001 8694	Lipg	lipase G, endothelial type	-1.22	-0.73	-1.11

Table 4-S4: Transcripts commonly affected across male treatment groups, part 2.

	ENSRNO G0000004 7860	Plin5	Perilipin 5	-1.19	-0.93	-0.81
	ENSRNO G0000001 2950	Efr3b	EFR3 Homolog B	0.96	0.98	0.96
	ENSRNO G0000001 4870	Slc13a5	Na(+)/Citrate Cotransporter	1.01	0.91	0.92
Cell cycle	ENSRNO G0000005 7729	Strip2	Striatin interacting protein 2	-0.92	-0.87	-0.73
	ENSRNO G0000001 7646	C16orf74	Chromosome 16 open reading frame 74	1.04	1.26	0.93
	ENSRNO G0000004 6379	Srm	Spermidine synthase	3.86	2.53	2.73
Cell-cell interaction	ENSRNO G0000000 0963	Tmem132 c	Transmembrane protein 132C	0.83	0.97	0.72
	ENSRNO G0000005 2405	Cdh4	Cadherin 4	1.16	1.06	1.02
	ENSRNO G0000001 8478	Myo3a	Myosin IIIA	-2.43	-1.68	-1.57
	ENSRNO G0000002 0151	Cdh1	Cadherin 1	1.28	1.69	1.42
Transporter /Receptor	ENSRNO G0000001 2830	Paqr8	Progestin and adipoQ receptor family member 8	0.90	0.83	1.01
	ENSRNO G0000000 1874	Slc7a4	Cationic amino acid transporter, Y+ System	-1.10	-0.90	-0.69
	ENSRNO G0000001 0296	Slc7a7	Solute carrier family 7 member 7	-0.90	-0.89	-0.75
	ENSRNO G0000001 9902	Folr1	Folate receptor alpha	-0.85	-0.84	-0.74
	ENSRNO G0000000 6076	Steap2	STEAP2 metalloreductase	-0.81	-0.63	-0.89
	ENSRNO G0000001 8567	Slc20a1	Solute carrier family 20 member 1	-0.67	-0.70	-0.65
	ENSRNO G0000000 7041	Abcg2	ATP binding cassette subfamily G member 2 (JR blood group)	0.97	0.83	1.01
	ENSRNO G0000002 6679	Scn4b	Sodium voltage- gated channel beta subunit 4	1.02	0.74	0.80
Miscellaneous	ENSRNO G0000002 9330	Car5b	Carbonic anhydrase 5b, mitochondrial	-0.62	-0.71	-0.73
	ENSRNO G0000006 1544	Spock2	SPARC (osteonectin), cwcv and kazal like domains proteoglycan 2	0.83	0.63	0.67
	ENSRNO G0000002 4435	Wbscr17	Polypeptide N- acetylgalactosaminyl transferase 17	0.90	0.96	0.65

Table 4-S5: Transcripts commonly affected across female treatment groups, part 1.

Category	ID	Symbol	Name	Log ₂ (FC) Low OPE	Log ₂ (FC) Middle OPE	Log ₂ (FC) High OPE
Adrenal related	ENSRNO G0000000 9734	Akr1b8	Aldo-keto reductase family 1, member B8	1.28	0.66	1.17
	ENSRNO G0000000 6841	Ano4	Anoctamin 4	1.40	1.39	1.31
	ENSRNO G0000002 5184	Prss35	Serine Protease 35	-0.97	-0.88	-1.43
	ENSRNO G0000001 4414	Qrfpr	Pyroglutamylated RFamide peptide receptor	0.73	0.62	1.06
	ENSRNO G0000000 1295	S100b	S100 calcium binding protein B	0.81	0.74	0.77
	ENSRNO G0000001 2847	Scgb1c1	Secretoglobulin Family 1C Member 1	-1.27	-1.06	-1.28
	ENSRNO G0000001 9978	Parg	Poly(ADP-ribose) glycohydrolase	0.64	0.61	1.03
Steroidogenesis	ENSRNO G0000001 9189	Acat2	Acetyl-CoA acetyltransferase 2	1.3	0.97	1.11
	ENSRNO G0000000 7234	Cyp51	Cytochrome P450, family 51	1.1	0.64	1.58
	ENSRNO G0000000 2826	Hsd17b7	Hydroxysteroid 17- beta dehydrogenase 7	0.7	0.64	1.48
	ENSRNO G0000001 6690	Idi1	Isopentenyl- diphosphate delta isomerase 1	2.3	1.06	2.70
	ENSRNO G0000000 6859	Insig1	Insulin induced gene 1	1.5	1.13	1.62
	ENSRNO G0000003 2297	Msmo1	Methylsterol monooxygenase 1	0.9	0.78	1.68
	ENSRNO G0000002 0989	Tm7sf2	Transmembrane 7 superfamily member 2	1.0	0.82	1.38
	ENSRNO G0000001 0468	Elov16	ELOVL fatty acid elongase 6	5.1	1.91	1.96
	ENSRNO G0000000 2921	Akap4	A-kinase anchoring protein 4	2.2	1.79	2.47
	ENSRNO G0000005 3577	Gramd1b	GRAM domain containing 1B	0.8	0.83	0.94
	ENSRNO G0000001 2786	Pgrmc1	Progesterone receptor membrane component 1	0.9	0.62	0.96
	ENSRNO G0000000 0461	Brd2	Bromodomain Containing 2	2.1	2.16	0.65
Immune	ENSRNO G0000000 3927	Cd55	CD55 molecule	1.4	1.02	0.93
	ENSRNO G0000003 6674	Cd7	Cluster of differentiation 7	1.3	1.04	1.46
	ENSRNO G0000000 6224	Klhl31	Kelch like family member 31	-1.2	-1.03	-1.49
	ENSRNO G0000001 8576	Rcan3	RCAN family member 3	-0.8	-0.65	-0.64
	ENSRNO G0000000 8045	Slamf9	SLAM family member	-1.0	-0.94	-1.26

Table 4-S5: Transcripts commonly affected across female treatment groups, part 2.

	ENSRNO G0000003 6711	Spn	Leukosialin	-0.8	-0.59	-1.01
	ENSRNO G0000001 3911	Nagk	N-acetylglucosamine kinase	0.9	0.67	0.83
Apoptosis	ENSRNO G0000005 8938	Camkv	CaM kinase like vesicle associated	-0.8	-0.91	-1.22
	ENSRNO G0000005 7078	Ddit4	DNA damage inducible transcript 4	0.8	0.99	0.86
	ENSRNO G0000001 3090	Gadd45g	Growth arrest and DNA damage inducible gamma	0.8	0.81	0.86
	ENSRNO G0000001 3712	Tex261	Testis expressed 261	1.1	0.61	0.86
	ENSRNO G0000001 6678	Angptl2	Angiopoietin like 2	-0.7	-0.82	-1.02
	ENSRNO G0000000 0195	Vwa5a	Von willebrand factor A domain containing 5A	1.8	2.01	1.47
	ENSRNO G0000003 0101	Traip	TRAF interacting protein	-0.8	-1.13	-1.22
	ENSRNO G0000000 8709	Arhgap32	Rho GTPase activating protein 32	1.5	0.59	1.47
G protein	ENSRNO G0000000 3895	Rgs1	Regulator of G protein signaling 1	1.2	0.99	1.46
	ENSRNO G0000000 3959	Rgs18	Regulator Of G protein signaling 18	-1.3	-1.09	-2.18
Lipid	ENSRNO G0000001 6769	Rab38	Rab-related GTP- binding protein	1.0	0.71	0.75
	ENSRNO G0000000 3870	C1qtnf2	Complement C1q tumor necrosis factor-related protein 2	-1.0	-0.73	-0.93
	ENSRNO G0000005 8193	Slc27a6	Solute carrier family 27 member 6	1.0	2.16	1.28
Cell cycle	ENSRNO G0000001 6483	Myo16	Myosin XVI	2.2	1.80	2.34
	ENSRNO G0000001 9587	Ptpn	Protein tyrosine phosphatase receptor type N	1.8	0.73	1.57
	ENSRNO G0000000 4084	Fam84a	Family with sequence similarity 84 member A	1.5	0.81	1.39
	ENSRNO G0000001 6980	Qprt	Quinolate phosphoribosyl transferase	-1.5	-1.30	-1.39
Cell-cell interaction	ENSRNO G0000004 5829	Thbs1	Thrombospondin 1	-1.2	-0.97	-1.00
	ENSRNO G0000001 3654	Cbln2	Cerebellin 2 precursor	1.8	1.44	2.08
	ENSRNO G0000000 5758	Btbd11	Ankyrin repeat and BTB domain containing 3	-0.9	-0.74	-0.69
	ENSRNO G0000001 8310	Eno4	Enolase 4	0.9	0.86	0.98
	ENSRNO G0000002 7171	Ndst2	N-deacetylase and N-sulfotransferase 2	-1.5	-2.56	-1.46
Transporter /Receptor	ENSRNO G0000001 5160	Gem	GTP binding protein overexpressed in skeletal muscle	1.0	0.88	1.98

Table 4-S5: Transcripts commonly affected across female treatment groups, part 3.

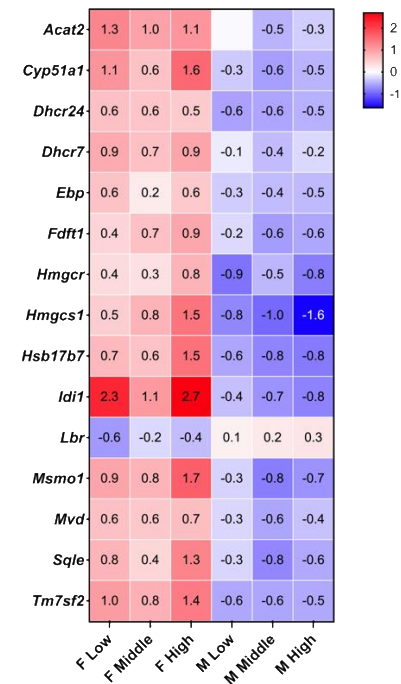
	ENSRNO G0000000 2391	Gla4	Glycine receptor alpha 4	-1.1	-0.69	-0.83
--	----------------------------	------	-----------------------------	------	-------	-------

	ENSRNO G0000003 9278	Mcart1	Mitochondrial nicotinamide adenine dinucleotide transporter	-0.7	-0.63	-1.93
	ENSRNO G0000005 0090	Slc6a17	Solute carrier family 6 member 17	0.7	0.79	1.11
	ENSRNO G0000000 8728	Unc79	Unc-79 homolog, NALCN channel complex subunit	1.0	0.65	1.11
Reactive oxygen species (ROS)	ENSRNO G0000000 8219	Ccdc33	Coiled-coil domain containing 33	3.3	3.10	3.54
	ENSRNO G0000005 9810	Txnrd3	Thioredoxin reductase 3	0.8	0.71	0.95
	ENSRNO G0000001 7716	Slc25a9	Solute carrier family 25 member 9	1.1	0.65	0.88
Miscellaneous	ENSRNO G0000001 9353	Ctrl	Chymotrypsin-like protease	1.1	1.00	1.09
	ENSRNO G0000000 8837	Ass1	Argininosuccinate synthase 1	1.3	0.72	2.44
	ENSRNO G0000003 2922	Dclk1	Doublecortin like kinase 1	1.4	0.67	1.66
	ENSRNO G0000000 3969	Fam20a	Golgi associated secretory pathway pseudokinase	0.9	0.81	1.08
	ENSRNO G0000000 8596	Ttl9	Tubulin--tyrosine ligase-like protein 9	0.7	0.78	0.91
	ENSRNO G0000005 0651	Zfp647	Zinc finger protein 647	-4.3	-4.95	-2.40

Table 4-S6: Transcripts that are in the top 10 commonly affected pathways.

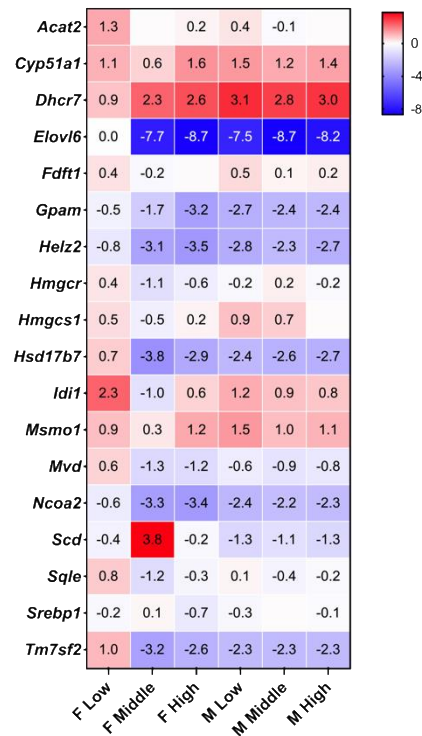
A) Cholesterol biosynthesis

ID	Symbol	Name
ENSRNOG00000019189	Acat2	Acetyl-CoA acetyltransferase 2
ENSRNOG00000007234	Cyp51a1	Cytochrome P450 family 51 subfamily A member 1
ENSRNOG00000006787	Dhcr24	24-dehydrocholesterol reductase
ENSRNOG00000020776	Dhcr7	7-dehydrocholesterol reductase
ENSRNOG00000004903	Ebp	EBP cholesterol delta-isomerase
ENSRNOG00000021314	Fdft1	Farnesyl-diphosphate farnesyltransferase 1
ENSRNOG00000016122	Hmgcr	HMG-CoA reductase
ENSRNOG00000016552	Hmgcs1	3-hydroxy-3-methylglutaryl-CoA synthase 1
ENSRNOG00000002826	Hsd17b7	Hydroxysteroid 17-beta dehydrogenase 7
ENSRNOG00000016690	Idi1	Isopentenyl-diphosphate delta isomerase 1
ENSRNOG00000005274	Lbr	Lamin B receptor
ENSRNOG00000032297	Msmo1	Methylsterol monooxygenase 1
ENSRNOG00000013376	Mvd	Mevalonate diphosphate decarboxylase
ENSRNOG00000009550	Sqle	Squalene Monooxygenase
ENSRNOG00000020989	Tm7sf2	Transmembrane 7 superfamily member 2



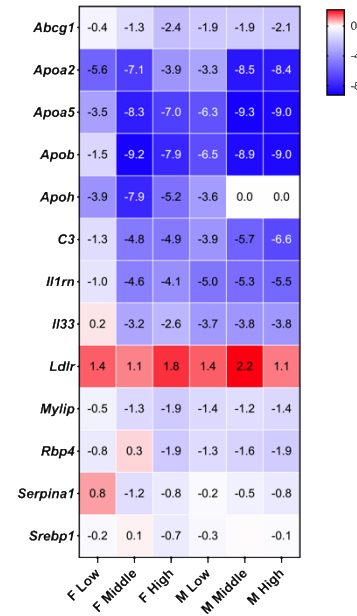
B) Activation of gene expression by SREBF (SREBP)

ID	Symbol	Name
ENSRNOG00000019189	Acat2	Acetyl-CoA acetyltransferase 2
ENSRNOG00000007234	Cyp51a1	Cytochrome P450 family 51 subfamily A member 1
ENSRNOG00000020776	Dhcr7	7-dehydrocholesterol reductase
ENSRNOG00000048949	Elov16	ELOVL fatty acid elongase 6
ENSRNOG00000021314	Fdft1	Farnesyl-diphosphate farnesyltransferase 1
ENSRNOG00000015124	Gpam	Glycerol-3-phosphate acyltransferase
ENSRNOG00000013267	Helz2	Helicase with Zinc finger 2
ENSRNOG00000016122	Hmgcr	HMG-CoA reductase
ENSRNOG00000016552	Hmgcs1	3-hydroxy-3-methylglutaryl-CoA synthase 1
ENSRNOG00000002826	Hsd17b7	Hydroxysteroid 17-beta dehydrogenase 7
ENSRNOG00000016690	Idi1	Isopentenyl-diphosphate delta isomerase 1
ENSRNOG00000032297	Msmo1	Methylsterol monooxygenase 1
ENSRNOG00000013376	Mvd	Mevalonate diphosphate decarboxylase
ENSRNOG00000007975	Ncoa2	Nuclear receptor coactivator 2
ENSRNOG00000046005	Scd	stearoyl-CoA desaturase
ENSRNOG00000009550	Sqle	Squalene monooxygenase
ENSRNOG00000003463	Srebp1	Sterol regulatory element-binding protein 1
ENSRNOG00000020989	Tm7sf2	Transmembrane 7 superfamily member 2



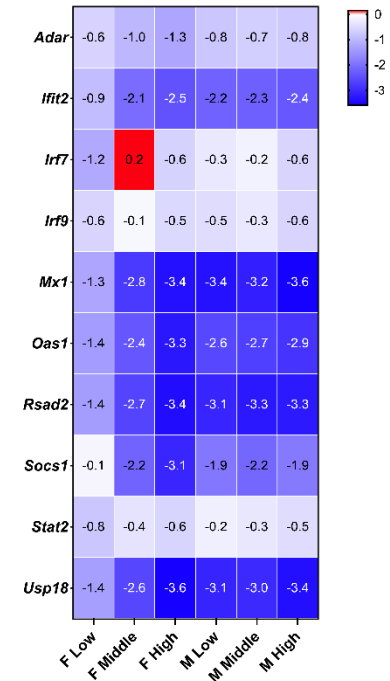
C) LXR/RXR activation

ID	Symbol	Name
ENSRNOG00000001158	Abcg1	ATP binding cassette subfamily G member 1
ENSRNOG00000003500	Apoa2	apolipoprotein A2
ENSRNOG000000018436	Apoa5	apolipoprotein A5
ENSRNOG000000005542	Apob	Apolipoprotein B
ENSRNOG000000003566	Apoh	apolipoprotein H
ENSRNOG000000046834	C3	complement C3
ENSRNOG000000005871	Il1rn	interleukin 1 receptor antagonist
ENSRNOG000000016456	Il33	Interleukin 33
ENSRNOG000000009946	Ldlr	low density lipoprotein receptor
ENSRNOG000000017579	Myip	myosin regulatory light chain interacting protein
ENSRNOG000000015518	Rbp4	retinol binding protein 4
ENSRNOG000000032669	Serpina1	serpin family A member 1
ENSRNOG000000003463	Srebp1	Sterol regulatory element-binding protein 1



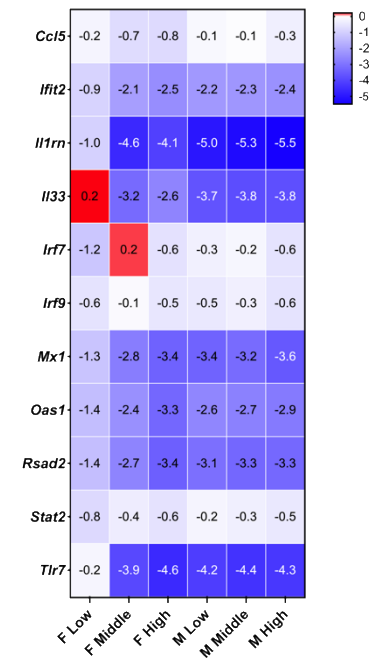
D) Interferon alpha/beta signaling

ID	Symbol	Name
ENSRNOG000000020744	Adar	Adenosine deaminase RNA specific
ENSRNOG000000036604	Ifit2	Interferon induced protein with tetratricopeptide repeats 2
ENSRNOG000000017414	Irf7	Interferon regulatory factor 7
ENSRNOG000000019478	Irf9	Interferon regulatory factor 9
ENSRNOG00000001959	Mx1	MX dynamin like GTPase 1
ENSRNOG000000047076	Oas1	2'-5'-oligoadenylate synthetase 1
ENSRNOG000000007539	Rsad2	Radical S-adenosyl methionine domain containing 2
ENSRNOG000000002568	Socs1	Suppressor of cytokine signaling 1
ENSRNOG000000031081	Stat2	Signal transducer and activator of transcription 2
ENSRNOG000000037198	Usp18	Ubiquitin specific peptidase 18



E) Role of hypercytokinemia/hyperchemokinememia in the pathogenesis of influenza

ID	Symbol	Name
ENSRNOG00000010906	Ccl5	C-C motif chemokine ligand 5
ENSRNOG00000036604	Ifit2	Interferon induced protein with tetratricopeptide repeats 2
ENSRNOG00000005871	Il1rn	Interleukin 1 receptor antagonist
ENSRNOG00000016456	Il33	Interleukin 33
ENSRNOG00000017414	Irf7	Interferon regulatory factor 7
ENSRNOG00000019478	Irf9	Interferon regulatory factor 9
ENSRNOG00000001959	Mx1	MX dynamin like GTPase 1
ENSRNOG00000047076	Oas1	2'-5'-oligoadenylate synthetase 1
ENSRNOG00000007539	Rsad2	Radical S-adenosyl methionine domain containing 2
ENSRNOG00000031081	Stat2	Signal transducer and activator of transcription 2
ENSRNOG00000004249	Tlr7	Toll-like receptor 7



F) Potassium channels

Category	ID	Symbol	Name
Voltage gated potassium channel	ENSRNOG00000055401	Kcnc1	Potassium voltage-gated channel subfamily C member 1
	ENSRNOG0000004077	Kcnc2	Potassium voltage-gated channel subfamily C member 2
	ENSRNOG00000024310	Kcnf1	Potassium Voltage-Gated Channel Modifier Subfamily F Member 1
	ENSRNOG00000003841	Kcnh1	Potassium voltage-gated channel subfamily H member 1
	ENSRNOG00000046949	Kcnb1	Potassium voltage-gated channel subfamily B member 1
Inwardly rectifying potassium channel	ENSRNOG00000033796	Kcnj5	Potassium inwardly rectifying channel subfamily J member 5
	ENSG00000162728	Kcnj9	Potassium Inwardly Rectifying Channel Subfamily J Member 9
Two-pore domain potassium channels	ENSRNOG00000009265	Kcnk9	Potassium two pore domain channel subfamily K member 9
Calcium-activated potassium channels	ENSRNOG00000029264	Kcnn1	Potassium calcium-activated channel subfamily N member 1
Hyperpolarization activated cyclic nucleotide gated potassium channel	ENSRNOG00000009450	Hcn4	Hyperpolarization activated cyclic nucleotide gated potassium channel 4
GABA receptor	ENSRNOG00000008431	Gabbr2	Gamma-aminobutyric acid type B receptor subunit 2

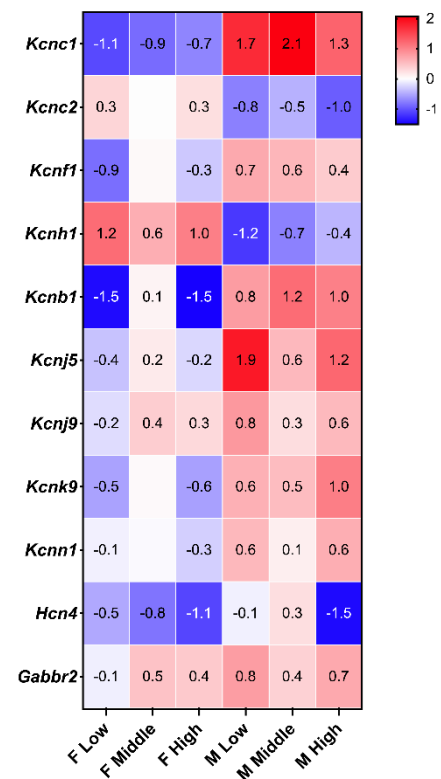


Figure 4-S1.

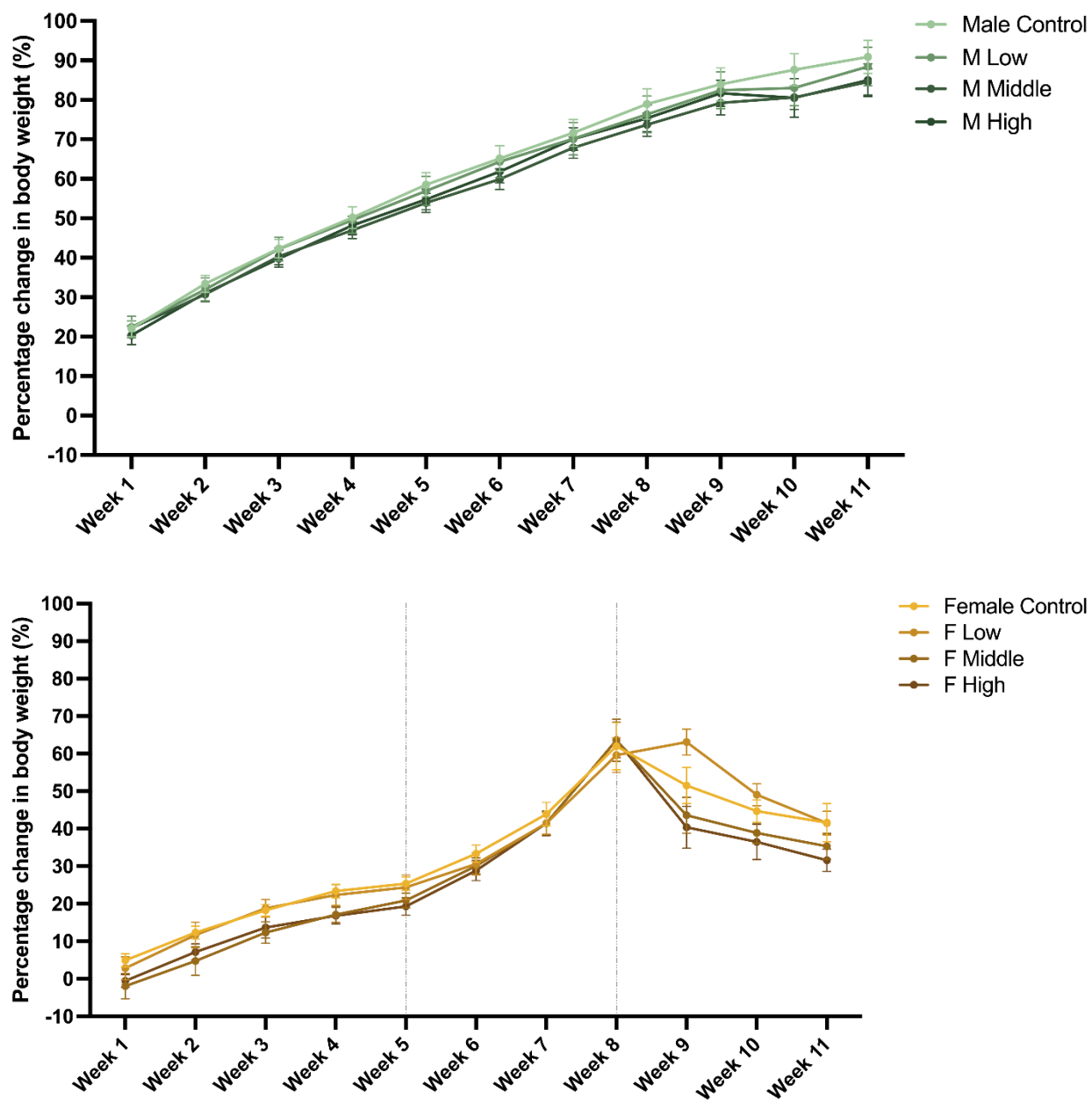


Figure 4-S1. Male and female percentage change in body weight following OPE exposure. Male rats were exposed to control, low, middle or high dose of the OPE mixture for 70 days followed by exposure during the mating period. Female rats were exposed for 30 days followed by exposure during gestation and lactation. Rats were measured weekly along with their food consumed. Female weights are shown for animals who were mated and gave birth. The dashed

lines correspond to the time of mating or parturition, respectively. No difference in food consumption between groups was observed (data not shown). N = 9-10.

Figure 4-S2.

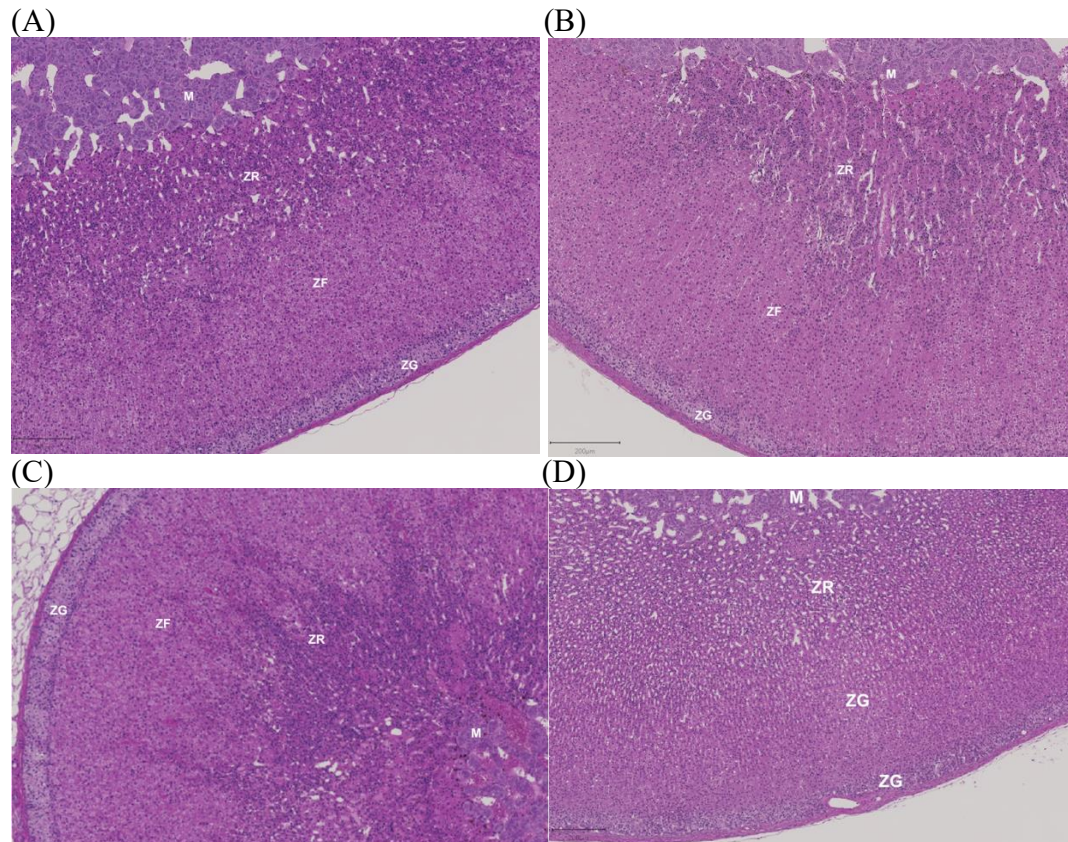


Figure 4-S2. Effects of the OPE mixture on adrenal gland morphology. Representative examples of adrenal histology from females on the (A) control or (B) high dose treatment group dose groups and from males on (C) control or (D) high dose treatment group. ZG, Zona Glomerulosa; ZF, Zona Fasciculata; ZR, Zona Reticularis; M, medulla. bar = 200 μ m

Figure 4-S3.

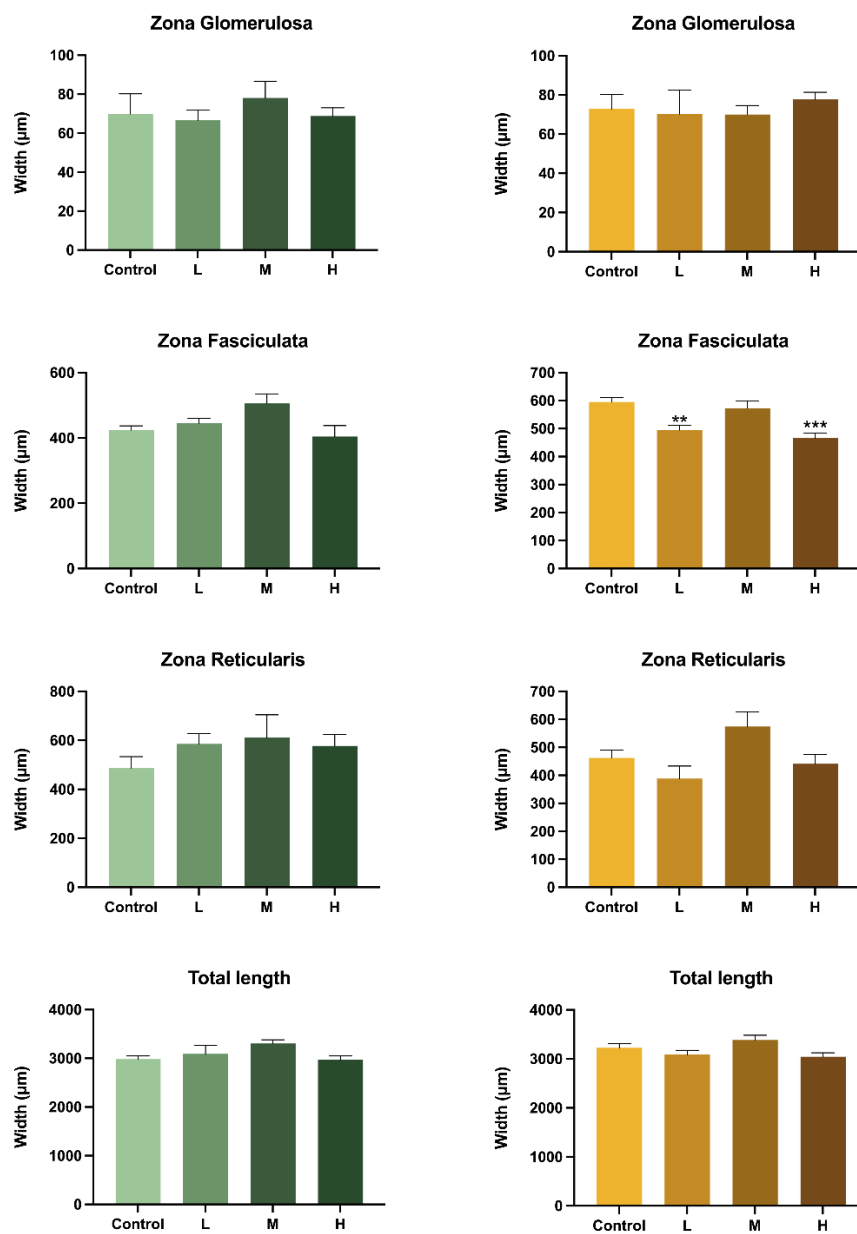


Figure 4-S3. Effect of OPE mixture exposure on the width of the zone in male and female adrenal glands. N = 5.

Figure 4-S4.

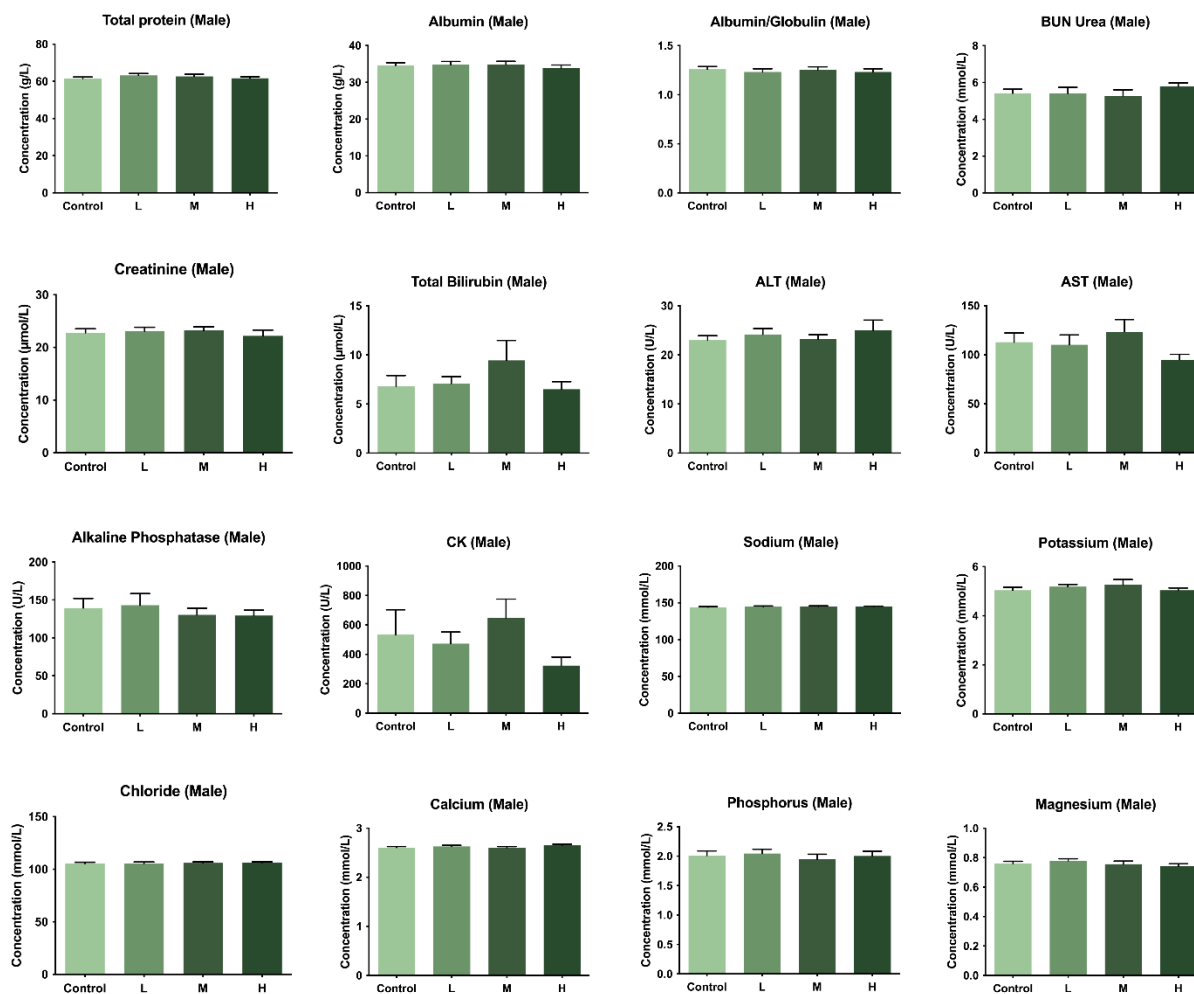


Figure 4-S4. Serum biochemistry for male rats. N = 9-10.

Figure 4-S5.

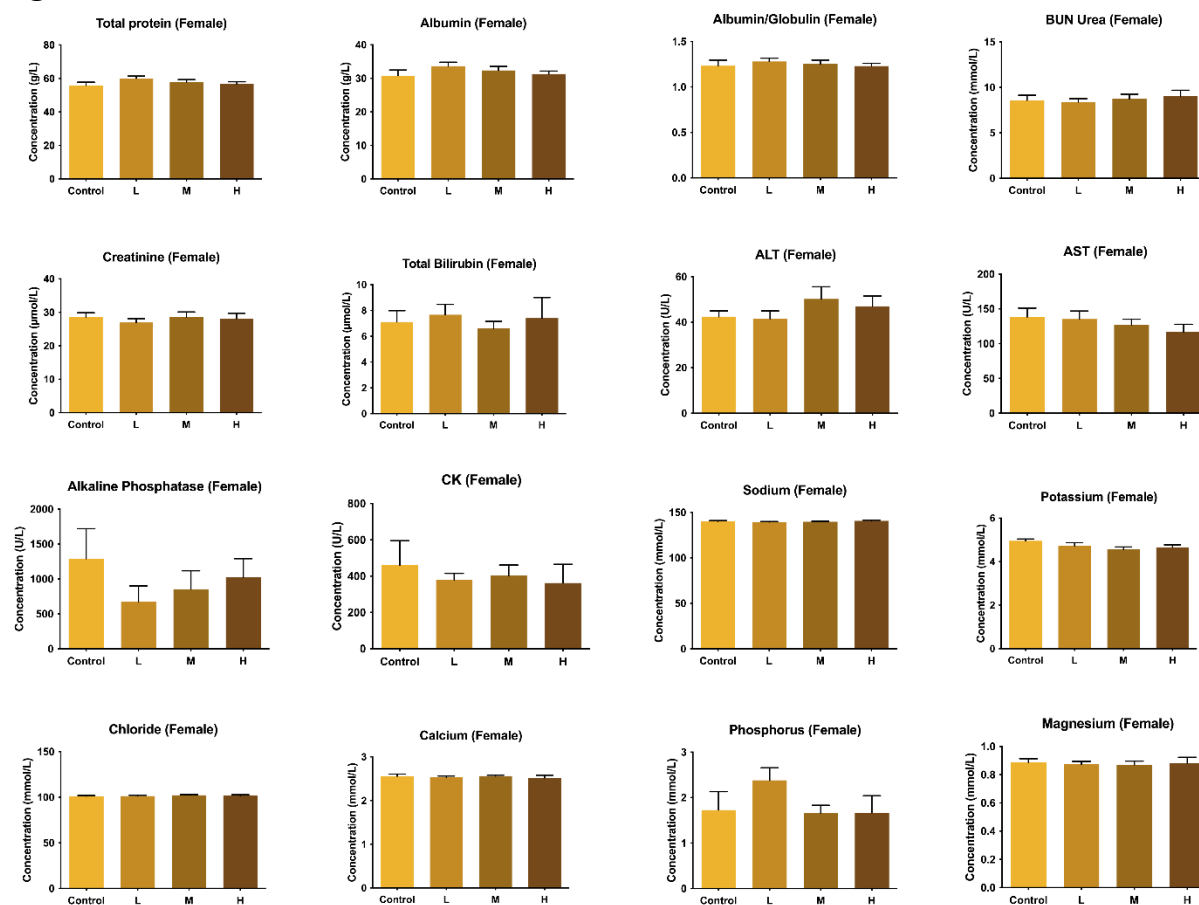


Figure 4-S5. Serum biochemistry for female rats. N = 9-10.

Figure 4-S6.

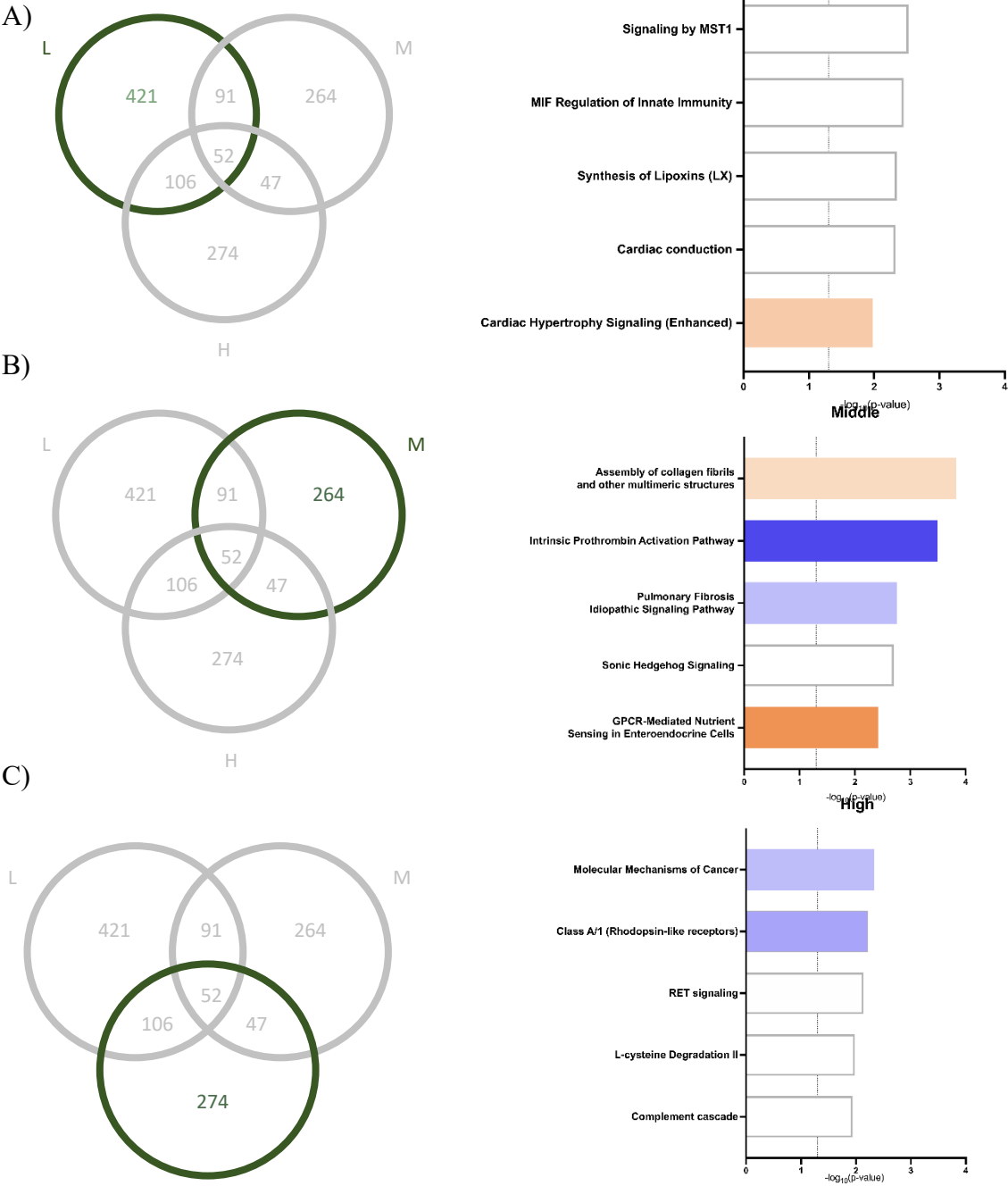


Figure 4-S6. Genes uniquely affected in (A) low, (B) middle, or (C) high OPE treatment group and the top 5 affected pathways identified by Ingenuity Pathway Analysis (IPA) related to each of the treatment group in males. Orange indicates pathway activation; blue indicates pathway inhibition; white indicates that insufficient DEGs (< 4) were associated with the pathway; grey indicates unknown direction of change of pathway activity.

Figure 4-S7.

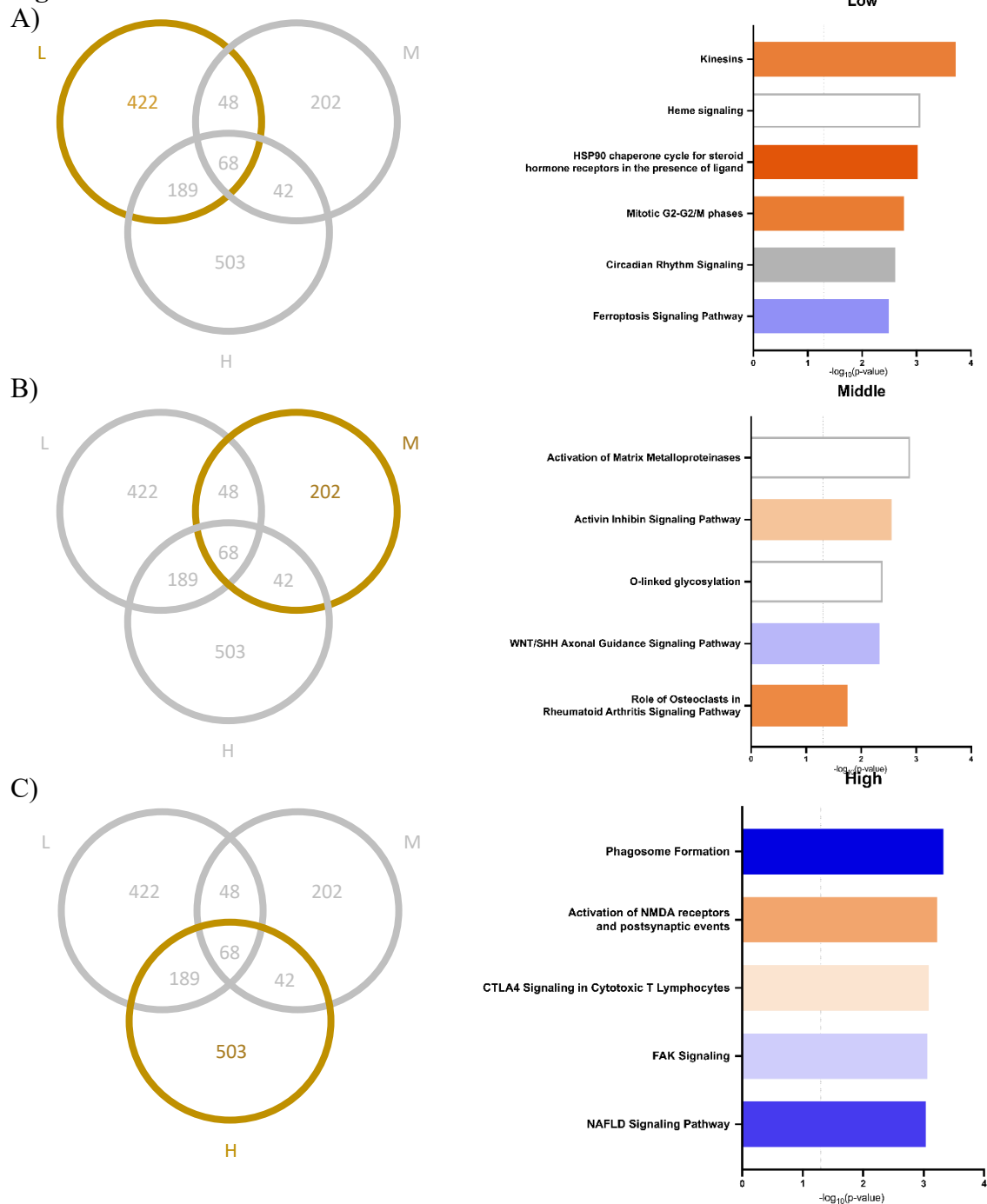


Figure 4-S7. Genes uniquely affected in low, (B) middle, or (C) high OPE treatment group and the top 5 affected pathways identified by Ingenuity Pathway Analysis (IPA) related to each of the treatment group in females. Orange indicates pathway activation; blue indicates pathway inhibition; white indicates that insufficient DEGs (< 4) were associated with the pathway; grey indicates unknown direction of change of pathway activity.

CHAPTER 5

DISCUSSION

5.1 Summary of findings

The studies presented in this thesis explores the *in vitro* and *in vivo* effects of a family of chemicals, the OPEs, on the adrenal glands. Chapter one provides the necessary background to understand the studies discussed throughout the thesis. In chapter two, we assessed the effects of six individual OPEs, commonly detected in Canadian house dust, on the phenotypic characteristics and functions of H295R human adrenal cells. A wide range of concentrations was tested, covering the higher end of human relevant exposure levels and doses that had previously induced adverse effects in toxicological studies. Potency ranking analyses based on the phenotypic outcomes revealed the relative potencies of OPEs in comparison to BDE-47. We identified potential "responsible replacements" of OPEs that showed little to no effects. Among the OPEs tested, several compounds sharing a common structural feature, the three phenol rings, were found to be more potent than BDE-47, and should be prioritized in further evaluations. Additionally, we found that triaryl OPEs disrupted hormone productions in H295R cells. The contrasting effects of these individual OPEs on cell functions were attributed to alterations in the expression of key transcripts involved in steroidogenesis and cholesterol biosynthesis. In chapter three, a mixture of OPEs was prepared based on the profile of OPEs measured in Canadian house dust samples. We determined its effect on the phenotypes and steroidogenic functions of H295R cells. Since the accumulation of lipid droplets was the most prominent phenotypic change induced by the house dust based OPE mixture, we further investigated its effects on the lipidome. Exposure to the OPE mixture altered the composition of lipid droplets through targeting the triglyceride, diglyceride, phosphatidylcholine, and cholesterol ester lipid subclasses. Importantly, our results demonstrated that individual OPEs, which exhibited minimal or no activity at low concentrations in isolation, induced significant effects when combined in mixtures. This suggests that studies focusing on single compounds may have underestimated the

potential health risks associated with OPEs. In chapter four, we assessed the *in vivo* effects of this OPE mixture on the adrenal glands of both male and female Sprague Dawley rats. We identified sex specific effects of OPEs on the weight, function, and transcriptome of the adrenal glands. A common mechanism observed in female rats, both *in vitro* and *in vivo*, involved the activation of the cholesterol biosynthesis pathway. In male rats, however, a potassium channel was consistently targeted. Similarly, *in vivo* exposure to the mixture affected the serum lipids, suggesting that disruptions in the level and composition of serum lipids could be a sensitive biomarker of OPE exposures.

Together, these studies represent the first comparison of the effects of OPEs with those of legacy PBDEs and elucidate the impact of an environmentally relevant mixture of OPEs on the adrenal glands. The *in vivo* component of this study highlighted the differential effects of the OPE mixture on male and female rats, emphasizing the importance of evaluating adrenal functions in both sexes. We propose that combining high-content screening, lipidomic, and transcriptomic approaches is effective in assessing the toxicity of environmental chemicals and identifying safer alternatives.

In the final chapter, we summarize the key findings of these studies, discuss their implications and draw connections between the results. We also address the limitations of the studies and propose future directions for further investigations into the effects of this class of chemicals on the function of the adrenal glands.

5.2 Common and cell specific effects of OPEs

In chapter two, we used a high-content screening strategy to assess the effects of commonly used OPEs on the phenotypes of the H295R cell. This standardized approach has

been used to test the effects of OPEs on cell lines from different organ systems, including the male reproductive system (TM4 mouse Sertoli cells (Rajkumar et al., 2022); MA-10 mouse Leydig cells, and C18-4 mouse spermatogonial cells (Wang et al., 2022)), the female reproductive system (KGN human granulosa cells (Wang et al., 2022)), and the liver (HepG2 human liver cells (Yu et al., 2024)). Here, we extend the comparison to all cell lines being tested to derive common and cell-specific effects of individual OPEs.

In the H295R cell, the most prominent effect was the accumulation of lipid droplets, which was induced by all six OPEs tested. This finding was consistent across the other cell lines, suggesting a common response to OPE exposure. Another significantly affected endpoint in H295R cells was the decrease in the number of lysosomes, an effect that was observed only in KGN cells (Wang et al., 2022), while it was either unaffected or increased in the other cell lines. When comparing the effects observed in H295R cells with all cell lines tested, we found that H295R cells shared more common profiles with reproductive cell lines, particularly KGN human granulosa cells. This could be partially attributed to their shared embryonic origins (discussed in the introduction). Importantly, these phenotypic changes were observed at concentrations that induced little to no cytotoxicity in all cell lines, indicating that phenotypic parameters were more sensitive indicators of cellular insult than traditional cytotoxicity assays.

There are also some endpoints that were only affected in certain cell lines. For example, calcein intensity increased exclusively in the male reproductive cell lines. Changes in calcein intensity were also commonly associated with alterations in oxidative stress levels (Wang et al., 2022). In these male reproductive cell lines, we observed increased oxidative stress, whereas in H295R and liver cells, calcein intensity remained unaffected, and oxidative stress levels were reduced (Yu et al., 2024). Additionally, the liver cell line exhibited more distinct effect profiles, with lysosomes and mitochondria being the predominant affected endpoints (Yu et al., 2024).

Lipid droplet accumulation was only mildly increased by one OPE in the liver cells. This may be partly due to the critical role liver cells play in autophagy and metabolism; the high abundance of lysosomes and metabolic enzymes in these cells may render them more resilient to lipid droplet accumulation compared to other cell types (Czaja et al., 2013).

The integration of Benchmark concentration (BMC) modeling with the Toxicological Prioritization Index (ToxPi) offers a powerful tool for ranking chemicals and visualizing their impacts across multiple biological endpoints. Among all the cell lines tested, the MA-10 mouse Leydig cell line exhibited the highest susceptibility to OPE exposures, with benchmark concentrations approximately ten times lower than those observed in other cell types (Wang et al., 2022). Moreover, ToxPi analysis revealed that the potency of OPEs varied depending on the cell line tested. For example, TDCIPP was the most potent OPE in MA-10 cells (Wang et al., 2022) and the second most potent in TM4 Sertoli cells (Rajkumar et al., 2022), yet it was the least potent in HepG2 liver cells (Yu et al., 2024). This variation can be explained by the fact that TDCIPP strongly affected up to six endpoints in MA-10 and TM4 Sertoli cells, while it only impacted cytotoxicity in HepG2 cells. Since ToxPi analysis considers all assessed endpoints, the ranking provides a comprehensive summary of the effects of each OPE on various cellular aspects. This also highlights the importance of evaluating not just cytotoxicity in risk assessment, as phenotypic effects may be overlooked.

Currently, most *in vitro* screening programs rely on monoculture assays using a single cell line for cost-efficiency (Health Canada, 2021a). However, the findings presented here suggest that responses observed in one cell type may not be generalizable to others. OPEs exhibit distinct bioactivities depending on the cell type tested, highlighting the need for a more comprehensive and integrated approach to toxicity assessment and risk evaluation.

5.3 Individual chemical vs mixture effects

In Chapter two, we tested six OPEs that were present at concentrations greater than 5% in Canadian house dust samples. The mixture used in Chapters three and four, which contained thirteen OPEs detected in Canadian homes, was employed to assess the *in vitro* and *in vivo* effects on the adrenal glands, respectively. This design allowed us to compare the effects of individual chemicals with those of the mixture. Additionally, the same mixture has been tested in other cell lines, including KGN cells (Wang et al., 2024), HepG2 liver cells (Yu et al., in preparation), and THP-1 human macrophages (Giles et al., 2024), enabling further comparison across different cell types.

To evaluate the impact of the mixture on cellular phenotypes, we employed a high-content screening strategy. We found that the only significantly affected endpoint was lipid droplet accumulation. In comparison to the individual chemicals, exposure to the mixture resulted in fewer affected endpoints, and the observed effects were less potent. These findings suggest that interactions between OPEs are more complex than simple additive effects of individual chemicals. Notably, 59.07% of the mixture was composed of TBOEP, a chemical identified as one of the less potent compounds in our study. Therefore, the relative proportion of potent components in a mixture may play a crucial role in predicting the effects of chemical mixtures.

However, the functional aspect of cellular steroid hormone production was significantly impacted by the mixture. Both basal and stimulated levels of aldosterone and cortisol were strongly upregulated following exposure to the OPE mixture. Importantly, regardless of the endpoint assessed, the mixture seemed to exert its effects at concentrations lower than the effective concentrations of the individual chemicals. For example, lipid droplet accumulation was observed at a dilution of 1/300,000 of the mixture, which contained a total of 6.9 μM of OPEs, including 0.68 μM of TMPP. However, when TMPP was tested in isolation, lipid droplet

accumulation only began at 1 μ M. Moreover, individual chemicals exhibited contrasting effects on hormone production: cortisol levels were increased by IPPP but decreased by TMPP or TPHP. These findings highlight that, while individual components may contribute to some of the responses observed following exposure to the mixture, it is not feasible to fully predict the effects of a chemical mixture based solely on data from single-exposure experiments. While assessing the effects of individual chemicals provides a foundation for identifying chemicals at risk, it is equally important to evaluate the effects of chemical mixtures directly to gain a comprehensive understanding of the potential risks associated with real-life exposure scenarios.

5.3.1 Effects of the mixture across different cell lines

Here, we extend the comparison to other cell lines, including KGN human granulosa cells, HepG2 liver cells, and THP-1 human macrophages. Similar to the individual OPEs, the mixture induced cytotoxicity and accumulation of lipid droplets across all cell lines tested, suggesting a common mechanism of action for this family of chemicals. However, when comparing the effect profiles, we found that unlike the individual OPEs, the KGN human granulosa cells were the most affected cell line (Wang et al., 2024), while the H295R cells were the least affected, with only lipid droplet accumulation observed. In line with the effects seen with individual OPEs, the mixture targeted lysosomes and lipid droplets in HepG2 cells. In THP-1 macrophages, a decrease in oxidative stress was also observed, in addition to alterations in lysosomes and lipid droplets (Giles et al., 2024). These findings highlight the importance of testing chemical mixtures in multiple cell models to gain a better understanding of the effects of chemicals on different biological systems.

5.4 Composition of lipids altered by the OPE mixture

Lipid droplets are increasingly recognized for their diverse functions beyond serving as simple energy storage sites. Their roles in mediating cellular signaling, modifying proteins, and sequestering lipophilic toxicants have been well-documented (Farese and Walther, 2009). Recent studies have also highlighted their contributions to disease processes, including metabolic disorders, neurodegeneration, and cancer, making them a key focus of cellular and biomedical research (Long et al., 2018; Sharma et al., 2023; Natesan et al., 2021). Therefore, we further investigated whether the composition of lipid droplets was altered by exposure to the OPE mixture through lipidomic analysis. This analysis was conducted in two additional cell lines, KGN human granulosa cells (Wang et al., 2024) and MA-10 mouse Leydig cells (in preparation), and is presented here as a comparison with the H295R cells.

The most significantly affected lipid category in H295R cells was glycerolipids, with triglycerides (TG) and diglycerides (DG) being the major subclasses impacted. Similarly, this lipid category was also the most affected in KGN human granulosa cells (Wang et al., 2024). Our transcriptomic data from the female adrenal glands suggest that the peroxisome proliferator-activated receptor (PPAR) signaling pathway was activated, which is consistent with previous reports of PPAR γ activation by individual OPEs (Negi et al., 2023; Fang et al., 2015) and the FM550 mixture (Pillai et al., 2014; Tung et al., 2017) in various cell types. Activation of the PPAR γ pathway has been linked to a reduction in TG levels, possibly indicating an adaptive response to lipid accumulation within cells (reviewed in Kersten, 2008).

In addition to glycerolipids, sterol lipids were another significantly affected category in both H295R and KGN cells, with a notable reduction in cholesterol esters found in both cell lines (Wang et al., 2024). Cholesterol, stored in ester form in lipid droplets, is a precursor for steroid hormone synthesis. A decrease in the level of cholesterol esters suggests that they could be mobilized for steroidogenesis. This is supported by the observed increase in cortisol and

aldosterone levels in H295R cells, as well as progesterone (P4) and 17 β -estradiol (E2) in KGN cells (Wang et al., 2024). Our transcriptomic data also revealed activation of the sterol regulatory element-binding protein (SREBP) pathway and inhibition of the liver X receptor (LXR) pathway. SREBP, when bound to its regulatory complex in the ER, activates genes involved in cholesterol homeostasis in response to reduced cholesterol levels, while LXR promotes cholesterol export (discussed in the introduction). Thus, we propose that in response to the decreased levels of cholesterol esters, the cells activate cholesterol biosynthesis and inhibit cholesterol export in an attempt to restore equilibrium. It has been reported that some OPEs had a medium to sub-high probability of binding to LXR (Wang et al., 2019), and inhibition of the LXR pathway by OPEs has been observed in other cell lines and organ systems. For example, in murine macrophages, exposure to TPHP and EHDPHP antagonized LXR activity, leading to inhibited cellular cholesterol efflux and the development of a cholesterol-laden cell phenotype (Hu et al., 2019). Inhibition of the LXR pathway by the same OPE mixture has also been observed in KGN cells (Wang et al., 2023b) and murine limb buds (Yan and Hales, 2021).

The lipidomic profile of MA-10 cells differed from the other two cell lines. A greater number of lipids were affected, although the prenol lipids category was not impacted in MA-10 cells. In contrast to H295R and KGN cells, the most significantly affected lipid category in MA-10 cells was glycerophospholipids, which include phosphatidylcholine (PC), a key component of the lipid droplet membrane (Koganti et al., 2022). The differences in lipid profiles between these cell lines could be attributed to several factors. The differences in cholesterol sources could influence lipid composition upon exposure to the OPE mixture. It is well established that in MA-10 cells, the plasma membrane is the primary source of cholesterol for the steroidogenic pathway, with membrane cholesterol gradually internalized into lipid droplets (Nagy and Freeman, 1990). The accumulation of lipid droplets resulting from increased rates of membrane

turnover in MA-10 cells may lead to membrane integrity damage, further enhancing the cellular uptake of OPEs and making these cells more susceptible to chemical exposures. Consequently, it is not surprising that MA-10 cells were affected to a greater extent. In comparison, intracellular lipids are preferred in the other two cell lines (reviewed in Azhar, 2003). Finally, the observed differences in OPE effects may also be partly attributed to species-specific variations, as rodent and human cells may respond differently to OPE exposure due to inherent biological differences.

5.5 Complementary roles of *in vitro* and *in vivo* studies

The assessment of both *in vitro* and *in vivo* effects of OPEs provides a comprehensive understanding of their toxicological profile. Most importantly, the *in vitro* cell line used in this study was derived from a female patient, and the inclusion of both male and female rats in the *in vivo* assessment enabled the identification of sex-specific effects of OPEs. Additionally, the evaluation of renin and ACTH levels in the animal model allowed us to assess the HPA axis, a critical function that cannot be fully captured in *in vitro* cell cultures. Moreover, it has been reported that some organophosphate di-esters are even more toxic than their respective tri-esters (Zhang et al., 2020). Thus, testing in the animal model which has the ability to metabolize OPEs reflect more closely to the real-world exposure effect.

The *in vitro* assessments, on the other hand, offer distinct advantages for screening chemicals in a high-throughout, cost-effective manner. The high-content screening of OPEs on various phenotypic endpoints provided an efficient way to identify chemicals of concern. Our findings suggest that OPEs containing halogen and aryl moieties are more toxic than alkyl OPEs, possibly due to enhanced cell membrane permeability and increased bioavailability, which allows for greater chemical uptake by cells (Finkelstein and Cass, 1968; Testa et al., 2000). These observations align with previous reports of similar effects in other cell types (Schang et al., 2016; Huang et al., 2017; Yu et al., 2024). Furthermore, we were able to determine the

adverse effect doses (AEDs) for each chemical, which represent the *in vivo* concentrations at which phenotypic alterations occurred. For instance, the lowest AED for TMPP-induced lipid droplet accumulation was calculated to be 0.0003 mg/kg body weight per day. While no phenotypic changes were observed with the OPE mixture in our animal study, Others assessing individual OPEs have reported lipid droplet accumulation in the adrenal glands at doses ranging from 5 to 1700 mg/kg body weight per day (National Toxicology Program, 1994; Latendresse et al., 1993, 1994, 1995; Wade et al., 2019; Akimoto et al., 2022). This suggests that our *in vitro* data provide valuable insight for deriving protective points of departure (PODs).

5.6 Potential mechanisms of action of OPEs

The assessment of OPEs using both *in vitro* and *in vivo* strategies provides a more comprehensive understanding of their overall toxic effects. At the cellular level, we were able to assess the acute exposure effects of OPEs on multiple phenotypic endpoints, while the animal model allowed us to evaluate the chronic, cumulative effects of exposure.

In female adrenal glands, exposure to individual OPEs for 48 hours resulted in significant accumulation of lipid droplets and a reduction in lysosome numbers. Lysosomes are critical in autophagy, a process that recycles cellular components, including proteins, organelles, and lipid droplets, by directing them for degradation in the lysosomes (Czaja et al., 2013). When autophagy specifically targets lipid droplets, it is referred to as lipophagy (Zhang et al., 2022). Within lipid droplets, cholesterol esters are stored and can be hydrolyzed by lysosomal enzymes to release free cholesterol, which serves as a precursor for steroid hormone synthesis. We propose that at the early stages of exposure to OPEs, the reduced lysosomal activity results in lipid droplet accumulation, which in turn triggers the activation of cholesterol biosynthesis pathways to provide the necessary cholesterol for steroid hormone production. Moreover, we observed an increase in the number of lipid droplets following exposure to all six OPEs.

Accumulating evidence suggests that the primary function of lipid droplet biogenesis is to alleviate cellular lipotoxicity, as well as stressors linked to disrupted ER homeostasis, oxidative damage, and nutrient deprivation (Henne et al., 2018; Zhang et al., 2003; Fei et al., 2009; Welte et al., 2017). It is possible that the accumulation of lipids was also partly due to lipid biogenesis in response to oxidative stress, and that we are observing a subsequent decrease in oxidative stress levels as a result.

Upon exposure to the OPE mixture for 48 hours, which contains 59.07% TBOEP (a chemical that does not significantly affect lysosomal function and oxidative stress levels), lipid droplet accumulation was the only phenotypic alteration observed. The mixture also activated cholesterol biosynthesis pathways, stimulating the production of steroid hormones. With prolonged exposure (weeks to months), the OPE mixture upregulated the expression of transcripts involved in the metabolism of aldosterone and corticosterone. Despite these transcriptional changes, no corresponding alterations in hormone levels were observed, suggesting that the cells may have been attempting to synthesize more steroid hormones. This increased demand for steroidogenesis may have triggered the activation of cholesterol biosynthesis via the SREBP-mediated pathway, which plays a key role in maintaining cholesterol homeostasis and supplying the necessary cholesterol within the cells for hormone production.

In contrast, the male adrenal glands exhibited a distinct response. The OPE mixture did not impact the expression levels of transcripts responsible for steroid hormone metabolism, suggesting that a different mechanism of action is involved here. The accumulation of potassium ions within the cells normally leads to depolarization, which activates calcium channels and triggers the production of aldosterone and corticosterone. However, exposure to the OPE mixture resulted in the upregulation of transcripts encoding potassium channels, promoting the efflux of

potassium ions from the cell. This prevents depolarization and calcium channel activation, ultimately reducing the production of aldosterone and corticosterone.

5.7 *In vitro* prediction of toxicity: Are we there yet?

In recent years, there has been a significant shift toward reducing the use of animals in toxicological testing, driven by ethical concerns, regulatory changes, and advances in alternative methods (Health Canada, 2024). For example, the 2016 amendments to the Toxic Substances Control Act (TSCA), administered by the Environmental Protection Agency (EPA), encourage the use of alternative testing methods for chemical safety evaluations, aiming to reduce and, where possible, replace the use of vertebrate animals in testing chemical substances or mixtures (US. EPA, 2016). Similarly, the Endocrine Disruptor Screening Program (EDSP) by EPA emphasizes the use of *in vitro* and high-throughput screening methods to assess the endocrine-disrupting potential of chemicals (US. EPA, 2024a). Consequently, *in vitro* assessment, utilizing human cell lines, organ-on-a-chip technologies, and high-throughput screening assays, has emerged as a promising alternative for evaluating chemical toxicity (reviewed in Zink et al., 2020). These methods offer several advantages, including higher throughput, cost-effectiveness, and the ability to better predict human-specific responses. Indeed, our study demonstrates that *in vitro* assays can efficiently screen phenotypic changes induced by OPEs, rank their potencies, and derive administered equivalent doses. The results presented here provide valuable input into the regulatory decision-making process.

While *in vitro* approaches have made considerable contributions to toxicological assessment, they still face notable limitations. Current *in vitro* screening assays do not fully replicate the complexity of whole-organism interactions, such as metabolic processes or the influence of multiple organ systems, which are essential for understanding the systemic effects of chemicals. As observed in our animal study, sex-specific effects, metabolic alterations, and

upstream regulators in the HPA axis all contributed to the differential effects observed *in vivo*. Additionally, the safe dose identified through *in vitro* screening methods may not always serve as a reliable protective surrogate in the absence of traditional hazard data. Point of departure (POD), which marks the beginning of a low-dose extrapolation on the dose–response curve, is commonly used in risk assessment to derive toxicity values for chemicals (Pradeep et al., 2020). In a study comparing *in vitro* and *in vivo* PODs, 48 of the 448 chemicals assessed had an *in vitro* POD that was higher than the corresponding *in vivo* POD. Notably, 24 of these substances shared chemical features indicative of carbamate or organophosphate pesticides. This suggested that, with current assays, *in vitro* approaches may not be suitable for prioritizing organophosphates and carbamates (Health Canada, 2021b). Therefore, despite the progress made in reducing animal use, there remains a need for integrated testing strategies that combine *in vitro* models with computational tools and carefully controlled animal studies, especially when assessing the organophosphate compounds.

5.8 Future directions

Based on our data, we first identified several OPEs that contain specific structural features, such as halogens and aryl moieties, which exhibit higher toxicity than alkyl OPEs in H295R cells. We hypothesize that these structural characteristics enabled higher cell membrane permeability and bioavailability of these chemicals, thereby increasing their potency. To further understand cell type and chemical-specific effects and validate this hypothesis, future studies could follow up on quantifying the intracellular concentrations of OPEs in different cell lines. By measuring the intracellular levels of OPEs and their metabolites across various cell types, it would be possible to determine whether specific cell types and/or structural characteristics are associated with higher concentrations of these chemicals, and whether this correlates with observed toxicity. Such data could provide valuable insights into the mechanisms of action of

OPEs and help identify cell types that are particularly vulnerable to OPE exposure.

Disruptions in the lipidome of cells appear to be a common and sensitive response to OPE exposures across different models (Witchey et al., 2022; Morris et al., 2014; Wang et al., 2021; Negi et al., 2023; Xiang and Wang, 2021). While our current analyses focus on the lipid droplet part of the cell, expanding lipidomic analyses to other cellular compartments such as the plasma membrane, mitochondria, and endoplasmic reticulum could offer a more comprehensive picture of how OPEs interact with cellular lipid structures. It has been reported that lipid composition of different cellular compartments such as the mitochondria, ER, cytoplasm, and plasma membrane, undergo dynamic remodeling during steroidogenesis in MA-10 cells (Venugopal et al., 2021). Since we have identified that OPEs affect steroidogenesis, determining how lipid distribution in subcellular fractions, beyond lipid droplets, changes upon exposure to OPEs is a field that deserves to be explored further. It could also provide insights into whether OPEs affect the cholesterol availability through targeting the trafficking of lipids in cells. Further, investigating lipidomic alterations across multiple cellular compartments may offer new biomarkers for OPE exposures.

Both our *in vitro* and *in vivo* studies suggest that exposure time may influence the effects of OPEs. For example, using the same mixture, it has been shown that oxidative stress levels were upregulated after 4 hours of exposure, but returned to baseline by 48 hours in THP-1 macrophages (Giles et al., 2024). In our study, we assessed the effects of OPEs at 48 hours of exposure. We found that although lipid droplets were upregulated in both H295R cells and KGN human granulosa cells, in KGN cells inhibition of cholesterol biosynthesis is observed (Wang et al., 2024). It is possible that any immediate transcriptional effects had dissipated by this time. Thus, it would be interesting to investigate whether H295R cells initially experience inhibition of this pathway, followed by compensatory positive feedback at 48 hours. Furthermore, we did not

observe phenotypic changes at the tissue level when rats were exposed to the OPE mixture for 70-72 days. In contrast, a two-year feeding study found that exposure to TMPP resulted in cytoplasmic vacuolization of the adrenal cortex and ovarian interstitial cell hyperplasia in female rats (National Toxicology Program, 1994). To more accurately mimic real-life exposure scenarios, it would be valuable to assess the effects of long-term exposure to OPE mixtures at low doses.

Our nontargeted transcriptomic data revealed that OPEs exert sex-specific effects on the adrenal glands. While these data provide valuable mechanistic insights, it is crucial to assess the expression and activity of molecular targets at the protein level to fully elucidate the effects of OPEs. Our data suggest that key mediators of OPE effects in females include rate-limiting enzymes in cholesterol biosynthesis, such as *Hmgcr*, and the upstream regulators, *Insig1*. In males, potassium channels, such as *Kcnk9*, appear to play a central role. To enhance our understanding of the relationship between transcriptional effects and functional alterations following OPE exposure, western blotting or immunohistochemistry analyses could be conducted. Additionally, knocking down these regulators, for example by using small interfering RNAs (siRNAs), would allow us to validate the mechanisms through which OPEs influence these pathways. Our transcriptomic data, along with other studies on individual OPEs, also suggest that nuclear receptors such as PPARs and LXRs are key targets of OPEs (Wang et al., 2019; Pillai et al., 2014; Chen et al., 2024; reviewed in Hu et al., 2022). However, the interaction between OPE mixtures and nuclear receptors, and how this mediates downstream effects in H295R cells, remains to be determined.

Our *in vitro* study was limited by the available cell lines that can be used to test the functional effects of OPEs. Thus, it is particularly important to test male-derived cell lines capable of producing steroid hormones, as we have identified sex-specific effects. Examining a

male adrenal cell line would provide further insight into whether the potency of OPEs varies between sexes.

The adrenal gland develops during embryonic stages (discussed in the introduction). Since we observed significant changes in the adult adrenal gland following OPE exposure, it would be valuable to assess whether exposure during critical windows of development results in alterations in adrenal function in the F1 generation. Such studies would help identify populations at greater risk. Furthermore, while current studies have focused primarily on the F0 generation, examining the developmental effects of OPEs on the adrenal gland in the F1 generation would fill an important gap in our understanding of the effects of OPEs. In addition, since the adrenal gland is only one of many endpoints being studied in this animal experiment, we adopted a comprehensive experimental design that would be compatible with studies on the reproductive system, liver, adrenals, and other tissues. As a result, the females were mated and underwent gestation and lactation. Although there have been no reports indicating that adrenal function is affected during this period, studying whether gestation and lactation impact the adrenal gland will help confirm the effects observed in the current animal study.

In our studies, we focused primarily on the cortex part of the adrenal gland. The H295R cells are derived from adrenocortical tumors, and our rat study examined hormones produced by the adrenal cortex and the overall adrenal gland transcriptome. Consequently, the medullary region of the adrenal gland has been partially overlooked. Thus, it would be interesting to explore the specific effects of OPEs on different regions of the adrenal gland. Standardized methods have been established for isolating and differentiating adrenocortical and adrenomedullary stem cells from mice (Friedrich et al., 2021). Investigating the distinct toxicological pathways in the cortex and medulla could help us distinguish which part of the adrenal gland is targeted by OPEs and provide further mechanistic insights.

Regulatory decisions regarding the risk of chemicals are based on a scientific evaluation of both the hazardous properties of chemicals and the extent of exposure to the substance (US EPA, 2024b). In our study, we identified the steady state administered equivalent dose, or point of departure (POD_{Bioactivity}), for six individual OPEs using HTTK modeling. The next step would be to incorporate the Margin of Exposure (MOE), calculated as the ratio of POD_{Bioactivity} to human exposure levels, to account for the exposure factor in assessing the risk of chemicals (Health Canada, 2022). This is especially important as we could be exposed to less potent chemicals at high levels. For example, TBOEP, although identified as one of the less potent OPEs, is present in over 50% of Canadian house dust and has been found at concentrations several to hundreds of times higher than other OPEs globally (reviewed in Liu et al., 2023). Looking only at the potency of the chemical would underestimate the risk it poses.

5.9 Final conclusions

In summary, we investigated the toxicity of prevalent OPEs commonly found in Canadian house dust using *in vitro* and *in vivo* strategies. Employing *in vitro* screening assays, we assessed the effects of OPEs on a range of phenotypic and functional endpoints in the human adrenal H295R cells, which serves as model for studying key endocrine functions of the adrenal glands. Our results demonstrate that combining the high-content imaging with potency ranking approaches provides ways for deriving administered equivalent dose of OPEs. The *in vitro* assessment of the impact of "house dust" OPE mixtures on the phenotype, function, and lipidome of the cells complements with the effects observed *in vivo*, and the results show the need for comprehensive assessments of chemical mixtures. Further, the transcriptome assessment of the male and female adrenal glands suggests that OPEs exert sex specific mechanism on the adrenal glands.

Collectively, the studies presented in this thesis show that exposure to several common OPEs disrupted adrenal cell functions to an extent comparable to or greater than that of legacy PBDEs. These findings suggest that current testing paradigms may not be sufficient for identifying potentially harmful alternatives and highlight the need for more rigorous evaluations of chemicals before they are adopted as replacements. Our research provides valuable mechanistic insights into the toxicity of OPEs and emphasizes the importance of evaluating the toxicological impacts of environmentally relevant mixtures in both sexes. Furthermore, our data highlight the adrenal gland as a critical endpoint in toxicological assessments. We propose that the combination of *in vitro* and *in vivo* approaches used in this thesis represents valuable tools for the comprehensive screening and prioritization of emerging chemicals in risk assessment.

LIST OF ORIGINAL CONTRIBUTIONS

1. Used standardized methods to compare the effects of OPEs on the phenotypes of adrenal cells to those of a predominant PBDE congener, BDE-47.
2. Ranked the chemical potencies of OPEs based on the phenotypic screening result using different potency ranking approaches: the ToxPi analysis, the lowest benchmark concentration method, and the lowest administered equivalent dose method.
3. The screening of phenotypic effects identified two OPEs, TCIPP and TBOEP, that may be less bioactive and could be potential safe alternatives to PBDEs.
4. The extrapolation of in vitro concentrations into in vivo doses using toxicokinetic modelling identified that OPEs may be bioactive at lower doses than those previously reported in the literature or their reference doses.
5. Elucidated the effects of six OPEs that are commonly detected in the environment or human matrices on the functions of H295R cells. The ability of the cells in synthesizing adrenal related steroids were not tested in most OPEs in previous studies.
6. First to identify the effects of environmentally relevant mixtures of OPEs on human adrenal H295R cells.
7. Identified that the OPE mixtures induced lipid accumulation through disrupting the cholesterol biosynthesis and steroidogenic pathway. Moreover, exposure to this mixture also altered the composition of lipids stored in intracellular lipid droplets.
8. First to identify the effects of environmentally relevant mixtures of OPEs on the adrenal glands of Sprague Dawley rats.
9. Identified sex specific mechanism of OPEs on the adrenal gland using a transcriptomic approach and provided mechanistic insights into the pathways that may mediate the toxicity induced by OPEs.

10. Identified the disruption of cholesterol homeostasis as a common and sensitive response to OPE exposures.

REFERENCE

(Introduction and Discussion)

Agency for Toxic Substances and Disease Registry (ATSDR). (2004). Toxicological Profile for Polybrominated Biphenyls and Polybrominated Diphenyl Ethers. Available at www.atsdr.cdc.gov/toxprofiles/tp68.pdf. Accessed on Oct 26, 2024.

Akimoto T, Kobayashi S, Nakayama A, et al. (2022). Toxicological effects of Tris (1,3-dichloro-2-propyl) phosphate exposure in adult male rats differ depending on the history of exposure in the neonatal period. *J. Appl. Toxicol.* **42**,1503-1509.

Antoniou-Tsigkos, A., Zapanti, E., Ghizzoni, L., et al. Adrenal Androgens. [Updated 2019 Jan 5]. South Dartmouth (MA): MDText.com, Inc. Available from: <https://www.ncbi.nlm.nih.gov/books/NBK278929/#>

Azhar, S. (2003). Cholesterol uptake in adrenal and gonadal tissues the SR BI and selective pathway connection. *Frontiers in Bioscience*, 8(6), s998-1029. <https://doi.org/10.2741/1165>

Ballesteros-Gómez, A., Erratico, C. A., Eede, N. V. den, Ionas, A. C., Leonards, P. E. G. and Covaci, A. (2015). In vitro metabolism of 2-ethylhexyldiphenyl phosphate (EHDPHP) by human liver microsomes. *Tox. Lett.* **232**, 203–212.

Bankhead, P., Loughrey, M. B., Fernández, J. A., Dombrowski, Y., McArt, D. G., Dunne, P. D., McQuaid, S., Gray, R. T., Murray, L. J., Coleman, H. G., James, J. A., Salto-Tellez, M., Hamilton, P. W. (2017). QuPath: Open source software for digital pathology image analysis. *Sci. Rep.* **7**, 16878.

Bansal, R., Tighe, D., Danai, A., Rawn, D. F., Gaertner, D. W., Arnold, D. L., Gilbert, M. E., and Zoeller, R. T. (2014). Polybrominated diphenyl ether (DE-71) interferes with thyroid hormone action independent of effects on circulating levels of thyroid hormone in male rats. *Endocrinology*. **155**, 4104–4112.

Behan, D. P., Heinrichs, S. C., Troncoso, J. C., Liu, X. J., Kawas, C. H., Ling, N., and De Souza, E. B. (1995). Displacement of corticotropin releasing factor from its binding protein as a possible treatment for Alzheimer's disease. *Nature*. **378**, 284–287.

Behan, D. P., Khongsaly, O., Owens, M. J., Chung, H. D., Nemeroff, C. B., and De Souza, E. B. (1997). Corticotropin-releasing factor (CRF), CRF-binding protein (CRF-BP), and CRF/CRF-BP complex in Alzheimer's disease and control postmortem human brain. *J. Neurochem*. **68**, 2053–2060.

Bi, R., Meng, W., & Su, G. (2023). Organophosphate esters (OPEs) in plastic food packaging: non-target recognition, and migration behavior assessment. *Environ. Int*, **177**, 108010.

Bird, I.M., Hanley, N.A., Word, R.A., Mathis, J.M., McCarthy, J.L., Mason, J.I. & Rainey, W.E. (1993). Human NCI-H295 adrenocortical carcinoma cells: a model for angiotensin-II- responsive aldosterone secretion. *Endocrinology*. **133**, 1555- 1561.

Bird, I.M., Mason, J.I., Rainey, W.E. (1994). Regulation of type 1 angiotensin II receptor messenger ribonucleic acid expression in human adrenocortical carcinoma H295 cells. *Endocrinology*. **134**, 2468–2474.

Birnbaum, L., and Staskal, D. (2004). Brominated flame retardants: Cause for concern? *Environ. Health. Perspect.* **112**, 9–17

Blum, A., Behl, M., Birnbaum, L., Diamond, M. L., Phillips, A., Singla, V., Sipes, N. S., Stapleton, H. M., and Venier, M. (2019). Organophosphate Ester Flame Retardants: Are They a Regrettable Substitution for Polybrominated Diphenyl Ethers?. *ES&T Letters*. **6**, 638–649.

Boron, F.W., and Boulpaep, L.M. (2017). The adrenal medulla bridges the endocrine and sympathetic nervous systems. *Medical Physiology*, 3rd Eds. Elsevier (HS-US), pp. 261-343.

Botteri Principato, N.L., Suarez, J.D., Laws, S.C. & Klinefelter, G.R. (2018). The use of purified rat Leydig cells complements the H295R screen to detect chemical-induced alterations in testosterone production. *Biol. Reprod.* **98**, 239-249.

Bui, T. T., Xu, F., Eede, N. V. den, Cousins, A. P., Covaci, A. and Cousins, I. T. (2017). Probing the relationship between external and internal human exposure of organophosphate flame retardants using pharmacokinetic modelling. *Environmental Pollution*, 230, 550–560.

Buonassisi, V., Sato, G., Cohen, A.I. (1962). Hormone-producing cultures of adrenal and pituitary tumor origin. *Proc. Natl. Acad. Sci. USA*. **48**, 1184–1190.

Butt, C. M., Hoffman, K., Chen, A., Lorenzo, A., Congleton, J., & Stapleton, H. M. (2016). Regional comparison of organophosphate flame retardant (PFR) urinary metabolites and tetrabromobenzoic acid (TBBA) in mother-toddler pairs from California and New Jersey. *Environment international*, 94, 627–634.

Carignan, C. C., Mínguez-Alarcón, L., Butt, C. M., Williams, P. L., Meeker, J. D., Stapleton, H. M., Toth, T. L., Ford, J. B., Hauser, R. and Team, E. S. (2017). Urinary Concentrations of Organophosphate Flame Retardant Metabolites and Pregnancy Outcomes among Women Undergoing in Vitro Fertilization. *Environmental Health Perspectives*, 125(8), 087018

Carlton, M., Voisey, J., Parker, T. J., Punyadeera, C., and Cuttle, L. (2021). A review of potential biomarkers for assessing physical and psychological trauma in paediatric burns. *Burns & trauma*. **9**, tkaa049.

Casella, M., Lori, G., Coppola, L., La Rocca, C., and Tait, S. (2022). BDE-47, -99, -209 and Their Ternary Mixture Disrupt Glucose and Lipid Metabolism of Hepg2 Cells at Dietary Relevant Concentrations: Mechanistic Insight through Integrated Transcriptomics and Proteomics Analysis. *International journal of molecular sciences*. **23**, 14465.

Casida J. E. (2017). Organophosphorus Xenobiotic Toxicology. *Annual review of pharmacology and toxicology*, 57, 309–327.

Castorina, R., Butt, C., Stapleton, H. M., Avery, D., Harley, K. G., Holland, N., Eskenazi, B., & Bradman, A. (2017). Flame retardants and their metabolites in the homes and urine of pregnant women residing in California (the CHAMACOS cohort). *Chemosphere*, 179, 159–166.

Cavieres, M. F., Jaeger, J., and Porter, W. (2002). Developmental toxicity of a commercial herbicide mixture in mice: I. Effects on embryo implantation and litter size. *Environmental health perspectives*. **110**, 1081–1085.

Cequier, E., Ionas, A. C., Covaci, A., Marcé, R. M., Becher, G., and Thomsen, C. (2014). Occurrence of a broad range of legacy and emerging flame retardants in indoor environments in Norway. *Environmental science & technology*, 48(12), 6827–6835.

Chen, F., Zhou, L., Bai, Y., Zhou, R., & Chen, L. (2014). Sex differences in the adult HPA axis and affective behaviors are altered by perinatal exposure to a low dose of bisphenol A. *Brain research*, 1571, 12–24.

Chen, X., Mo, J., Zhang, S., Li, X., Huang, T., Zhu, Q., Wang, S., Chen, X., & Ge, R. S. (2019). 4-Bromodiphenyl Ether Causes Adrenal Gland Dysfunction in Rats during Puberty. *Chemical research in toxicology*, 32(9), 1772–1779.

Chen, Y., Huang, B., Liang, H., Ji, H., Wang, Z., Song, X., Zhu, H., Song, S., Yuan, W., Wu, Q., & Miao, M. (2024). Gestational organophosphate esters (OPEs) exposure in association with placental DNA methylation levels of peroxisome proliferator-activated receptors (PPARs) signaling pathway-related genes. *The Science of the total environment*, 947, 174569.

Chourpiliadis, C., Aeddula, N.R. Physiology, Glucocorticoids. [Updated 2023 Jul 17]. Treasure Island (FL): StatPearls Publishing. Available from: <https://www.ncbi.nlm.nih.gov/books/NBK560897/>

Cock, M. de, Boer, M. R. de, Govarts, E., Iszatt, N., Palkovicova, L., Lamoree, M. H., Schoeters, G., Eggesbø, M., Trnovec, T., Legler, J. and Bor, M. van de. (2017). Thyroid- stimulating hormone levels in newborns and early life exposure to endocrine-disrupting chemicals: analysis of three European mother–child cohorts. *Pediatric Research*, 82(3), 429–437.

Cohen, A.I., Bloch, E., Celozzi, E. (1957). In vitro response of experimental adrenal tumors to corticotropin (ACTH). *Proc. Soc. Exp. Biol. Med.* **95**, 304–309.

Compagnone, N.A., Bair, S.R., Mellon, S.H. (1997). Characterization of adrenocortical cell lines produced by genetically targeted tumorigenesis in transgenic mice. *Steroids*. **62**, 238–243.

Cooper, G.M. *The Cell: A Molecular Approach*. 2nd edition. (2000). Sunderland (MA): Sinauer Associates. Cell Membranes. Available from: <https://www.ncbi.nlm.nih.gov/books/NBK9928/>

Coutinho, A.E. and Chapman, K.E. (2011). The anti-inflammatory and immunosuppressive effects of glucocorticoids, recent developments and mechanistic insights. *Mol. Cell. Endocrinol.* **335**, 2-13.

Costa, L. G., and Giordano, G. (2011). Is decabromodiphenyl ether (BDE-209) a developmental neurotoxicant?. *Neurotoxicology*, 32(1), 9–24.

Costa L. G. (2018). Organophosphorus Compounds at 80: Some Old and New Issues. *Toxicological sciences : an official journal of the Society of Toxicology*, 162(1), 24–35.

Cuprak, L.J., Lammi, C.J., Bayer, R.C. (1977). Scanning electron microscopy of induced cell rounding of mouse adrenal cortex tumor cells in culture. *Tissue Cell*. **9**, 667–680.

Czaja, M. J., Ding, W.-X., Donohue, T. M., Friedman, S. L., Kim, J.-S., Komatsu, M., Lemasters, J. J., Lemoine, A., Lin, J. D., Ou, J. J., Perlmutter, D. H., Randall, G., Ray, R. B., Tsung, A. and Yin, X.-M. (2013). Functions of autophagy in normal and diseased liver. *Autophagy*, 9(8), 1131–1158.

Daft J. L. (1982). Identification of aryl/alkyl phosphate residues in foods. *Bulletin of environmental contamination and toxicology*, 29(2), 221–227.

Darnerud, P. O., & Risberg, S. (2006). Tissue localisation of tetra- and pentabromodiphenyl ether congeners (BDE-47, -85 and -99) in perinatal and adult C57BL mice. *Chemosphere*, 62(3), 485–493.

Demeneix B. A. (2019). Evidence for Prenatal Exposure to Thyroid Disruptors and Adverse Effects on Brain Development. *European thyroid journal*, 8(6), 283–292

Dingemans, M. M., van den Berg, M., and Westerink, R. H. (2011). Neurotoxicity of brominated flame retardants: (in)direct effects of parent and hydroxylated polybrominated diphenyl ethers on the (developing) nervous system. *Environmental health perspectives*. **119**, 900–907.

Doherty, B. T., Hammel, S. C., Daniels, J. L., Stapleton, H. M., & Hoffman, K. (2019a). Organophosphate Esters: Are These Flame Retardants and Plasticizers Affecting Children's Health?. *Current environmental health reports*, 6(4), 201–213.

Doherty, B. T., Hoffman, K., Keil, A. P., Engel, S. M., Stapleton, H. M., Goldman, B. D., Olshan, A. F., & Daniels, J. L. (2019b). Prenatal exposure to organophosphate esters and behavioral development in young children in the Pregnancy, Infection, and Nutrition Study. *Neurotoxicology*, 73, 150–160.

Dou, M., and Wang, L. (2023). A review on organophosphate esters: Physiochemical properties, applications, and toxicities as well as occurrence and human exposure in dust environment. *Journal of environmental management*, 325(Pt B), 116601.

Dungar, B. M., Schupbach, C. D., Jacobson, J. R., & Kopf, P. G. (2021). Adrenal Corticosteroid Perturbation by the Endocrine Disruptor BDE-47 in a Human Adrenocortical Cell Line and Male Rats. *Endocrinology*, 162(11), bqab160.

Endocrine Disruptor Screening and Testing Advisory Committee (EDSTAC). (1998). Endocrine disruptor screening and testing advisory committee final report. Office of Research and

Development, Washington, DC. Available from:

<https://www.ncbi.nlm.nih.gov/books/NBK230219/>

Environmental Protection Agency (EPA). (2009). “Polybrominated Diphenyl Ethers (PBDEs) Action Plan Summary.” Available at www.epa.gov/oppt/existingchemicals/pubs/actionplans/pbdes_ap_2009_1230_final.pdf. Accessed on Oct 26, 2024.

Environment Canada. (2013). Canadian Environmental Protection Act, 1999 Federal Environmental Quality Guidelines Polybrominated Diphenyl Ethers (PBDEs). Available at: <https://www.ec.gc.ca/ece-ees/default.asp?lang=En&nav=05DF7A37-1>. Accessed Oct 28, 2024.

Eriksson, P., Viberg, H., Jakobsson, E., Orn, U., & Fredriksson, A. (2002). A brominated flame retardant, 2,2',4,4',5-pentabromodiphenyl ether: uptake, retention, and induction of neurobehavioral alterations in mice during a critical phase of neonatal brain development. *Toxicological sciences : an official journal of the Society of Toxicology*, 67(1), 98–103.

European Parliament. (2019). Endocrine Disruptors: from Scientific Evidence to Human Health Protection. Available at [https://www.europarl.europa.eu/RegData/etudes/STUD/2019/608866/IPOL_STU\(2019\)608866_EN.pdf](https://www.europarl.europa.eu/RegData/etudes/STUD/2019/608866/IPOL_STU(2019)608866_EN.pdf). Accessed Oct 31, 2024.

Fair, P. A., Stavros, H. C., Mollenhauer, M. A. M., DeWitt, J. C., Henry, N., Kannan, K., Peden-Adams, M. M. (2012). Immune function in female B₆C₃F₁ mice is modulated by DE-71, a commercial polybrominated diphenyl ether mixture. *Journal of Immunotoxicology*. **9**, 96–107.

Fan, X., Kubwabo, C., Rasmussen, P. E., & Wu, F. (2014). Simultaneous determination of thirteen organophosphate esters in settled indoor house dust and a comparison between two sampling techniques. *The Science of the total environment*, 491-492, 80–86.

Fang, M., Webster, T. F., Ferguson, P. L. and Stapleton, H. M. (2015). Characterizing the Peroxisome Proliferator-Activated Receptor (PPAR γ) Ligand Binding Potential of Several Major Flame Retardants, Their Metabolites, and Chemical Mixtures in House Dust. *Environmental Health Perspectives*, 123(2), 166–172.

Farese, R. V. and Walther, T. C. (2009). Lipid Droplets Finally Get a Little R-E-S-P-E-C-T. *Cell*, **139**, 855–860.

Fei, W., Wang, H., Fu, X., Bielby, C. and Yang, H. (2009). Conditions of endoplasmic reticulum stress stimulate lipid droplet formation in *Saccharomyces cerevisiae*. *Biochem. J.* **424**, 61–67.

Finkelstein, A. and Cass, A. (1968). Permeability and electrical properties of thin lipid membranes. *J Gen Physiology*, **52**, 145–172.

Fommei, E., Turci, R., Ripoli, A., Balzan, S., Bianchi, F., Morelli, L., & Coi, A. (2017). Evidence for persistent organochlorine pollutants in the human adrenal cortex. *Journal of applied toxicology : JAT*, 37(9), 1091–1097.

Friedrich, L., Schuster, M., Rubin de Celis, M. F., Berger, I., Bornstein, S. R., & Steenblock, C. (2021). Isolation and in vitro cultivation of adrenal cells from mice. *STAR protocols*, 2(4), 100999.

Friedman, K.P., Gagne, M., Loo, L.-H., Karamertzanis, P., Netzeva, T., Sobanski, T., Franzosa, J.A., Richard, A.M., Lougee, R.R., Gissi, A., Lee, J.-Y. J., Angrish, M., Dorne, J.L., Foster, S., Raffaele, K., Bahadori, T., Gwinn, M.R., Lambert, J., Whelan, M., Thomas, R. S. (2019). Utility of In Vitro Bioactivity as a Lower Bound Estimate of In Vivo Adverse Effect Levels and in Risk-Based Prioritization. *Toxicological Sciences*. **173**, 202–225.

Gazdar, A.F., Oie, H.K., Shackleton, C.H., Chen, T.R., Triche, T.J., Myers, C.E., Chrousos, G.P., Brennan, M.F., Stein, C.A. and La Rocca, R. V. (1990). Establishment and characterization of a human adrenocortical carcinoma cell line that expresses multiple pathways of steroid biosynthesis. *Cancer. Res.* **50**, 5488-5496.

Geyer, H. J.; Schramm, K.-W.; Darnerud, P. O.; Aune, M.; Feicht, E. A.; Fried, K. W.; Henkelmann, B.; Lenoir, D.; Schmid, P.; McDonald, T. A. (2004). Terminal elimination half-lives of the brominated flame retardants TBBPA, HBCD, and lower brominated PBDEs in humans. *Organohalogen Compd.* 66, 3867– 3872

Giles, B. H., Kukolj, N., Mann, K. K., & Robaire, B. (2024). Phenotypic and Functional Outcomes in Macrophages Exposed to an Environmentally Relevant Mixture of Organophosphate Esters in Vitro. *Environmental health perspectives*, 132(8), 87002.

Givertz M. M. (2001). Manipulation of the renin-angiotensin system. *Circulation*. **104**, E14–E18.

González-Hernández, J.A., Bornstein, S.R., Ehrhart-Bornstein, M., Geschwend, J.E., Adler, G., and Scherbaum, W.A. (1994). Macrophages within the human adrenal gland. *Cell and tissue research*. **278**, 201–205.

Gore, A. C., Martien, K. M., Gagnidze, K., & Pfaff, D. (2014). Implications of prenatal steroid perturbations for neurodevelopment, behavior, and autism. *Endocrine reviews*, 35(6), 961–991.

Gorini, F., Iervasi, G., Coi, A., Pitto, L., & Bianchi, F. (2018). The Role of Polybrominated Diphenyl Ethers in Thyroid Carcinogenesis: Is It a Weak Hypothesis or a Hidden Reality? From Facts to New Perspectives. *International journal of environmental research and public health*, 15(9), 1834.

Gospodarowicz, C.R., Hornsby, P.J., et al. (1977). Control of bovine adrenal cortical cell proliferation by fibroblast growth factor. Lack of effect of epidermal growth factor. *Endocrinology*. **100**, 1080–1089.

Government of Canada. (2021). Notice to stakeholders on the use of flame-retardant chemicals in certain consumer products in Canada. Available at <https://www.canada.ca/en/health-canada/services/consumer-product-safety/legislation-guidelines/guidelines-policies/notice-stakeholders-flame-retardant-chemicals-certain-consumer-products.html>. Accessed Oct 26, 2024.

Government of Canada. (2020). Evaluation of the effectiveness of risk management for polybrominated diphenyl ethers. ISBN: 978-0-660-35044-8. Available at: <https://www.canada.ca/en/environment-climate-change/services/evaluating-existing-substances/evaluation-effectiveness-risk-management-polybrominated-diphenyl-ethers.html>. Accessed Oct 28, 2024.

Grabek, A. et al. (2019). The adult adrenal cortex undergoes rapid tissue renewal in a sex-specific manner. *Cell Stem Cell*. **25**, 290–296.

Greaves, A. K., Su, G., Letcher, R. J. (2016). Environmentally relevant organophosphate triesters in herring gulls: in vitro biotransformation and kinetics and diester metabolite formation using a hepatic microsomal assay. *Toxicology and Applied Pharmacology*, 308, 59–65.

Greaves, A. K., & Letcher, R. J. (2017). A Review of Organophosphate Esters in the Environment from Biological Effects to Distribution and Fate. *Bulletin of environmental contamination and toxicology*, 98(1), 2–7.

Greep, R.O. and Deane, H.W. (1949). Histological, cytochemical and physiological observations on the regeneration of the rat's adrenal gland following enucleation. *Endocrinology*. **45**, 42–56.

Grimaldi, M., Boulahtouf, A., Toporova, L., & Balaguer, P. (2019). Functional profiling of bisphenols for nuclear receptors. *Toxicology*, 420, 39–45.

Govarts, E., Gilles, L., Martin, L. R., Santonen, T., Apel, P., Alvito, P., Anastasi, E., Andersen, H. R., Andersson, A.-M., Andryskova, L., Antignac, J.-P., Appenzeller, B., Barbone, F., Barnett-Itzhaki, Z., Barouki, R., Berman, T., Bil, W., Borges, T., Buekers, J., ... Schoeters, G. (2023). Harmonized human biomonitoring in European children, teenagers and adults: EU-wide exposure data of 11 chemical substance groups from the HBM4EU Aligned Studies (2014–2021). *International Journal of Hygiene and Environmental Health*, 249, 114119.

Harvey, P.W. (2010). Toxic responses of the adrenal cortex. *Comprehensive toxicology* (Second Edition). 11, 265-289.

Haggard, D. E., Karmaus, A. L., Martin, M. T., Judson, R. S., Setzer, R. W., and Paul Friedman, K. (2018). High-Throughput H295R Steroidogenesis Assay: Utility as an Alternative and a Statistical Approach to Characterize Effects on Steroidogenesis. *Toxicological sciences: an official journal of the Society of Toxicology*. **162**, 509–534.

Hakk, H., Larsen, G., & Klasson-Wehler, E. (2002). Tissue disposition, excretion and metabolism of 2,2',4,4',5-pentabromodiphenyl ether (BDE-99) in the male Sprague-Dawley rat. *Xenobiotica; the fate of foreign compounds in biological systems*, 32(5), 369–382.

- Hammel, S. C., Hoffman, K., Webster, T. F., Anderson, K. A., & Stapleton, H. M. (2016). Measuring Personal Exposure to Organophosphate Flame Retardants Using Silicone Wristbands and Hand Wipes. *Environmental science & technology*, 50(8), 4483–4491.
- Hales, B. F. & Robaire, B. (2020). Effects of brominated and organophosphate ester flame retardants on male reproduction. *Andrology*, 8(4), 915–923.
- Hanley, N.A., Wester, R.M., Carr, B.R., et al. (1993). Parathyroid hormone and parathyroid hormone-related peptide stimulate aldosterone production in the human adrenocortical cell line, NCI-H295. *Endocr. J.* 1, 447–450.
- Harley, K. G., Marks, A. R., Chevrier, J., Bradman, A., Sjödin, A., & Eskenazi, B. (2010). PBDE concentrations in women's serum and fecundability. *Environmental health perspectives*, 118(5), 699–704.
- He, C., Wang, X., Thai, P., Baduel, C., Gallen, C., Banks, A., Bainton, P., English, K., & Mueller, J. F. (2018a). Organophosphate and brominated flame retardants in Australian indoor environments: Levels, sources, and preliminary assessment of human exposure. *Environmental pollution* (Barking, Essex : 1987), 235, 670–679.
- He, C., Wang, X., Tang, S., Thai, P., Li, Z., Baduel, C., & Mueller, J. F. (2018b). Concentrations of Organophosphate Esters and Their Specific Metabolites in Food in Southeast Queensland, Australia: Is Dietary Exposure an Important Pathway of Organophosphate Esters and Their Metabolites?. *Environmental science & technology*, 52(21), 12765–12773.

Health Canada (2021a). Draft Screening Assessment Flame Retardants Group. Available at: <https://www.canada.ca/en/environment-climate-change/services/evaluating-existing-substances/draft-screening-assessment-flame-retardants-group.html>. Accessed October 31, 2024.

Health Canada. (2021b). Science approach document - Bioactivity exposure ratio: Application in priority setting and risk assessment. Available at <https://www.canada.ca/en/environment-climate-change/services/evaluating-existing-substances/science-approach-document-bioactivity-exposure-ratio-application-priority-setting-risk-assessment.html>. Accessed Nov 18, 2024.

Health Canada. (2022). Use of margins of exposure and risk quotients in risk assessment. Available at <https://www.canada.ca/en/health-canada/services/chemical-substances/fact-sheets/margins-risk-quotient-risk-assessment.html>. Accessed Nov 22, 2024.

Health Canada. (2024). Draft Strategy to Replace, Reduce or Refine Vertebrate Animal Testing under the Canadian Environmental Protection Act, 1999. Available at <https://www.canada.ca/en/health-canada/programs/consultation-draft-strategy-replace-reduce-refine-vertebrate-animal-testing/document.html>. Accessed Nov 19, 2024.

Hecker, M., Newsted, J.L., Murphy, M.B., Higley, E.B., Jones, P.D., Wu, R. and Giesy, J.P. (2006), Human adrenocarcinoma (H295R) cells for rapid in vitro determination of effects on steroidogenesis: Hormone production. *Toxicol. Appl. Pharmacol.* **217**, 114-124.

Hilbers, U., Peters, J., Bornstein, S.R., et al. (1999). Local renin-angiotensin system is involved in K⁺ induced aldosterone secretion from human adrenocortical NCI-H295 cells. *Hypertension*. **33**, 1025–1030.

Henne, W. M., Reese, M. L. & Goodman, J. M. (2018). The assembly of lipid droplets and their roles in challenged cells. *EMBO J*. **37**, e98947.

Hoffman, K., Daniels, J. L., & Stapleton, H. M. (2014). Urinary metabolites of organophosphate flame retardants and their variability in pregnant women. *Environment international*, 63, 169–172.

Hoffman, K., Butt, C. M., Webster, T. F., Preston, E. V., Hammel, S. C., Makey, C., Lorenzo, A. M., Cooper, E. M., Carignan, C., Meeker, J. D., Hauser, R., Soubry, A., Murphy, S. K., Price, T. M., Hoyo, C., Mendelsohn, E., Congleton, J., Daniels, J. L., & Stapleton, H. M. (2017). Temporal Trends in Exposure to Organophosphate Flame Retardants in the United States. *Environmental science & technology letters*, 4(3), 112–118.

Hooper, K. and T.A. McDonald. (2000). The PBDEs: An Emerging Environmental Challenge and Another Reason for Breast-Milk Monitoring Programs. *Environ. Health. Perspec.* 108, 387-392.

Horton, J. D., Goldstein, J. L., and Brown, M. S. (2002). SREBPs: activators of the complete program of cholesterol and fatty acid synthesis in the liver. *The Journal of clinical investigation*. **109**, 1125–1131.

Hou, R., Huang, C., Rao, K., Xu, Y., Wang, Z. (2018). Characterized in vitro metabolism kinetics of alkyl organophosphate esters in fish liver and intestinal microsomes. *Environmental Science and Technology*, 52(5), 3202–3210.

Hu, W., Gao, P., Wang, L., & Hu, J. (2022). Endocrine disrupting toxicity of aryl organophosphate esters and mode of action. *Critical Reviews in Environmental Science and Technology*, 53(1), 1–18.

Hu, W., Jia, Y., Kang, Q., Peng, H., Ma, H., Zhang, S., Hiromori, Y., Kimura, T., Nakanishi, T., Zheng, L., Qiu, Y., Zhang, Z., Wan, Y., & Hu, J. (2019). Screening of House Dust from Chinese Homes for Chemicals with Liver X Receptors Binding Activities and Characterization of Atherosclerotic Activity Using an in Vitro Macrophage Cell Line and ApoE^{-/-} Mice. *Environmental health perspectives*, 127(11), 117003.

Huang, C., Li, N., Yuan, S., Ji, X., Ma, M., Rao, K., and Wang, Z. (2017). Aryl- and alkyl-phosphorus-containing flame retardants induced mitochondrial impairment and cell death in Chinese hamster ovary (CHO-k1) cells. *Environ. Pollut.* 230, 775–786.

le Roux, C. W., Chapman, G. A., Kong, W. M., Dhillon, W. S., Jones, J., and Alaghband-Zadeh, J. (2003). Free cortisol index is better than serum total cortisol in determining hypothalamic-pituitary-adrenal status in patients undergoing surgery. *The Journal of clinical endocrinology and metabolism*. **88**, 2045–2048.

Ji, Y., Yao, Y., Duan, Y, et al. (2021). Association between urinary organophosphate flame retardant diesters and steroid hormones: a metabolomic study on type 2 diabetes mellitus cases and controls. *Sci. Total. Environ.* **756**, 143836.

Jiménez-Canino, R., Fernandes, M. X., & Alvarez de la Rosa, D. (2016). Phosphorylation of Mineralocorticoid Receptor Ligand Binding Domain Impairs Receptor Activation and Has a Dominant Negative Effect over Non-phosphorylated Receptors. *The Journal of biological chemistry*, 291(36), 19068–19078.

Jopek, K., Celichowski, P., Szyszka, M., et al. (2017). Transcriptome Profile of Rat Adrenal Evoked by Gonadectomy and Testosterone or Estradiol Replacement. *Front. Endocrinol.* **8**, 26.

Karmaus, A.L., Toole, C.M., Filer, D.L., Lewis, K.C. & Martin, M.T. (2016). High-throughput screening of chemical effects on steroidogenesis using H295R human adrenocortical carcinoma cells. *Toxicol. Sci.* **150**, 323-332.

Kersten, S. (2008). Peroxisome proliferator activated receptors and lipoprotein metabolism. *PPAR research*, 2008, 132960.

Kiciński, M., Viaene, M. K., Den Hond, E., Schoeters, G., Covaci, A., Dirtu, A. C., Nelen, V., Bruckers, L., Croes, K., Sioen, I., Baeyens, W., Van Larebeke, N., & Nawrot, T. S. (2012). Neurobehavioral function and low-level exposure to brominated flame retardants in adolescents: a cross-sectional study. *Environmental health : a global access science source*, 11, 86.

Kitay, J.I. (1963). Pituitary-adrenal function in the rat after gonadectomy and gonadal hormone replacement. *Endocrinology*. **73**, 253–260.

Kodavanti, P. R., Coburn, C. G., Moser, V. C., MacPhail, R. C., Fenton, S. E., Stoker, T. E., Rayner, J. L., Kannan, K., & Birnbaum, L. S. (2010). Developmental exposure to a commercial PBDE mixture, DE-71: neurobehavioral, hormonal, and reproductive effects. *Toxicological sciences: an official journal of the Society of Toxicology*. **116**, 297–312.

Koganti, P. P., Tu, L. N., & Selvaraj, V. (2022). Functional metabolite reserves and lipid homeostasis revealed by the MA-10 Leydig cell metabolome. *PNAS nexus*, 1(4), pgac215.

Kojima, H., Takeuchi, S., Sanoh, S., Okuda, K., Kitamura, S., Uramaru, N., Sugihara, K., & Yoshinari, K. (2019). Profiling of bisphenol A and eight its analogues on transcriptional activity via human nuclear receptors. *Toxicology*, 413, 48–55.

Kowal J, Fiedler R. (1968). Adrenal cells in tissue culture. I. Assay of steroid products steroidogenic responses to peptide hormones. *Arch. Biochem. Biophys*. **128**, 406–421

Kubwabo, C., Fan, X., Katuri, G.P., Habibagahi, A., & Rasmussen, P.E. (2021). Occurrence of aryl and alkyl-aryl phosphates in Canadian house dust. *Emerging Contaminants*.

Lam, K. Y., Chan, A. C., & Lo, C. Y. (2001). Morphological analysis of adrenal glands: a prospective analysis. *Endocrine pathology*, 12(1), 33–38.

Latendresse JR, Azhar S, Brooks CL, Capen CC. (1993). Pathogenesis of Cholesteryl Lipidosis of Adrenocortical and Ovarian Interstitial Cells in F344 Rats Caused by Tricresyl Phosphate and Butylated Triphenyl Phosphate. *Toxicol Appl Pharm.* 122(2):281-289.

Latendresse JR, Brooks CL, Capen CC. (1994). Pathologic Effects of Butylated Triphenyl Phosphate-Based Hydraulic Fluid and Tricresyl Phosphate on the Adrenal Gland, Ovary, and Testis in the Fischer-344 Rat. *Toxicol Pathol.* 22(4):341-352.

Latendresse, J. R., Brooks, C. L. & Capen, C. C. (1995). Toxic Effects of Butylated Triphenyl Phosphate-based Hydraulic Fluid and Tricresyl Phosphate in Female F344 Rats. *Veterinary Pathology*, 32(4), 394–402.

Leonetti, C., Butt, C. M., Hoffman, K., Hammel, S. C., Miranda, M. L., and Stapleton, H. M. (2016). Brominated flame retardants in placental tissues: Associations with infant sex and thyroid hormone endpoints. *Environ. Health* 15, 113.

Li, W., Wang, Y., Asimakopoulos, A. G., Covaci, A., Gevao, B., Johnson-Restrepo, B., Kumosani, T. A., Malarvannan, G., Moon, H.-B., Nakata, H., Sinha, R. K., Tran, T. M. and Kannan, K. (2019). Organophosphate esters in indoor dust from 12 countries: Concentrations, composition profiles, and human exposure. *Environment International*, 133(Pt A), 105178.

Li, R., Zhan, W., Ren, J., Gao, X., Huang, X., & Ma, Y. (2022). Associations between organophosphate esters concentrations and markers of liver function in US adolescents aged 12-19 years: A mixture analysis. *Environmental pollution* (Barking, Essex : 1987), 314, 120255.

Liao, K., Zhao, Y., Qu, J., Yu, W., Hu, S., Fang, S., Zhao, M., & Jin, H. (2023). Organophosphate esters concentrations in human serum and their associations with Sjögren syndrome. *Environmental pollution (Barking, Essex : 1987)*, 331(Pt 1), 121941.

Lin, J., Deng, L., Sun, M., Wang, Y., Lee, S., Choi, K., & Liu, X. (2021). An in vitro investigation of endocrine disrupting potentials of ten bisphenol analogues. *Steroids*, 169, 108826.

Liu, B., Ding, L., Lv, L., Yu, Y. and Dong, W. (2023). Organophosphate esters (OPEs) and novel brominated flame retardants (NBFRs) in indoor dust: A systematic review on concentration, spatial distribution, sources, and human exposure. *Chemosphere*, 345, 140560.

Liu, X., Ji, K., & Choi, K. (2012). Endocrine disruption potentials of organophosphate flame retardants and related mechanisms in H295R and MVLN cell lines and in zebrafish. *Aquatic toxicology (Amsterdam, Netherlands)*, 114-115, 173–181.

Liu, L. Y., Salamova, A., He, K., and Hites, R. A. (2015). Analysis of polybrominated diphenyl ethers and emerging halogenated and organophosphate flame retardants in human hair and nails. *Journal of chromatography. A*, 1406, 251–257.

Liu, L. Y., He, K., Hites, R. A., and Salamova, A. (2016). Hair and Nails as Noninvasive Biomarkers of Human Exposure to Brominated and Organophosphate Flame Retardants. *Environmental science & technology*, 50(6), 3065–3073.

Liu, X., Sakai, H., Nishigori, M., Suyama, K., Nawaji, T., Ikeda, S., Nishigouchi, M., Okada, H., Matsushima, A., Nose, T., Shimohigashi, M., & Shimohigashi, Y. (2019). Receptor-binding affinities of bisphenol A and its next-generation analogs for human nuclear receptors. *Toxicology and applied pharmacology*, 377, 114610.

Long, J., Zhang, C. J., Zhu, N., Du, K., Yin, Y. F., Tan, X., Liao, D. F., & Qin, L. (2018). Lipid metabolism and carcinogenesis, cancer development. *American journal of cancer research*, 8(5), 778–791.

Lotti, M., & Moretto, A. (2005). Organophosphate-induced delayed polyneuropathy. *Toxicological reviews*, 24(1), 37–49.

Lund, B. O., Bergman, A., & Brandt, I. (1988). Metabolic activation and toxicity of a DDT-metabolite, 3-methylsulphonyl-DDE, in the adrenal zona fasciculata in mice. *Chemico-biological interactions*, 65(1), 25–40.

Lyraki, R., and Schedl, A. (2021). Adrenal cortex renewal in health and disease. *Nature reviews. Endocrinology*. **17**, 421–434.

Ma, Y., Xie, Z., Lohmann, R., Mi, W., & Gao, G. (2017). Organophosphate Ester Flame Retardants and Plasticizers in Ocean Sediments from the North Pacific to the Arctic Ocean. *Environmental science & technology*, 51(7), 3809–3815.

Maddela, N. R., Venkateswarlu, K., Kakarla, D. and Megharaj, M. (2020). Inevitable human exposure to emissions of polybrominated diphenyl ethers: A perspective on potential health risks. *Environmental Pollution*. **266**, 115240.

Makey, C. M., McClean, M. D., Braverman, L. E., Pearce, E. N., Sjödin, A., Weinberg, J., & Webster, T. F. (2016). Polybrominated diphenyl ether exposure and reproductive hormones in North American men. *Reproductive toxicology* (Elmsford, N.Y.), *62*, 46–52.

Marchitti, S. A., Fenton, S. E., Mendola, P., Kenneke, J. F., and Hines, E. P. (2017). Polybrominated Diphenyl Ethers in Human Milk and Serum from the U.S. EPA MAMA Study: Modeled Predictions of Infant Exposure and Considerations for Risk Assessment. *Environmental health perspectives*. **125**, 706–713.

Martinez-Arguelles, D. B., Guichard, T., Culty, M., Zirkin, B. R., & Papadopoulos, V. (2011). In utero exposure to the antiandrogen di-(2-ethylhexyl) phthalate decreases adrenal aldosterone production in the adult rat. *Biology of reproduction*, *85*(1), 51–61.

Martinez-Arguelles, D. B., McIntosh, M., Rohlicek, C. V., Culty, M., Zirkin, B. R., & Papadopoulos, V. (2013). Maternal in utero exposure to the endocrine disruptor di-(2-ethylhexyl) phthalate affects the blood pressure of adult male offspring. *Toxicology and applied pharmacology*, *266*(1), 95–100.

Martinez-Arguelles, D. B., & Papadopoulos, V. (2015). Mechanisms mediating environmental chemical-induced endocrine disruption in the adrenal gland. *Frontiers in endocrinology*, *6*, 29.

Martín-Pozo, L., Cantarero-Malagón, S., Hidalgo, F., Navalón, A., & Zafra-Gómez, A. (2020). Determination of endocrine disrupting chemicals in human nails using an alkaline digestion prior to ultra-high performance liquid chromatography-tandem mass spectrometry. *Talanta*, 208, 120429.

Mattson, P. and Kowal, J. (1978). The ultrastructure of functional mouse adrenal cortical tumor cells in vitro. *Differentiation*. **11**, 75–88

Mazdai, A., Dodder, N. G., Abernathy, M. P., Hites, R. A., and Bigsby, R. M. (2003). Polybrominated diphenyl ethers in maternal and fetal blood samples. *Environmental health perspectives*. **111**, 1249–1252.

Medwid, S., Guan, H., & Yang, K. (2019). Bisphenol A stimulates steroidogenic acute regulatory protein expression via an unknown mechanism in adrenal cortical cells. *Journal of cellular biochemistry*, 120(2), 2429–2438

Megha, R., Wehrle, C.J., Kashyap, S., et al. (Updated 2022 Oct 17). *Anatomy, Abdomen and Pelvis: Adrenal Glands (Suprarenal Glands)* StatPearls Publishing. Available from: <https://www.ncbi.nlm.nih.gov/books/NBK482264/>

Mellon, S.H., Miller, W.L., Bair, S.R., et al. (1994). Steroidogenic adrenocortical cell lines produced by genetically targeted tumorigenesis in transgenic mice. *Mol. Endocrinol.* **8**, 97–108.

Meng, S., Chen, X., Gyimah, E., Xu, H., and Chen, J. (2020). Hepatic oxidative stress, DNA damage and apoptosis in adult zebrafish following sub-chronic exposure to BDE-47 and BDE-153. *Environmental toxicology*. **35**, 1202–1211.

McKenna, S.T., Birtles, R., Dickens, K., Walker, R.G., Spearpoint, M.J., Stec, A.A. and Hull, T.R. (2018). Flame retardants in UK furniture increase smoke toxicity more than they reduce fire growth rate. *Chemosphere*. **196**, 429–439.

Mitsche, M. A., McDonald, J. G., Hobbs, H. H., and Cohen, J. C. (2015). Flux analysis of cholesterol biosynthesis in vivo reveals multiple tissue and cell-type specific pathways. *eLife*, 4, e07999.

Mitty H. A. (1988). Embryology, anatomy, and anomalies of the adrenal gland. *Seminars in roentgenology*, 23(4), 271–279.

Morris, P. J., Medina-Cleghorn, D., Heslin, A., King, S. M., Orr, J., Mulvihill, M. M., Krauss, R. M. and Nomura, D. K. (2014). Organophosphorus flame retardants inhibit specific liver carboxylesterases and cause serum hypertriglyceridemia. *ACS Chemical Biology*, 9(5), 1097–1103.

Mountjoy, K.G., Bird, I.M., Rainey, W.E., et al. (1994). ACTH induces up-regulation of ACTH receptor mRNA in mouse and human adrenocortical cell lines. *Mol. Cell. Endocrinol.* **99**, 17–20.

Mukai K, Nagasawa H, Agake-Suzuki R, et al. (2002). Conditionally immortalized adrenocortical cell lines at undifferentiated states exhibit inducible expression of glucocorticoid synthesizing genes. *Eur. J. Biochem.* **269**, 69–81.

Nagy, L., & Freeman, D. A. (1990). Cholesterol movement between the plasma membrane and the cholesteryl ester droplets of cultured Leydig tumour cells. *The Biochemical journal*, 271(3), 809–814.

Natesan, V., & Kim, S. J. (2021). Lipid Metabolism, Disorders and Therapeutic Drugs - Review. *Biomolecules & therapeutics*, 29(6), 596–604.

National Toxicology Program. (1994). NTP Toxicology and Carcinogenesis Studies of Tricresyl Phosphate (CAS No. 1330-78-5) in F344/N Rats and B6C3F1 Mice (Gavage and Feed Studies). *Natl Toxicol Program Tech Rep Ser.* 433, 1-321.

Negi, C. K., Gadara, D., Kohoutek, J., Bajard, L., Spáčil, Z. and Blaha, L. (2023). Replacement Flame-Retardant 2-Ethylhexyldiphenyl Phosphate (EHDPP) Disrupts Hepatic Lipidome: Evidence from Human 3D Hepatospheroid Cell Culture. *Environmental Science and Technology*, 57(5), 2006–2018.

Netter, H.F. (1965). Histology of the suprarenal (adrenal) glands. *The CIBA Collection of Medical Illustrations*. CIBA, p.81.

Nicolaides, N.C., Willenberg, H.S., Bornstein, S.R., et al. (Updated 2023 Jun 12). Adrenal Cortex: Embryonic Development, Anatomy, Histology and Physiology. South Dartmouth (MA): MDText.com, Inc. Accessed Sep 13, 2024. Available from: <https://www.ncbi.nlm.nih.gov/books/NBK278945/>

OECD. (2022). Test No. 456: H295R Steroidogenesis Assay: OECD Guidelines for the Testing of Chemicals. OECD Publishing. Section 4.

O'Hare MJ, Neville AM. (1973). Morphological responses to corticotrophin and cyclic AMP by adult rat adrenocortical cells in monolayer culture. *J. Endocrinol.* **56**, 529–536.

Ospina, M., Jayatilaka, N. K., Wong, L.-Y., Restrepo, P. & Calafat, A. M. (2018). Exposure to organophosphate flame retardant chemicals in the U.S. general population: Data from the 2013–2014 National Health and Nutrition Examination Survey. *Environment International*, 110, 32–41

Oster, H., Challet, E., Ott, V., Arvat, E., de Kloet, E. R., Dijk, D. J., Lightman, S., Vgontzas, A., & Van Cauter, E. (2017). The Functional and Clinical Significance of the 24-Hour Rhythm of Circulating Glucocorticoids. *Endocrine reviews*, 38(1), 3–45.

Oulhote, Y., Chevrier, J., and Bouchard, M. F. (2016). Exposure to Polybrominated Diphenyl Ethers (PBDEs) and Hypothyroidism in Canadian Women. *The Journal of clinical endocrinology and metabolism*, 101(2), 590–598.

Palmer, L.G., and Schnermann, J. (2015). Integrated control of Na transport along the nephron. *Clinical journal of the American Society of Nephrology : CJASN*. **10**, 676–687.

Panagiotidou, E., Zerva, S., Mitsiou, D. J., Alexis, M. N., & Kitraki, E. (2014). Perinatal exposure to low-dose bisphenol A affects the neuroendocrine stress response in rats. *The Journal of endocrinology*, 220(3), 207–218.

Pankratz, D.S. (1931). The development of the suprarenal gland in the albino rat with a consideration of its possible relation to the origin of foetal movements. *Anat. Rec.* **49**, 31–49.

Paravati, S., Rosani, A., Warrington, S.J. Physiology, Catecholamines. [Updated 2022 Oct 24]. Treasure Island (FL): StatPearls Publishing. Available from: <https://www.ncbi.nlm.nih.gov/books/NBK507716/>

Payne, J., Rajapakse, N., Wilkins, M., and Kortenkamp, A. (2000). Prediction and assessment of the effects of mixtures of four xenoestrogens. *Environmental health perspectives*, 108(10), 983–987.

Payne, A. H., and Hales, D. B. (2004). Overview of steroidogenic enzymes in the pathway from cholesterol to active steroid hormones. *Endocrine reviews*. **25**, 947–970.

Piao, Y., Liu, Y., Xie, X. (2013). Change Trends of Organ Weight Background Data in Sprague Dawley Rats at Different Ages. *J. Toxicol. Pathol.* **26**, 29-34.

Pihlajoki, M., Dörner, J., Cochran, R. S., Heikinheimo, M., & Wilson, D. B. (2015).

Adrenocortical zonation, renewal, and remodeling. *Frontiers in endocrinology*. **6**, 27.

Pillai, H. K., Fang, M., Beglov, D., Kozakov, D., Vajda, S., Stapleton, H. M., Webster, T. F. and Schlezinger, J. J. (2014). Ligand Binding and Activation of PPAR γ by Firemaster® 550: Effects on Adipogenesis and Osteogenesis in Vitro. *Environmental Health Perspectives*, 122(11), 1225–1232.

Pinto, C.L., Markey, K., Dix, D. & Browne, P. (2018). Identification of candidate reference chemicals for in vitro steroidogenesis assays. *Toxicol. In Vitro*. **47**, 103-119.

Percy, Z., La Guardia, M. J., Xu, Y., Hale, R. C., Dietrich, K. N., Lanphear, B. P., Yolton, K., Vuong, A. M., Cecil, K. M., Braun, J. M., Xie, C., & Chen, A. (2020). Concentrations and loadings of organophosphate and replacement brominated flame retardants in house dust from the home study during the PBDE phase-out. *Chemosphere*, 239, 124701.

Pierson, R.W.J. (1967). Metabolism of steroid hormones in adrenal cortex tumor cultures. *Endocrinology*. **81**, 693–707

Pinto, D.E., Setzer, R.W., Judson, R.S. & Paul Friedman, K. (2019). Development of a prioritization method for chemical- mediated effects on steroidogenesis using an integrated statis- tical analysis of high-throughput H295R data. *Regul. Toxicol. Pharmacol.* **109**, 104510.

Poma, G., Glynn, A., Malarvannan, G., Covaci, A., & Darnerud, P. O. (2017). Dietary intake of phosphorus flame retardants (PFRs) using Swedish food market basket estimations. *Food and chemical toxicology : an international journal published for the British Industrial Biological Research Association*, 100, 1–7.

Pradeep, P., Friedman, K. P., & Judson, R. (2020). Structure-based QSAR Models to Predict Repeat Dose Toxicity Points of Departure. *Computational toxicology (Amsterdam, Netherlands)*, 16(November 2020), 10.1016/j.comtox.2020.100139.

Rainey, W. E., Saner, K., and Schimmer, B. P. (2004). Adrenocortical cell lines. *Molecular and cellular endocrinology*. **228**, 23–38.

Rajapakse, N., Silva, E., & Kortenkamp, A. (2002). Combining xenoestrogens at levels below individual no-observed-effect concentrations dramatically enhances steroid hormone action. *Environmental health perspectives*, 110(9), 917–921.

Rajkumar, A., Luu, T., Hales, B. F. and Robaire, B. (2022). High-content imaging analyses of the effects of bisphenols and organophosphate esters on TM4 mouse Sertoli cells. *Biology of Reproduction*, 107(3), 858–868.

Rasmussen, P. E., Beauchemin, S., Chénier, M., Levesque, C., MacLean, L. C., Marro, L., Jones-Otazo, H., Petrovic, S., McDonald, L. T., & Gardner, H. D. (2011). Canadian house dust study: lead bioaccessibility and speciation. *Environmental science & technology*, 45(11), 4959–4965.

Rasmussen, P. E., Levesque, C., Chénier, M., Gardner, H. D., Jones-Otazo, H., & Petrovic, S. (2013). Canadian House Dust Study: population-based concentrations, loads and loading rates of arsenic, cadmium, chromium, copper, nickel, lead, and zinc inside urban homes. *The Science of the total environment*, 443, 520–529.

Reardon, A.J.F., Farmahin, R., Williams, A., Meier, M.J., Addicks, G.C., Yauk, C.L., Matteo, G., Atlas, E., Harrill, J., Everett, L.J., Shah, I., Judson, R., Ramaiahgari, S., Ferguson, S.S. and Barton-Maclaren, T.S. (2023). From vision toward best practices: Evaluating in vitro transcriptomic points of departure for application in risk assessment using a uniform workflow. *Front. Toxicol.* **5**, 1194895.

Robb, E. L., Regina, A. C., & Baker, M. B. (2023). Organophosphate Toxicity. In StatPearls. StatPearls Publishing.

Robin, J., Lefevre, S., Guihenneuc, J., Cambien, G., Dupuis, A., & Venisse, N. (2024). Analytical methods and biomonitoring results in hair for the assessment of exposure to endocrine-disrupting chemicals: A literature review. *Chemosphere*, 353, 141523.

Rodgers, T. F. M., Truong, J. W., Jantunen, L. M., Helm, P. A., & Diamond, M. L. (2018). Organophosphate Ester Transport, Fate, and Emissions in Toronto, Canada, Estimated Using an Updated Multimedia Urban Model. *Environmental science & technology*, 52(21), 12465–12474.

Rodgers, K.M., Bennett, D., Moran, R., Knox, K., Stoiber, T., Gill, R., Young, T. M., Blum, A., and Dodson, R.E. (2021). Do flame retardant concentrations change in dust after older upholstered furniture is replaced?. *Environment international*. **153**, 106513.

Rodriguez, H., Hum, D.W., Staels, B. & Miller, W.L. (1997). Transcription of the human genes for cytochrome P450scc and P450c17 is regulated differently in human adrenal NCI-H295 cells than in mouse adrenal Y1 cells. *J. Clin. Endocrinol. Metab.* **82**, 365-371.

Ragazzon, B., Lefrancois-Martinez, A.M., Val, P., et al. (2006). Adrenocorticotropin-dependent changes in SF-1/DAX-1 ratio influence steroidogenic genes expression in a novel model of glucocorticoid-producing adrenocortical cell lines derived from targeted tumorigenesis. *Endocrinology*. **147**, 1805–1818.

Rainey, W.E., Bird, I.M., Sawetawan, C., Hanley, N.A., McCarthy, J.L., McGee, E.A., Wester, R. & Mason, J.I. (1993). Regulation of human adrenal carcinoma cell (NCI-H295) production of C19 steroids. *J. Clin. Endocrinol. Metab.* **77**, 731-737.

Rodriguez, H., Hum, D.W., Staels, B. (1997). Transcription of the human genes for cytochrome P450scc and P450c17 is regulated differently in human adrenal NCI-H295 cells than in mouse adrenal Y1 cells. *J. Endocrinol. Metab.* **82**, 365–371.

Sala, B., Giménez, J., Fernández-Arribas, J., Bravo, C., Lloret-Lloret, E., Esteban, A., Bellido, J. M., Coll, M., & Eljarrat, E. (2022). Organophosphate ester plasticizers in edible fish from the

Mediterranean Sea: Marine pollution and human exposure. *Environmental pollution* (Barking, Essex : 1987), 292(Pt B), 118377.

Salgado-Freiría, R., López-Doval, S., & Lafuente, A. (2018). Perfluorooctane sulfonate (PFOS) can alter the hypothalamic-pituitary-adrenal (HPA) axis activity by modifying CRF1 and glucocorticoid receptors. *Toxicology letters*, 295, 1–9.

Salih Al-Omran, L. (2019). *Physiochemical Properties and Environmental Levels of Legacy and Novel Brominated Flame Retardants*. IntechOpen.

Schang, G., Robaire, B. and Hales, B. F. (2016). Organophosphate Flame Retardants Act as Endocrine-Disrupting Chemicals in MA-10 Mouse Tumor Leydig Cells. *Toxicological Sciences*, 150(2), 499–509. <https://doi.org/10.1093/toxsci/kfw012>

Schechter, A., Johnson-Welch, S., Tung, K. C., Harris, T. R., Päpke, O., and Rosen, R. (2007). Polybrominated diphenyl ether (PBDE) levels in livers of U.S. human fetuses and newborns. *Journal of toxicology and environmental health*. **70**, 1–6.

Schteingart, D. E., Sinsheimer, J. E., Counsell, R. E., Abrams, G. D., McClellan, N., Djanegara, T., Hines, J., Ruangwises, N., Benitez, R., & Wotring, L. L. (1993). Comparison of the adrenalytic activity of mitotane and a methylated homolog on normal adrenal cortex and adrenal cortical carcinoma. *Cancer chemotherapy and pharmacology*. **31**, 459–466.

Schmeisser, S., Miccoli, A., von Bergen, M., Berggren, E., Braeuning, A., Busch, W., Desaintes, C., Gourmelon, A., Grafström, R., Harrill, J., Har, T., Herzler, M., Kass, G. E. N., Kleinstreuer, N., Leist, M., Luijten, M., Marx-Stoelting, P., Poetz, O., van Ravenzwaay, B., Roggeband, R., Tralau, T. (2023). New approach methodologies in human regulatory toxicology - Not if, but how and when!. *Environment international*, 178, 108082.

Scott, J.H., Menouar, M.A., Dunn, R.J. Physiology, Aldosterone. [Updated 2023 May 1]. Stat Pearls Treasure Island (FL): StatPearls Publishing. Available from: <https://www.ncbi.nlm.nih.gov/books/NBK470339/>

Sharkey, M., Harrad, S., Abou-Elwafa Abdallah, M., Drage, D. S., & Berresheim, H. (2020). Phasing-out of legacy brominated flame retardants: The UNEP Stockholm Convention and other legislative action worldwide. *Environment international*. **144**, 106041.

Sharma, S., Saini, A., & Dhawan, D. K. (2023). Lipid Metabolic Disorders in Neurodegenerative Diseases – Role of Androgen Receptor. *The Eurasian Journal of Medicine*, 55(1), S1–S8.

Sjödin, A., Mueller, J.F., Jones, R., Schütze, A., Wong, L.-Y., Caudill, S.P., Harden, F.A., Webster, T.F. and Toms, L.-M. (2020). Serum elimination half-lives adjusted for ongoing exposure of tri- to hexabrominated diphenyl ethers: Determined in persons moving from North America to Australia. *Chemosphere*. **248**, 125905.

Sparrow, R. A., & Coupland, R. E. (1987). Blood flow to the adrenal gland of the rat: its distribution between the cortex and the medulla before and after haemorrhage. *Journal of anatomy*, 155, 51–61.

Siddique, S., Farhat, I., Kubwabo, C., Chan, P., Goodyer, C. G., Robaire, B., Chevrier, J., & Hales, B. F. (2022). Exposure of men living in the greater Montreal area to organophosphate esters: Association with hormonal balance and semen quality. *Environment international*, 166, 107402.

Sigala, S.B.C., Penton, D., Abate, A., Peitzsch, M., Cosentini, D., Tiberio, G.A.M., Bornstein, S.R., Berruti, A., Hantel, C. (2022). A comprehensive investigation of steroidogenic signaling in classical and new experimental cell models of adrenocortical carcinoma. *Cells*. 2022. **11**, 1439.

Stapleton, H.M., Sharma, S., Getzinger, G., Ferguson, P.L., Gabriel, M., Webster, T.F. and Blum, A. (2012). Novel and High Volume Use Flame Retardants in US Couches Reflective of the 2005 PentaBDE Phase Out. *Environ Sci & Tech*, **46**, 13432–13439.

State of California (2013). Technical bulletin 117-2013: Requirements, test procedure and apparatus for testing the smolder resistance of materials used in upholstered furniture.

Sacramento, CA. Available at: https://bhgs.dca.ca.gov/about_us/tb117_2013.pdf (Accessed Oct 26, 2024)

Stroth, N., Liu, Y., Aguilera, G., and Eiden, L. E. (2011). Pituitary adenylate cyclase-activating polypeptide controls stimulus-transcription coupling in the hypothalamic-pituitary-adrenal axis

to mediate sustained hormone secretion during stress. *Journal of neuroendocrinology*. **23**, 944–955.

Struzina, L., Pineda Castro, M. A., Kubwabo, C., Siddique, S., Zhang, G., Fan, X., Tian, L., Bayen, S., Aneck-Hahn, N., Bornman, R., Chevrier, J., Misunis, M., and Yargeau, V. (2022). Occurrence of legacy and replacement plasticizers, bisphenols, and flame retardants in potable water in Montreal and South Africa. *The Science of the total environment*. **840**, 156581.

Teuschler, L., Klaunig, J., Carney, E., Chambers, J., Conolly, R., Gennings, C., Giesy, J., Hertzberg, R., Klaassen, C., Kodell, R., Paustenbach, D., & Yang, R. (2002). Support of science-based decisions concerning the evaluation of the toxicology of mixtures: a new beginning. *Regulatory toxicology and pharmacology : RTP*, 36(1), 34–39.

Testa, B., Crivori, P., Reist, M. and Carrupt, P.A. (2000). The influence of lipophilicity on the pharmacokinetic behavior of drugs: concepts and examples. *Perspect Drug Discov*, **19**, 179–211.

Thayer, K. A., Doerge, D. R., Hunt, D., Schurman, S. H., Twaddle, N. C., Churchwell, M. I., Garantziotis, S., Kissling, G. E., Easterling, M. R., Bucher, J. R. and Birnbaum, L. S. (2015). Pharmacokinetics of bisphenol A in humans following a single oral administration. *Environment International*, 83, 107–115.

Tian, Y., Baukal, A.J., Sandberg, K., et al. (1996). Properties of AT1a and AT1b angiotensin receptors expressed in adrenocortical Y-1 cells. *Am. J. Physiol.* **270**, E831–E839.

Tung, E. W. Y., Peshdary, V., Gagné, R., Rowan-Carroll, A., Yauk, C. L., Boudreau, A. and Atlas, E. (2017). Adipogenic Effects and Gene Expression Profiling of Firemaster® 550 Components in Human Primary Preadipocytes. *Environmental Health Perspectives*, 125(9), 097013.

Ueno, M., Nakashima, J., Akita, M., Ban, S. I., Nakanoma, T., Iida, M., and Deguchi, N. (2001). Characterization of a newly established cell line derived from human adrenocortical carcinoma. *International journal of urology: official journal of the Japanese Urological Association*. **8**, 17–22.

Utiger, R. D. (2010). Adrenal gland. *Encyclopedia Britannica*. Accessed Sep 20, 2024. Available from: <https://www.britannica.com/science/adrenal-gland>

US. EPA. (2016). Frank R. Lautenberg Chemical Safety for the 21st Century Act. House Reports: No. 114-176.

US. EPA. (2000). Supplementary Guidance for Conducting Health Risk Assessment of Chemical Mixtures. EPA 630/R-00/002. Washington, DC:U.S. Environmental Protection Agency, Risk Assessment Forum.

US. EPA. (2024a). Endocrine Disruptor Screening Program (EDSP) in the 21st Century. Available at <https://www.epa.gov/endocrine-disruption/endocrine-disruptor-screening-program-edsp-21st-century>. Accessed Nov 19, 2024.

US. EPA. (2024b). Conducting a Human Health Risk Assessment. Available at <https://www.epa.gov/risk/conducting-human-health-risk-assessment>. Accessed Nov 20, 2024.

van den Dungen, M. W., Rijk, J. C., Kampman, E., Steegenga, W. T., & Murk, A. J. (2015). Steroid hormone related effects of marine persistent organic pollutants in human H295R adrenocortical carcinoma cells. *Toxicology in vitro : an international journal published in association with BIBRA*, 29(4), 769–778.

Van den Eede, N., Maho, W., Erratico, C., Neels, H., & Covaci, A. (2013). First insights in the metabolism of phosphate flame retardants and plasticizers using human liver fractions. *Toxicology letters*, 223(1), 9–15.

Van den Eede, N., Erratico, C., Exarchou, V., Maho, W., Neels, H., Covaci, A. (2015). In vitro biotransformation of tris(2-butoxyethyl) phosphate (TBOEP) in human liver and serum. *Toxicology and Applied Pharmacology*, 284(2), 246–253.

Van der Veen, I., and van der de Boer, J. (2012). Phosphorus flame retardants: Properties, production, environmental occurrence, toxicity and analysis. *Chemosphere*. **88**, 1119– 1153.

van Weerden, W.M., Bierings, H.G., van Steenbrugge, G.J., de Jong, F.H., and Schröder, F.H. (1992). Adrenal glands of mouse and rat do not synthesize androgens. *Life sciences*. **50**, 857–861.

Venugopal, S., Galano, M., Chan, R., Sanyal, E., Issop, L., Lee, S., Taylor, L., Kaur, P., Daly, E., & Papadopoulos, V. (2021). Dynamic Remodeling of Membranes and Their Lipids during Acute Hormone-Induced Steroidogenesis in MA-10 Mouse Leydig Tumor Cells. *International journal of molecular sciences*, 22(5), 2554.

Vinson, G.P., Pudney, J.A., and Whitehouse, B.J. (1985). The mammalian adrenal circulation and the relationship between adrenal blood flow and steroidogenesis. *J. Endocrinol.* **105**, 285–294.

Voorhees, H., Aschenbrenner, J., Carnes, J., et al. (1984). Rounding and steroidogenesis of enzyme and ACTH-treated Y-1 mouse adrenal tumor cells. *Cell. Biol. Intl.* **8**, 483–497

Vuong, A. M., Yolton, K., Xie, C., Webster, G. M., Sjödin, A., Braun, J. M., Dietrich, K. N., Lanphear, B. P., & Chen, A. (2017). Childhood polybrominated diphenyl ether (PBDE) exposure and neurobehavior in children at 8 years. *Environmental research*, 158, 677–684.

Wade MG, Kawata A, Rigden M, Caldwell D, Holloway AC. (2019). Toxicity of Flame Retardant Isopropylated Triphenyl Phosphate: Liver, Adrenal, and Metabolic Effects. *Int J Toxicol.* 38(4):279-290.

Wagner C.A. (2014). Effect of mineralocorticoids on acid-base balance. *Nephron. Physiology*, **128**, 26–34.

Wang, X., Zhang, R., Song, C. and Crump, D. (2019). Computational evaluation of interactions between organophosphate esters and nuclear hormone receptors. *Environmental Research*, 182, 108982.

Wang, X., Liu, Q., Zhong, W., Yang, L., Yang, J., Covaci, A. and Zhu, L. (2020). Estimating renal and hepatic clearance rates of organophosphate esters in humans: Impacts of intrinsic metabolism and binding affinity with plasma proteins. *Environment International*, 134, 105321

Wang, Y., Hong, J., Shi, M., Guo, L., Liu, L., Tang, H. and Liu, X. (2021). Triphenyl phosphate disturbs the lipidome and induces endoplasmic reticulum stress and apoptosis in JEG-3 cells. *Chemosphere*, 275, 129978.

Wang, X., Luu, T., Beal, M. A., Barton-Maclaren, T. S., Robaire, B., & Hales, B. F. (2022). The Effects of Organophosphate Esters Used as Flame Retardants and Plasticizers on Granulosa, Leydig, and Spermatogonial Cells Analyzed Using High-Content Imaging. *Toxicological sciences : an official journal of the Society of Toxicology*, 186(2), 269–287.

Wang, X., Lee, E., Hales, B. F., & Robaire, B. (2023a). Organophosphate Esters Disrupt Steroidogenesis in KGN Human Ovarian Granulosa Cells. *Endocrinology*, 164(7), bqad089.

Wang, X., Rowan-Carroll, A., Meier, M. J., Williams, A., Yauk, C. L., Hales, B. F., & Robaire, B. (2023b). Toxicological Mechanisms and Potencies of Organophosphate Esters in KGN Human Ovarian Granulosa Cells as Revealed by High-throughput Transcriptomics. *Toxicological sciences : an official journal of the Society of Toxicology*, 197(2), 170–185.

Wang, X., Rowan-Carroll, A., Meier, M. J., Yauk, C. L., Wade, M. G., Robaire, B., & Hales, B. F. (2024). House dust-derived mixtures of organophosphate esters alter the phenotype, function, transcriptome, and lipidome of KGN human ovarian granulosa cells. *Toxicological sciences: an official journal of the Society of Toxicology*, 200(1), 95–113.

Welte, M. A. and Gould, A. P. Lipid droplet functions beyond energy storage. (2017). *Biochim. Biophys. Acta* **1862**, 1260–1272.

Welshons, W. V., Thayer, K. A., Judy, B. M., Taylor, J. A., Curran, E. M., & vom Saal, F. S. (2003). Large effects from small exposures. I. Mechanisms for endocrine-disrupting chemicals with estrogenic activity. *Environmental health perspectives*. **111**, 994–1006.

Witchey, S. K., Doyle, M. G., Fredenburg, J. D., Armour, G. S., Horman, B., Odenkirk, M. T., Aylor, D. L., Baker, E. S. and Patisaul, H. B. (2022). Impacts of Gestational FireMaster 550 (FM 550) Exposure on the Neonatal Cortex are Sex Specific and Largely Attributable to the Organophosphate Esters. *Neuroendocrinology*.

Wolkersdörfer, G. W., Lohmann, T., Marx, C., Schröder, S., Pfeiffer, R., Stahl, H. D., Scherbaum, W. A., Chrousos, G. P., and Bornstein, S. R. (1999). Lymphocytes stimulate dehydroepiandrosterone production through direct cellular contact with adrenal zona reticularis cells: a novel mechanism of immune-endocrine interaction. *J. Clin. Endocrinol. Metab.* **84**, 4220–4227.

Wu, K.D., Chen, Y.M., Chu, T.S., et al. (2001). Expression and localization of human dopamine D2 and D4 receptor mRNA in the adrenal gland, aldosterone-producing adenoma, and pheochromocytoma. *J. Clin. Endocrinol. Metab.* **86**, 4460–4467.

Xiang, D., and Wang, Q. (2021). PXR-mediated organophorous flame retardant tricresyl phosphate effects on lipid homeostasis. *Chemosphere*, 284, 131250.

Xing, Y., Lerario, A.M., Rainey, W., and Hammer, G.D. (2015). Development of adrenal cortex zonation. *Endocrinology and metabolism clinics of North America*. **44**, 243–274.

Yamamoto, M., Yanai, R., & Arishima, K. (2004). Study of migration of neural crest cells to adrenal medulla by three-dimensional reconstruction. *The Journal of veterinary medical science*, 66(6), 635–641.

Yan, H., & Hales, B. F. (2020). Exposure to tert-Butylphenyl Diphenyl Phosphate, an Organophosphate Ester Flame Retardant and Plasticizer, Alters Hedgehog Signaling in Murine Limb Bud Cultures. *Toxicological sciences : an official journal of the Society of Toxicology*, 178(2), 251–263.

Yan, H., and Hales, B. F. (2021). Effects of an Environmentally Relevant Mixture of Organophosphate Esters Derived From House Dust on Endochondral Ossification in Murine Limb Bud Cultures. *Toxicological sciences : an official journal of the Society of Toxicology*, 180(1), 62–75.

Yasumura, Y., Buonassisi, V., Sato, G. (1966). Clonal analysis of differentiated function in animal cell cultures. I. Possible correlated maintenance of differentiated function and the diploid karyotype. *Cancer. Res.* **26**, 529–535.

Yilmaz, B., Terekeci, H., Sandal, S. & Kelestimur, F. (2020). Endocrine disrupting chemicals: exposure, effects on human health, mechanism of action, models for testing and strategies for prevention. *Reviews in Endocrine and Metabolic Disorders*, 21(1), 127–147.

Yu, D., Hales, B. F., & Robaire, B. (2024). Organophosphate ester flame retardants and plasticizers affect the phenotype and function of HepG2 liver cells. *Toxicological sciences : an official journal of the Society of Toxicology*, 199(2), 261–275.

Zhang, Q. et al. *Schizosaccharomyces pombe* cells deficient in triacylglycerols synthesis undergo apoptosis upon entry into the stationary phase. (2003). *J. Biol. Chem.* **278**, 47145–47155.

Zhang, Q., Wang, J., Zhu, J., Liu, J., & Zhao, M. (2017). Potential Glucocorticoid and Mineralocorticoid Effects of Nine Organophosphate Flame Retardants. *Environmental science & technology*, 51(10), 5803–5810.

Zhang, Q., Yu, C., Fu, L., Gu, S., & Wang, C. (2020). New Insights in the Endocrine Disrupting Effects of Three Primary Metabolites of Organophosphate Flame Retardants. *Environmental science & technology*, 54(7), 4465–4474.

Zhang, X., Wang, K., Zhu, L., & Wang, Q. (2021). Reverse Cholesterol Transport Pathway and Cholesterol Efflux in Diabetic Retinopathy. *Journal of diabetes research*, **2021**, 8746114.

Zhang, S., Peng, X., Yang, S., Li, X., Huang, M., Wei, S., Liu, J., He, G., Zheng, H., Yang, L., et al. (2022). The regulation, function, and role of lipophagy, a form of selective autophagy, in metabolic disorders. *Cell Death Dis.* **13**, 132.

Zhao, X., Chen, T., Wang, D., Du, Y., Wang, Y., Zhu, W., Bekir, M., Yu, D., and Shi, Z. (2020). Polybrominated diphenyl ethers and decabromodiphenyl ethane in paired hair/serum and nail/serum from corresponding chemical manufacturing workers and their correlations to thyroid hormones, liver and kidney injury markers. *The Science of the total environment*. **729**, 139049.

Zink, D., Chuah, J. K. C., & Ying, J. Y. (2020). Assessing Toxicity with Human Cell-Based In Vitro Methods. *Trends in molecular medicine*, 26(6), 570–582.

COPYRIGHT INFORMATION AND LICENSING

This Agreement between Zixuan Li ("You") and Oxford University Press ("Oxford University Press") consists of your license details and the terms and conditions provided by Oxford University Press and Copyright Clearance Center.

CHAPTER 2

License Number	5917750416067
License date	Nov 28, 2024
Licensed content publisher	Oxford University Press
Licensed content publication	Endocrinology
Licensed content title	The Organophosphate Esters Used as Flame Retardants and Plasticizers Affect H295R Adrenal Cell Phenotypes and Functions
Licensed content author	Li, Zixuan; Robaire, Bernard
Licensed content date	Jul 31, 2023
Type of Use	Thesis/Dissertation
Institution name	
Title of your work	EFFECTS OF ORGANOPHOSPHATE ESTERS ON THE ADRENAL GLAND
Publisher of your work	McGill University
Expected publication date	Dec 2024
Title of new work	EFFECTS OF ORGANOPHOSPHATE ESTERS ON THE ADRENAL GLAND
Institution name	McGill University
Expected presentation date	Dec 2024
The Requesting Person / Organization to Appear on the License	Zixuan Li
Requestor Location	Zixuan Li 3655 Promenade Sir William Osler Room 110 McGill University Montreal, QC H3G 1Y6 Canada
Order reference number	9727
Publisher Tax ID	GB125506730
Billing Type	Invoice
Billing Address	Zixuan Li 3655 Promenade Sir William Osler Room 110 McGill University Montreal, QC H3G 1Y6 Canada

CHAPTER 3

License Number	5917750944942
License date	Nov 28, 2024
Licensed content publisher	Oxford University Press
Licensed content publication	Endocrinology
Licensed content title	Impact of Exposure to a Mixture of Organophosphate Esters on Adrenal Cell Phenotype, Lipidome, and Function
Licensed content author	Li, Zixuan; Hales, Barbara F
Licensed content date	Feb 20, 2024
Type of Use	Thesis/Dissertation
Institution name	
Title of your work	EFFECTS OF ORGANOPHOSPHATE ESTERS ON THE ADRENAL GLAND
Publisher of your work	McGill University
Expected publication date	Dec 2024
Title of new work	EFFECTS OF ORGANOPHOSPHATE ESTERS ON THE ADRENAL GLAND
Institution name	McGill University
Expected presentation date	Dec 2024
The Requesting Person / Organization to Appear on the License	Zixuan Li
	Zixuan Li McGill University 3655 Promenade Sir William Osler Room 110 Montreal, QC H3G 1Y6 Canada Attn: McGill University
Requestor Location	
Order reference number	9727
Publisher Tax ID	GB125506730
Billing Type	Invoice
	Zixuan Li McGill University 3655 Promenade Sir William Osler Room 110 Montreal, QC H3G 1Y6 Canada Attn: McGill University
Billing Address	